UNIVERSIDADE D
COIMBRA

Sílvia Maria do Couto Rodrigues

DISSECTING THE MECHANISMS GOVERNING SKIN WOUND HEALING INDUCED BY AN UMBILICAL CORD BLOOD-DERIVED PRODUCT

Tese no âmbito do Doutoramento em Biologia Experimental e Biomedicina, Biotecnologia e Saúde, orientada pela Doutora Joana Rita Simões Correia, pelo Doutor Renato Manuel Soares Cardoso e pelo Doutor João Ramalho-Santos e apresentada ao Instituto de Investigação Interdisciplinar da Universidade de Coimbra.

Agosto de 2020

Instituto de Investigação Interdisciplinar da Universidade de Coimbra

DISSECTING THE MECHANISMS GOVERNING SKIN WOUND HEALING INDUCED BY AN UMBILICAL CORD BLOOD-DERIVED PRODUCT

INFLAMMATION AND IMMUNOMODULATION AS HALLMARKS IN THE TREATMENT OF DIFFERENT SKIN LESIONS

Sílvia Maria do Couto Rodrigues

Tese no âmbito do Doutoramento em Biologia Experimental e Biomedicina, Biotecnologia e Saúde, orientada pela Doutora Joana Rita Simões Correia, pelo Doutor Renato Manuel Soares Cardoso e pelo Doutor João Ramalho-Santos e apresentada ao Instituto de Investigação Interdisciplinar da Universidade de Coimbra.

Agosto de 2020

1 2 9 0

UNIVERSIDADE D COIMBRA

This thesis was developed with the support of:

Individual PhD grant attributed to Sílvia Rodrigues: SFRH/BD/137633/2018

Exogenus Therapeutics, SA

Institut Curie

Centre for Neuroscience and Cell Biology – PhD program Experimental Biology and Biomedicine

Acknowlegments

I would like to express my sincere gratitude to my advisor and mentor, Joana Correia, for introducing me to the wonders and frustrations of scientific research. Her guidance, encouragement, and support were fundamental for the development and completion of this research project. At first, she believed in me and gave me the opportunity to pursue my PhD when no one did and then she supported me in all my academic, professional, and personal decisions.

I would like to thank my colleagues at Exogenus Therapeutics, Renato, Filipe, Cláudia, Inês and both "Patricias" for their support at all times. I feel very fortunate to have had the privilege to work with you all and learn a lot with you in different areas.

I am also grateful to Graça Raposo for her advice and suggestions throughout this path and for having accepted join this project. Her extraordinary knowledge and relevant recommendations were crucial for the improvement of this study.

I would also like to thank Ricardo Neves for teaching me and influence in my scientific perception and critical thinking. I am grateful for new opportunities he gave me to explore new thematic under this PhD thesis.

I would like to thank our collaborators at *Centro Nacional de Investigaciones Cardiovasculares Carlos III* (CNIIC), specially to Danay and Raquel for welcoming and making my time at Madrid very enjoyable.

I would like to express my heartfelt thanks to my family for their endless love, support, and encouragement throughout my life and studies. Thank you for guiding me and molding me into who I have become and I couldn´t be happier.
Finally, I would like to thank João for always believing in me and even from far away he was always there for me. To Margarida, that was just a project when I wrote this thesis, for inspiring me and to show how to be simply happy.

Resumo

As doenças de pele estão entre as condições mais comuns de doença onde a maioria das lesões de pele está relacionada com o sistema imunológico. O controlo e equilíbrio dos fatores patológicos deste sistema deve ser uma prioridade no tratamento desses distúrbios. A investigação de terapias baseadas em vesículas extracelulares (EVs) aumentou substancialmente nos últimos anos, tornando-os produtos extremamente atraentes e inovadores para o mercado de medicamentos. Um produto inovador enriquecido em EVs pequenas (sEVs) derivadas de células mononucleares do sangue do cordão umbilical (UCB-MNCs) mostrou, previamente, resultados promissores na aceleração da cicatrização de feridas *in vitro* e *in vivo*. No entanto, outras potencialidades poderão ser atribuídas às EVs derivadas de UCB-MNCs. Assim, esta tese de doutoramento visa avaliar o potencial das UCB-MNCs-EVs como ferramenta para o tratamento de lesões cutâneas relacionadas com o sistema imunológico, caracterizando a sua capacidade de atuar na inflamação e/ou como imunomodulador.

Após a otimização de uma nova metodologia para isolar e purificar as EVs, a composição biofísica e bioquímica das UCB-MNCs-sEVs foi caracterizada. Demonstramos que desta nova metodologia resulta um produto final enriquecido em EVs pequenas (~90%) com um tamanho médio de 102.7±10.55nm. Estas vesículas apresentam características típicas de sEVs como a presença de marcadores clássicos (CD9 e CD63) e não clássicos (CD15) e várias anexinas. Também, apresentam um conteúdo lipídico maioritariamente composto por fosfatidilcolinas e fosfatidilserinas, são isentas de DNA genómico, e contem diversas espécies de RNA de tamanho pequeno. As sEVs obtidas por essa nova metodologia mostraram eficácia superior na cicatrização de feridas quando comparados às sEVs obtidas por metodologias padrão. Ao dia 10, em ratinhos com diabetes tipo I induzida, as feridas tratadas com sEVs isoladas com a nova metodologia mediam menos 37% do que as correspondentes feridas tratadas com sEVs derivadas da metodologia padrão.

O potencial anti-inflamatório e imunomodulador das UCB-MNCs-sEVs também foi testado. Estas sEVs são capazes de afetar a polarização dos macrófagos, diminuindo a razão M1/M2, em ambiente fisiológico e mais pronunciadamente em ambiente inflamatório (estímulo de LPS), alterando o seu padrão de expressão génica e secreção de citocinas. Este impacto no microambiente dos macrófagos induziu a proliferação de fibroblastos assim como um fenótipo menos inflamatório, diminuindo a produção de IL-8 e modulando a expressão genética de fatores de crescimento e moléculas da matriz extracelular. As UCB-MNCs-sEVs também medeiam a supressão da proliferação, diferenciação e ativação de linfócitos T *in vitro.* Estas vesículas potenciam a imunotolerância,

aumentando a abundância de células T reguladoras (T_{regs}) e diminuindo as células T auxiliares 17 (T_H17).

Este potencial foi confirmado *in vivo* por avaliação da expressão genética de feridas tratadas e não tratadas com UCB-MNCs-sEVs ao dia 3 em murganhos com diabetes tipo I induzida. Dos genes relacionados com a resposta inflamatória e imune, aproximadamente 70% estão sub-expressos. A expressão de alguns destes genes foi validada, confirmando o potencial imunomodulador das UCB-MNCs-sEVs.

Num modelo *in vitro* tridimensional de doença psoriática, demonstramos que as UCB-MNCs-sEVs modelam a expressão génica de citocinas (IL-6, IL-8 e CXCL10), péptidos antimicrobianos (psoriasin e beta-defensin 4), e outros fatores anti-inflamatórios considerados críticos na patogénese da psoríase. Adicionalmente, estas vesículas diminuem a secreção de TNF-α e CCL20 em 40 e 30%, respetivamente. *In vivo*, num modelo de ratinho de psoríase induzida pela aplicação tópica de imiquimode, a aplicação tópica de UCB-MNCs-sEVs emulsionados numa formulação de hidrogel diminuiu a espessura da epiderme e aumentou o número de T_{regs} na pele em comparação aos animais não tratados. Quando administrados intravenosamente, UCB-MNCs-sEVs diminuíram o número de células T efetoras observados e a expressão de citocinas pro-inflamatórias. Adicionalmente, células dos gânglios linfáticos e do baço estimuladas *in vitro* tratadas com estas vesículas diminuíram a secreção de IFN-γ e aumentaram a expressão de IL-10.

Estes resultados suportam fortemente um efeito imunomodulador das UCB-MNCs-sEVs tanto *in vitro* (humano) como *in vivo* (ratinho). Os resultados indicam que as UCB-MNCs-sEVs atuam por estimulação da diferenciação dos linfócitos T em T_{regs}, o que pode conduzir à ativação de vias anti-inflamatórias em detrimento das pró-inflamatórias.

Os resultados positivos observados na psoríase abrem as portas para futuros estudos sobre o efeito das UCB-MNCs-sEVs noutras doenças inflamatórias da pele, onde se pensa que a disfunção T_H17/ T_{reg} desempenha um papel crucial (por exemplo, vitiligo, alopecia areata), posicionando-as como uma ferramenta terapêutica muito promissora para doenças inflamatórias da pele.

PALAVRAS-CHAVE: Exossomas, Vesículas Extracelulares, Modo de ação, reparação, regeneração, inflamação, lesões cutâneas.

Abstract

Skin diseases are among the most common human disease conditions where most skin lesions are immune-related. Controlling and balancing pathological factors in this system should be a priority in the treatment of these disorders. Over the last few years, investigation of extracellular vesicles (EVs)-based therapies has grown substantially, making them an extremely attractive and innovative product for medicine market. An innovative product enriched in small EVs (sEVs) derived from umbilical cord blood mononuclear cells (UCB-MNCs) have previously shown promising results in accelerating wound healing *in vitro* and *in vivo*. Yet, other potentialities of EVs derived from UCB-MNCs remain to be elucidated. Thus, this doctoral thesis aims to evaluate the potential of UCB-MNCs-EVs as a tool for the treatment of immune-related skin lesions, characterizing their ability to act on inflammation and/or as an immunomodulator.

After optimizing a new methodology to isolate and purify the EVs, the biophysical and biochemical composition of UCB-MNCs-sEVs was characterized. We demonstrate that this new methodology results in a final product enriched in small EVs (~ 90%) with an average size of 102.7 ± 10.55nm. These vesicles have characteristics typical of sEVs such as the presence of classical (CD9 and CD63) and non-classical (CD15) markers and several annexins. Also, they have a content mostly composed of phosphatidylcholines and phosphatidylserines, free of genomic DNA and made up of several small RNA species. UCB-MNCs-sEVs obtained by this new methodology showed superior efficacy in wound healing when compared to the sEVs obtained by standard methodologies. On day 10, in mice with induced type I diabetes, wounds treated with sEVs isolated with the new methodology measured 37% less than the corresponding wounds treated with sEVs derived from the standard methodology.

In addition, their inflammatory and immunomodulatory potential was tested. Mechanistically, these EVs were able to affect the polarization of macrophages, decreasing the M1/M2 ratio, in a physiological environment and more pronouncedly in an inflammatory environment (LPS stimulus). Its pattern of gene expression and cytokine secretion was also modulated. This impact on the macrophage microenvironment was able to induce the proliferation of fibroblasts as well as a less inflammatory phenotype, leading to decreased production of IL-8 and modulation of the genetic expression of growth factors and extracellular matrix molecules. UCB-MNCs-sEVs also mediate suppression of proliferation, differentiation, and activation of T lymphocytes *in vitro*. These vesicles enhance immunotolerance, increasing the abundance of regulatory T cells (Tregs) and decreasing auxiliary T cells 17 (T_H17). This potential was further confirmed *in vivo* by sequencing the genetic profile of type I-induced diabetes mice wounds treated or not with UCB-MNCs-sEVs on day 3. Of the genes related to the inflammatory and the immune responses,

approximately 70% of these were downregulated. The expression of many of these genes was validated, confirming the immunomodulatory potential of UCB-MNCs-sEVs in the skin.

In a three-dimensional *in vitro* model of psoriatic disease, we demonstrated that UCB-MNCs-sEVs modulate the gene expression of cytokines (IL-6, IL-8 and CXCL10), antimicrobial peptides (psoriasin and beta-defensin 4), and other anti-inflammatory factors considered critical in the pathogenesis of psoriasis. In addition, these vesicles decrease the secretion of TNF-α and CCL20 by 40 and 30%, respectively. *In vivo*, in a mouse model of psoriasis induced by topical application of imiquimod, topical application of emulsified UCB-MNCs-sEVs in a hydrogel formulation decreased the thickness of the epidermis and increased the number of Tregs on the skin compared to untreated animals. When administered intravenously, UCB-MNCs-sEVs decreased the number of effector T cells observed and the expression of proinflammatory cytokines. In addition, *in vitro* stimulated lymph nodes and spleen cells treated with these vesicles decreased IFN-γ secretion and increased IL-10 expression.

These results strongly support an immunomodulatory effect of UCB-MNCs-sEVs both *in vitro* (human) and *in vivo* (mouse). UCB-MNCs-sEVs probably act by stimulating differentiation of T lymphocytes in Tregs, which can lead to the activation of anti-inflammatory pathways in detriment of pro-inflammatory ones.

The positive results observed in psoriasis open the door to future studies on the effect of UCB-MNCs-sEVs on other inflammatory skin diseases, where T_H17/Treg dysfunction is thought to play a crucial role (e.g. vitiligo, alopecia areata). In general, they have shown to be a very promising therapeutic tool for inflammatory skin diseases.

.

***KEYWORDS**:* Exosomes, Extracellular vesicles, Mode of action, Repair, Regeneration, Inflammation, Skin lesions

Graphical Abstract

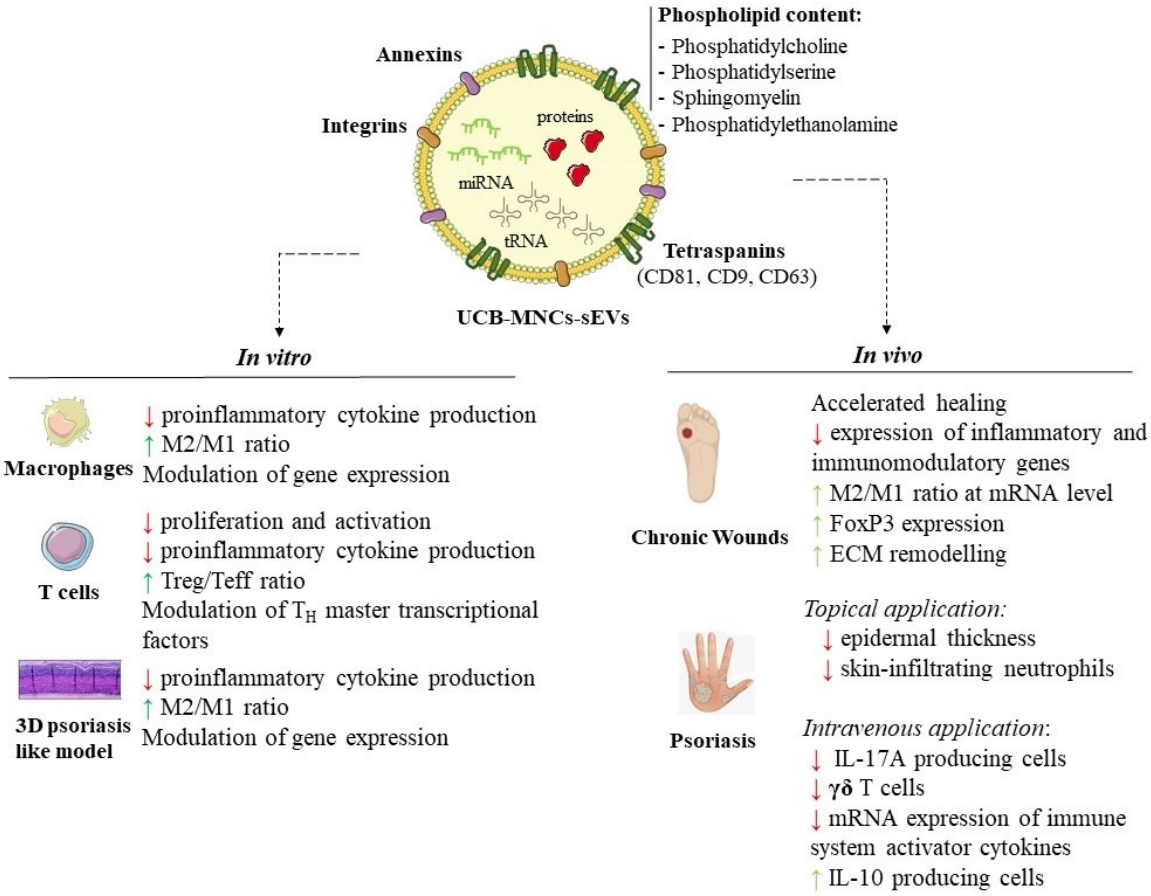

Publications resulting from the thesis:

Patent:

PCT/IB2019/058462 – "Compositions comprising small extracellular vesicles derived from umbilical cord blood mononuclear cells with anti-inflammatory and immunomodulatory properties and process for obtaining them" – Inventors: Joana Correia, Renato Cardoso, Sílvia C. Rodrigues

Peer-reviewed articles:

"Development of an optimized and scalable method for isolation of umbilical cord blood-derived small extracellular vesicles for future clinical use"
Cardoso, R.M.S.*, Rodrigues, S.C.*, Gomes, C. F., Duarte, F.V., Romao, M., Leal, E.C, Freire, P.C., Neves, R., and Simões-Correia, J. (*co-authors) – *Stem Cell Translation Medicine* (Accepted)

"Toxicological profile of umbilical cord blood-derived small extracellular vesicles"
Rodrigues, S.C., Cardoso, R.M.S., Gomes, C. F., Duarte, F.V., Freire, P.C., Neves, R., and Simões-Correia, J. – *Scientific Reports* (in preparation)

"Extracellular vesicles from umbilical cord blood mononuclear cells exert an immunomodulatory function in psoriatic skin, via regulatory T-cells"
Rodrigues, S.C., Gomes, C. F., Cardoso, R.M.S., Freire, P.C., Neves, R., and Simões-Correia, J. – *Journal of Investigative Dermatology* (in preparation)

"Minimal information for studies of extracellular vesicles 2018 (MISEV2018): a position statement of the International Society for Extracellular Vesicles and update of the MISEV2014 guidelines."
Théry C, Witwer KW, Aikawa E, et al.
Journal of Extracellular Vesicles. 2018;7(1):1535750. Published 2018 Nov 23. doi:10.1080/20013078.2018.1535750

Poster presentations:

"Development of a fast-standardized exosome production process for clinical use"
Sílvia C. Rodrigues, Renato Cardoso, Filipe Duarte, Cláudia Gomes, Joana Simões Correia
Annual meeting of International Society of Extracellular Vesicles. Barcelona, May 2018

"The impact of automatizing umbilical cord blood processing in the production of an exosome-based medicinal product"

Sílvia C. Rodrigues, Renato Cardoso, Filipe Duarte, Cláudia Gomes, Joana Simões Correia

Vesicular biology Meeting. Coimbra, February 2018

Table of contents

List of Figures

List of tables

Abbreviations and symbols

3D	Three-dimensional
ACTB	β-actin
AKT	Protein B serine/threonine kinase
AMPs	Antimicrobial peptides
APCs	Antigen presenting cells
ATP	Adenosine triphosphate
bp	Base pair
Ca^{2+}	Calcium
CCL	Chemokine (C-C motif) ligand
cDNA	Complementary DNA
CE	Choleteryl esters
CFSE	Carboxyfluorescein succinimidyl ester
CM	Conditioned medium
Col1a1	Collagen type I (Col1a1)
Col3a1	Collagen type III
COX-2	Cyclooxygenase 2
cryo-TEM	Cryogenic TEM
CXCL	Chemokine (CXC motif) ligand
DAG	Diacylglycerol
DALYs	Disability-Adjusted Life Years
DCs	Dendritic cells
DMSO	Dimethyl sulfoxide
DSS	Dextran sulfate sodium
ECM	Extracellular Matrix
ESCRT	Endosomal sorting complex required for transport
EU	5-ethynyl uridine
EVs	Extracellular Vesicles
FBS	Fetal bovine serum
FGF	Fibroblast Growth Factor
Fn	Fibronectin
GAPDH	Glyceraldehyde-3-phosphate dehydrogenase
gDNA	Genomic DNA

GVHD	Graft-versus-host disease
HE	Haematoxylin/eosin
HPG	Homopropargylglycine
IBMC	Instituto de Biologia Molecular e Celular
IC	Immunocapture
IFN	Interferon
Ig	Immunoglobin
IG	Iodixanol gradient
IGF	Insulin-like growth factor
IL	Interleukin
IMQ	Imiquimod
iNOS	Inducible nitric oxide synthase
ISEV	International Society for Extracellular Vesicles
KGF	Keratinocyte growth factor
KRT	Keratin
LCs	Langerhans cells
lncRNA	Long non-coding RNA
LNs	Lymph nodes
LPS	Lipopolysaccharide
MAPK	Mitogen-activated protein kinases
MCP-1	Monocyte chemoattractant protein 1
Mg^{2+}	Magnesium
MHC	Major histocompatibility complex
MIP1a	Macrophage inflammatory protein 1a
miRNA	MicroRNA
MMPs	Matrix Metalloproteinases
MNCs	Mononuclear Cells
mRNA	messenger RNA
MS	Mass Spectrometry
MSCs	Mesenchymal stem cells
NDHF	Normal human dermal fibroblasts
NETs	Neutrophils extracellular traps
NF-κB	Nuclear factor kappa-light-chain-enhancer
NK	Natural killer
NO	Nitric oxide
NS	Non-stimulated
NSAIDs	Non-steroid anti-inflammatory drugs

nt	Nucleotides
NT	Non-treated
NTA	Nanoparticle tracking analysis
PA	Phosphatidic Acid
PAMPs	Pathogen-associated molecular patterns
PBMNCs	Peripheral blood mononuclear cells (PBMNCs)
PC	Phosphatidylcholine
PCR	Polymerase chain reaction
PDGF	Platelet Derived Growth Factor
PE	Phosphatidylethanolamine
PG	Phosphatidylglycerol
PHA	Phytohemagglutinin
PI	Phosphatidylinositol
piRNA	Piwi-interacting
PlGF	Placental growth factor
PMA	Phorbol 12-myristate-13-acetate
PRRs	Pattern-recognition receptors
PS	Phosphatidylserine
PTEN	Phosphoinositide-phosphatase
qPCR	Quantitative real time polymerase chain reaction
RBCs	Red blood cells
rIL-10	Recombinant IL-10
RNA	Ribonucleic acid
ROS	Reactive oxygen species
rRNA	Ribosomal RNAs
SEC	Size-exclusion chromatography
SEM	Standard error of mean
SFM	Serum free medium
SG	Sucrose gradient
SNARE	Soluble N-ethylmaleimide-sensitive factor attachment protein receptor
snoRNA	Small nucleolar RNA
snRNA	Small nuclear RNA
SPM	Sphingomyelin
SRP-RNA	Signal recognition particle RNA
STAT3	Signal transducer and activator of transcription 3
STZ	Streptozotocin
SUC	Sequential centrifugation

TAG	Triacylglycerol
TEM	Transmission electron microscopy
TGF-β	Transforming growth factor beta
T_H	T helper
TIMP	Tissue inhibitor of metalloproteinase
TLRs	Toll-like receptors
TNF-α	Tumor Necrosis Factor-alpha
T_{reg}	T regulatory cells
T_{RM}	Resident memory T cells
tRNA	Transference RNA
UC	Ultracentrifugation
UCB	Umbilical Cord Blood
UF	Ultrafiltration
uFCS	Ultracentrifuged fetal calf serum
VEGF	Vascular endothelial growth factor
YLD	Years Lost Due to Disability
α-SMA	Alpha-smooth muscle actin

Chapter 1: Introduction

Skin diseases are among the most common human conditions, causing a huge burden in the global context of health[1]. They can occur at all ages and affect in similar way individuals of all cultures[2]. Some skin conditions are manageable, while others are severe enough to kill. Collectively, skin pathologies were the 4th leading cause of nonfatal burden expressed as Years Lost Due to Disability (YLD) in 2010 and 2013, directly following iron-deficiency anemia, tuberculosis, and sense organ diseases [2]. Excluding mortality, YLDs from skin diseases (36.4 million) are larger than those caused by diabetes mellitus (29.5 million) and migraines (28.9 million)[3]. In 2013, skin conditions contributed 1.79% to the total global burden of disease measured in disability-adjusted life years (DALYs) across 306 diseases and injuries[3,4]. Skin wounds/burns, inflammatory skin diseases (e.g. eczema/dermatitis, psoriasis) and skin infections (e.g. impetigo, scabies) are among the most common skin lesions worldwide **(Figure 1.1)**[1].

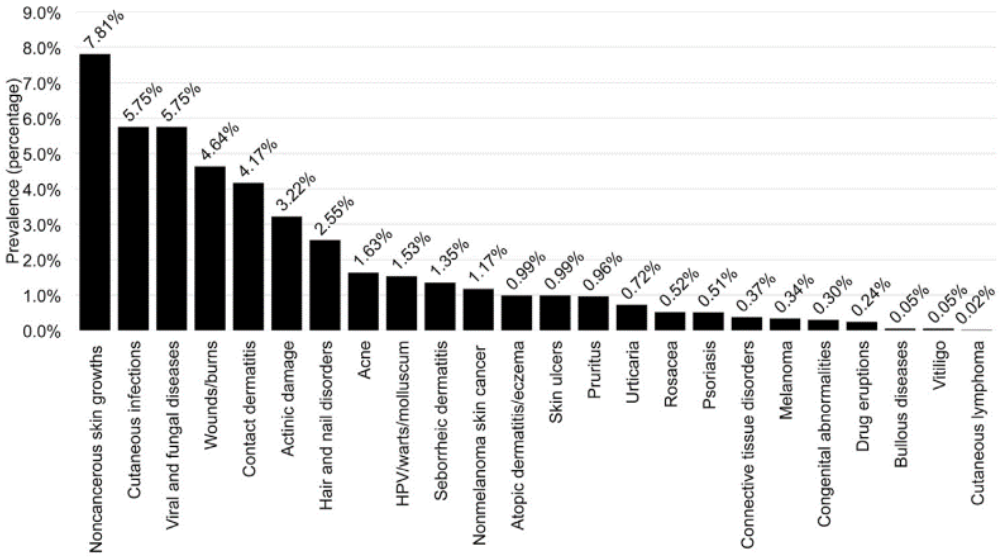

Figure 1.1. Prevalence of skin disease in 2013. The histogram shows the 24 skin disease categories sorted by claims-based prevalence for the United States population in 2013. Adapted from [1].

The majority of skin lesions are immune-related, occurring in individuals in which skin immunity is compromised, being the increased immune dysregulation considered as the leading cause of skin disorders[5]. Therefore, targeting the malfunctioning factors at the core of the immune system should be a priority in the management of these skin disorders.

New and more effective drugs and treatment options for skin diseases are being introduced in the market, albeit at higher costs than older treatments[1]. Current treatments in cancer and infectious

diseases target hazardous elements either by chemotherapy and checkpoint inhibitors[6] or by antibacterial therapy[7], respectively. Immunotherapy is also used to intensify the immune response in these pathologies[8]. Conversely, in skin inflammation, the detrimental effects are a result of immune upregulation, thus its suppression is the primary therapeutic goal. This can be attained by targeting the immune system as a whole, for instance, with glucocorticoids or non-steroid anti-inflammatory drugs (NSAIDs). Histamine, one of the primary mast cell mediators which is implicated in pathogenesis of inflammation, has been a therapeutic target for the past thirty years[9]. Many antagonists of histamine receptors, termed antihistamines, are continuously being developed for the purpose of abrogating allergic inflammation[5]. Additionally, antibodies against specific biomolecules such as tumor necrosis factor-alpha (TNF-α) or interleukin (IL)-12/23 and IL-17A are also being used in autoimmune diseases like psoriasis and arthritis rheumatoid, shutting down the exacerbated immune response through a strong immunosuppressant effect[10]. For chronic wounds, besides conventional therapies such as wound cleaning, debridement and coverage, other treatments exist. Engineered skin, skin grafts, and wound therapy devices are some examples of the more advance therapies available in the market[11]. Still, modulation of inflammation is a hallmark mechanism and several active ingredients are being developed, aiming to improve healing through a reduction in neutrophil infiltration and macrophage accumulation[12]. Nevertheless, current treatments in the field of inflammation are still unsatisfactory and newer avenues are being developed.

Regenerative medicine is focused on repairing damaged or malfunctioning tissue through both cellular and non-cellular therapies and this biological strategy is applicable to a wide spectrum of processes, including those governing skin diseases[13]. While it has long been accepted that direct cell-cell interactions and the replacement of injured tissues with injected cells exerts therapeutic effects, it is currently believed that the paracrine factors released from different cell types activate cytoprotective, immunomodulatory and regenerative processes[14]. In specific contexts, cells are now seen as bioreactors that produce and release soluble factors and extracellular vesicles (EVs) that might be used as therapeutic tools[13,15].

EVs are emerging as significant regulators of skin homeostasis and skin diseases, and some authors have already reported examples of how EVs participate in skin homeostasis, disease, and repair[16]. Interestingly, EVs from different cell sources have already been implicated in the regulation of cutaneous pigmentation, immune response and also wound healing[17–22].

The following sections provide a brief overview of essential concepts regarding skin structure and function, regulation of cutaneous immune system and its fragilities in pathologic conditions. Also, this chapter summarizes the basic concepts about EVs biogenesis, their biophysical and biochemical composition as well as different methods of purification and characterization. Finally, the EVs role as future therapeutics for skin disorders is discussed.

1.1. Skin in health and disease

1.1.1. Skin tissue architecture

The skin can be defined as a thin layer of tissue that forms the natural outer covering of the body, presenting critical functions such as physical protection and homeostasis[23]. This organ protects the organism against harmful environmental agents, such as abrasion and ultraviolet light, and it also keeps the body free of microorganisms. In addition, skin reduces water loss and thus prevents dehydration. The body temperature is regulated by the activity of sweat glands and by the amount of blood flow through the skin. In the skin, there are also nerve endings that are responsible for sensation[24]. Moreover, vitamin D, an important regulator of calcium homeostasis, is a product of the exposure of skin to ultraviolet light. Finally, this organ is also essential to the excretion of small amounts of waste products. Thus, any damage on the integrity of the skin may weaken the individual, leading to pathological conditions, such as loss of fluid, electrolyte imbalance and infections[23]. In general, the skin is capable of regeneration following a wound; however when the damage is too extensive, therapeutic intervention is required[23].

Structurally, the skin is composed of three layers: the hypodermis, the dermis and the epidermis[25] **(Figure 1.2)**. Beneath dermis and above the muscle, hypodermis, or subcutaneous tissue, is found, being composed mostly by adipocytes. This layer of loose connective tissue connects the skin to underlying muscle or bone[23]. Above hypodermis lies dermis; this layer is responsible for the structural strength and elasticity of skin through extracellular matrix (ECM). The dermis supports blood vessels and nerve endings of skin and it forms a basis for the epidermis to attach to. Epidermis is the outmost layer of skin. It is an epithelial tissue primarily constituted by keratinocytes and forms the body's first protective barrier against pathogens and dehydration. The dermis and the epidermis are the main layers of skin and they represent the most part of skin functions[26].

Dermis consists of connective tissue that houses fibroblasts, myofibroblasts, and immune cells such as macrophages, lymphocytes (αβ T cells, γδ T cells and B cells), natural killer (NK) cells, and mast cells[27]. Dermal fibroblasts are the most prevalent cell type in human dermis, responsible for structure maintenance and function of the dermis, having important roles in cutaneous wound healing. Dermal fibroblasts are responsible for the production and conservation of ECM, which is an essential component of skin[28]. The ECM present in dermis is composed of a network of multiple biomolecules which serves as scaffold to cells and other structures. ECM comprises two major biomolecule classes fibrous proteins and glycosaminoglycans, which are usually linked to protein forming proteoglycans[29]. The fibrous proteins can be structural proteins, such as collagen and elastin, or specialized proteins, which include fibronectin (Fn) or laminin. These last ones connect matrix elements one to another and to cells. Glycosaminoglycans, such as hyaluronic acid and proteoglycans, permit elasticity and lubrication. The ECM provides structural support to hair

follicles, nerve endings, glands and other structures. The dermis can be further divided in two distinct layers: the reticular layer and the papillary layer. The reticular layer is the deeper and the main layer of the dermis. This layer is composed of dense irregular connective tissue and is continuous with the subcutaneous tissue. The ECM in this layer of dermis forms a network of irregularly arranged fibers that are resistant to stretching. The papillary layer is loose connective tissue which has projections, that are extended towards to the epidermis. The ECM in papillary layer has thin fibers that are rather loosely organized. In its composition it is possible to detect blood vessels that supply the covering epidermis with nutrients and oxygen, remove waste products, and aid in regulating body temperature[30].

Epidermis is the superficial layer of the skin and it is divided into four typical cell layers: *stratum basale*, *stratum spinosum*, *stratum granulosum* and *stratum corneum*, from the deepest to the most superficial **(Figure 1.2).** Only in thick skin, there is still a fifth layer, found between the *stratum corneum* and *stratum granulosum*: the *stratum lucidum*[25]. The epidermis is composed of several types of cells, such as melanocytes, Langerhans cells (LCs), Merkel cells and keratinocytes. Melanocytes produce melanin that contributes to skin colour[31], while LCs contribute to immune protection[32]. Merkel cells are associated with nerve endings, which are responsible for detecting superficial pressure and light. Keratinocytes are the main cellular type of the epidermis. These cells, which are responsible for production of keratin, give the epidermis its ability to resist abrasion and reduce water loss. Additionally, keratinocytes participate in an important process of renewal of epidermis, named keratinization[33]. This process of continuous cytodifferentiation, begins in the deepest layer of the epidermis, where keratinocyte stem cells undergo mitosis and new keratinocytes are produced. During the process of keratinization, they migrate up from the basement membrane toward the *stratum corneum*. As they move from the deeper epidermal layers to the surface, keratinocytes differentiate, changing shape and accumulating keratin (KRT). Thus, these different stages are responsible for the five layers that constitute the epidermis. When these cells reach the *stratum corneum,* they eventually die and produce an outer layer of dead cells that resist abrasion forming a barrier. Then, they are either sloughed off or rubbed off by friction in a process called desquamation.

Appropriate functioning of the skin requires close communication and collaboration among a number of cell types, including stromal cells (keratinocytes, fibroblasts, endothelial cells, and adipocytes) as well as those derived from bone marrow (dendritic cells, macrophages, NK cells, mast cells, T cells, and others)[34].

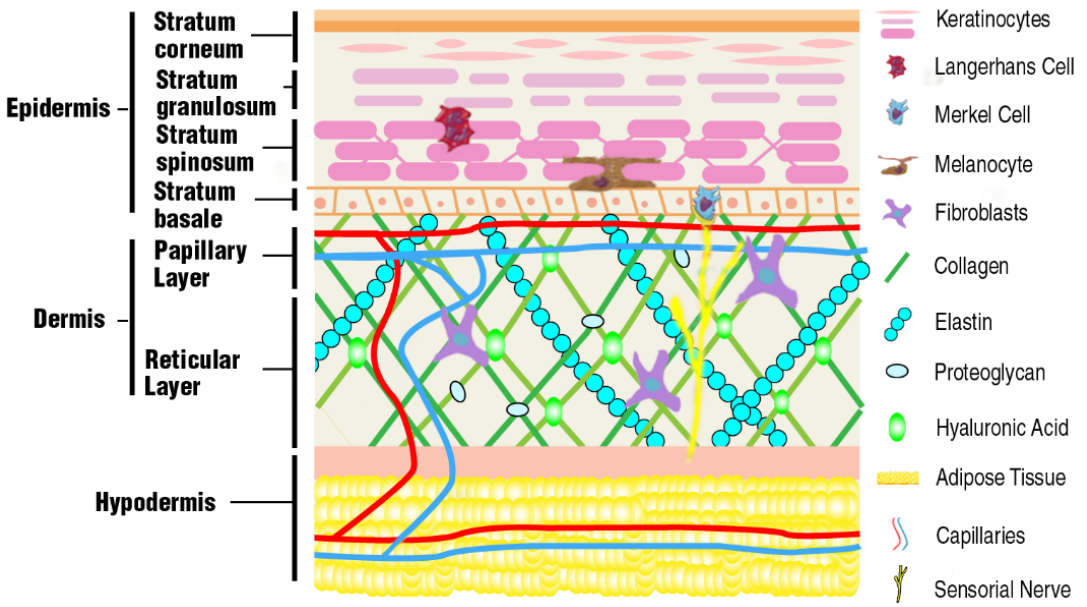

Figure 1.2. Schematic representation of the structure of the skin. The main layers of the skin are depicted - hypodermis, dermis and epidermis – as well as its main cellular and molecular constituents. The deepest layer of skin, hypodermis, is composed mainly by adipocytes and connects the skin to underlying muscle or bone. The dermis is responsible for the structural strength of skin, given support to cells and biological structures. The most superficial layer of skin, epidermis, have keratinocytes as principal constituent and forms a primary barrier of human body. Adapted from [23,35,36].

Murine models are commonly used in dermatological research[37,38]. These models are of great value and mimic many pathological aspects observed in human skin disorders. However, it is important to note that there are differences in the skin structure between mice and humans[23]. Murine epidermis is thinner than that of human', which depending on the area of the body, is between six and 32 layers[37]. The human epithelium, in contrast to murine skin, contains rete ridges, which are extensions that project into the underlying tissue[23,39]. In contrast to humans, the murine dermis lacks sweat glands, excluding the mammary glands in female mice. Furthermore, mice contain a dermal muscular layer, also known as the panniculus carnosus, which is absent in humans[37]. In addition, there are differences in the immune cell populations that colonize the epithelium in the epidermis and hair follicles **(Figure 1.3)**. In contrast to mice, humans have a larger proportion of interfollicular epidermis relative to hair follicle epithelium while γδ T cell receptor expressing dendritic epidermal T cells are abundant in mouse skin but are sparse in human skin. It is important to take these differences into account when interpreting the inflammatory skin phenotypes observed in mouse models in relation to the mechanisms that drive the pathogenesis of human inflammatory skin diseases[38]. The skin of other animals such as pigs more closely resembles that of humans[40], so these animals are increasingly employed in experimental settings. However, murine models are still widely used due to easy access, lower costs and ethical concerns and have proved effective for the study of inflammatory diseases of the skin[41–43].

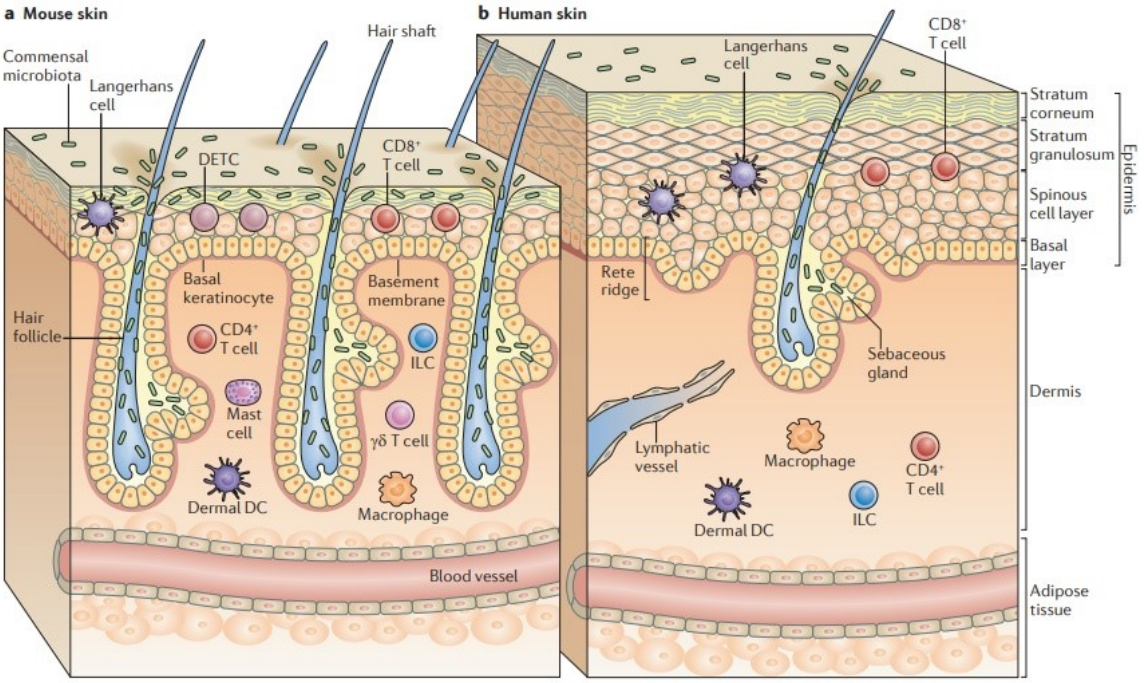

Figure 1.3. Comparative diagram between mouse (a) and human (b) skin. Mouse skin has densely packed hair follicles, whereas human skin has larger areas of interfollicular skin with sparse hair follicles. Human skin has a thicker epidermis (with more cell layers) and a thicker dermis than mouse skin and is characterized by downward projections of the epidermal rete ridges. The most prevalent immune cell types in human epidermis are Langerhans cells and CD8 T cells. In mouse epidermis, there is a prominent population of dendritic epidermal T cells, which are absent from human epidermis. Human and mouse dermis are populated by macrophages, mast cells, conventional αβ T cells and a small population of innate lymphoid cells. In mouse skin, there is an important contribution from recruited γδ T cells to skin immune surveillance and IL-17 production. Adapted from [44].

1.1.2. Cutaneous immune system

A wide array of mechanisms and responses spread across the epidermal and dermal layers compose the cutaneous immune system[24]. Skin-resident immune cells maintain tissue function in homeostasis and play as sentinels by actively patrolling the microenvironment looking for antigens. Some of these immune cells migrate to lymph nodes (LNs) to either induce peripheral tolerance to tissue self-antigens or start intense immune responses. In the event of a challenge, such as infections or tissue injury, immune cells resident in the skin and those infiltrating from the periphery interact to create a well-orchestrated defence network to minimize the insult and restore the tissue to its original state[27].

The maintenance of immune homeostasis in the skin relies on a finely tuned equilibrium of well-regulated interactions between different cellular and microbial components and, the dysregulation of this equilibrium contributes to the pathogenesis of inflammatory skin diseases such as psoriasis[38].

A proper immune response is usually initiated by dendritic cells (DCs). These cells regularly take up proteins within the skin and further distinguish whether they are presented in a dangerous context like infection or malignancy, or a safe context like normal cell turnover during tissue homeostasis. DCs recognize non-self-molecular patterns or pathogen-associated molecular patterns (PAMPs), through receptors called pattern-recognition receptors (PRRs) that alert immune cells to danger. PRRs are located both on surface and in the intracellular space allowing the recognition of pathogens in that regions[34]. Activation of these receptors leads to antigen processing and presentation, up-regulation of costimulatory receptors for T-cell activation, and secretion of proinflammatory cytokines such as IL-6, IL-1β, TNF-α, therefore, initiating a proinflammatory response[24] **(Figure 1.4)**. Upon secretion of proinflammatory cytokines that promote the recruitment of innate effector cells, including neutrophils, monocytes, and NK cells, these cells initiate their tasks by secreting more cytokines and chemokines and phagocytosing debris and apoptotic cells. This first response characterizes the innate immune response. Nevertheless, an effective immune response usually requires the subsequent involvement of the adaptive immune system[44].

Adaptive immune populations form slower pathogen-specific responses to infection through unique antigen-specific receptors. Thus, DCs must interact with T cells to identify the cells with the capacity to recognize the specific invading pathogens. To optimize this process, DC migrate to LNs and efficiently survey millions of potential responders finding those that can participate in any particular response. Following the successful activation of an antigen-specific T cell, that cell will proliferate, exit the LN into the bloodstream and migrate to the skin. This homing process is mediated by cytokines and adhesion molecules at the site of inflammation which guide those cells to the correct site[45] **(Figure 1.4)**. Already on the affected site, T cells are polarized towards a specific subset with specialized functions. These cells can be cytotoxic, have suppressive responses, and can oversee and help to shape the response through the secretion of cytokines. However, mixed responses may also occur, creating a significant level of complexity that has yet to be fully understood for all such responses *in vivo*.

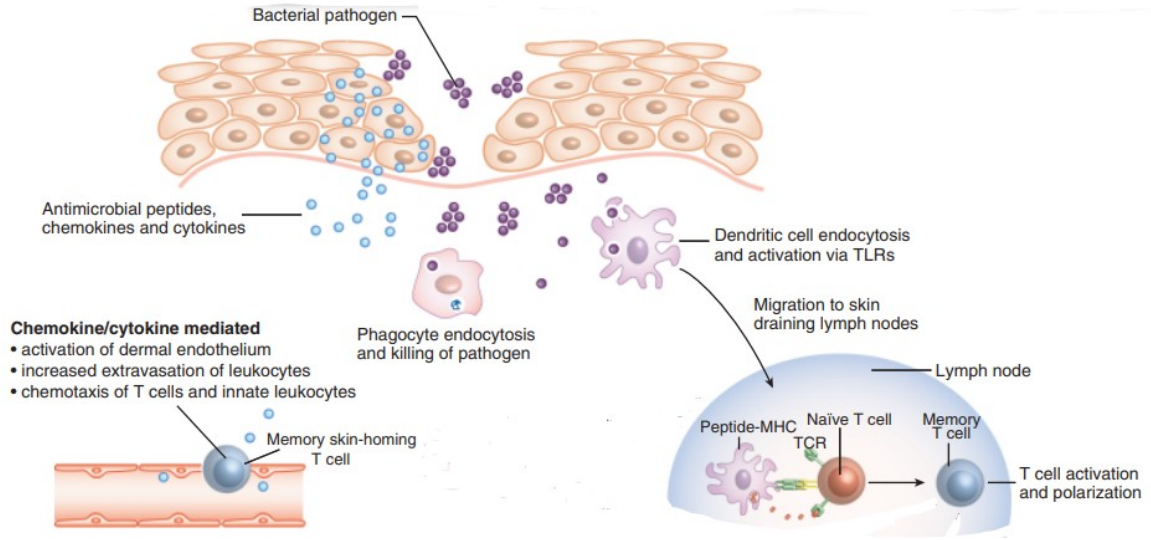

Figure 1.4. Cutaneous immune response. In response to an insult that breaches the epithelial barrier, keratinocytes synthesize anti-microbial peptides, chemokines, and cytokines. These factors lead to activation of DCs, inducing the migration of innate leukocytes and memory T cells into the skin via chemotactic gradients. Bacterial antigens and PAMPs activate innate phagocytes (neutrophils and macrophages) to kill ingested organisms and activate DCs to migrate to the skin-homing LN. In the LN, DCs present bacterial antigens to naïve and central memory T cells, leading to stimulation of pathogen-specific cells. Effector CD8 cells exit the lymph node, home to inflamed skin and kill pathogens. Adapted from [46].

1.1.3. Skin resident immune cells

Both myeloid and lymphoid cell subsets are found in the skin in steady state[24]. Each of these subsets play an important role on a complex network to resolve the insult and to restore the tissue to its original state **(Figure 1.5)**.

1.1.3.1. Myeloid Cells

Skin-resident myeloid cells include LCs, dermal dendritic cells, macrophages and granulocytes, and the latter include neutrophils, eosinophils, basophils, and mast cells. These innate immune cell populations can be recruited to the skin following activation of a tissue-resident cell and subsequent release of chemokines and activation of the endothelium **(Figure 1.5)**. Neutrophils are rarely present in healthy skin and thus are not considered as skin-resident cells. However, in inflammatory conditions and after a wound, neutrophils populate the skin[34].

Skin-resident myeloid cells promote skin homeostasis by secreting growth factors essential for the survival of keratinocytes, fibroblasts, and endothelial cells. In addition, they sustain optimal tissue function by phagocytosing debris and apoptotic cells, supporting vasculature integrity, and promoting tolerance[27]. In inflammatory conditions, myeloid cells respond immediately and produce

pro-inflammatory mediators that drive the activation of cells in the local vicinity and infiltration of peripheral immune cells into the affected site. Skin myeloid cells also serve as a link between the innate and adaptive immune system[34].

In the skin, mast cells are specialized for first-line surveillance functions owing to the presence of a plethora of preformed pro-inflammatory mediators that are stored within their cytoplasmic granules and can be rapidly released upon contact with antigens[34,38]. Mast cells granules are particularly enriched in histamine and so they are traditionally known as typical allergy cells. This reaction is initiated when their Fcε receptors are crosslinked via immunoglobin (Ig) E-antigen complexes[47,48]. Nevertheless, recent studies prove their remarkable internal and external plasticity and critical role in vital processes such as wound healing, skin inflammation, angiogenesis, immune tolerance, and cancer[49,50]. Intriguingly, the skin's microbiome regulates the population of mast cells in that organ. The intradermal injection of staphylococcal-derived lipoteichoic acid in germ-free mice, that contain fewer mature mast cells in the dermis, induced the expression of stem cell factor in keratinocytes, ultimately resulting in the rescue of the dermal mast cell population[51].

Dermal DCs are resident cells in dermis that are able to migrate to the LNs. These cells are efficient at priming adaptative immune responses due to their antigen-presenting capacities[27]. Recently, Tordessillas *et al*. showed that these cells can also induce tolerance to topically applied antigens encountered in the hair follicles[27,52]. Moreover, dermal DCs maintain homeostatic interactions between the host and skin-resident commensal bacteria.

Plasmacytoid DCs are a subset, found in the skin exclusively under inflammatory conditions. These cells are massive producers of interferon (IFN)-α, which is essential for viral defense[53]. Besides their preponderant antiviral activity, plasmacytoid DCs also play a role in autoimmune skin disorders such as psoriasis[54] and fibrosis[55].

LCs are another DC subset that spend the majority of their time in the epidermis, forming a dense network with keratinocytes[34]. This network potentiates the sensing of potential invaders through LCs dendritic process. LCs promote tolerance to environmental antigens, including commensal bacteria and fungi, and help to polarize T cells into a particular inflammatory response[56].

Interestingly, the subpopulation of DC that initiates the immune response and the signals present during the initiation can influence the nature of that response. For instance, in a LC-deficient mouse exposed to an allergenic substance, the immune response was exacerbated supporting LCs immunotolerant role in skin. On the other hand, plasmacytoid DC-deficient mice did not trigger an immune response, suggesting this DC population is proinflammatory in this context[57].

Macrophages are skin-resident immune cells with high phagocytic capacity and motility[53]. Although they are less likely than dendritic cells to present antigen to T cells, due to relative cell numbers, they are capable of activating immune responses through PRRs and cytokine secretion[34]. Resident skin macrophages engulf and eliminate debris from dead or dying cells, invading pathogens, allergens or environmental insults, preventing the trigger of an inflammatory response[58].

In turn, blood circulating monocytes migrate towards sites of inflammation in the skin where they differentiate into mature macrophages[53].

Macrophages are located in the dermis and hypodermis and, in case of an insult, secrete chemokines that drive the recruitment of neutrophils, setting the beginning of the inflammatory phase necessary for healing[59]. Interestingly, although macrophage ablation in a transgenic mice impaired skin healing, the absence of these cells did not affect the accumulation of neutrophils, indicating that dermal macrophages are not indispensable for neutrophil infiltration[60]. Besides, macrophages have also been implicated in skin sodium salt balance and homeostatic hair regeneration[61].

Macrophages are plastic cells and so, it is possible to categorize them according to their effector functions. Macrophages are designated as "M1" or classically activated macrophages when they present a pro-inflammatory phenotype whilst macrophages with anti-inflammatory/pro-repair functions are denominated "M2" or alternatively activated macrophages[62,63]. Of note, bona fide M1 and M2 macrophages are generated only *in vitro* once *in vivo* macrophages may simultaneously express M1 and M2 markers[27]. Although some controversy exist in the field about M1/M2 denomination namely due to the an oversimplification of the complex biological system[64], we will use this nomenclature to describe and categorize the functions of macrophages as pro-inflammatory (M1) or anti-inflammatory (M2).

M1 macrophages express inducible nitric oxide synthase (iNOS) and at the cell surface, they are identified by CD80 or CD86[65]. Also, they secrete inflammatory cytokines such as TNFα, IL-1β, and IL-6 and chemokines to recruit additional leukocytes to the injured site[27]. This recruitment leads to the induction of inflammatory cytokine production by T cells which in turn acts on the macrophage enhancing cytokine secretion, antigen-presentation and bactericidal activity. Such cytokine activity is critical for establishment of effective host defense against intracellular pathogens[27,58]. Although these cells contribute to the pathogenicity of inflammatory diseases, displaying enhanced production of inflammatory cytokines IL-12 and IL-23, for instance, in psoriasis[66], they have a preponderant role in skin wound healing by shortening the inflammatory phase[67].

In turn, M2 macrophages, adopt an anti-inflammatory and/or pro-repair phenotype, expressing cell surface CD163 and CD206[65]. They have potent anti-inflammatory effects due to their production of IL-10 and transforming growth factor beta (TGF-β) and lack of IL-12 production, failing the generation of toxic intermediates that compromise their antimicrobial activity[58]. M2 macrophages have suppressive effect on T-cell proliferation and inflammatory responses[58,65,68]. Additionally, anti-inflammatory phenotype macrophages have been described to have a potential role on angiogenesis and ECM deposition[27].

The M1 to M2 polarization, or switch, reflects the macrophage differentiation process that shifts cells from inflammation to proliferation functions[63,69]. This polarization is a vital step in wound

healing and is brought about by IL-4, IL-10, glucocorticoids, prostaglandins, and modulators of glucose and lipid metabolism[70] **(Figure 1.5)**.

Although they are not skin-resident cells, neutrophils are typically the first cell type recruited to the skin following activation of DCs and/or macrophages in response to PAMPs encountered during infection. Neutrophils follow platelets as principal effector cells in the initiation of the inflammatory phase at sites of acute inflammation or infection[71]. When neutrophils migrate into skin, they are capable of efficiently phagocytosing and killing pathogens[72]. While neutrophils play a role in re-establishing tissue homeostasis, excessive neutrophil activity contributes to the development of nonhealing wounds[73].

Neutrophils have also recently been shown to produce extracellular traps (NETs) by expelling the DNA from their nucleus, effectively trapping pathogens like flies caught in a spider web[24]. Moreover, neutrophils engage in cellular crosstalk via cell-cell contact where numerous cytokines, chemokines, and angiogenic factors activate resident hematopoietic cells, macrophages, dendritic cells, B cells, T cells, and natural killer cells modulating the innate and adaptive immune responses[74].

1.1.3.2. Lymphoid Immune Cells

The skin is composed of different types of lymphoid cells namely T and B lymphocytes, all of which are important in both steady state and inflammatory responses[24]. Of note, skin is a reservoir of approximately 20 billion T cells, nearly twice the number present in the entire blood volume[24,75]. Both human and murine skin contain γδ T lymphocytes and αβ T lymphocytes, along with natural killer T cells[38]. γδ T cells are the dominant T cell population in murine skin, while αβ T cells are the dominant T cell population in human skin[45].

Initially, the perception of skin immunosurveillance was based on T cells that migrate between skin draining LNs and peripheral tissues. However, the resident rather than recruited T cells creates skin immune homeostasis[27].

αβ T lymphocytes are found in the epidermis and dermis[76] and traffic to the skin from the periphery with the assistance of endothelial cells that express E-selectin to interact with cutaneous lymphocyte antigen[27]. These cells are the resident memory T cells (T_{RM}), which are long-lived and distinct from their circulating counterparts[27]. Epidermal T_{RM} express predominantly CD8 and the activation marker CD69[76]. Due to their strategic position, T_{RM} exert sentinel-like functions by promoting recruitment of other memory T cells from the periphery to sites of infection[27,58].

$CD4^+$ T_{RM} cells also make up a significant portion of the skin-resident lymphocyte population and are found in both the epidermis and dermis[45]. Although the function of CD4 T cells in the skin is not studied to the same extent as CD8 T_{RM}, CD4 T_{RM} cells may have important roles in protective immunity by secreting cytokines in response to infection, tissue damage and tumors[77].

CD4 memory skin T cells or CD4 skin infiltrating cells are subdivided in specific subsets[58]. T helper (T_H) subsets are usually designated with a number to delineate which types of cytokines they produce which is also intrinsically connected with their function. These subsets are differentiated by antigen-presenting cells such as DCs and LCs and are determined by the type of antigen, inflammatory cues and cytokine signals in the local microenvironment[53] **(Figure 1.5)**. T_H1 cells primarily produce IFN-γ, TNF-α and IL-12 in response to intracellular pathogens that disrupt the skin barrier while T_H2 cells fight extracellular pathogens and are involved in atopic diseases by secreting IL-4, IL-13, IL-24, IL-25, and IL-3[45]. T_H17 cells are essential for first-line defense against various fungal and bacterial infections, producing IL-17, IL-21, and IL-22[58]. These different cytokine patterns are usually associated with recruitment of slightly different types of immune effector populations. For example, T_H2 responses recruit basophils, eosinophils, and mast cells to coordinate an antiparasitic response, whereas T_H1 responses result in recruitment of circulant cytotoxic lymphocytes for an antiviral or antitumor response, and T_H17 promotes an antibacterial or antifungal response through the recruitment of neutrophils and production of cytokines and antimicrobial peptides[34,38]. T_H1 and T_H17 responses may also promote autoimmunity, whereas T_H2 responses may mediate allergy[58]. Albeit not as commonly, T_H2 may also promote autoimmunity.

Another important CD4 T_{RM} subset are T-regulatory cells (T_{reg}), comprising 5–10% of the T cells resident in normal human skin[78]. These cells typically express FoxP3, a critical transcription factor for their development and CD25, a high-affinity IL-2 receptor[79]. Their role is to suppress immune responses as a major contributor to peripheral tolerance, helping to prevent autoimmunity and to resolve inflammation once a threat has been controlled[79]. Of note, there are different T_{reg} subsets according to their generation site: whereas central T_{reg} develop in the thymus, peripheral T_{reg} are generated during immune responses in lymphoid organs and/or tissues, where asymmetric division of effector cells allows for generation of a small population of T_{reg}[34].

Other dermis skin resident cells are NK T cells, classified by their expression of both NK cell receptors and the universal T-cell marker CD3[24], providing immunoregulation and control over αβ T-cell-mediated.

Unlike naïve αβ T lymphocytes, skin γδ T cells reside in the epidermis in a pre-activated state[27]. In contrast to αβ T cells, γδ T cells are able to inhibit skin tumor responses and to regulate epithelial homeostasis and contact hypersensitivity[24,45]. Recently, IL-23 responsive skin γδ T cells have been described as the major IL-17 producers, a pivotal cytokine in psoriasis progression and skin inflammation[24,80]. Moreover, skin γδ T cells act as primary responders to damage and wound repair due to their ability to produce growth factors participating in wound repairing [24]. As they are also able to produce antimicrobial peptides, skin γδ T cells together with NK T cells participate in antimicrobial defense. Activated NKT cells can maintain high levels of TNF-α and increase DCs migration from the skin to draining LNs in a mouse model of hypersensitivity[45]. Both populations respond to lipid antigens[24].

B cells are sparse in the homeostatic skin and thus, it is unclear whether they are indeed skin resident cells and how they are characterized[27]. However, during skin inflammatory diseases, B cells are found in the dermis and their role is well studied. In humans, B cells are found in elevated levels in cutaneous diseases such as atopic eczema, cutaneous leishmaniasis, and cutaneous sclerosis where they are responsible for the high production of immunoglobulins such as IgM, IgE and IgG[27,81]. Upon activation, B cells are converted into plasma cells responsible for the production of antibodies that are passively delivered to the skin through the circulation. Although activated B cells may also be recruited to the skin during inflammation, they more often remain within the LNs or bone marrow[34].

1.1.3.3. Non-immune cells

Although keratinocytes are not an integral part of the immune system they have an unexpected role in both innate and adaptive immunity[24,82]. Beyond physiological barrier, reaction to temperature changes and protection against ultraviolet radiation[23], modulation of the immune system and the skin immune status strongly depends on functional keratinocytes that, similarly to neutrophils, produce antimicrobial peptides and other small molecules responsible for the first skin defense against an insult[24]. However, atypical production of these bioproducts could lead to the development of inflammatory skin diseases and susceptibility to microbial infections[24]. For instance, in atopic dermatitis, defective function or decrease of some antimicrobial peptides (AMPs) such as cathelicidin and β-defensins is described[83] whereas high expression of AMPs is observed in psoriatic lesions[84]. Expression of AMPs can be upregulated by some pro-inflammatory cytokines such as interleukin IL-17 and IL-22[24].

Keratinocytes release primary inflammation-associated cytokines such as IL-1β and TNF-α, enhancing the immune response[85]. The production of these classical pro-inflammatory cytokines promotes T_H1 responses, aiding the perpetuation of the immune response since local skin cells are sensitive to immune cell-products like IFN-γ[58]. Skin fibroblasts and melanocytes have similar abilities, secreting IL-6, TNF-α and keratinocyte growth factor (KGF) that further facilitate an immune response initiated by keratinocytes[85]. Moreover, plasticity of keratinocytes in production of chemokines and chemokine receptors empowers them to communicate and cooperate with other cell types during immune response in particular with T cells activating them or inducing antigen-specific tolerization[82]. Therefore, malfunction of keratinocytes can lead to pathological conditions such as autoimmunity and cancer[58].

Similarly to keratinocytes, dermal fibroblasts not only act as sentinels by producing inflammatory mediators (cytokines, chemokines, and growth factors) but also act in response to infections driven by several microorganisms[86]. Fibroblasts have been shown to express a variety of PPRs, including Toll-like receptors (TLRs)[87], and the subsequent ligand activation of those receptors can directly

activate fibroblasts and promote their differentiation into collagen-producing myofibroblasts[88]. Additionally, when challenged with microorganisms such as *Staphylococcus. aureus*, skin fibroblasts can synthesize proinflammatory cytokines such as IFN-γ, IL-6, and IL-8[86]. Fibroblasts are also capable of synthesizing growth factors including vascular endothelial growth factor (VEGF-A),known to promote inflammatory response-induced neovascularization, allowing recruitment of monocytes/macrophages[89].

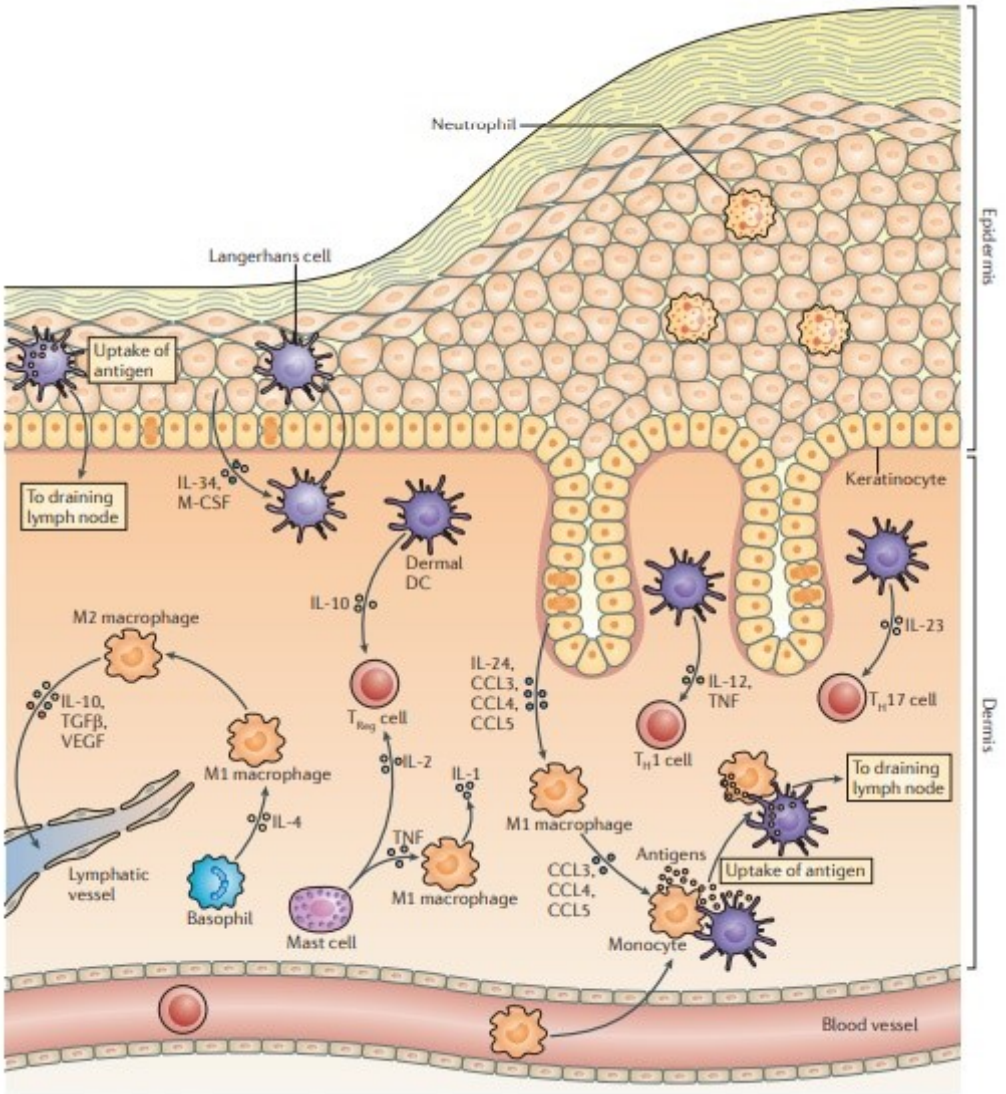

Figure 1.5. Skin resident immune cells. The skin is populated by resident and trafficking myeloid and lymphoid cells. LCs migrate to the epidermis in response to a gradient of molecules produced by epidermal keratinocytes. Monocytes migrate from the blood and patrol through the dermis. DCs and monocytes can take up antigen and transport it to lymph nodes. Basophils, mast cells and dermal DCs establish a balance of pro-inflammatory and anti-inflammatory mechanisms by producing cytokines that facilitate or dampen inflammatory responses, respectively. IL-4 stimulates the differentiation of M1 macrophages into M2 macrophages that produce anti-inflammatory cytokines such as IL-10, TGF-β and VEGF, which facilitates the growth of lymphatic vessels for rapid antigen elimination. Mast cells and dermal DCs produce IL-2 and IL- 10, respectively, which facilitates the generation of T_{reg} cells. Conversely, mast cells can release TNF that stimulates pro-inflammatory IL-1 production by M1 macrophages. Dermal DCs present antigen to T cells and enable T cell polarization towards T_H1 or T_H17 phenotypes under the influence of cytokines such as IL-12, TNF and IL- 23. Adapted from [44].

1.1.4. Skin inflammatory mechanisms

Inflammation is a complex biological response of the immune system that can be triggered by a variety of factors, including pathogens, damaged cells, and toxic compounds. The inflammatory response is an essential mechanism of the innate immune response[90] and is coordinated by activation of signaling pathways that regulate inflammatory mediator levels in skin resident tissue cells and inflammatory cells recruited from the blood[91].

Proper inflammatory responses provide a broad protection against infections and orchestrate long-term adaptive immunity toward specific pathogens[90]. In contrast, chronic and uncontrolled inflammation are a common major pathogenicity in several skin disorders[38,92] . In this way, different regulatory mechanisms have been developed to adjust the initiation, progression, and resolution of inflammation.

As a consequence of injury, resident skin cells are exposed to danger signals which are recognized by PRRs among which TLRs are the best characterized ones[93]. TLRs are constitutively expressed on host cells and stimulation of TLRs induces the activation of intracellular signaling pathways, including the nuclear factor kappa-light-chain-enhancer (NF-κB) of activated B cells and mitogen-activated protein kinases (MAPK) pathways[91]. This interaction leads to the expression of a large number of genes, including cytokines, chemokines and antimicrobial peptides, to initiate and perpetuate the inflammatory response[91].

The inflammatory phase starts with the recruitment of neutrophils that rapidly migrate into the injured skin[70,92]. The rapidity of this response and the resulting microbicidal activity is essential to kill bacteria and prevent the establishment of biofilms and other stable microbial communities[92]. Invading pathogens are controlled by neutrophil secretion of several antimicrobial substances such as reactive oxygen species (ROS), AMPs and antimicrobial proteases and also by the release of NETs[73]. During their spontaneous apoptosis, neutrophils secrete cytokines and growth factors that act as chemoattractants to inflammatory cells namely monocytes. Further, neutrophils can even amplify the inflammatory immune response by secreting potent chemoattractants such as IL-8 and leukotriene B4, which recruit other neutrophils to the injury site[27,94].

Monocyte-derived and skin resident macrophages have been widely studied in the context of wound healing, and are often considered to be the most important immune cell type in this process contributing to a proper healing[61,95].Upon initial infiltration, proinflammatory macrophages remove cellular debris, damaged matrix, microbes, and neutrophils[70]. They also secrete proinflammatory cytokines and growth factors (including IL-1, fibroblast growth factor (FGF)]-2, platelet derived growth factor (PDGF), and VEGF), which mobilize more immune cells, and promote the proliferation of keratinocytes, fibroblasts, and epithelial cells[96]. During the progress of inflammatory phase, cues derived from the surrounding environment trigger macrophages to transition into a functionally and phenotypically anti-inflammatory state. One of these cues is the

engulfment of apoptotic neutrophils by human phagocytes[94]. This phenomenon promotes anti-inflammatory signaling, prevents neutrophil lysis, and inhibit the immune responses. Macrophage phenotypic transition towards an anti-inflammatory phenotype marks the resolution of inflammatory phase, and it is a hallmark for a successful healing[97]. At this point, M2 macrophages secrete anti-inflammatory cytokines, such as TGF-β1, which promotes ECM synthesis and wound contraction[73]. In the final stage of wound healing, anti-inflammatory macrophages stimulate ECM reorganization and debris phagocytosis[98]. Moreover, anti-inflammatory macrophages play an indirect role in angiogenesis by degrading the ECM to create tunnels that guide endothelial proliferation and migration and by releasing angiogenic factors, such as VEGF, FGF and placental growth factor (PlGF)[27,70].

T cells are also critical in tissue remodeling and the resolution of inflammation[27,70]. Macrophages and neutrophils are the mediator cells in the recruitment of these adaptative immunes cells. T cells are attracted to wound site by macrophages that secrete IFN-γ during the inflammatory phase[34] which polarizes CD4 T cells into T_H1, contributing to the initial proinflammatory wound microenvironment[73]. In addition, human cutaneous T_H type 22 cells produce IL-22, IL-17, and other cytokines that further stimulate keratinocyte production of antimicrobial peptides and proteins and directly induce keratinocyte proliferation, collagen and fibronectin production[76].

Tissue resident γδT cells also play a role in regulating skin wound healing. These cells are able to support and regulate keratinocyte proliferation and differentiation via secretion of various growth factors, such as FGF-7, FGF-10, and insulin-like growth factor (IGF)-1[73,99]. Additionally, T_{reg} are also described as fundamental in wound closure and resolution of inflammation[79]. This T cell subset secretes arginase and anti-inflammatory cytokines, including IL-10 and TGF-β1, which encourages anti-inflammatory macrophage polarization and suppress the inflammatory response. A recent study, using Foxp3 transgenic mice where T_{reg} were depleted, showed that wound healing is slower in T_{reg} depleted mice compared with wild-type controls[100].A similar study demonstrated that depletion of T_{reg} in mice resulted in a decrease in the numbers of mature endothelial cells associated with myofibroblasts after excision injury, highlighting T_{reg} role in maturation of new blood vessels[101]. Contrastingly, NK T cells have an inhibitory role on wound healing in mouse. Two studies have shown that depleting NK T cells increases wound closure rate[102,103].

1.1.5. Skin pathologies: Improper immune response

The effectiveness of the skin immune system strongly depends on the close interplay and communication between immune cells and the skin environment. Under normal circumstances, when skin recovers from an acute challenge or injury, cutaneous immune responses are self-limiting, and the skin returns to a quiescent state. However, during pathological events, whether chronic disease, an acute response to skin challenge, or a wound, there is an aberrant and inappropriate activation and perpetuation of pro-inflammatory signals which become harmful[91]. The critical contribution of immune system dysregulation and pro-inflammatory cytokines to chronic skin disease is evidenced by the efficacy of drugs, both topical and systemic, that target either immune cells directly, or their secreted molecules[34].

1.1.5.1. Chronic inflammation

The immune response is central during the entirety of the healing process[34]. In physiological conditions, when the skin barrier is breached, acute wound healing follows a well-coordinated series of processes, comprising homeostasis, inflammation, proliferation, and remodeling phases. The acute inflammatory response tends to resolve the skin insult, but persistent inflammatory stimuli or dysregulation of inflammatory mechanisms usually leads to chronic inflammation. This chronicity contributes to a variety of chronic inflammatory diseases with skin manifestation, namely atopic dermatitis and psoriasis[91,104]. Additionally, persistent inflammation is the hallmark of chronic wounds that are arrested in this phase without the ability to adequately pass the needed cues for wound closure[72].

Chronic inflammatory microenvironment is associated with the release of various pro-inflammatory and oncogenic mediators such as nitric oxide (NO), cytokines (IL-1β, IL-2, IL-6), and TNF-α, growth factors, and chemokines by innate immune cells[105]. In turn, several molecular signaling cascades such as NF-κB, MAPK, nuclear factor erythroid 2-related factor 2, phosphoinositide-3-kinase, Janus kinases/STAT, Wnt/B-catenin, and cyclic AMP response element binding protein are induced by these pro-inflammatory mediators[67].

Excess of neutrophils at the injured site is a critical factor to perpetuate chronic inflammation[67], leading to over-production of ROS, causing direct damage to ECM, cell membrane and subsequently, premature cell senescence. In addition, neutrophils release proteases such as elastase and matrix metalloproteinases (MMPs) specifically the neutrophil collagenase (MMP-8) which degrade important growth factors such as PDGF and TGF-β and inactivates components of the ECM[73]. Adding to this fact, neutrophil apoptosis is also dysregulated. In a chronic wound mouse model, neutrophil apoptosis was diminished although their number in comparison with the control was higher. Also, decreased neutrophil apoptosis was correlated with impaired clearance by

macrophages and prolonged production of proinflammatory TNF-α, that sustained the proinflammatory state[106].

Macrophages are often defined as master regulators of inflammation[107] and, in normal conditions, they are able to efficiently remove neutrophils and debris from the damage site. However, in chronic inflammatory conditions, these cells no longer maintain the same capacity further increasing the abundance of proinflammatory cells[108]. Beyond phagocytizing neutrophils and other apoptotic cells and debris, macrophages phenotypic conversion is crucial for inflammation resolution[67]. Using iron to modulate macrophages phenotypic switch, wound healing process was impaired[109]. The authors verified an uncontrolled inflammatory environment sustained by macrophages that induced fibroblast senescence. The lack of conversion phenotype also leads to decrease growth factor production, which hinders the transition to proliferative phase[107]. As described previously, M1 macrophages secrete preferentially proinflammatory mediators, such as TNF-α, IL-17 and IL-1β, ROS and iNOS, which have negative effects on the wound microenvironment at high concentrations. In this point of view, promoting macrophage phenotype transition is crucial for chronic inflammation resolution.

Although M2 macrophages can promote the resolution of inflammation, the accumulation of these cells could lead to undesirable effects. In fact, if M2-like macrophages remain for too long in the wound site, there may be excessive collagen formation, resulting in scarring[108].

In human skin, T lymphocytes are also crucial to the establishment of pathogenicity of chronic inflammatory skin diseases. In chronic wounds, beside the reduced number of T cells, they are also in an unresponsive and functionally impaired state[73]. In fact, although both αβ and γδ T cells are capable of producing IGF-1 and IL-2 in physiological state, γδ and αβ T cells isolated from human chronic wounds fail to secrete these cytokines impairing keratinocyte proliferation[99]. Notwithstanding, depletion of T lymphocytes in a mouse model did not impair wound healing[73].

In psoriatic biopsies, although the causes are unclear, the number of dermal T cells are increased from about 1 to 15% when compared with normal skin. This increase in lymphocytes allied with concomitantly augment in macrophages and DCs intensify the inflammatory microenvironment. Special emphasis has been done for γδ T cells that produce more IL-17 when stimulated with IL-23. These cytokines lead to the recruitment of more lymphocytes, neutrophils, and myeloid cells creating a positive feedback loop that maintains cutaneous inflammation and causes epidermal hyperplasia[45,80].

Interestingly, independent of their role in immune suppression, T_{reg} have an important role on resolution of inflammation, more specifically on wound healing. Specific deletion of these cells early during the wound-healing process attenuates wound closure and re-epithelialization[100]. T_{reg} absence resulted in IFN-γ dependent accumulation of M1 macrophages.

1.1.5.2. Autoimmunity

Autoimmunity occurs when the immune system targets self-cells and tissues, resulting in destruction, and, potentially, organ failure[34]. Normally, it results from an imbalance between effector T cells and functional T_{reg} cells[110]. Although there are checkpoints to prevent the immune system from targeting self-tissues, in autoimmune disease, these mechanisms are bypassed. In physiological conditions, the immune system is regulated through maintenance of central tolerance by deletion of autoreactive T and B cells in the thymus, peripheral tolerance through the action of T_{reg}, production of anti-inflammatory cytokines, such as IL-10 and TGF-β, and down-modulation of proinflammatory cytokine production[34].

Skin DCs and T_{reg} cells play a critical role in coordinating extrinsic mechanisms of peripheral tolerance. In mice, DCs are able to mediate T cell tolerance by presenting exogenous self-antigens in the steady state to induce unresponsiveness of self-reactive CD8 T cells. In humans, the majority of circulatory T_{reg} express skin-homing receptors comprising up to 10% of the resident T cells in normal skin[34]. Accordingly, lack of skin-homing molecules CD103, CCR4, and P- and E-selectin ligands severely affects the migration and/or retention of T_{reg} cells within the skin and results in impaired pathogen clearance and skin-specific autoimmunity[34,79].

On the other hand, in autoimmunity, there is a progressive increase of the effector to regulatory cells ratio that is mainly driven by an accumulation of effector T cells in the tissues. Interestingly, this may be accompanied by a relative decline in T_{reg} number, or increased numbers of dysfunctional T_{reg}[110]. Currently, therapies for autoimmune diseases are mainly focused on resolution of inflammation which is a consequence of a decrease and defective role of T_{reg} that fail in resolving this phase. Therefore, the future development of therapeutic strategies to autoimmune diseases may attempt to reset the effector T cell/T_{reg} balance.

Low-dose IL-2 therapy is under development aiming to preferentially augment T_{reg} numbers and/or function. This therapy has shown clinical benefits in patients with chronic graft-versus-host disease (GVHD), autoimmune vasculitis, and alopecia areata[111,112]. In addition, adoptive transfer of large numbers of *ex vivo* expanded T_{reg} has been shown to be efficacious in preventing acute GVHD and is currently being explored for the treatment of autoimmune diseases[113].

Autoimmunity can also be a result of an excess in autoantibodies production or a defective function in B cells population[34]. For instance, autoimmune bullous diseases are characterized by the presence of autoantibodies that are reactive to structural proteins of the epidermis. In pemphigus vulgaris, desmoglein-3 autoantibodies lead to the formation of blisters in the skin[27]. Besides, depletion of B cells in an imiquimod-induced murine psoriasis model increased the severity of symptoms when compared to their controls. These findings suggest that B cells play a therapeutic role in relieving the disorder and can be a suitable target for therapeutic solutions[114].

1.1.5.2.1. Psoriasis

Psoriasis is a highly chronic inflammatory disease of the skin with a strong genetic predisposition and autoimmune pathogenic traits. It afflicts 2-3% of the world population but varies according to regions. Lower prevalence in Asian and some African populations are observed whereas up to 11% of Caucasian and Scandinavian populations manifest this disease[115].

In skin, classical clinical manifestations are pruritus, pain, erythema, occasional pustules, and thickened scales. Histologically, it is characterized by epidermal acanthosis, vascular proliferation, and a significant inflammatory infiltrate consisting of neutrophils, T cells, DCs, and other populations[116]. In psoriatic lesions, the granular layer of the epidermis is greatly reduced or absent and as a result, the *stratum corneum* is formed by incomplete cornified keratinocytes with retention of nuclei (parakeratosis)[117]. In comparison with normal skin, the mitotic rate of the basal keratinocytes is increased, originating a thickened epidermis (acanthosis) with elongated rete ridges. The disappearance of late differentiation markers such as profilaggrin and loricrin is observed in psoriasis due to the acceleration of keratinization combined with premature cell death [117].

Much efforts have been devoted to understanding the primary pathogenic mechanisms and the cell components responsible for the onset of the disease[118]. Nevertheless, a consensus has not yet been reached. Different studies have described cathelicidin antimicrobial peptides (LL37), nucleic acid complexes, lipid antigens, thrombospondin type 1 motif-like 5, as well as pathogens of viral or bacterial origin as possible initial psoriatic triggers[115,118]. In response to these triggers, keratinocytes produce significant levels of antimicrobial peptides, and cytokines IL-23, IL-17, IL-6, and IL-22 that appear to play a prominent role in pathogenesis[34]. The secretion of these molecules induces further recruitment and activation of DCs and neutrophils to skin plaque lesions which increments inflammation. KRT1 and KRT10 are reduced in the psoriatic involved epidermis, whereas proteins absent in healthy skin are expressed in psoriasis, such as SKALP/elafin, KRT6, KRT16 and KRT17.

The infiltration of inflammatory immune cells plays an influential role in the disease pathophysiology[119]. They trigger the inflammatory cascade by interaction with and activation of keratinocytes, resulting in disease progression. Psoriasis was initially considered to be a T_H1 cell-mediated disease due to the presence of large numbers of CD4 T_H1 and CD8 cytotoxic T cells type 1 and elevated levels of IFN-γ, TNF-α and IL-12[120]. In addition, interaction of T cells with DCs leads to the secretion of T_H1 type cytokines, thus creating a 'type 1' inflammatory environment **(Figure 1.6)**. Further research, however, demonstrated the added role of IL-17-producing T_H17 cells in the pathogenesis of psoriasis, and their downstream effector molecules such as IL-17A, IL-17F, IL-22, IL-21 and TNF-α. A third subset of T_H cells has been implicated in the pathogenesis of psoriasis, namely the T_H22 cells, due to their abundant secretion of IL-22. In fact, dermal CD3 T

cells are increased in psoriatic skin where compared to healthy controls. These cells increase from 1 to 15% in psoriatic samples. The same was verified to dermal γδ T cells, increasing from 15 to 40%[45,80]. Both αβ and γδ dermal T cells have the ability to secrete IL-17 when stimulated with IL-23, inducing inflammatory cytokines. This effect was demonstrated to be intensified in dermal γδ T cells isolated from psoriasis patients. Furthermore, monocytes, which are important pro-inflammatory cells found in psoriasis skin lesions, respond by secreting high amounts of TNF-α, IL-12, and IL-23[119].

Activated DCs migrate into draining lymph nodes and secrete TNF-α, IL-23, and IL-12, with the latter two modulating the differentiation and proliferation of T_H17 and T_H1 cell subsets, respectively[115] **(Figure 1.6).** These activated T cells can migrate to the epidermis, secrete cytokines, including IL-22, mediating epidermal hyperproliferation and activation of keratinocytes. These cytokines lead to the recruitment of more lymphocytes, neutrophils, and myeloid cells creating a positive feedback loop that maintains cutaneous inflammation and causes epidermal hyperplasia, in a vicious cycle[45,121].

Current available treatments for psoriasis comprise the use of topical preparations, phototherapy, systemic treatments, or the use of biotechnological drugs[122]. Their application strongly depends on disease severity. The first two are the first line treatment for mild to moderate disease while the others are considered in cases of moderate to severe disease[123]. The biotechnological drugs target specific biomolecules such as TNF-α, IL-12/IL-23, IL-17A and IL-17A receptor, shutting down the exacerbated immune response through a strong immunosuppressant effect[10,123]. Although these products are effective in controlling psoriasis symptoms, they significantly increase the risk of getting severe infections, or developing cancer, due to the constant artificial shut down of the immune system. The long-term consequences of their use are yet to be fully understood. Accordingly, there is a need to develop other treatment options that increase the tolerance of the immune system, without strongly suppressing its main functions, consequently reducing secondary side.

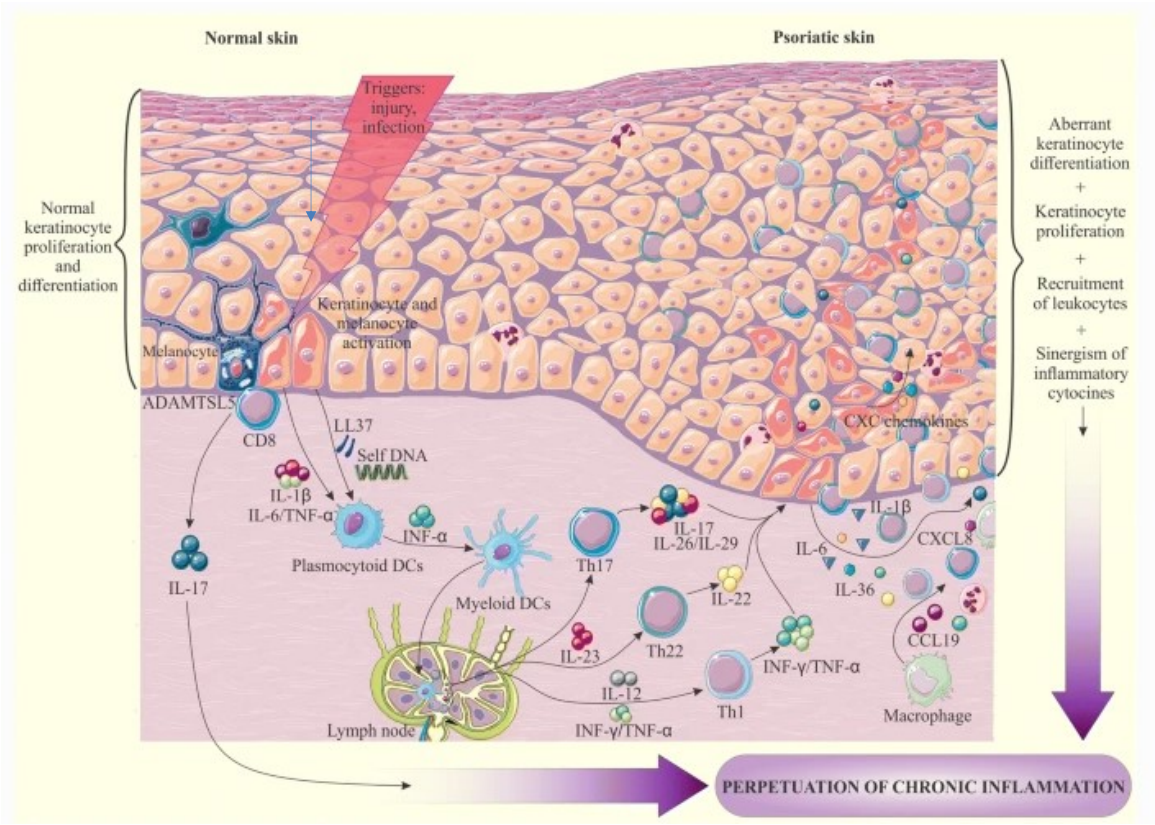

Figure 1.6. The pathogenesis of psoriasis. Early upstream events in psoriasis activate both keratinocytes and innate immune cells such as DCs and neutrophils. During this initial phase, keratinocytes produce antimicrobial peptides, such as β-defensins and S100 proteins, together with chemokines and cytokines of IL-1 family. These microenvironment drives expansion of T lymphocytes, mostly T_H17, T_H22 and CD8. The IL-23/IL-17 axis is activated in a feedforward loop that favors keratinocyte proliferation, eventually forming a psoriatic plaque. In lymph nodes, activate DCs polarize naïve T cells into T_H1, T_H17, and CD8 cells by cytokine stimulation. Adapted from [124].

1.1.5.3. Allergy

Allergy is an improper immune response to an foreign antigen[125]. The pathophysiology of allergic responses starts when there is a sensitization to a specific antigen[34]. Although we are all continuously being exposed to harmless antigens, only a certain percentage of individuals experience adverse immunological reactions to these antigens. Similarly to autoimmune responses, this is related with abrogation of tolerance or failure to induce tolerance that leads to the induction and perpetuation of active immune responses[126].

Allergens are recognized and presented to naïve T cells by antigen-presenting cells (APCs) that induce T cell activation, differentiation and expansion of T_H2 cells. The key cytokines responsible for the allergic response include IL-4, IL-5, and IL-13. These ILs act on B cells, promoting Ig class switching to IgE which when occurring repeatedly stimulates the release of histamine and other mediators responsible for the immediate symptoms of allergic disease. Effector cells (i.e., mast

cells, basophils, and specifically, eosinophils) release additional inflammatory mediators and cytokines, perpetuating the proinflammatory response[126].

In skin, keratinocytes also have an important role in perpetuating allergic responses. This inflammatory environment causes oxidative stress in keratinocytes, resulting in release of reactive oxygen species and danger signals, such as ATP. This response further increases an influx of T cells to the skin, resulting in tissue damage and in inflammatory eruption[125].

1.2. Extracellular vesicles

1.2.1. The discovery of extracellular vesicles

EVs are a group of small, naturally-derived particles, which, until recently, represented an overlooked and underappreciated component of the cellular secretome[127]. The secretion of EVs is a process that appears to be conserved throughout evolution, since both eukaryotes and prokaryotes cells have been demonstrated to release vesicles into the extracellular environment[128]. Two major categories of EVs have been defined - microvesicles and exosomes -, predominantly based upon vesicle biogenesis, but also in differences in size, composition and even function[129,130] **(Figure 1.7)**. EVs, namely exosomes, were initially identified in the early 80s mediating the recycling of the transferrin receptor in reticulocytes[131]. In this first report, the release of EVs was described as part of a disposal mechanism to discard unwanted materials from cells. Some years later, exosomes were reported to be secreted by B lymphocytes[132] and dendritic cells[133] with potential functions related to immune regulation. Nevertheless, succeeding research has also brought to light a more glorious role of EVs as important mediators of intercellular communication, involved not only in normal physiology but also in pathological conditions[128,134]. In fact, they are described as significant factors in inflammation and immune responses, antigen presentation, cancer progression and metastasis, immunomodulation, coagulation, tissue regeneration, organ repair, cell-cell communication, senescence, proliferation and differentiation in the body[135].

Exosomes or small EVs (sEVs) are formed when the peripheral membrane of multivesicular bodies (MVBs) undergo reverse budding to form small lipidic nanovesicles (30-200 nm in diameter) that are released when MVBs fuse with the cytoplasmic membrane[130]. Exosome secretion is described in many different cell types and both amount and molecular composition of released exosomes depend on the state of the parent cell. Morphologically exosomes resemble viral particles, being able to elastically deform while maintaining their integrity[136].

In turn, microvesicles are larger in size (up to 1 μm) and are produced during shedding or outward budding of the cytoplasmic membrane[130]. This EV subset was primarily described as subcellular material originating from platelets in normal plasma and serum[137]. Similarly to exosomes, microvesicles have been reported to have a role in cell–cell communication in various cell types, including cancer cells, where they are generally called oncosomes[138]. In this case, vesicles are larger with diameters up to 10 μm.

EVs nomenclature is still not consistent in the vesicle field due the lack of consensus on specific markers assigning EVs to a particular biogenesis pathway, overlapping range of size, similar morphology and variable composition[139].

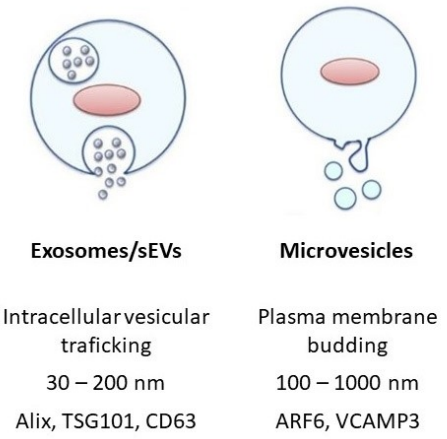

Figure 1.7. Comparison of pathways, size, and markers of the two major EVs subtypes.

1.2.2. EVs biogenesis and secretion

Both small and medium/large EVs (exosomes and microvesicles) biogenesis involve membrane trafficking process. These two EVs categories have distinct biogenesis pathways occurring at distinct sites but share many intracellular mechanisms and sorting machinery components in the process.

sEVs or exosomes are generated within the endosomal system which consists of highly dynamic membrane compartments that are responsible not only for the internalization of extracellular ligands or cellular components but also for their recycling to the plasma membrane and/or their degradation[128]. sEVs formation starts at early endosomes that mature into late endosomes [140], which during this process accumulate intraluminal vesicles (ILVs). Due to their appearance, late endosomes are generally referred to as multivesicular endosomes or MVBs. In most cells the MVBs have two possible fates: fusion with lysosomes and consequently degradation or fusion with plasma membrane, releasing their content to the extracellular space. Usually, the second scenario is associated with MVBs bearing molecules such as CD63 and lysosomal-associated membrane proteins LAMP1 and LAMP2[128]. Other molecules have been implicated in this process showing that not all MVBs can fuse with the plasma membrane[141]. For instance, cholesterol content of MVBs in B-lymphocytes seemed to modulate the ability of these compartments to fuse with the plasma membrane and release exosomes[142].

Specifically sorted proteins and lipids form ILVs by inward budding of the early endosomal membrane[128]. This dual role of first mediating the sequestration of cargo at the endosomal membrane, and then inducing budding and scission of the endosome membrane away from the cytosol forming cargo-specific ILVs are usually mediated by endosomal sorting complex required for transport (ESCRT) machinery[143] **(Figure 1.8).** The ESCRT machinery is a modular system consisting of four subcomplexes named ESCRT-0, -I, -II, and -III. The ESCRT-0 complex

recognizes and sequesters ubiquitinated transmembrane proteins in the endosomal membrane, whereas the ESCRT-I and -II complexes appear to be responsible for membrane deformation into buds with sorted cargo, and ESCRT-III components subsequently drive vesicle scission[143]. Interestingly, depletion of the ESCRT-0 proteins, Hrs and TSG101, and the ESCRT-I protein, STAM1, reduces the secretion of exosomes[141]. Briefly, at the endosome membrane, ubiquitin-binding proteins, such as the Vps27/HRS complex or ESCRT-0, bind to clathrin to form a clathrin coat and to recruit ESCRT-I. ESCRT-I is a trimeric complex of Vps23, Vps37 and Vps28 which interacts with mono-ubiquitinylated proteins. ESCRT-I activates ESCRT-II, a trimer of Vps22, Vps36 and Vps25. ESCRT-II initiates the formation of ESCRT-III by oligomerization of Vps20, Vps24, Vps2 and Snf7. ESCRT-III acts by concentrating the protein cargo and recruits a number of other factors; these factors include Bro1 which in turn recruits the de-ubiquitinating enzyme Dos4, and Vps4, which dissociates the ESCRT machinery[128]. The canonical ESCRT pathway can be intersected by syntenin and the ESCRT accessory protein ALG2 interacting protein X (ALIX; also known as programmed cell death 6-interacting protein), which bridge cargoes and the ESCRT-III subunit vacuolar protein sorting associated protein 32 (VPS32; also known as CHMP4)[130].

Of note, exosomes can also be generated by distinct pathways independent of ESCRT. After inhibition of ESCRT-dependent pathway by depleting cells of key subunits of all four ESCRTs, MVBs with CD63-bearing ILVs were still formed[144]. Indeed, in the last years, several distinct molecules have been described as regulators of sEVs biogenesis on ESCRT-independent pathways. The first ESCRT-independent mechanism of sEVs described was dependent on ceramide. Trajkovic et al. proposed that this sphingolipid can promote domain-induced budding and curvature of the membrane leaflets in MVBs[145]. Alternatively, it was also described that ceramide could be metabolized to sphingosine-1-phosphate to activate G protein-coupled S1P receptor that appears essential for cargo sorting into exosomal ILVs[146]. In addition to lipids, tetraspanins proteins were also described as regulators of this endosomal pathway. These proteins are able to form clusters among themselves and dynamic structures with different transmembrane and cytosolic proteins, promoting the formation of microdomains that will bud[130]. For instance, CD63 that besides being enriched in sEVs surface was shown to be involved in endosomal sorting in melanocytes[147,148] and in the biogenesis of exosomes in different cell types[149–151]. The tetraspanins CD81, CD82 and CD9 are also directly involved in the sorting of various cargoes to exosomes[130,141].

Once ILVs are formed, MVBs need to be transported to the plasma membrane to be released. Rab protein family are important for intracellular transport pathways along with actin and tubulin. They are also important for the release of sEVs, although the exact mechanism is not known[141]. Accordingly, the loss of Rab27a and Rab27b[152] and Rab7[153] expression strongly reduced the release of exosome. Moreover, Rab proteins are not continuously expressed, suggesting that different cell types develop their own vesicle release pattern[130]. Small GTPases of other families such as the Rho/Rac/cdc42 family might also play a role in sEVs transport and release[141]. The specific

molecular machinery for fusion of MVBs with the plasma membrane is not well characterized[154]. Nevertheless, it is well suggested that this fusion mechanism is mediated by soluble N-ethylmaleimide-sensitive factor attachment protein receptor (SNARE) proteins[130], tethering factors, Rabs, and other Ras GTPases[141].

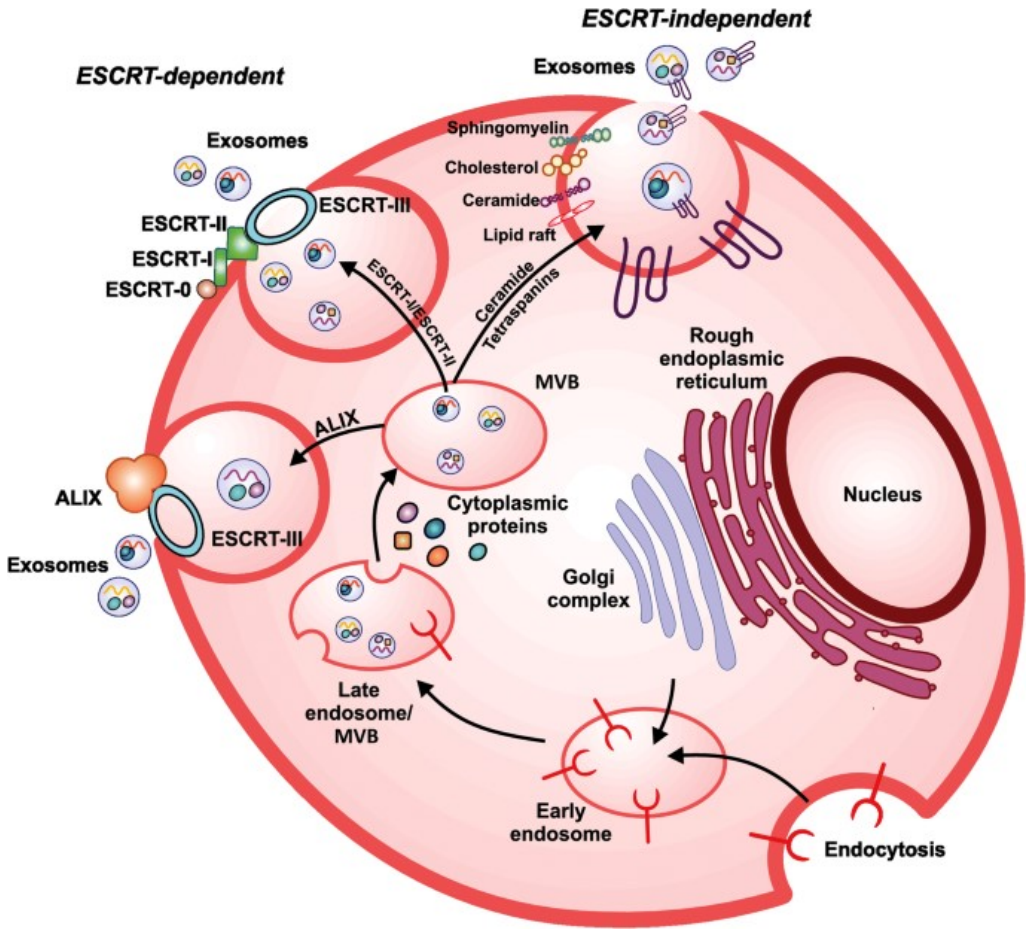

Figure 1.8. ESCRT-dependent and independent exosome biogenesis. Exosomes are formed inside the secreting cells in endosomal compartments MVBs. It involves inward budding of the cell membrane and encompasses bioactive molecules, leading to the formation of the endosome Exosome biogenesis process can be or not coordinated by ESCRT pathways. ESCRT complex is composed of approximately thirty proteins that assemble into four complexes, namely ESCRT-0, ESCRT-I, ESCRT-II and ESCRT-III. ESCRT complex is usually recruited to the endosomal membrane for the sorting of selected protein to ILVs, which requires ubiquitination of the cytosolic tail of endocytosed receptors. Adapted from [155].

In turn, microvesicle biogenesis follows a different path which requires several molecular rearrangements within the plasma membrane, including changes in lipid components, protein composition and calcium (Ca^{2+}) levels[130]. Membrane budding and microvesicle formation is favored by Ca^{2+} dependent enzymatic machineries including aminophospholipid translocases (flippases and floppases), scramblases and calpain which promote rearrangements in the asymmetry of membrane phospholipids (e.g. translocation of phosphatidylserine from the inner leaflet to the

cell surface), causing physical bending of the membrane and restructuring of the underlying actin cytoskeleton[130].

Lipids were shown to be crucial in this process. Del Conde et al. investigated the possibility that microvesicles arise from cholesterol-rich lipid rafts. After cholesterol depletion in blood monocytes and in the monocytic cell line THP-1, microvesicle shedding was significantly reduced. Another evidence of lipids role on microvesicle biogenesis was demonstrated on platelets[156]. A genetic defect in the activity of the lipid scramblase suppresses the exposure of phosphatidylserine, which impairs the production of these vesicles[157]. In addition to lipids, cytoskeletal elements and their regulators are certainly required for microvesicle biogenesis. Nevertheless, the release of microvesicles from the plasma membrane of healthy cells and the mechanisms involved in this secretion have only recently started to emerge[130].

Interestingly, ESCRT machinery also acts on microvesicle release[128]. Depletion of different ESCRT subcomplexes significantly decrease microvesicle budding[158]. Additionally, SNARE, Rab and other GTPases are also important for microvesicle biogenesis, sharing common mechanisms with SEV formation.

1.2.3. EVs composition

Most studies of biochemical composition of EVs involved analysis of bulk populations of vesicles as different modes of isolation and characterization are used. Although a lot of efforts have been made to isolate specific EVs population, the actual composition of each subtype of EV is unknown[128,139]. Globally, EVs are nanometric particles limited by a lipid bilayer, containing biologically active cargo of nucleic acids, proteins, lipids and metabolites that can be altered based on the precise state of the cell or external stimulus **(Figure 1.9).** Herein, we summarize the current state of the literature regarding lipids, proteins and nucleic acid mostly associated with EVs and linked with specific sorting mechanisms.

1.2.3.1. Lipids

EVs are built up by a lipid bilayer containing distinct lipid classes such as cholesterol, phosphatidylserine (PS), phosphatidylcholine (PC) and sphingomyelin (SM)[128]. Although EV lipidomic studies are scarce, several evidences show an enrichment of specific lipid classes in EVs when compared with total cell membranes. These studies report 2–3 times enrichment from cells to EVs for cholesterol, SM, glycosphingolipids and PS. In contrast, EVs generally contained less PC than their parent cells, and only small changes were reported for phosphatidylethanolamine (PE) in most studies[159].

Curiously, although lipids involved in EVs biogenesis like ceramide and its derived were identified in EVs samples, lysobisphosphatic acid, a lipid present in membranes of the intraluminal vesicles of MVBs, was not[128]. It is described that this lipid contributes to lysosomal stability and integrity and to be an essential cofactor for sphingolipid catabolism in lysosomes[159].

Besides the lipid species, other publications focused on the saturation level of fatty acyl groups in lipids in EVs were published[159]. When compared with parent cells, there is an enrichment of phospholipid species with two saturated fatty acyl groups. For PC, this is mainly due to an increase in PC 14:0/16:0 and 16:0/16:0[145,160]. However, EVs are also highly abundant in monounsaturated fatty acyl groups. Although depending on the secreting cells, PC 16:0/18:1 and PC 16:0/16:1 were the two dominating PC species in EVs from PC-3 cells[160], PC 34:1 and PC 32:1 were among the most common species in EVs from oligodendrocytes neuronal cells[145], and PC 34:1 accounted for approximately 60% of the PC species in prostasome preparations[161].

Beyond structural function, EVs can transport various lipid species including eicosanoids, prostaglandins, fatty acids and cholesterol as well as lipid translocases, thereby contributing to the regulation of important cell biological processes such as inflammation and immune system modulation[130,162]. For example, ceramides in EVs induce apoptosis in oligodendroglioma cells[163], and promote macrophage chemotaxis in a mouse model[164]. Enzymes capable of producing leukotrienes, potent lipid mediators that promote granulocyte migration, were identified in EVs generated from healthy human monocyte dendritic cells and monocyte-derived macrophages[165], as well as in epithelial cancer cells from the lung[166]. Importantly, differences in the abundance of ceramides, modified ceramides, and phosphatidylglycerol in airway EVs also contributes to drive inflammatory responses and exacerbate inflammation in asthmatics[167]. In cancer, EVs produced from rat basophilic leukemia cells, containing a cocktail of prostaglandins, cyclooxygenases 1 and 2 and free fatty acids (including arachidonic acid), showed a potent ability to modulate the immune responses potentiating tumor growth[168,169]. Contrarily, EVs containing phospholipid hydrolases, such as phospholipases and the phosphoinositide (PIP3)-phosphatase (PTEN) participate in reducing tumor growth when these molecules are transferred to recipient cells[162,170]. In summary, delivery of different EVs contents to recipient cells can produce opposing physiological outcomes.

1.2.3.2. Proteins

EVs also contain a large diversity of proteins, many of which are common among themselves[171]. The overlap is a consequence of the biogenesis pathways as such proteins are those involved in the MVB formation of EVs like ESCRT proteins and others are related to the membrane transport and plasma membrane fusion, as described for the Rab proteins[128,152].

EVs protein content when compared to their parental cell membrane is commonly enriched in tetraspanins, such as CD9, CD63 and CD81, a group of proteins involved in EVs formation and

protein sorting[171–175]. Besides, tetraspanins are also central in the regulation of ESCRT-independent vesicle formation and due to their transmembrane domains these proteins are involved in various biological functions such as cell adhesion and membrane fusion[176]. Originally, it was thought that tetraspanin proteins were specific markers of exosomes, however, these proteins have also been identified in MVs and apoptotic bodies[172,177,178]. Interestingly, while CD9, CD63 and CD81 have been identified in exosome like vesicles, only CD9 was present on plasma membrane associated vesicles, i.e. microvesicles[179].

In addition, ESCRT proteins and its accessory proteins (Alix, TSG101, HSC70, and HSP90β) are expected to be found in EVs regardless of the type of cell from which they originate[180]. Syndecan was shown to recruit Alix and Syntenin and support their essential interaction for intraluminal budding of the endosomal membrane, a function that is blocked in the absence of Rab7[153].

Rab proteins, the largest family of small GTPases, are commonly identified in EVs samples[171,180]. Referring to Exocarta (www.exocarta.org), a web-based compendium for exosomal cargo, more than 28 Rab isoforms have been characterized. Within those, most of the Rabs characterized are GTPases involved in the endocytic pathway, while Rab proteins having a role in endoplasmatic reticulum and Golgi transport are less frequently found[181]. This highlights the endosomal origin of the multivesicular compartment, resulting from various membrane transport steps regulated by Rabs. RAB4, RAB5 and RAB11 are localized in early endosomes mediating endocytosis and endosome fusion of clathrin-coated vesicles while RAB7 and RAB9 membrane domains are present in late endosomes [182].

In addition to Rabs, exosomes are rich in annexins (annexins I, II, IV, V, VI, VII and X1) which aid in membrane trafficking and fusion events and also in other exosomal proteins including metabolic enzymes (GAPDH, enolase 1, aldolase 1, PKM2, PGK1, PDIA3, GSTP1, DPP4, AHCY, TPL1, peroxiredoxins, P4HB, LDH, cyclophilin A, FASN, MDH1 and CNP), ribosomal proteins (RPS3), transmembrane (PIGR, LAMP1 and CD59), signal transduction (syntenin, 14-3-3, G proteins, ARF1, CDC42, stomatin, SLC9A3R1, RALA, PDCD6, rack1, mucin 1, EHD1, RAN, PEBP1, MIF, RRAS2, RAC1, NRAS and EHD4), adhesion (MFGE8 and integrins), ATPases (VCP, ATP1A1, DYNC1H1, ATP5B and ACLY), cytoskeletal (actins, tubulins, cofilin 1, ezrin, profilin 1, moesin, radixin, myosin, perlecan, THBS1, IQGAP1, keratins, gelsolin, FN1 and LGALS3BP) and ubiquitin molecules (ubiquitins B and C)[171].

In general, EVs protein content is believed to be reflective of their cell of origin, on the health status of the cell and the stimuli that induced EVs secretion[130]. For instance, EVs derived from APCs like DCs carry major histocompatibility complex (MHC) class II molecules and other DC related markers such as costimulatory molecules[180].

The scientific community researching EVs has been making the effort of creating different databases and continuously updating them to incorporate the results of EVs characterization. Firstly, Exocarta was created and then it was extended to a more comprehensive database named

Vesiclepedia, which also includes data from other types of EVs (http://microvesicles.org)[128,183]. Both databases include data not only on proteins but also on nucleic acids and lipids, as well as on the purification procedures used.

Although the database continuous updating makes them a crucial tool to improve comprehension of EV complexity, the different isolation procedures and characterization methods are confound methods that difficult the determination of a single EVs protein signature. To overcome this issue, Lo Ciccero et al. compile a few of mass spectrometry (MS) data obtained from EVs isolated equally from dendritic cells, melanocytes, Schwann cells, neurons, intestinal epithelial cells[180]. Table 1 summarizes examples of common proteins that are present in vesicles with exosomal features released by different cells.

Similar to lipids, EVs proteins have also been described with functional role in recipient cells, modulating basilar cell functions. Heat-shock protein Hsp72, expressed in EVs, can activate the Stat3 signaling pathway by inducing IL-6 secretion[184]. Furthermore, EVs can carry specific antigens with the ability to induce a specific immune response. For instance, Sheng et al. found that EVs contain unique antigens that activate autoreactive T cells to produce T_H1 cytokine IFN-γ[185] while another report demonstrated that adipose-derived stem cells release exosomes that drive macrophage differentiation into IL-10–secreting M2 cells[186]. When transporting Fas ligand and galectin 9, EVs induce apoptosis of the surrounding immune cells, promoting immunosuppression[187]. This functionality could have beneficial impact on systems showing exacerbated immune response but can also promote tumor growth by decreasing the immune surveillance.

Table 1.1. Examples of common proteins that are present in vesicles with exosomal features released by different cells. The protein content was determined by MS analysis of exosomes from dendritic cells, melanocytes, Schwann cells, neurons, intestinal epithelial cells. Adapted from [180].

Classification	Proteins
Antigen Presentation	MHC class I, MHC class II
Adhesion Molecules	Tetraspanin: CD63, CD81, CD9, CD37, CD53, CD82 Integrins: α3, α4, αM, αL, β1
Membrane Trafficking	Annexins: I, II, IV, VI, VII, XI Syndecan-1 Rab 2, Rab 5c, Rab 10, Rab 7
ESCRT proteins	Alix, Tsg101
Heat-shock proteins	Hsc70, Hsp90
Cytoskeletan proteins	Actin, Cofilin 1, Moesin Tubulin: α1, α2, α6, β5, β3
Enzymes	Pyruvate kinase Alpha enolase GAPDH
Signal transduction	14-3-3 ξ, γ, ε
Lipid raft	Flotillin-1, Flotillin-2
Others	Lactadherin Elongation factor 1α, Lamp2

1.2.3.3. Nucleic acids

EVs also carry different ribonucleic acid (RNA) species, including messenger RNA (mRNA), long non-coding RNA (lncRNA) and microRNA (miRNA), which are safely protected from degradation by RNases for transportation to the recipient cell[188]. The presence of nucleic acids in EVs was firstly described in 2007[188]. Strikingly, it was further demonstrated that these small molecules can be transferred inside of EVs to acceptor cells and interfere in gene expression in the latter[188,189]. From then on, a new perspective on the possible roles of EVs emerged as vectors of genetic information able to modify the range of genes expressed within recipient cells.

EVs RNA content is highly influenced by the used isolation technique and the purity of the vesicle preparation[139,190]. Nevertheless, the majority of studies report a high abundance of small RNA, with a low molecular weight and the absence or small amount of ribosomal RNAs (rRNA) (18S and 28S)[191]. Depending on the cell type, abundance of each small RNA species in EVs is highly variable[191].

In a pioneering work, Nolte-'t Hoen et al. characterized small RNA content in EVs released by the immune cells in culture using deep sequencing[192]. Interestingly, the majority of total RNA isolated from EVs consisted of small RNAs (<200 nucleotides), with minor amounts of 18S and 28S rRNA[192]. Besides protein coding mRNA and repeats, the EV fractions contained all types of structural RNAs such as vault RNA, Y-RNA, small nuclear RNA (snRNA), small nucleolar RNA (snoRNA), signal recognition particle RNA (SRP-RNA), and transference RNA (tRNA), as well as fragments deriving from long non-coding RNAs and pseudogenes. Of note, many of the small non-coding transcripts were enriched in EVs relative to cellular RNA, indicating that RNA species are possibly packed into the EVs in a strictly regulated manner.

In particular, miRNAs have been shown to be differentially sorted to EVs depending on their sequence (presence of specific motifs)[193,194]. Several miRNAs are more highly represented in EVs than in cells (such as miRNA-575, miRNA-451, miRNA-125a-3p, miRNA-198, miRNA-601 and miRNA-887) while other are more highly represented in cells than in EVs (such as miRNA-17, miRNA-29a, let-7a, miRNA-142-3p, miRNA-181a and miRNA-18a)[193]. These findings hypothesize a possible regulation of nucleic acid incorporation into EVs, however, the relative contributions of passive and active loading of RNAs remain unclear[130]. A recent study showed that EVs from a metastatic breast cancer cell line used different mechanisms of miRNA sorting, one selective and the other non-selective[195]. Using biochemical and genetic tools, the authors identified the Lupus La protein as a sorting mediator of selectively packaged miRNAs as well as two motifs embedded in miRNA-122 responsible for high-affinity binding to Lupus La.

Additionally, EVs can also transport DNA sequences[196,197] which may be genomic[198,199] or mitochondrial[200–202]. Depending on the cell line and context, DNA may be single- or double-stranded, and may reside within the lumen or on the surface of EVs. Surface-bound DNA can alter the ability of EVs to adhere to fibronectin[200], suggesting it may help determine how EVs interact with extracellular matrix molecules. Luminal DNA, like other cargo types, can be transferred from donor to recipient cells resulting in increased messenger RNA and protein production. Similarly to RNA species little is known regarding how DNA is sorted into EVs[203].

To complement the physiological role of lipids and proteins associated with and transported by EVs, genetic modulation by delivered small pieces of nucleic acids added another powerful feature on top of that. Current knowledge about EVs nucleic acid cargo outlined their role in physiologic and pathologic contexts and they are currently being explored not only as biomarkers[197,204] but also as therapeutic tools for a myriad of diseases[203,205–208]. The role of nucleic acid cargo will be further address in this work mainly focused on their influence on inflammatory and immunomodulatory mechanisms.

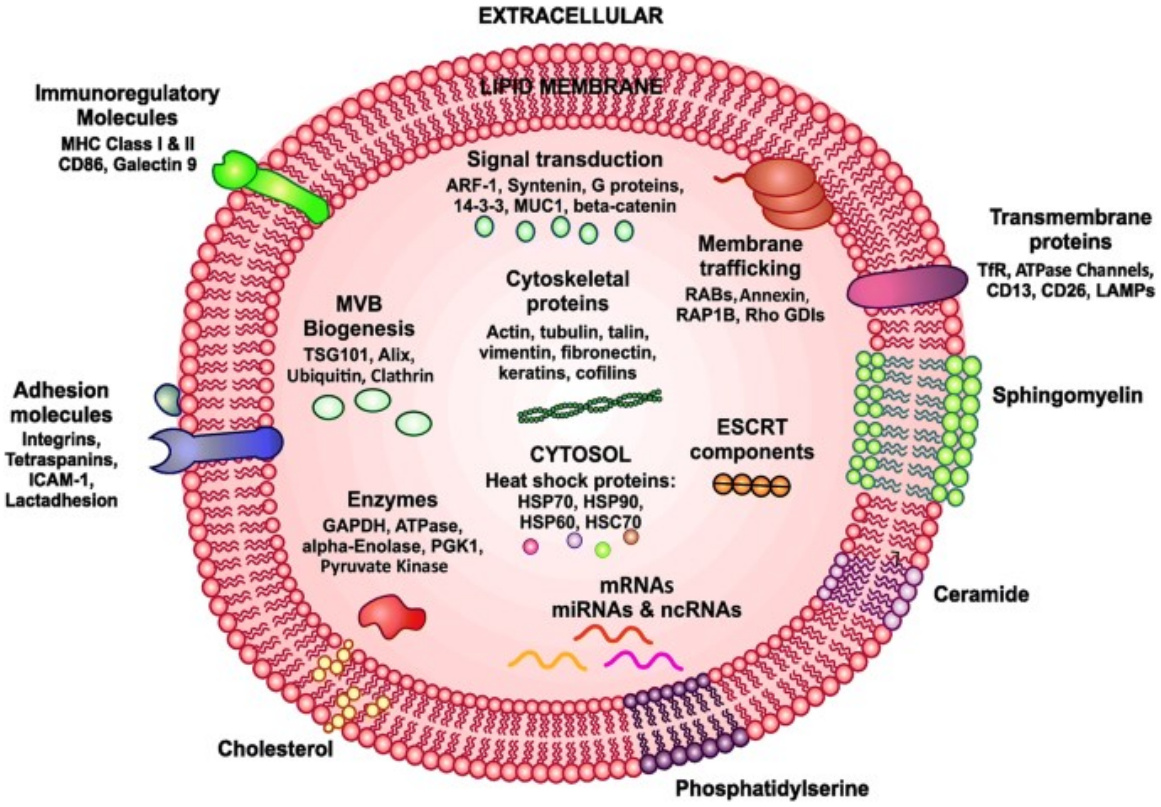

Figure 1.9. Schematic representation of exosome composition comprising different families of proteins, lipids, and nucleic acids. Adapted from [155].

1.2.4. EVs isolation methodologies

The release of EVs in the extracellular space allows for their recovery from cell culture supernatants and biological fluids. Therefore, a good isolation protocol is critical to characterize them, to understand their mechanisms of action and for their use as a therapeutic tool. Nevertheless, EVs nanometric sizes make their isolation difficult. Thus, various techniques have been adopted and developed to facilitate the isolation of EVs and, to date, different isolation methods of EVs have been widely used. These procedures comprise ultracentrifugation (UC), ultrafiltration (UF), chromatography and size, immunoaffinity capture, precipitation, and microfluidic-based methods[209].

The initial protocol used to purify EVs was UC. This method is based on differential centrifugation, whereby the smallest vesicles (including sEVs) are sedimented at 100 000 ×g. Before UC, larger vesicles were eliminated by successive centrifugations at increasing speeds to sediment these vesicles without artificially creating small vesicles from large ones by direct high-speed centrifugation[210]. It is not expected that the recovery fraction is composed purely of exosomes, as their size overlaps to some extent with that of microvesicles. However, further characterization of

these samples confirmed their enrichment in exosomes[141]. Moreover, if present, lipoparticles from serum, protein aggregates, nucleosomal fragments, apoptotic bodies and lipid droplets would be co-isolated together with EVs during UC. To improve EVs fraction purity, several variants of this method are used nowadays that can involve higher-speed ultracentrifugation or include different steps before final ultracentrifugation, such as filtration to eliminate debris and vesicles larger than 220 nm[128]. Combining UC with size-exclusion chromatography (SEC) is also a reliable strategy to recover entities larger than 50,000 kDa and thus eliminate soluble proteins[211,212]. Additionally, UC is often used in conjugation with density gradients like sucrose density gradients or sucrose cushions which separates EVs according to their floatation densities. In this way, protein aggregates sediment through sucrose whereas lipid-containing vesicles float upward[128,141].

Using the same logic, to purify larger EVs (microvesicles, for instance), lower centrifugation speed is used. Most protocols adopt speeds ranging from 10,000 ×g to 50,000 ×g[128]. In any case, depending on the EVs purpose, UC is time-consuming, labor-intensive and requires costly instrumentation which hamper UC implementation in good-manufacturing practice (GMP) production unit for generation of clinical grade EVs.

To face UC methodological challenges, size-based methods were adapted to EVs isolation. Ultrafiltration (UF) is an example of these methods and by using them, EVs isolation is only dependent on size or molecular weight. Besides, UF is faster than UC, and does not require costly equipment[213]. Nevertheless, at the end, it is difficult to remove protein contaminants. The combination of UF and SEC is the best approach to achieve high-purity EV preparations[141,212]. SEC separates EVs by fractioning, however it is not capable of distinguishing between protein aggregates, lipoparticles, macromolecules, and particulate matter[135]. EV separation based on size can be achieved by their differential passage through physical barriers, using filters or chromatography columns. Immunoaffinity methods are suitable for isolating EVs based on their enrichment of protein at surface. With these methods is possible to purify EVs based on the interaction of those specific EV proteins with their antibodies[209]. Immuno-affinity methods are rapid, easy, and compatible with routine laboratory equipment. This approach employs magnetic beads covalently coated with streptavidin, which can be coupled to a high-affinity capture antibody. The most common antibodies to capture EVs are anti-CD63, -CD9, and -CD81. Interestingly, the specificity and yield of exosomes isolated by immunoaffinity methods are comparable to yields from UC. To improve this method, submicron-sized magnetic particles have been used for immunoaffinity capture-magneto-immunocapture and shown to yield 10 to 15 times higher quantities of exosomes than UC[135,214].

Commercially available kits are mainly based on precipitation methods. These procedures are based on capturing and collecting EVs with sizes ranging from 50 to 150 nm, in ‘‘polymer nets’’ using simple, rapid, low-speed centrifugation on the bench top at 1500 ×*g*[135]. Although these methods are easy to use and do not require any costly or specialized equipment, there is no specificity for EVs,

co-isolating contaminant material, such as protein aggregates. Besides and depending on the future EVs application, there is the need to ensure that the polymer used to precipitate EVs is innocuous and do not elicit immune responses *in vitro* or *in vivo*. Similarly to UF/SEC, this method does not separate small from larger EVs nor protein aggregates, or lipoparticles[128].

Microfluidics-based EVs isolation techniques were developed to face the challenges of conventional methods such as low yield and purity, time intensiveness, a high cost, and difficulties in standardization. Thus, these technologies have become important techniques for isolation, detection, and analysis of exosomes, using both their physical and biochemical properties. This technique uses the basic EVs characteristics like size, density, and immunoaffinity in combination with innovative sorting mechanisms, such as acoustic, electrophoretic, and electromagnetic manipulations, nanowire-based traps, nano-sized deterministic lateral displacement, and viscoelastic flow[135].

Because none of these methods is perfect, efforts to develop new technologies are currently under way, but none has reached worldwide use yet. Regardless of the protocol used, each technique must be validated for any given cell type— or biological fluid, as a source of EVs—to confirm the identity of the purified vesicles. This requires the use of a combination of several methods to determine their morphological, biochemical, and physical features.

1.2.5. EVs characterization

Several methods can be applied for EVs visualization and characterization. One of them is transmission electron microscopy (TEM) where structure, morphology, and size of various biological components is possible to be determined. The working principle of TEM is the creation of images as a beam of electrons passes through a sample, where a secondary electron is generated. These electrons are collected and magnified using special lenses[172]. By using TEM, exosomes were first described to have a cup shaped morphology[210]. However, this appearance was likely caused by extensive sample preparation, which involves multiple steps, and may induce changes in the morphology of the EVs. Moreover, in some cases, the electron beam may also damage biological samples. Later on, by using cryogenic TEM (cryo-TEM), exosomes were described to have a round appearance[215]. Cryo-EM is free from the effects of dehydration and fixation, because the samples are kept in liquid nitrogen and, under these conditions, remain intact, with no ultrastructural changes or redistribution of elements. Cryo-TEM is considered the best method for visualizing nanoparticles and proteins without dehydration artifacts[135]. Allied to EM, immunogold is a good method to label, visualize specific surface EVs proteins and also to trace different cargos inside EVs, contrarily to the use of specific fluorescent dyes whose fluorescence is exaggerated[135].

Flow cytometry is also an alternative technique to characterize EVs surface proteins. Despite being a standardized and robust method for analysis of cells at a rate of a thousand cells per minute,

application to EVs is a major challenge because of the low detection sensitivity for EVs under 500 nm[216]. To overcome this issue, EVs are fixed to latex beads of a size that is in the detection range of a flow cytometer and then are labeled with fluorophore-conjugated antibodies to be analyzed[210]. Although this technique allows a rapid semiquantitative characterization, EVs sample heterogenicity is not completely evaluated as samples are analyzed at population-level. To increase the high-throughput, numerous multiplexing approaches have been developed to simultaneously analyze the presence of a pre-designated set of surface protein markers on EVs. For instance, one platform uses flow cytometry after capture on an array of 37 beads, each bearing a specific antibody[139,217]. Nowadays, highly specialized flow cytometers can visualize and determine EVs size by the integration of a high-power 488 nm laser and by introducing special modifications of the optical detection system to decrease the forward scattering detection angle and enhanced both the scatter intensity and fluorescence signals coming from the EVs. Nevertheless, it is important to stress that heterogeneity of the membrane and cargo composition of EVs affects their level of scattering and potentially introduces errors. In this way, International Society for Extracellular Vesicles (ISEV) and several multi-center initiatives continuously encourage the report of experimental details so that the improvement of the standardization of microparticle quantification using flow cytometry be possible[139,216]. Other commonly applied methods for EVs phenotyping are ELISA for surface markers and western blot for proteins enriched inside of EVs.

One of the most common method used to estimate the size distribution and concentration of vesicles is nanoparticle tracking analysis (NTA)[135]. NTA is an optical particle tracking technique which can measure the concentration and size distribution of EVs in the 10 nm to 2 µm range by tracking the Brownian motion of nanoparticles in a liquid suspension. Although it has been questioned whether NTA is robust enough to determine the vesicle concentration and give reproducible results[139], this technique has several advantages. Besides NTA being able to detect different EVs population within the same sample and to measure small particles with diameters as low as 10 nm, sample preparation is very quick and easy using this method and the measurement itself only takes minutes[135].

Evaluating the RNA profile of EVs can be very challenging. Chip-based capillary electrophoresis is one of the most sensitive RNA quantification methods currently available, with a lower detection limit of 50 pg μl^{-1}. Notably, it requires only 1 µl of sample and gives electrophoresis-like length profiles which are useful for estimating the size distribution of RNA in EV samples[190]. Individual RNAs species can be analyzed by RNA sequencing, RNA microarrays and polymerase chain reaction (PCR). Of note, EVs RNA isolation method of choice has been shown to influence the yield and quality of the extracted RNA[139,190,218]. Taken together, applying several methods is recommended for EV characterization, in order to have a complete picture of EVs samples.

1.2.6. Extracellular vesicles for regenerative and anti-inflammatory therapies

EVs have emerged as significant regulators of the immune system both promoting and inhibiting the immune response, depending on their cell of origin and on the signals present in the microenvironment. Notably, the first study identifying a connection between EVs and the immune system was the observation that B cell-derived exosomes carried MHC class II molecules that could present peptides to CD4 T cells and induce an antigen-specific response *in vitro*[132] . This finding unveiled new perspectives of EVs usage as immune modulators and motivated further investigation in this area. Interestingly, EVs originating from APCs carried MHC class I and class II molecules and are, therefore, potential inducers of CD8 and CD4 T cell responses, respectively[219,220]. It has been shown that when free EVs interacted directly with T cells, they induced a low immune-stimulatory effect 10 to 20 fold less potent than that of parental cells[221]. Besides direct antigen presentation by EVs, indirect antigen presentation by cross-dressing APCs can also occur. In this case, EVs are engulfed by DCs or other APCs and the EVs-MHC/peptide complexes are transferred to the cell surface[222]. Another possibility would be that exosomes stay attached to the APC surface to interact with the T cell directly, resorting to the presence of co-stimulatory proteins[221]. EVs that do not transport MHC peptide can also affect the immune cells status. Mechanistically, this can occur by (i) a direct uptake of RNAs from the vesicles leading to a genetic reprogramming of the recipient cells; (ii) an acquisition of new properties after the transfer of mature vesicular proteins or mRNAs; (iii) a direct effect of EV-contained cytokines exerting an immunosuppressive effect; (iv) eliciting signals via the triggering of membrane receptors on immune cells, leading to the production of inflammatory factors[221,223].

Regarding cutaneous immune response, skin counts on both the nervous system and the immune system to accomplish critical functions as reviewed in the previous sections[16]. EVs are able to convey pathogen molecules (proteins, nucleic acids, lipids, sugars) and serve as antigen presenters to activate host defense, rendering them as putative components of immune-based therapies and vaccine preparations for different diseases namely immune-related skin lesions [224]. EVs can be used as carriers of DAMPs and molecules that regulate T-cell function can exert either a direct effect on stem cells or an indirect effect through the activation of immune cells involved in the inflammatory response. This can mimic molecular signals that participate in the activation of skin stem cells in response to skin damage, although it remains unknown whether EVs are involved in this type of mechanism during physiological skin homeostasis and repair[225]. Kotzerke et al. showed that murine keratinocyte-derived EVs could stimulate dendritic cells to develop a mature phenotype, increasing CD40 expression and producing IL-6, IL-10, and IL-12[226]. Moreover, it was shown that EVs secreted by monocytes contained proteins with the ability to increase the secretion of matrix metalloproteinases by dermal fibroblasts, facilitating cell migration[227]. In this way, EVs can be

envisioned as a new strategy to tackle skin inflammatory and/or autoimmune diseases, tightly regulating immune system functions. Moreover, EVs in blood circulation may serve as biomarkers and predict the onset of a dermatologic disease before visible symptoms arise.

EV-based therapies have advantages when compared to cell-based therapies, nanotechnology or even small-molecules. These vesicles are highly stable *in vivo* and are able to naturally cross biological barriers and deliver their cargo in a bioactive form, orchestrating complex biological activities[228]. Additionally, from the regulatory point of view, EVs reduce most of the difficulties and risks associated to cell transplantation and immune rejection[229]. EVs-based therapeutics have a lower risk for teratoma formation and embolization, which are major concerns for stem cell-based therapeutics[230].

A lot of attention has already been paid to EVs, namely those that are derived from mesenchymal stem cells (MSCs) and immune system cells due to their strong anti-inflammatory and immunomodulatory potential[231,232]. Notably, several authors reported that EVs stimulate wound healing both in normal and diabetic mouse models[20,21,233] by modulating the intensity of the inflammatory response. Excess inflammation is a major hallmark in the dysregulation of normal wound healing. Therefore, further limiting inflammation effectively accelerates healing by prompting the transition to the proliferative phase[70]. As key players in the inflammatory phase, neutrophils and macrophages can secrete molecules able to amplify inflammation at the early stages, or shut down the inflammatory phase of healing[59,234]. Human umbilical cord MSCs-derived EVs, for example, stimulate recipient macrophages (human monocytic cell line THP-1) toward the anti-inflammatory M2 phenotype. Activation, differentiation, and proliferation of B lymphocytes and suppression of T-lymphocyte proliferation was also induced by these EVs. Moreover, MSC-derived EVs can polarize activated T lymphocytes into a T-regulatory phenotype, thereby exerting immunosuppressive effects[235]. Human umbilical cord MSC pretreated with lipopolysaccharide (LPS) release EVs enriched with microRNA let7b. When internalized, let7b can regulate macrophage polarization by the inhibition of the TLR4/NF-κB pathway and by activating the signal transducer and activator of transcription 3 (STAT3)/protein B serine/threonine kinase (AKT). This would resolve chronic inflammation[235]. MSC-EVs could reduce high levels of various chemokines such as chemokine (CXC motif) ligand 10 (CXCL10), monocyte chemoattractant protein 1 (MCP-1), CXCL9, and tissue inhibitor of metalloproteinase-1 (TIMP-1) accumulated by cytotoxic macrophage in colitis-induced colons[236]. In addition, EV-derived microRNAs can enhance the M1 inhibitory ability of MSC-EV treatment in the context of aortic aneurysm formation after elastase infusion[237]. In this model, the severity of elastase-induced aortic damage correlated with proinflammatory cytokine levels. MSC-EVs successfully ameliorated aortic dilation and immune cell infiltration partly by downregulation of proinflammatory and chemokine signaling. Importantly, inhibition of M1 macrophage-derived cytokines including high-mobility group box 1, chemokine (C-C motif) ligand 5 (CCL5), and macrophage inflammatory protein 1a (MIP1a) was

miRNA-147 dependent, given that the miRNA-147 inhibitor mitigated the beneficial effects of MSC-EVs.

Moreover, EVs from umbilical cord stem cells can attenuate burn-induced inflammation. Li and colleagues [238] found that burn injury stimulated an inflammatory reaction in macrophages exposed to LPS, with higher strong secretion of TNF-α and IL-1β accompanied by decreased IL-10 levels and that EVs from umbilical cord MSCs successfully reversed this reaction. Transference of miRNA-181c by EVs to macrophages with a consequent suppression of the TLR4 signaling pathway and inflammatory response alleviation was hypothesized as the mechanism responsible for this effect. Similarly, EVs derived from bone marrow MSCs transfer miRNA-223, regulating macrophage polarization through pknox1. EVs treatment led to an increase of M2 macrophages at the wound site, promoting accelerated healing[239]. Moreover, an interesting study conducted by Kou and collaborators showed that TNF-α promotes EVs-IL-1RA exocytosis from MSCs, mediated via Fas/Fap-1/Cav-1. As IL-1RA is an antagonist to IL-1B, this could control inflammation in microenvironments[240].

Beyond modulating inflammation, EVs can also display immunosuppressive properties. MSC-EVs similarly to anti-inflammatory properties, exert a dose-dependent inhibitory activity on B cells, reducing the production of different immunoglobulins like IgM, IgG, and IgA[241]. Their role on T cells was also studied. In a rodent model, bone marrow derived EVs inhibited the proliferation of T lymphocytes and induced apoptosis in activated T cells. Interestingly, this inhibition was associated with an increased proportion of regulatory T cells[242]. Similarly, *in vitro*, Del Fattore et al. showed that although the addition of MSC-EVs to activated peripheral blood mononuclear cells (PBMNCs) did not affect proliferation of T cells as a whole, they did induce the apoptosis of specific T_H sub-populations and increased the proliferation and the apoptosis of T_{reg}. Moreover, MSC-EV treatment increased the T_{reg}/T_{eff} ratio and the concentration of the immunosuppressive cytokine IL-10 in culture medium[243]. *In vivo* comparable results are reported. In an animal model of inflammatory bowel disease induced by dextran sulfate sodium (DSS), mice receiving daily MSC-EVs treatment showed less weight loss, improved disease activity index and a less severe reduction in colon length when compared to DSS/vehicle-treated controls. Furthermore, quantitative PCR analysis performed on RNA extracted from colon tissue revealed a strong inhibition of the induction of inflammatory cytokines with respect to untreated animals. Notably, a case of successful treatment with MSC-EVs in a patient with steroid-resistant GVHD was recently reported[244].

EVs secreted by immature DCs can induce tolerogenic, rather than effector immune responses, promoting graft survival[245] and reduce inflammation in animal models of arthritis[246], of inflammatory-bowel disease[247] and of septic shock[248,249]. Activated T cells secrete exosomes bearing FasL, which induce apoptosis of neighboring T cells, suggesting their participation in the regulation of immune response by a negative feedback mechanism. Interestingly, placenta secreted

EVs seem to contribute to fetomaternal tolerance, reducing the cytotoxicity of NK and CD8 T cells[231,250].

Nevertheless, additional work both *in vitro* and *in vivo* is needed in order to better understand both the potency and the mechanisms of action of EVs as potential immunosuppressive tools.

1.3. Aims

Over the last few years, investigation of EVs-based therapies has grown substantially, making them an extremely attractive and innovative product for the medicine market. Exogenus Therapeutics is a Portuguese biotechnology company envisioning becoming a reference in the use of EVs for the treatment of skin lesions. Exogenus Therapeutics was founded with the focus on regenerative medicine with access to an exclusive license for the patent protecting the "Use of Umbilical Cord Blood derived exosomes for tissue repair" (PCT/IB2017/000412; WO2017163132). This work drove the development of Exogenus' leading product for chronic wounds treatment, which is a small EV-enriched product derived from pre-conditioned mononuclear umbilical cord blood cells (UCB-MNCs), a privileged biologic human material enriched in immature and stem-like cells, with a high capacity to regenerate damaged tissues[251,252]. Notably, UCB-MNCs-sEVs have shown promising results in accelerating wound healing *in vivo* being the pro-healing activity mediated at tissue/cell level by an increase in skin neovascularization and re-epithelization[253]. In this study, the authors identified hsa-miRNA-150-5p as a key biomolecule for the regenerative effect.

Nevertheless, other potentialities of EVs derived from UCB-MNCs remain to be elucidated. Scrutinizing UCB-MNCs-EVs mechanism of action is crucial for the product development and for future regulatory approval, and will also strengthen the companies' knowhow, potentiating the development of its product's pipeline. Therefore, this project envisions to evaluate UCB-MNCs-EVs potential as a valuable tool for treatment and management of immune-related skin lesions, characterizing their capacity to act on inflammation and/or as an immunomodulator. It is worth noting that EVs derived from UCB-MSCs have therapeutic effects on the treatment of GVHD and chronic kidney disease in the clinic, and in a variety of pre-clinical immune disease models[254–256]. Achieving this aim, the company will strengthen its pipeline with products for a promising area, of diseases with high unmet needs and strong commercial potential, opening the access to new markets.

Hence, four major aims were delineated:

(i) Validate the molecular composition of UCB-MNCs-sEVs produced with an optimized process developed for future GMP production and clinical application;

(ii) Evaluate the UCB-MNCs-sEVs effect in inflammation;

(iii) Characterize the immunomodulatory properties of UCB-MNCs-sEVs;

(iv) Perform proof-of-concept studies in a disease model (psoriasis).

Chapter 2: Materials and Methods

2.1. Manual or automatic isolation of human UCB mononuclear cells

The human UCB samples were obtained upon signed informed consent, in compliance with Portuguese legislation. The collection was approved by the ethical committees of Centro Hospitalar e Universitário de Coimbra, Portugal. The samples were stored and transported to the laboratory in sterile bags with anticoagulant solution (citrate-phosphate-dextrose). Samples were processed within 48 h after collection. Mononuclear cells (MNCs) were isolated by density gradient separation (Lymphoprep TM - StemCell Technologies SARL, Grenoble, France). In the automatic isolation the UCB units were processed in an accredited cryobank (Crioestaminal®) using an automated system AXP, according to the manufacturer recommendations. Briefly, cord blood is transferred into the processing bagset which is placed in the AXP device and then centrifuged. The AXP device fits into most standard blood bank centrifuge buckets allowing up to six samples to be processed simultaneously. During centrifugation, component stratification and separation occurs. RBCs are transferred to a separate sterile bag, the buffy coat which contains the MNC rich layer is delivered to a separate sterile freezing bag while the plasma remains in the processing bag[257].

2.2. UCB cell culture

The UCB-MNCs (2 000 000 cells/mL) were cultured at 37 ºC in X-VIVO 15 serum-free cell-culture medium (Lonza Group Ltd, Basel, Switzerland) supplemented with 0.5 ug/mL of FMS-like tyrosine kinase-3 and 0.5 µg/mL of stem-cell factor, under ischemia (0.5% O_2) conditions. After 18 hours of secretion the conditioned media was carefully removed to proceed with the sEVs purification

2.3. sEVs isolation by differential ultracentrifugation

EVs were purified by differential centrifugation as described in Thery C. et al. (2006)[210]. Briefly, the conditioned media was subjected to sequential centrifugation steps of 300 xg (10 min), 2000 xg (20 min), and two times at 10 000 xg (35 minutes), for removal of cells, cell debris, and microvesicles, respectively. The supernatant was filtrated through a 0.22 µm pore followed by a 2:18h centrifugation at 100 000 xg in a SW32Ti swinging bucket rotors (Beckman). The pellet

was then washed with 20 mL of PBS and centrifuged at 100 000 xg for another 2:18h. The pellet containing the exosomes was re-suspended in 250µL of sterile PBS. The exosomes were quantified based on their protein content using a Micro BCA™ Protein Assay Kit from ThermoScientific.

2.4. sEVs isolation by Ultrafiltration and Size Exclusion Chromatography

The conditioned media was cleared by 2 sequential centrifugation steps of 300 xg (10 min) and 2000 xg (20 min). After these steps, the supernatant was collected and subjected to two filtration steps using a syringe, first using a 0.45 µm filter and afterwards a 0.22 µm. After this initial clearance, the media was filtered in ultrafiltration step using a pressure-controlled device (VivaCell 250®). The supernatant was subject to a 3 bar pressure through a 100 kDa filter in a Vivacell (Sartorius) device and the supernatant containing the exosomes was recovered in the top compartment after a washing step with filtered PBS. Then, 15 mL of the concentrated solution were submitted to a SEC using a Superose 6 pre-packed XK 26/70 (GE Healthcare). The equipment for SEC is a FPLC- Akta Avant Chromatographic system. A Filtered PBS solution was used as elution buffer at a flow rate of 3 mL/min (XK 26/70) and UV absorbance was detected at three wavelengths: 220, 260 and 280 nm. Fractions of 5 mL were collected, using a refrigerated automatic fraction collector coupled with the equipment.

2.5. Nanoparticle Tracking analysis (NTA)

The size distribution and concentration of the sEVs was measured in Nanosight LM 10 (Malvern Instruments Ltd, Malvern UK) equipped with a 638 nm laser, and the data was analyzed with NTA software. The measurements were performed with a detection threshold set to 3, camera level set to 13 and a screen gain of 10. The blur and Max Jump Distance were set to 2. The sEVs samples were diluted to obtain a particle number per frame between 15 and 30. Readings were taken in 5 captures during 30s each at manual monitoring of temperature.

2.6. Transmission Electron Microscopy and immunolabeling

The samples were mounted on 300 mesh formvar copper grids, stained with uranyl acetate 1%, and were examined using a Jeol JEM 1400 transmission electron microscope (Tokyo). Images were digitally recorded using a Gatan SC 1000 ORIUS CCD camera (Warrendale, PA, USA), and photomontages were performed using Adobe Photoshop CS software (Adobe Systems, San Jose,

CA), at the HEMS / IBMC - Institute for Molecular and Cell Biology (IBMC) of the University of Porto, Portugal.

For the CD63 immunogold labeling, sEVs were prepared according to Thery C. et al. (2006). sEVs were fixed with 2% PFA and underwent single immunogold labeling with protein A conjugated to gold particles 10 nm or 15 nm in diameter (Cell Microscopy Center, Department of Cell Biology, Utrecht University). Grids were analyzed on a Tecnai Spirit G2 electron microscope (FEI, Eindhoven, The Netherlands) and digital acquisitions were made with a 4k CCD camera (Quemesa, Olympus, Münster, Germany).

2.7. Lipidomics

Lipids were extracted using chloroform and methanol. The samples were spiked with specific internal standards prior to extraction. The mass spectra were acquired on a hybrid quadrupole/Orbitrap mass spectrometer equipped with an automated nano-flow electrospray ion source in both positive and negative mode. The identification of lipids was performed using LipotypeXplorer on the raw mass spectra. For MS-only mode, lipid identification was based on the molecular masses of the intact molecules. MS/MS mode included the collision induced fragmentation of lipid molecules and lipid identification was based on both the intact masses and the masses of the fragments. This technique was executed at Lypotype GmbH.

The total choline concentration was quantified by Phospholipid assay kit (Sigma Aldrich). Approximately $1x10^{11}$ part/mL of each sample was used. The kit was used according to manufacturer instructions[258].

2.8. Mass Spectrometry

35µL of each purified sEVs sample was run on a 4-12% Bis-Tris gel, under denaturing conditions, for 5 min at 200 V with MES Running Buffer (NuPAGE, Invitrogen™). The whole run was cut, reduced and alkylated with 10 mM of DTT (45 min at 56 °C) and with 55 mM iodoacetamide (IAA, 30 min at 20 °C in the dark), respectively, and digested with trypsin overnight at 37 °C with a 10 ng/µl concentration (Sequencing Grade Modified Trypsin V5111, Promega). The tryptic peptides were extracted from the gel with acetonitrile (ACN), desalted using C18 microcolumns (Empore, 3M) and dried on a SpeedVac (ThermoSavant™ Scientific). The peptides were resuspended with LCMS water 0.1% formic acid (Fisher Chemicals) prior to LCMS analysis. For protein identification, an information-dependent acquisition (IDA) analysis by NanoLC-MS using TripleTOF 6600 (ABSciex, Framingham, MA, USA) was used. Peptides were separated through reversed-phase chromatography (RP-LC) in a trap-and-elute mode. Trapping was performed at 2

µl/min with 100% solvent A (0.1% formic acid in water, Fisher Chemicals), for 10 min, on a Nano cHiPLC Trap column (Sciex 200 µm x 0.5 mm, ChromXP C18-CL, 3 µm, 120 Å). Separation was performed on a Nano cHiPLC column (Sciex 75 µm x 15 cm, ChromXP C18-CL, 3 µm, 120 Å) at a flow rate of 300 $\mu L.min^{-1}$, applying a 90 min linear gradient of 5% to 30% (v/v) of solvent B (0.1% formic acid in acetonitrile, Fisher Chemicals).

Peptides were sprayed into the MS through an uncoated fused-silica PicoTip™ emitter (360 µm O.D., 20 µm I.D., 10 ± 1.0 µm tip I.D., New Objective). The source parameters were set as follows: 12 GS1, 0 GS2, 30 CUR, 2.4 keV ISVF and 100 ºC IHT. An information dependent acquisition (IDA) method was set with a TOF-MS survey scan (400-2000 m/z) for 250 msec. The 50 most intense precursors were selected for subsequent fragmentation and the MS/MS were acquired in high sensitivity mode (150–1800 m/z for 40 ms each) with a total cycle time of 2.3 sec. The selection criteria for parent ions included a charge state between +2 and +5, and count above a minimum threshold of 125 counts per second. Ions were excluded from further MS/MS analysis for 12 sec. Fragmentation was performed using rolling collision energy with a collision energy spread of 5. The following parameters were used to select peptide precursors: up to 1 missed cleavage; 6-45 amino acid-long; cysteine with carbamidomethylation; mass range of 400-1500 m/z; 2-6 precursor charges. In addition, a manual filter was also imposed and several precursors with z=6 were removed. Any duplicate m/z values (rounded up to the second decimal value) were removed automatically by Analyst. The obtained spectra were processed and analyzed using ProteinPilot™ software, with the Paragon search engine (version 5.0, Sciex). The following search parameters were set: search against Uniprot/SwissProt reviewed database restricted to *Homo sapiens* (accessed in May 2017); Iodoacetamide, as Cys alkylation; Tryspsin, as digestion; TripleTOF 6600, as the Instrument; ID focus as biological modifications and Amino acid substitutions; search effort as thorough; and a FDR analysis. Only the proteins with Unused Protein Score above 1.3 and 95% confidence were considered. Data was provided/obtained by the UniMS – Mass Spectrometry Unit, ITQB/IBET, Oeiras, Portugal.

The second UCB-MNCs-sEVs MS characterization was performed at CNC in Mass Spectrometry Unit. The used technique as well as procedure was identical to the previous described. Nonetheless, a greater amount of sample material was used: 50µg of three independent samples were analyzed. Besides, instead of one single run per sample, UCB-MNCs-sEVs proteins were segmented into three bands **(Figure 2.1).** The first one corresponds to high molecular weight protein until approximately 67kDa, the second corresponds to albumin band situated between 65-67 kDa, the third band groups proteins with molecular weight below 65kDa but higher than 20kDa and the last sections correspond to proteins with a molecular weight lower than 20kDa.

The obtained data was analyzed by functional enrichment analysis tool Funrich V3.0 and Panther online software.

Total protein quantification was performed by using Micro BCA™ Protein assay kit (Thermo Scientifics). A minimum of $1x10^{10}$part/mL of UCB-MNCs-sEVs were used to quantify protein content, according to manufacturer instructions.

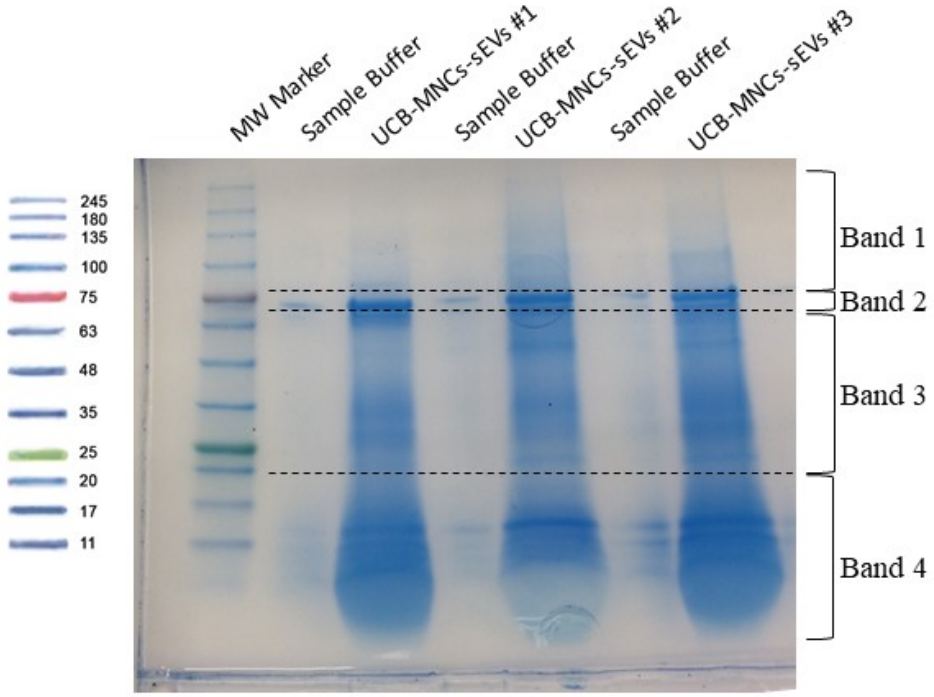

Figure 2.1. MS strategy to analyze UCB-MNCs-sEVs protein content. After running three UCB-MNCs-sEVs samples onto a polyacrylamide gel, four bands were excised for analysis. The first one corresponds to high molecular weight proteins until approximately 67kDa, the second corresponds to the albumin band situated between 65-67 kDa; the proteins in Band 3 have a molecular weight below 65kDa but higher than 20kDa; Band 4 corresponds to proteins with a molecular weight lower than 20kDa.

2.9. Flow cytometry for UCB-MNCs-sEVs

Flow cytometry data was acquired using a BD Accuri™ C6 (BD Biosciences). Briefly, $1x10^{10}$ particles of sEVs were incubated, during 15 minutes at room temperature, with 10µL of 3.8 µm aldehyde/sulphate latex, 4% (m/v) beads (Molecular probes® Lot. 1743119). A Phosphate Buffered Saline Solution (PBS) was added to a final volume of 1 mL and the solution was kept overnight at 4 ºC under a constant stirring in a microtube rotator. After the addition of 110 µL of glycine for 30 minutes the exosome coated beads were washed two times with 1 mL of PBS/0.5% BSA and resuspended in 500 µL of PBS/ 0.5% BSA. The coated beads were incubated, at 4 ºC for 30 minutes, with the fluorescent antibodies and their corresponding isotype control **(Table 2.1).** The labeled exosomes were washed twice with PBS/ 0.5% BSA and resuspended in 200 µL for analysis. Data was analyzed in FlowJo software v10.

Table 2.1. Conjugated Antibodies and respective isotype controls used for UCB-MNCs-sEVs characterization.

Antibodies	Reference
Human CD81 Allophycocyanin	FAB4615A, R&D System
Human CD63 Phycoerythrin	ADI-SPA-815-488-E, Enzo Life Sciences
Human CD9 Phycoerythrin	FAB1880P, R&D System
Human CD45 Alexa Fluor 488	345808, BD Biosciences
Anti-Human CD15 Allophycocyanin	17-0158-42, LabClinics
Mouse IgG1 Alexa Fluor 488 Isotype Control	IC002G, R&D System
Mouse IgG2B Phycoerythrin Isotype Control	IC0041A, R&D System
Mouse IgG2B Allophycocyanin Isotype Control	IC0041P, R&D System

2.10. Western Blot

UCB-MNCs-sEVs lysates were incubated in sample buffer with or without 350 mM 2-mercapthethanol (Sigma), boiled for 5 min, and fractionated by SDS-PAGE using polyacrylamide gel (10%) and transferred onto polyvinylidene difluoride (PVDF) membranes (Amersham™ Hybond®). The membranes were blocked in PBS/0.1%Tween-20 (PBS/T) with 5% non-fat dried milk, incubated with the indicated primary antibody diluted in PBS/T, washed four times in blocking solution, and finally incubated with HRP-conjugated secondary antibody followed by washing in PBS/T. Blots were developed using the ECL Plus Western blotting detection system (GE Healthcare) according to the manufacturer's instructions. Signal intensities were quantified with Image J software. Anti-CD63 and anti-calnexin antibodies were kindly provided by Graça Raposo (Institut Curie, Paris, France).

2.11. ELISA

Commercially available ELISA kits were used to quantify specific proteins in UCB-MNCs-sEVs samples. Each kit was prepared according to manufacturer instructions. Human serum albumin and hemoglobin were quantified using Human Serum Albumin ELISA Kit (ab179887, Abcam) and Human Hemoglobin ELISA Kit (ab157707, Abcam), respectively. CD63 and Annexin 2 were quantified employing Aviva System biology kits (ASB-OKEH01943 and ASB-OKEH01382, respectively).

2.12. RNA extraction and quality assessment

Total RNA was extracted from sEVs with the miRNACURY™ RNA Isolation Kit – Cell & Plant (EXIQON) using the Lysate Preparation from Cultured Animal Cells protocol (Section 1A) and then the Total RNA Purification from All Types of samples (Section 2). The following modifications to the standard protocol were carried out: 1) in Section 1A, Step 2/3, the lysis was performed with 700µl lysis solution plus 7µl β-mercaptoethanol by vortexing for 1 min. 400 µl of ethanol were then added to the lysate; 2) in Section 2, Step 2/3, the wash step was done with 700 µl of Wash Solution (3X). RNA elution was performed in two elution steps of 25 µl + 25 µl (instead of one elution with 50 µl). The amount and quality of total RNA and small RNA were assessed using the RNA 6000 Pico kit and the Small RNA kit in the Agilent 2100 Bioanalyzer (Agilent Technologies), respectively. Technical procedures were performed in accordance with manufacturer instruction.

2.13. RNA-Seq library preparation and next-generation sequencing

UCB-MNCs-sEVs RNA was isolated using EXIQON miRNACURY™ Isolation kit (Cell & Plants) and small RNA quality and quantification were performed in Bioanalyzer 2100 (Agilent). To construct each library, 1.5 ng of small RNA was hybridized and ligated to Ion Adapters v2 (Ion Total RNA-Seq Kit v2, Life Technologies, Carlsbad, CA). Small RNA samples were reverse transcribed to cDNA using adapter specific Ion RT primers v2 (Life Technologies, Carlsbad, CA) as described in Hill (2017)[259]. Purified cDNA samples were size-selected and amplified by PCR followed by further purification and size selection. cDNA samples were barcoded using Platinum PCR SuperMix High Fidelity polymerase with IonXpress RNA 3′ Barcode primer and unique 5′ Ion Xpress RNA-Seq Barcode Primers using the Ion Xpress RNA-Seq Barcode 1–16 Kit (catalog #4471250, Life Technologies, Carlsbad, CA). Yield and size distribution of the cDNA libraries were assessed using the Agilent 2100 BioAnalyzer DNA1000 chip (catalog #5067–1504, Agilent Technologies, Santa Clara, CA). Total barcoded cDNA within the 50–300 base pair range was considered to be derived from small RNA. 50 picomoles of each barcoded library were pooled and clonally amplified onto Ion Sphere™ Particles (ISPs), enriched and loaded in a Ion 530™ Chip Kit (catalog #A27764, Life Technologies, Carlsbad, CA) using the Ion Chef™ system (Life Technologies, Carlsbad, CA) and the Ion 520&530™ Kit-Chef (catalog #A27757, Life Technologies, Carlsbad, CA). Enriched ISPs were sequenced on the Ion S5™ Next Generation Sequencing system with 500 flows. Small RNA sequencing technique was performed at the Genomics i3S Scientific Platform.

2.14. RNA-Seq data processing, alignment and analysis

Data derived from the small-RNA sequencing of the 6 UCB-MNCs-sEVs samples provided was submitted to the program FASTQC for quality control. No hard sample trimming was performed, and it was used the aligner's own ability to ignore regions in reads which did not map to the human genome. Alignment was performed using aligner *Bowtie2* and then samples were aligned to the *RefSeq* genome GRCh38 (GCF_000001405.26_GRCh38_genomic), as it matches the genome used by the database MIRNABASE for identification and annotation of miRNAs. Cufflinks tool was used for annotation and estimation of the relative abundance of each gene in each sample. Cufflinks was performed using annotation against the whole human genome by RefSeq, to detect all small RNAs. The obtained data was generated by Bioinf2Bio.

2.15. Quantitative real time polymerase chain reaction on UCB-MNCs-sEVs

The analysis of genetic expression was performed mainly to evaluate and validate microRNA content of UCB-MNCs-sEVs. After RNA extraction and analysis, the absolute quantification of miRNANAs was performed by quantitative real time polymerase chain reaction (qPCR). Complementary DNA (cDNA) was synthesized by using miRNACURY™ LNA™ miRNANA RT Kit (339340, Qiagen). After RNA mixture with enzyme and kit buffer, samples were incubated for 60 min at 42ºC followed by 5 min at 95ºC. At the end, samples were diluted to 1:10 in RNase-free water and store at -20ºC. qPCR was performed using the NZYSpeedy qPCR Green Master Mix (2x), ROX in a 96-well format in CFX96 Touch™ Real-Time PCR Detection System (BioRad). The following conditions were used for qPCR, 95°C for 2min, followed by 40 cycles at 95°C for 5 s, 60°C for 30 s, 72°C for 20 s (measuring the fluorescence) were used for the qPCR. miRNACURY LNA miRNANA PCR Assays were used as primers in accordance with the desired sequence to be analyzed.

Due to the hurdles to define a reference gene/miRNANA for relative quantification, a calibration curve based on a miRNANA-mimic was used. For that, miRNAIDIAN microRNA (Horizon) were diluted in sequential RNA concentrations, transcribed to cDNA and run in qPCR at the same conditions as samples.

2.16. Evaluation of genomic DNA

An intronic gene region of CYP1B1 with 649 base pair (bp) was amplified in UCB-MNCs-sEVs samples in order to determine whether genomic DNA (gDNA) was or not present in the samples.

The used primers have the following sequences: CYPB1-E2F2 5' CATGATGCGCAACTTCTTCA-3' and CYPB1-E2R2 5'–ACTCCGCCTTTTTCAGAGG-3'. PCR reaction was performed using 0.26 U of Phusion enzyme (ThermoScientific, Waltham, Massachusetts), 1x Phusion HF buffer, 0.2 µM of each primer, 0.2 mM dNTPs (Bioron, Ludwigshafen am Rhein, Germany) and 0.75 µL of sample in a total volume of 12.5 µL. PCR reaction included an initial denaturation at 98ºC for 30s, followed by 35 cycles of 10 s at 98ºC, 45 s at 64 ºC and 60 s at 72 ºC. At the end. a final extension was done at 72ºC for 10 min. PCR layout included two controls: negative (water) and positive (37.5ng of cellular gDNA). The amplicons were visualized on an electrophoretic agarose gel (1% (p/v)).

2.17. Cell culture

Two different cell lines were used in the scope of this doctoral thesis. Normal human dermal fibroblasts (NHDF, ATCC ®, PCS-201-012TM) and human monocytic cells (THP-1, ATCC ®, TIB-202 TM). Cell lines were cultured in T75 culture flasks and, maintained in an incubator with controlled temperature (37 ºC), CO_2 level (5%) and humidity (90%).

NHDF cells were cultured in Fibroblasts Basal Medium (ATCC® PCS-201-030) supplemented with Fibroblast Growth Kit–Serum-Free (ATCC® PCS-201-040)), phenol red (33 µM) and Penicillin-Streptomycin-Amphotericin B Solution (Penicillin: 10 Units/mL, Streptomycin: 10 µg/mL, Amphotericin B: 25 ng/mL). Cells were subcultured when reaching ~80% confluence. Briefly, cells were washed with pre-warmed PBS (without Ca^{2+} and Mg^{2+}), detached with trypsin 0.05% at 37 ºC and then the reaction was stopped with complete culture medium. After that, cells were centrifuged for 5min at 300xg and suspended in culture medium. Cells were then counted using a Neubauer chamber and trypan blue, and then plated in the adequate cell plate format for the experiments.

THP-1 cells were cultured in RPMI-1640 Medium (Catalog No. 30-2001, ATCC®), supplemented with 2-mercaptoethanol to a final concentration of 0.05 mM and fetal bovine serum to a final concentration of 10%. Cultures were maintained by the addition of fresh medium at 2-4 x 10^5 viable cells/mL. Subculture was performed when cell concentration reached 8-10x10^5cells/mL

PBMNCs were collected from human blood samples obtained from the Hospital Universitário de Coimbra. These donations were derived from healthy volunteers after providing their informed consent. PBMNCs were isolated by Lymphoprep™ gradient centrifugation. PBMNCs were frozen and stored in liquid nitrogen. For *in vitro* experiments, cell aliquots were thawed at 37°C, added to 10 mL of RPMI 1640 and centrifuged at 300g for 5min to eliminate dimethyl sulfoxide (DMSO). Pellet was resuspended in RPMI 1640 supplemented with 10% of fetal bovine serum (FBS). PBMNCs were plated on 96-well flat bottom culture plates (Corning-Costar, Celbio,

Milan, Italy) at the density of 2-3 x 10^5 cells/well and cultured with RPMI 1640 medium containing 10 % FBS. For T cell activation, plate-bound anti-CD3 (5µg/ml) plus anti-CD28 (2µg/ml) were used.

2.18. *In vitro* transcription and translation assays

To assess cell capacity to transcribe and translate, NDHF were used. 10 000 cells were sedimented on µ-Slide Angiogenesis ibiTreat (81506, iBidi). Cells were seeded for at least 24h and according to experimental conditions, the medium was renewed to complete or starvation medium. UCB-MNCs-sEVs were administrated at 1x10^{10}part/mL After 18h incubation, cells were incubated for 30min or 4h with 5-ethynyl uridine (EU) (1mM) and homopropargylglycine (HPG) (500µM).
30 min before adding HPG, medium was changed for a pre-warmed L-methionine-free medium. Cells were then fixed with 4% PFA for 15 minutes at room temperature. The incorporation of EUTP was assessed with Click-iT® RNA Alexa Fluor® 488 Imaging Kit (Molecular Probes) according to manufacturer's protocol. The incorporation of HPG was measured by Click-iT® HPG Alexa Fluor™ 488 Protein Synthesis Assay Kit. Both readouts were obtained by confocal imaging (LSM 710, Carl Zeiss) and cell image analysis by Cell Profiler and Fiji. A new routine in Cell profiler was created. RGB-images were converted into black and white, and after applying a threshold, maximum values were counted to identify RNA polymerase I. A mask algorithm was applied to DAPI images and overlap with EU staining after subtraction of RNA polymerase I signal. Thus, mean intensity was measured to determine RNA polymerase II activity. While RNA polymerase II has a disperse and diffuse signal in the nuclei staining by EU, RNA polymerase I is identified as very bright spots where there is no DAPI staining. As RNA polymerase I requires nucleolin to transcribe we have confirmed this distinction between the two polymerases by staining with anti-nucleolin. As shown in **figure 2.2.**, there is the co-localization of both EU signal (green) and nucleolin (red).

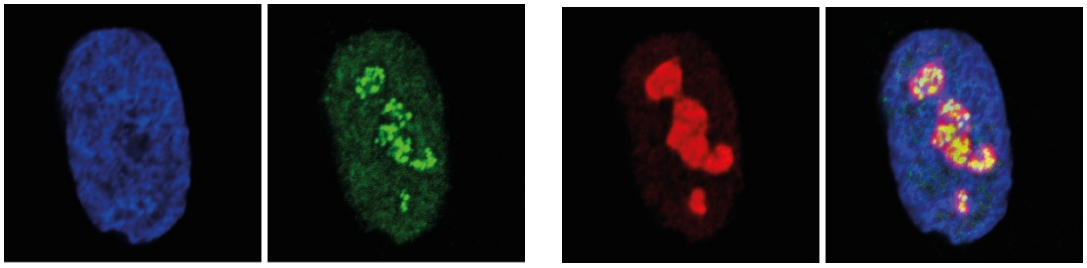

Figure 2.2. Validation of RNA polymerase transcription sites. Nuclei was observed at blue channel stained by DAPI, while EU is seen as green and nucleolin as red.

2.19. *In vivo* wound healing model

Animal testing protocols were approved by the Portuguese National Authority for Animal Health (DGAV), and all the surgical and necropsy procedures were performed according to the applicable national regulations respecting international animal welfare rules. Male C57BL/6 wild-type mice (8-10 week-old), purchased from Charles River (France) and weighing between 20 and 30 g, were housed in a conventional animal facility on a 12 h light/12 h dark regimen and fed a regular chow *ad libitum*. Diabetes mellitus was induced in mice by consecutive intraperitoneal injection of streptozotocin (50 mg/kg; in citrate buffer, pH 4.5; STZ, Sigma-Aldrich). The intraperitoneal injection was maintained once a day during 5 consecutive days. Glycemia was weekly monitored after STZ treatment with a glucometer with glucose test strips (Accu-Chek Aviva, Roche) and only animals with blood glucose levels greater than 300 mg/dL were used in this study (6-8 weeks after induction). Insulin (16-32 U/Kg or 0.4-0.8 U/mouse, Sigma-Aldrich) was injected only for weight maintenance, if necessary. To induce wounds in these animals, they were anesthetized by intramuscular injection of a xylazine/ketamine solution (ketamine hydrochloride, 10 mg/mL, (Imalgene®, Merial, Barcelona, Spain), 50 mg/kg of body weight, and xylazine hydrochloride, 2 mg/mL, (Rompun®, Bayer Healthcare, Germany), 10 mg/kg of body weight), then shaved and the dorsum disinfected with a povidone-iodine solution (Betadine®). Two 6 mm diameter full-thickness excision wounds were performed with a sterile biopsy punch in the dorsum of each animal separated by 5 cm. The treatments were applied immediately after the wound creation and were repeated when mentioned. Animals were kept in individual cages with food and water *ad libitum* and observed daily during the total period of the experiment.

2.20. Animal testing: wound treatment and healing monitoring

The animals were divided in different groups accordingly to the treatment applied. sEVs were applied topically in the wound bed, as a single application after wound infliction (day 0), twice a day until 10 days, during the experimental time the animals were kept in individual cages with food and water *ad libitum*. The progress of wound closure was monitored daily by measuring the wound area. The excision wounds were traced onto an acetate and wound size was determined with the ImageJ software (NIH). The percentage of wound area was presented as percentage of original wound (day 0) and calculated following the equation: (area of actual wound / area of original wound) × 100%.

2.21. *In vivo* gene expression analysis on wounds

The total RNA from mice skin wound biopsies was extracted using Trizol reagent (NZYol; NZYTech). Before initiate the RNA extraction, samples were incubated at room temperature for 5 minutes. Chloroform for molecular biology, DNase, RNase and protease free (Fisher Bioreagents) was added. The solution was shacked vigorously for 15s, incubated for 5 min at room temperature and then centrifuged at 12 000 xg for 15 minutes at 4ºC. After this step, the aqueous phase (upper) was collected and then the RNA was precipitated with addiction of isopropanol for molecular biology (Enzymatic). The solution was incubated at room temperature for 10 minutes and then centrifuged at 12000xg for 10 minutes at 4ºC. The resulting pellet was washed with 75% ethanol absolute for molecular biology (Fisher Bioreagents) solution and centrifuged at 7 500xg for 5 minutes at 4ºC. When dry, the resulting pellet was resuspended in 20 µL of ddH2O (NZYTech) and RNA concentration was measured in Nanodrop (Thermo Scientific). All RNA samples were stored at -80ºC.

QuantSeq technology has been used as alternative to microarrays and conventional RNA-seq, in order to measure gene expression. cDNA libraries for each sample were generated at Gene Expression Unit (Instituto Gulbenkian de Ciência, Portugal) from 50 ng of total RNA using the Quantseq 3′ mRNA-Seq Library Prep kit for Illumina (Lexogen) following the manufacturer's instructions. FASTQ files were processed using the QuantSeq 3′ mRNA-seq pipeline followed by differential expression pipeline implemented on the Bluebee genomic platform (Bluebee). To identify pathways and biological processes affected in response to UCB-MNCs-sEVs, Funrich software and IPA were used. For this analysis, only differential expressed genes with a p-value smaller than 0.05 and count number higher than 10 were considered.

Some of the identified genes were validated by qPCR. For that, RNA was reverse transcribed according to manufacturer's instructions of SuperScript IV VILO Master Mix (Invitrogen). After reverse transcription, the cDNA was immediately used for qPCR or were preserved at -20ºC. qPCR was performed using the NZYSpeedy qPCR Green Master Mix (2x), ROX in a 96-well format in CFX96 Touch™ Real-Time PCR Detection System (BioRad). The following conditions, 95°C for 2min, followed by 40 cycles at 95°C for 5 s, 60°C for 30 s, 72°C for 20 s (measuring the fluorescence) were used for the qPCR. At least three biological replicates were used. The primers are listed in **Table 2.2**. GAPDH was used as an endogenous control to normalize each sample. The resulting data was analysed using Bio-Rad CFX Manager software.

Table 2.2. Mouse primer sequences used on wounded skin.

Target Gene	Forward Sequence	Reverse Sequence
IL-6	TAGTCCTTCCTACCCCAATTTCC	TTGGTCCTTAGCCACTCCTTC
IFN-γ	CGGCACAGTCATTGAAAGCCTA	GTTGCTGATGGCCTGATTGTC
IL-1β	TCCAGGATGAGGACATGAGCAC	GAACGTCACACACCAGCAGGTTA
TNF-α	GTTCTATGGCCCAGACCCTCAC	GGCACCACTAGTTGGTTGTCTTTG
CCL20	ACTGTTGCCTCTCGTACATACA	GAGGAGGTTCACAGCCCTTTT
CXCL-1	GCTTGAAGGTGTTGCCCTCAG	AGAAGCCAGCGTTCACCAGAC
CD163	CAGACTGGTTGGAGGAGAAATC	TGACTTGTCTCTGGAAGCTG
IL-10	GACCAGCTGGACAACATACTGCTAA	GATAAGGCTTGGCAACCCAAGTAA
Arginase-1	AAGAAAAGGCCGATTCACCT	CACCTCCTCTGCTGTCTTCC
iNOS	TCTCCCTTTCCTCCCTTCTT	AAACTCAACCTCCTGACTGAAG
FoxP3	CACCCAGGAAAGACAGCAACC	GCAAGAGCTCTTGTCCATTGA
TGF-β	CTTCAATACGTCAGACATTCGGG	GTAACGCCAGGAATTGTTGCTA
Fn	GCTCCTCTTAGGGGCCACT	CCACGTCTCACCATTGGGG
Col1a1	GCTCAGCAAATCGTGCAGC	CTAGGTAGGTCCGTTCCCACT
Col3a1	CCTGGCTCAAATGGCTCAC	GACCTCGTGTTCCGGGTAT
keratin 10	CGAAGAGCTGGCCTACCTAAA	GGGCAGCGTTCATTTCCAC
GAPDH	AGCTTGTCATCAACGGGAAG	TTTGATGTTAGTGGGGTCTCG
β-actin	ACCACACCTTCTACAATGAG	ACGACCAGAGGCATACAG

2.22. Flow cytometry and cell sorting

PBMNCs were collected and erythrocytes were osmotically lysed in red blood cell lysis buffer. When evaluating THP-1 cell surface markers, cells were collected, washed in PBS before cell staining. For cell surface staining, single-cell suspensions were incubated for 30 min with saturating concentrations of monoclonal antibodies **(Table 2.3).**

To evaluate specifically FoxP3 expression, cells were stained for the above identified cell surface markers, fixed 30 min at 4°C, permeabilized with the Foxp3/Transcription Factor Staining Buffer set (eBioscience) for 15 min at 4°C, and lastly incubated for 1 hour at 4°C with the above identified antibodies in permeabilization buffer.

Samples were acquired using BD accuri C6 (BD Biosciences). Data were analyzed using FlowJo 7.0.0. software.

When CD4 T lymphocytes were sorted, PBMNCs followed the same staining procedure as for flow cytometry analysis. At the end, cells were passed through cell sorter (FACS Aria II ^{TM}, BD bioscience) and collected directly on RNA lysis buffer to further RNA extraction.

Table 2.3. Antibodies for PBMNCs T cell phenotyping.

Antibody	Reference
Anti-Human CD25 FITC	555431, BD Bioscience
Anti-Human FoxP3 Alexa Fluor 647	560045, BD Bioscience
Anti-Human CD4 PE	555347, BD Bioscience
Anti-human IFN-gamma	502502, BioLegend
7-AAD Staining Solution	559925, BD Bioscience
Anti-Human CD3 Pacific Blue	558117, BD Bioscience
Anti-human CD127 (IL-7Ralpha) PE/Cy7	351320 (453431), BioLegend
Anti-Human CD3 APC	555335, BD Bioscience
Anti-human CD45 FITC	345808, BD Bioscience
Anti-Human CD14 PE-Cy7	557742, BD Bioscience
Anti-Human CD 163 PE	556018, BD Bioscience
Anti-Human CD86 APC	555660, BD Bioscience
Anti-Human CD8 PerCP-Cy5.5	565310, BD Bioscience
Anti-Human IL-17A Alexa Fluor 647	560437, BD Bioscience

2.23. Gene expression analysis

RNA samples were extracted by RNAeasy Mini kit (Qiagen) according to manufacture recommendation. RNA concentration was quantified with total RNA chips in Bioanalyzer 2100 (Agilent). All RNA samples were stored at -80ºC. RNA was reverse transcribed according to manufacturer's instructions of SuperScript IV VILO Master Mix (Invitrogen). After reverse transcription, the cDNA was immediately used for qPCR or were preserved at -20ºC. qPCR was performed using the NZYSpeedy qPCR Green Master Mix (2x), ROX in a 96-well format in CFX96 Touch™ Real-Time PCR Detection System (BioRad). The following conditions, 95°C for 2min, followed by 40 cycles at 95°C for 5 s, 60°C for 30 s, 72°C for 20 s (measuring the fluorescence) were used for the qPCR. At least three biological replicates were used. The primers are listed in **Table 2.4.** β-actin (ACTB) or GAPDH were used as an endogenous control to normalize each sample. The resulting data was analysed using Bio-Rad CFX Manager software.

Table 2.4. List of human primers used in this study.

Target Gene	Forward Sequence	Reverse Sequence
Fn	CCATAGCTGAGAAGTGTTTTG	CAAGTACAATCTACCATCATCC
Col1a1	GCTATGATGAGAAATCAACCG	TCATCTCCATTCTTTCCAGG
Col3a1	ATTCACCTACACAGTTCTGG	TGCGTGTTCGATATTCAAAG
VEGF	AATGTGAATGCAGACCAAAG	GACTTATACCGGGATTTCTTG
TGF-β	AACCCACAACGAAATCTATG	CTTTTAACTTGAGCCTCAGC
β-actin	GACGACATGGAGAAAATCTG	ATGATCTGGGTCATCTTCTC
α-SMA	AGATCAAGATCATTGCCCC	TTCATCGTATTCCTGTTTGC
bFGF	TGGCTTCTAAATGTGTTACG	GTTTATACTGCCCAGTTCG
PDGF	GGGCAGGGTTATTTAATATGG	AATCAGGCATCGAGACAG
VEGFA	AATGTGAATGCAGACCAAAG	GACTTATACCGGGATTTCTTG
COX2	ATCTACCCTCCTCAAGTCCC	TACCAGAAGGGCAGGATACAG
KRT10	AAGAGCAAGGAACTGACTAC	CGTCTCAATTCAGTAATCTCAG
IL-1β	CTAAACAGATGAAGTGCTCC	GGTCATTCTCCTGGAAGG
IL8	GTTTTTGAAGAGGGCTGAG	TTTGCTTGAAGTTTCACTGG
TNF-α	AGGCAGTCAGATCATCTTC	TTATCTCTCAGCTCCACG
IFN-γ	GGTAACTGACTTGAATGTCC	TTTTCGCTTCCCTGTTTTAG
IL-6	GGTACATCCTCGACGGCATCT	GT GCCTCTTTGCTGCTTTCAC
CXCL10	TTCAAGGAGTACCTCTCTCTAG	CTGGATTCAGACATCTCTTCTC
DEFβ4	ATCAGCCATGAGGGTCTTGT	GAGACCACAGGTGCCAATTT
S100A7	CCAAACACACACATCTCACTCA	TCAGCTTGAGTGTTGCTCATC
FoxP3	GCTTCATCTGTGGCATCATC	TGGAGGAACTCTGGGAATGT
Gata3	CGCCTGCGGGCTCTATC	CCTTCGCTTGGGCTTAATGA
t-bet	GATGTTTGTGGACGTGGTCTTG	CTTTCCACACTGCACCCACTT
RORγδ	TGGACCACCCCCTGCTGAGAA	CTTCAATTTGTGTTCTCATGACT

2.24. Three dimensional "Epidermis-like" model

The three-dimensional (3D) *in vitro* “Psoriasis like” Reconstructed Human Epidermis was obtained from Sterlab (205HTSPSO model; France). Cultures were maintained with supplied culture media. The supplied inserts were placed into a 12 well feeder-plate and allowed to equilibrate for a day at 37 ºC with 5% CO_2 before exposures, as described in the manufacturer’s instructions. Each insert was treated with 20 µL of UCB-MNCs-sEVs ($4x10^9$part/cm^2 which corresponds to $1x10^{10}$part/mL) or PBS daily for 5 consecutive days.

mRNA transcripts were evaluated by qPCR. RNA extraction and cDNA synthesis were performed as described previously. At the end of experiment, supernatant of each insert was collected, and protein quantification was performed. Three commercial kits from Biolegend were used: Human

TNF-alpha ELISA MAX™ Deluxe (430205), Human CCL20 (MIP-3alpha) ELISA MAX™ Deluxe (441404) and Human IL-17A ELISA MAX™ Deluxe (433915).

2.25. Imiquimod-induced psoriasis-like mice model

60 C57BL/6 background mice (8-12 weeks) were used for *in vivo* experiments. All animals were kept in pathogen-free conditions at the CNIC animal facility. Experimental procedures were approved by the local Committee for Research Ethics and are in accordance with Spanish and European guidelines. Mice were shaved on the back skin and received daily, for 6 consecutive days, topical applications of imiquimod (IMQ) (3.125 mg) from a commercially available cream (5%) (Aldara; 3M Pharmaceuticals). After 1hour of IMQ application, topic-UCB-MNCs-sEVs ($3.3x10^9$ part/cm^2) treatment was applied. Intravenous injection of UCB-MNCs-sEVs was administrated in vein tail in 50µL of saline solution.

Mice were sacrificed and skin, LN, spleen and blood samples were collected. Skin samples were divided in three pieces. The first one was used for haematoxylin/eosin (HE) staining, the second was rapidly frozen in liquid nitrogen for subsequent isolation of total RNA or detection of tissue cytokines and the last one was digested with Liberase TM (Roche) and used for flow cytometry analysis. LNs and spleen samples were divided in two where one part was also rapidly frozen in liquid nitrogen for subsequent isolation of total RNA or detection of tissue cytokines and the other half was used for flow cytometry and cell culture. Finally, blood sample was used for flow cytometry analysis and serum collection for further cytokine detection.

HE staining was completed on 5 µm thick paraffin sections using standard protocols. Epidermal thickness was quantified using NanoZoomer Digital Pathology (NDP.view 2.7.25) software. For each animal, 5 measurements were taken for one section (20 measurements per animal). Epidermal thickness was measured from the *stratum basale* to *stratum granulosum*, and excluded the *stratum corneum* and hair follicles.

Incubation of cell suspensions derived from skin, blood, LNs and spleens with anti-FcRII/III (clone 2.4G2) was always conducted prior to staining. For flow cytometry analysis, the following anti-mouse antibodies were used: CD45, GL3, CD25, and γδTCR obtained from eBioscience, CD11c, CD11b, Ly6G, Ly6C, CD44, CD62L, FoxP3 CD3, CD4 and CD8 from BD Bioscience. Absolute count of cells in the skin was conducted using BD Trucount Tubes (BD).

LN isolated cells from IMQ-treated animals and controls were incubated for 48 h on plate-bound anti-CD3 (5µg/ml), soluble anti-CD28 (2µg/ml) and IL23 plus IL-1β (10ng/ml each one). 4h before sample staining preparation for flow cytometry, brefeldin A (1µg/ml) was added to the culture. *In vitro* stimulated were fixed and permeabilized with Fix & Perm solution (BD Biosciences) and stained with anti-IL-22, anti-IFN-γ (E-Bioscience) and anti-IL10 and anti-IL-17 (BD Pharmingen). IFN-γ production in the culture supernatants was quantified with the Mouse

IFN-gamma ELISA MAX™ Deluxe kit (430804, eBioscience). RNA was extracted as previously described in "2.23 - Gene expression analysis" and gene-specific primers are listed in **Table 2.5.**

Table 2.5. Mouse primer sequences used on psoriatic-like skin and lymph nodes.

Target Gene	Forward Sequence	Reverse Sequence
IFN-γ	CGGCACAGTCATTGAAAGCCTA	GTTGCTGATGGCCTGATTGTC
TNF-α	GTTCTATGGCCCAGACCCTCAC	GGCACCACTAGTTGGTTGTCTTTG
CXCL-1	GCTTGAAGGTGTTGCCCTCAG	AGAAGCCAGCGTTCACCAGAC
IL-17A	TTTAACTCCCTTGGCGCAAAA	CTTTCCCTCCGCATTGACAC
IL-22	ATGAGTTTTTCCCTTATGGGGAC	GCTGGAAGTTGGACACCTCAA
FoxP3	CACCCAGGAAAGACAGCAACC	GCAAGAGCTCTTGTCCATTGA
RORγδ	CACGGCCCTGGTTCTCAT	GCAGATGTTCCACTCTCCTCTTCT
CCL20	ACTGTTGCCTCTCGTACATACA	GAGGAGGTTCACAGCCCTTTT
β-actin	ACCACACCTTCTACAATGAG	ACGACCAGAGGCATACAG
GAPDH	AGCTTGTCATCAACGGGAAG	TTTGATGTTAGTGGGGTCTCG

2.26. Statistical Analysis

Bar graphs are showed as mean ± standard error of mean (SEM). The statistical significance was assessed by two-tailed unpaired Student's t test, one-way ANOVA with Tukey's multiple comparison or two-way ANOVA with Bonferroni multiple comparison post-test, as required. All analysis was performed with GrapPhad software (Version 7.04). Differences were considered significant at $p<0.05$. * for p-value<0.05, ** for p-value< 0.01, *** for p-value <0.001 and **** for p-value<0.0001. When no indication appears, no statistical differences were detected.

Chapter 3: Characterization of optimized clinically transferable umbilical cord blood-derived small extracellular vesicles

Previous results demonstrated that UCB-MNCs-sEVs accelerate skin regeneration by promoting the proliferation of endothelial cells, fibroblasts and keratinocytes[253]. These vesicles are biologically active in cutaneous wound healing context, promoting tissue regeneration in wounds with a normal or delayed healing profile (excisional wounds performed in mouse models of diabetes). Topical application of UCB-MNCs-sEVs in these wounds had a better outcome than treatment with PDGF-BB, an approved therapy for wound regeneration[253]. Moreover, this data is protected under patent - PCT/IB2017/000412 - "USE OF UMBILICAL CORD BLOOD DERIVED EXOSOMES FOR TISSUE REPAIR".

Nevertheless, a standardized and up scalable method for isolation of EVs secreted by UCB-MNCs, which can be easily transferred into a GMP-compliant production unit has not been stablished. As part of the product development, we felt the need to implement several modifications into the sEVs manufacturing process, to increase scalability and to implement quality control measures that allow the future transference to GMP-compliant conditions in order to produce clinically compatible sEVs. Previously, UCB units were processed manually, MNCs where collected after by density gradient separation, ands EVs were isolated using sequentially UC. The combination of these steps posed many challenges namely: i) high variability; ii) user dependent; iii) time consuming; iv) low yield and v) limitations in scaling-up which would make their clinical applications unfeasible. To overcome these issues, automatic UCB processing was outsourced to Crioestaminal™ which is an authorized and accredited company that cryopreserves UCB. Additionally, we implemented an alternative UCB-MNCs-sEVs isolation process which is based in UF and SEC. This two techniques are currently being used for the isolation of EVs[209,260], presenting several advantages: i) easily standardized ii) up-scalable and easy to transfer to a GMP-compliant unit and iii) increased EVs yield and purity. To further increase scalability and decrease variability among batches, a donor pooling strategy was also adopted. In this work, each replicate of UCB-MNC-sEVs is a combination of vesicles obtained from 5 UCB units.

The new purification method is expected to increase the yield and the purity of UCB-MNCs-sEVs while generally maintaining the vesicles' molecular signature and their morphological

characteristics. In this chapter, we characterized the biophysical and biochemical properties of UCB-MNCs-sEVs in depth and addressed the regenerative potential of these clinically compatible EVs *in vivo* using a diabetic mouse model of wound healing. We envisioned that profound molecular characterization of the EVs would help us to identify the mode of action and potentially open new therapeutic opportunities.

3.1. Biophysical Characteristics

In 2018, the ISEV board members published a Position Editorial detailing their recommendations, based on their own established expertise, on the "minimal experimental requirements for definition of extracellular vesicles and their functions"[139]. Since consensus has not yet emerged on specific markers of EV subtypes, such as endosome-origin "exosomes" and plasma membrane-derived "ectosomes" (microparticles/microvesicles), assigning an EV to a particular biogenesis pathway remains extraordinarily difficult. Therefore, physical characteristics of EVs, such as size are recommended as an attribute to define EV subtypes[139]. In this way, "small EVs" (sEVs) are considered to be less than 200 nm while "medium/large EVs" are characterized by sizes higher than 200nm.

NTA is a technique based on the ability to track the Brownian motion of particles in suspension that enables the acquisition of particle parameters such as average particle size, modal value and size distribution[261]. Using NTA, the size distribution of the particles isolated with the optimized production process was characterized **(Figure 3.1A).** The profile of the curve is centered in sizes below 200 nm, and the average modal size obtained is close to 100 nm (102.7 ± 10.55 nm) **(Figure 3.1B)**. These values are compatible with the expected size of sEVs that is well reported in the literature to be within 50-200 nm[130,139,210]. Taking this into consideration and combined with MISEV2018 guidelines, we opted to designate the purified EVs from UCB-MNCs as UCB-MNCs-sEVs.

The broad size distribution profile obtained in our samples anticipated the presence of microvesicles, which we further described to be around 10%, with sizes within the range of 200-400 nm **(Figure 3.1C).** The contamination due to larger particles (>400nm) is negligible (less than 5%).

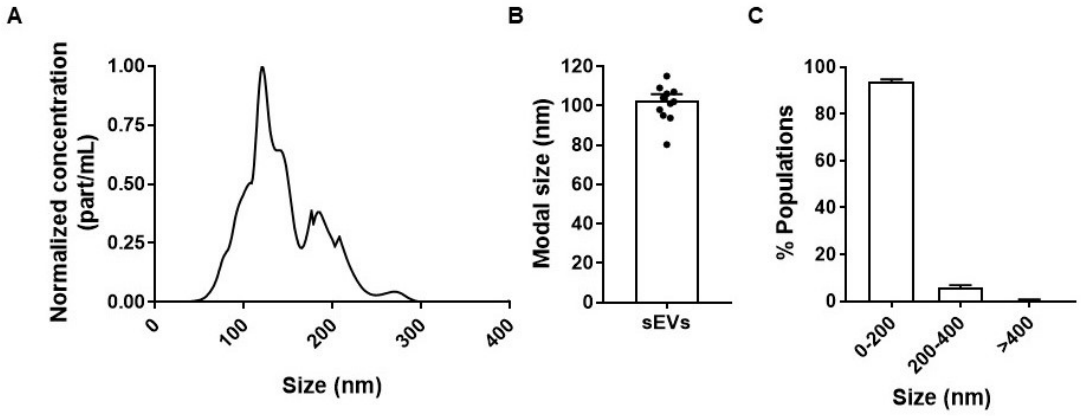

Figure 3.1. Morphological characterization of UCB-MNCs-sEVs isolated by the optimized procedure. (A) Representative size distribution of UCB-MNCs-sEVs normalized by concentration in particles/mL. Modal size (B) and populations distribution (C) of the UCB-MNCs-sEVs were evaluated by NTA. (n=12).

Interestingly, when compared with the previous isolation method (UC), the size distribution profile is significantly different specially in what concerns the presence of particles between 200 and 400nm (**Figure 3.2A)**. These differences are reflected in the modal size that is significantly higher in standard conditions of sEVs isolation when compared with the optimized procedure (**Figure 3.2B)**. Moreover, the final yield of particles obtained when using the new optimized purification method is significantly higher **(Figure 3.2C).**

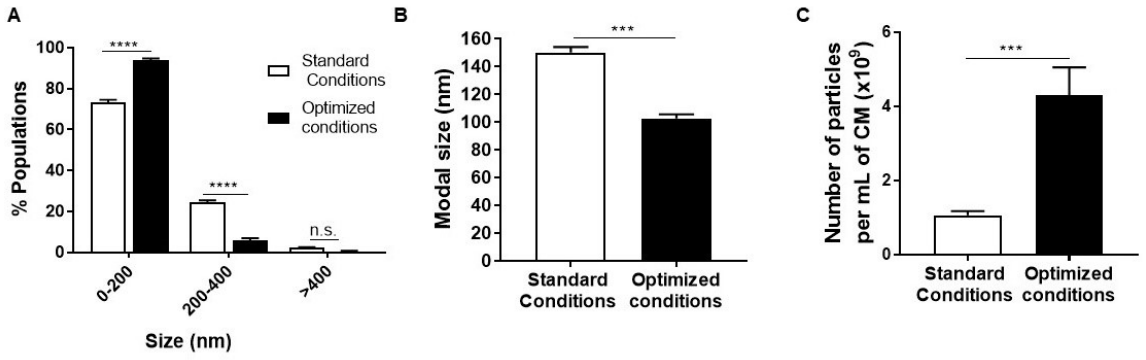

Figure 3.2. Optimized isolation procedure enriches UCB-MNCs-sEVs in vesicles with smaller size and increases the yield. NTA comparative analyses between sEVs isolated by two implemented methods showed higher abundance of smaller sEVs in optimized conditions (A) which leads to smaller EVs modal size (B). (C) Assessment of the number of total EVs in conditioned media (CM) reveals an increase in the recovery of particles using the optimized procedure. p-values were calculated by using unpaired t-test. (at least n=12).

Transmission Electron Microscopy (TEM) was also used for EVs visualization and determination of EVs diameter. As expected, sEVs presented a 'cup shaped' morphology. TEM data confirms that the fraction collected with the new purification method is significantly enriched in vesicles **(Figure 3.3A)** with diameter ranging from 100 to 150nm **(Figure 3.3B)**. This data corroborates NTA analysis not only in the mean size but also confirms the dominance of sEVs in the mixture (~80%) **(Figure 3.3C).**

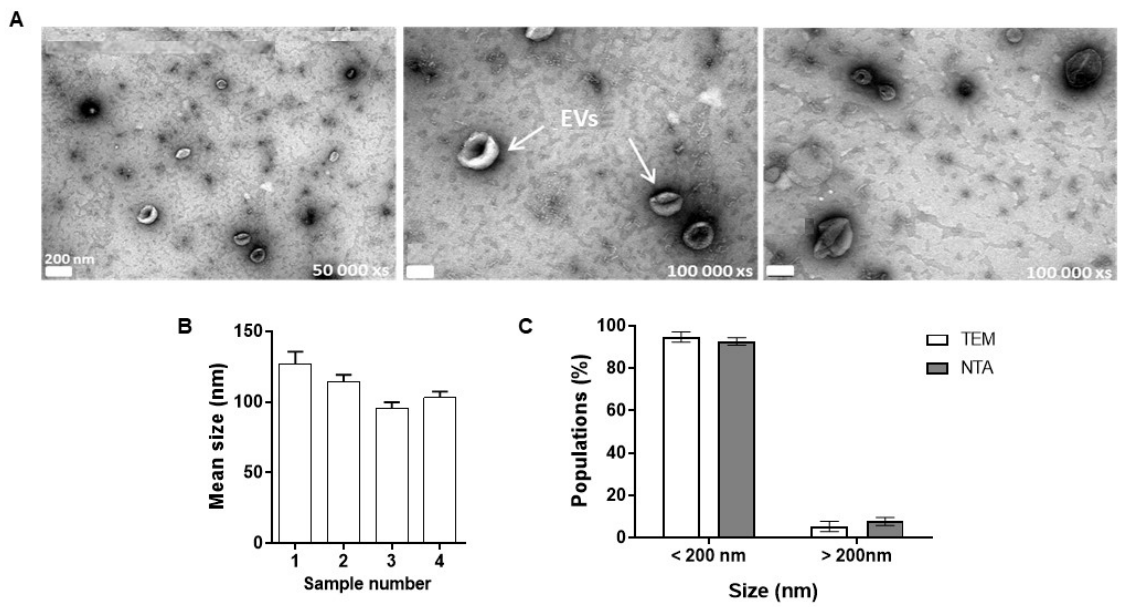

Figure 3.3. Morphological characterization of UCB-MNCs-sEVs isolated in the optimized conditions by TEM. (A) Representative TEM images of UCB-MNCs-sEVs with different magnification. Scale bar: 100 nm (middle and right image). (B) The sEVs mean sizes is about 100 nm when measured directly in the TEM images. (C) Comparison of population distribution between TEM and NTA. (at least n=3).

The extensive and multistep preparations needed for electron microscopy can easily induce changes in the morphology of the EVs[261]. It has been reported by several studies that EVs are spherical, however, other EVs are heterogeneous in shape[216,262]. To counter these problems, cryo-EM is being applied for EVs analysis, which introduces a different protocol for sample preparation. In this method, the specimen is kept and studied on vitreous ice at the temperature of liquid nitrogen, thus, the invasive steps such as dehydration or fixation are omitted [261].This avoids ultra-structural changes and redistribution of elements. In collaboration with Graça Raposo laboratory at Institut Curie (Paris, France), UCB-MNCs-sEVs were analyzed by cryo-TEM and immunolabeled with CD63. In fact, when compared with TEM images, cryo-TEM revealed a round structure of EVs variable in size, however not exceeding 200 nm. Moreover, this specific staining with CD63 antibody suggested that at least a proportion of UCB-MNCs-sEVS is likely to have an endosomal origin (**Figure 3.4).**

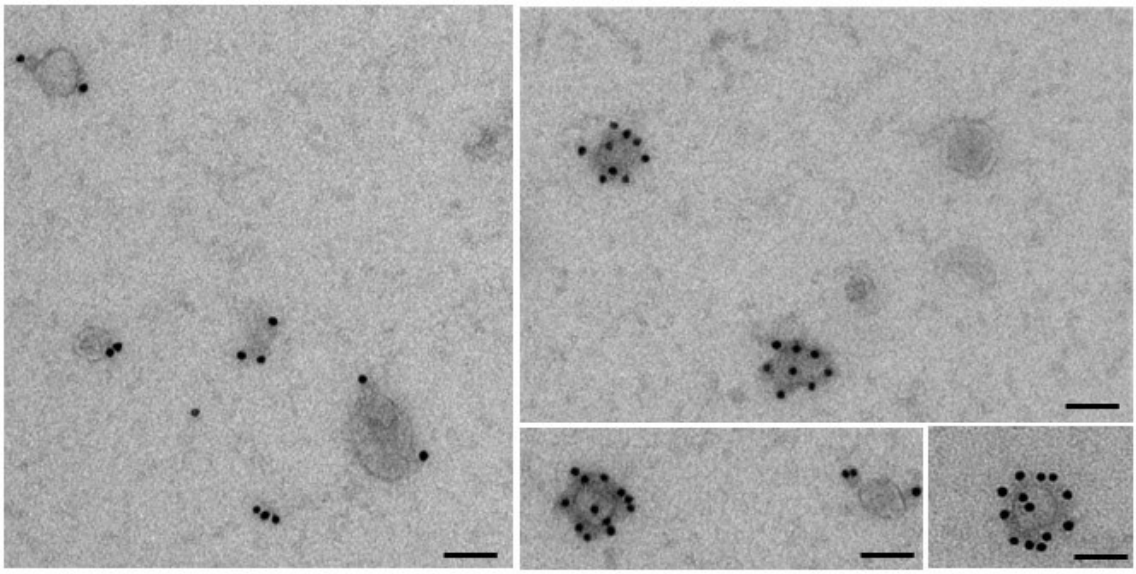

Figure 3.4. Immunolabeling of UCB-MNCs-sEVs with anti-CD63. An heterogenous EVs population is observed both in size and origin. CD63-stained vesicles are likely to have endosomal origin. Scale bar: 100 nm.

3.2. Biochemical Properties

3.2.1. Lipids

Lipids are not only an important structural component of sEVs comprising up to two-third of their volume[263], but they also have a key role in the interaction of sEVs with recipient cells. Additionally, these biomolecules have been implicated in multiple aspects of EV biogenesis and function. Due to the presence of lipid raft-associated proteins, including flotillin-1, in EVs, it is thought that lipid rafts may be influencing selective protein sorting into EVs[264]. Cholesterols, sphingomyelins and phosphatidylserine are the major components of lipid rafts and it is reported that all these three lipids are enriched in EVs when compared to their secreting cells[265].

To have some insight regarding the lipid composition of the purified UCB-MNCs-sEVs, we have used shotgun MS to identify the most abundant lipid species. 6 samples were analyzed after lipid extraction using chloroform and methanol[266]. Samples yielded between 7 900-16 200 pmol of lipids **(Figure 3.5A)** and these values are within the optimal range for lipidomic measurement. A total of 194 molecular lipid species were quantitatively identified in UCB-MNCs-EVs samples among which 118 were present in all samples**.** In average, UCB-MNCs-sEVs samples had 143.7 ± 31.3 pmol of DAG, 393.1 ± 159.3 pmol of PA; 3644.6 ± 696.2 pmol of PC; 1551.7 ± 370.9 pmol of PE; 27.3 ±11.6 pmol of PG; 450.0 ± 120.6 of PI; 3608.6 ± 1301.5 of PS; 2145.4 ± 584.6 pmol of SM and 7.0 ± 10.4 pmol of TAG (**Figure 3.5B**). From the results we observed that PC and PS compose almost 60% of the total lipid identifications, while SM and PE represent the other 30% (**Figure**

3.5C). The phospholipids containing a choline group (SPM and PC) represent almost 50% of the identifications**.** The cholesterol content of UCB-MNCs-sEVs was not also evaluated.

UCB-MNCs-sEVs are composed of very-long- fatty acid chains being SM (34:1), PS (38:4) and PC (34:1) the most abundant ones. The top 10 lipid species found in UCB-MNCs-sEVs are summarized in **Figure 3.5D.** These results are in line with what is described for sEVs obtained from other cell sources[159,265].

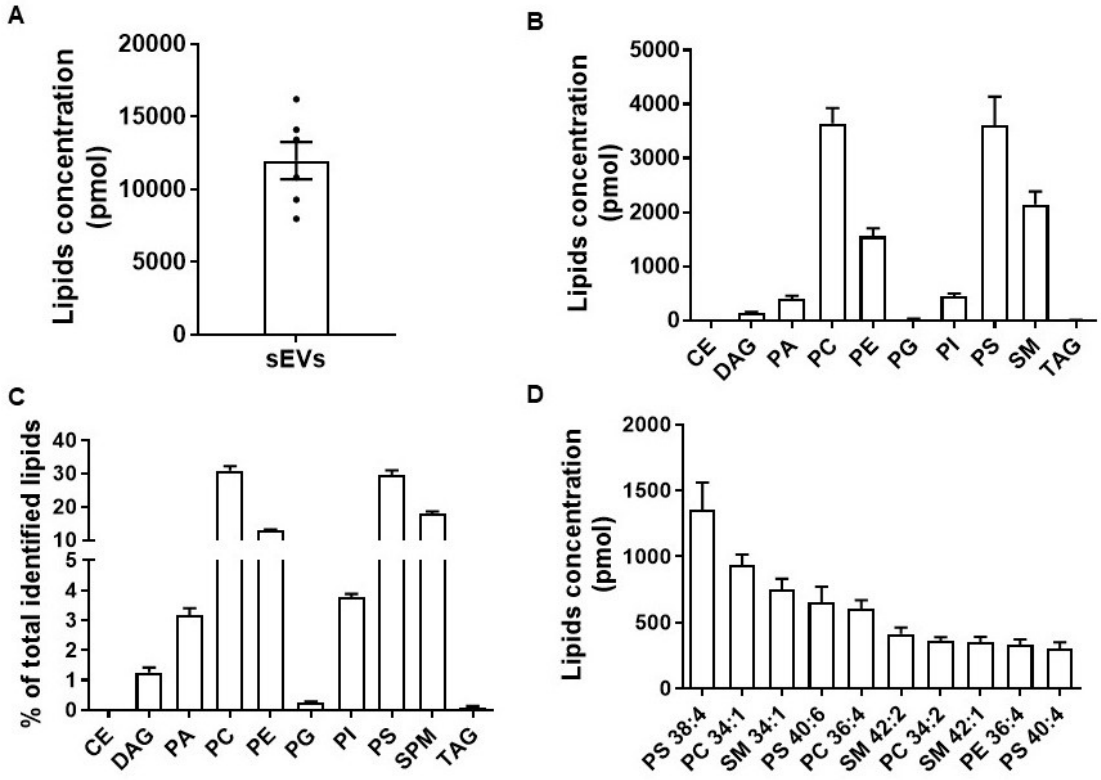

Figure 3.5. UCB-MNCs-sEVs lipid profile. (A) An average of 12 000 pmol of lipids extracted from 6 samples of UCB-MNCs-sEVs were analyzed by shotgun MS. Lipid distribution od the identified classes according to their concentration (B) and their relative abundance in the EVs preparation (C). In (D), the top 10 list is presented according to quantification of each lipid species in the sample. (n=6)

Lipid distribution was analyzed within each lipid class. Considering the PC, 31 different species were found and PC 34:1 and PC 36:4 are the two most represented molecules that together comprised around 45% of this lipid class **(Figure 3.6**). Within PS, 60% are resumed to PS 38:4 and PS 40:6 among the 23 biomolecules identified **(Figure 3.7)**. 15 SMs were identified and SM 34:1: SM 42:1 and SM 42:2 relative abundance within this class sum up to 70% **(Figure 3.8**). Finally, half of the PE class is composed by PE 34:1; PE 36:6 and PE 38:4 (**Figure 3.9**).

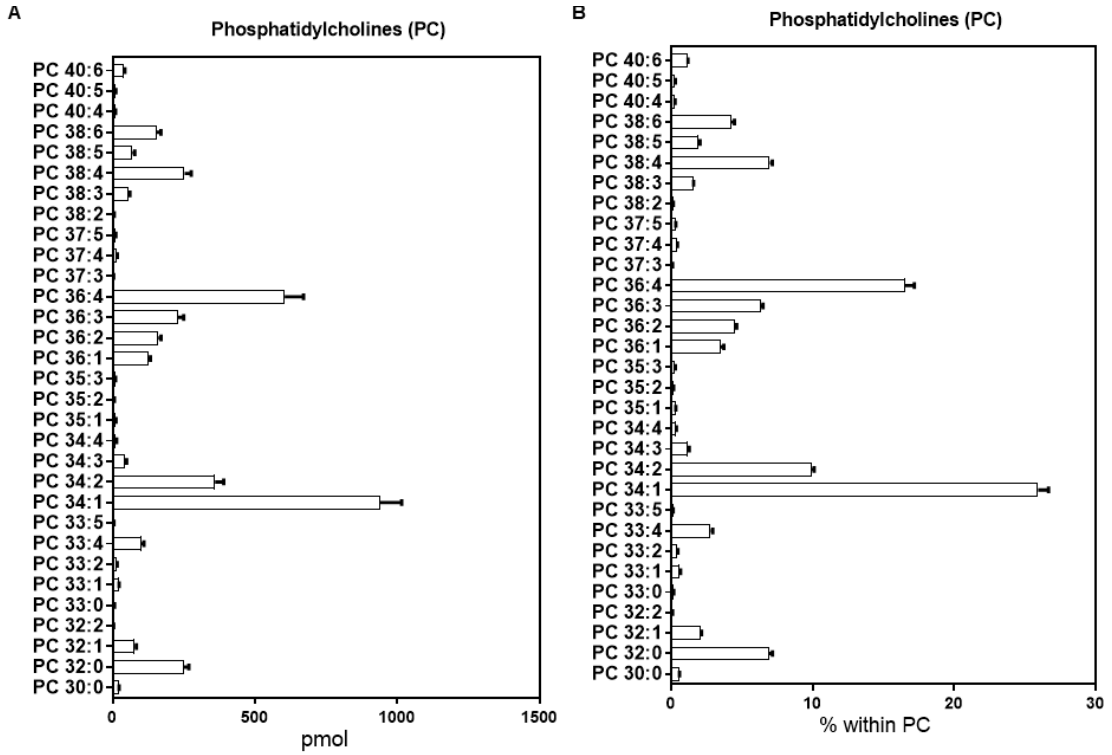

Figure 3.6. PC species composition of UCB-MNCs-sEVs. Graphs show (A) the mean absolute quantification of each lipid species in the PC class and (B) the mean percentages of each lipid species within PC. (n=6).

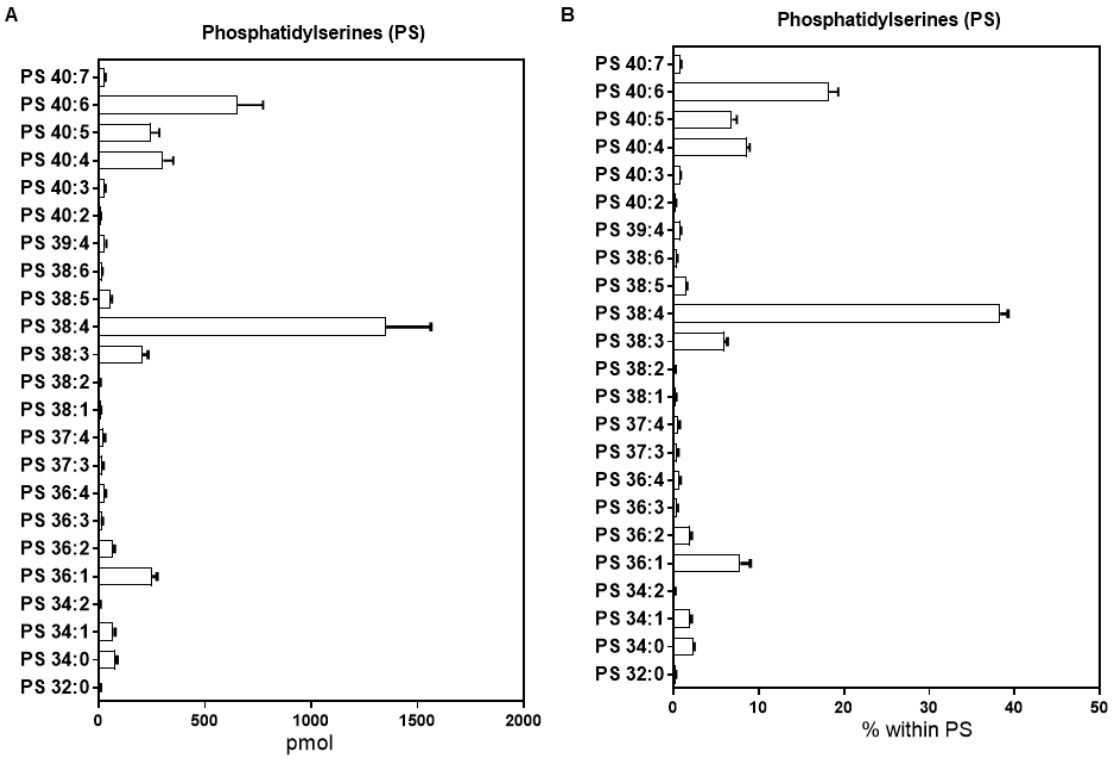

Figure 3.7. PS species composition of UCB-MNCs-sEVs. Graphs show (A) the mean absolute quantification of each lipid species in the PS class and (B) the mean percentages of each lipid species within PS. (n=6).

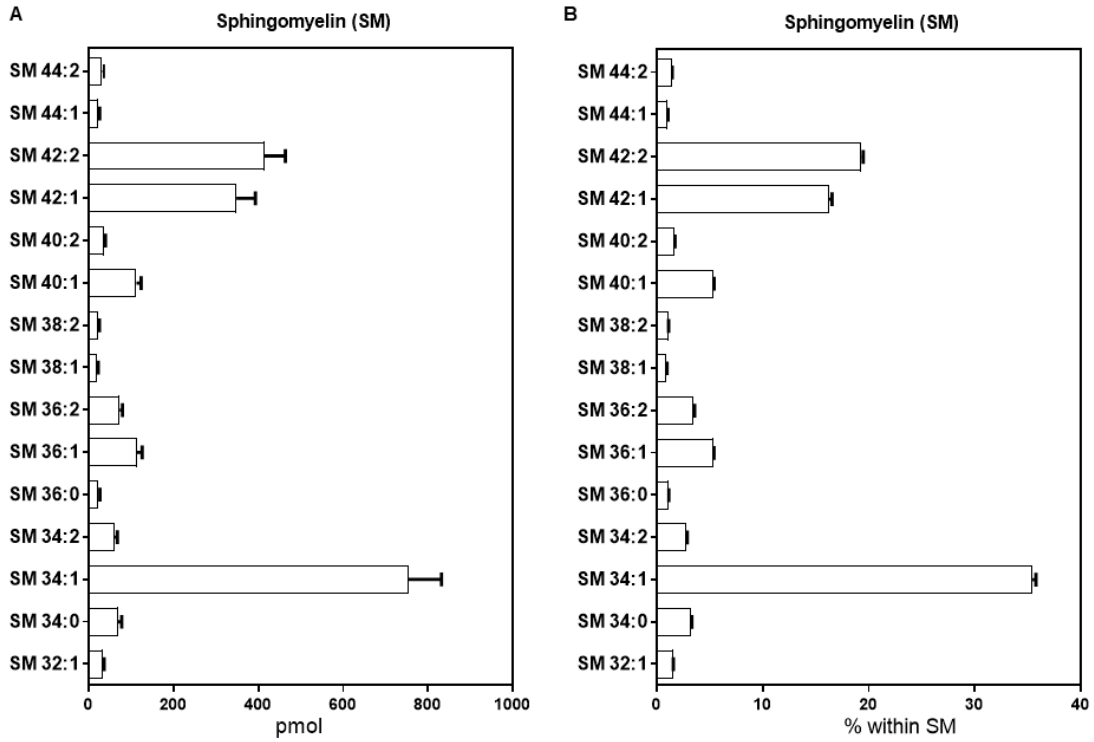

Figure 3.8. SM species composition of UCB-MNCs-sEVs. Graphs show (A) the mean absolute quantification of each lipid species in the SM class and (B) the mean percentages of each lipid species within SM. (n=6).

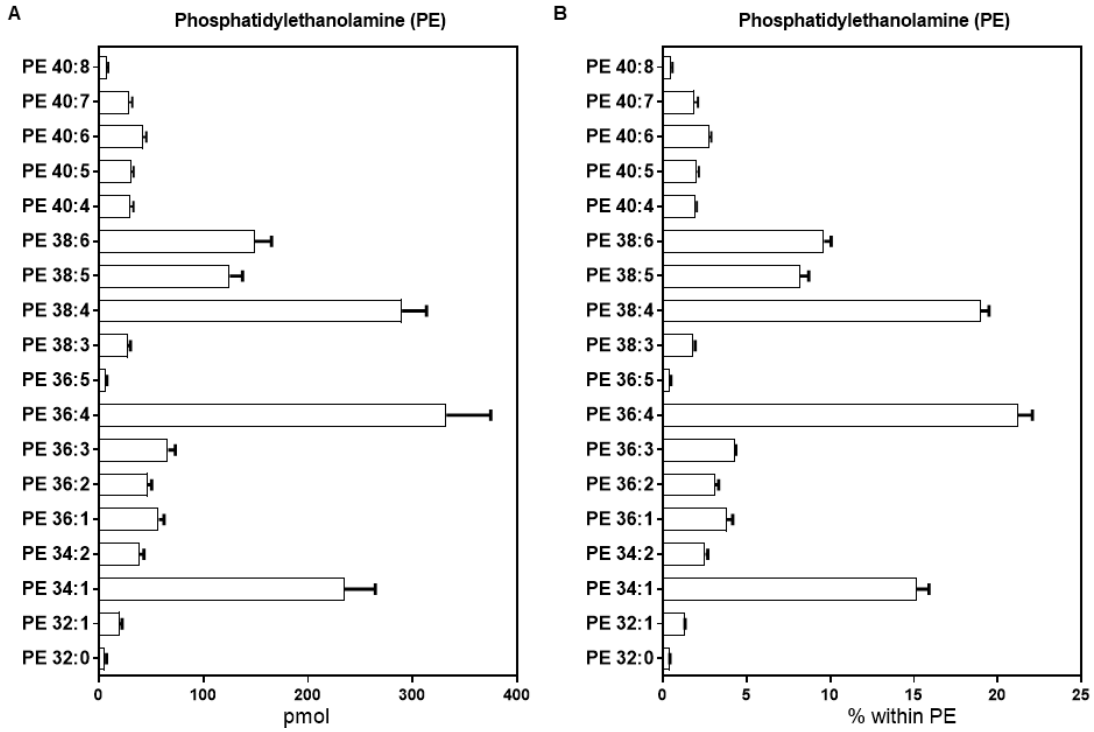

Figure 3.9. PE species composition of UCB-MNCs-sEVs. Graphs show (A) the mean absolute quantification of each lipid species in the PE class and (B) the mean percentages of each lipid species within PE. (n=6).

Due to sEVs biogenesis by inward budding of plasma membrane, it is expectable that their lipid composition agrees with the composition of cellular lipid bilayer. It is well established that there is an asymmetric distribution of lipid classes in the two leaflets of the plasma membrane[267]. Thus, sphingolipids and PC are mostly present in the outer leaflet, and the other lipid classes (PS, PE and PI) are mainly located in the inner leaflet [267]. In our samples, these lipidic groups represent more than 90% of the total lipid amount studied. Additionally, all lipid identified molecules are described in Vesiclepedia as reported by other authors when characterizing EVs preparations.

Lipidomic analysis of EVs derived from other cell sources showed several similarities in terms of lipidic composition[145,160,268–272] **(Table 3.1).** Excluding cholesterol content, UCB-MNC-sEVs have percentages of each lipid class similar to platelets and cell line derived-EVs, having comparable percentages of SM, PC, PS and PE. The biggest difference was between UCB-MNC-sEVs and adipocytes EVs. While our samples have similar percentages of PC and PS (~30%), adipocyte EVs showed 60% of PC and only 2% of PS. Although several similarities exist between all these EVs preparations, it is difficult to compare some of these results with the mentioned MS studies. In older studies of EVs derived from B-lymphocytes[269], mast cells[270] and dendritic cells[270] , lipid analyses were performed with thin layer chromatography (TLC) and/or gas liquid chromatography (GLC). In these studies, some lipid classes migrated as one band, including PS and PI, which can hinder the results interpretation as PS was later reported to be enriched from cells to exosomes while PI has an opposite tendency[273–275]. Recently, Haraszti et al. published regarding the composition of MSCs-EVs secreted in serum-deprived conditions[276]. In general, UCB-MNCs-sEVs composition is similar to those from MSCs having the same percentages of SM (18% versus 13%); PC (31% versus 37.3%), PE (13.0% versus 9.1%) and PA (3.2% versus 5.0%). However, discrepancies exist when PS and DAG abundance is compared. UCB-MNCs-sEVs have more PS (29.4% versus 9.3%) and less DAG (1.3% versus 20.1%).

Table 3.1. Lipid composition of EVs released by individual cell types in comparison with UCB-MNCs-sEVs. Adapted from [273]

	PC-3 cells	Oli-neu cells	HepG2/C3a	B-lymphocytes	Mast cells	Dendritic cells	Reticulocytes	Platelets	Adipocytes	UCB-MNCs-sEVS
SM	28.9	13.5	16.9	17.2	12.5	20.0	15.9	25.5	23.2	18.0
PC	27.1	44.0	34.8	15.2	29.2	26.0	44.4	32.4	61.2	31.0
PS	20.8	24.5	27.2	15.2	16.7	19.0	11.2	21.4	2.0	29.4
PE	10.3	18.0	12.9	10.9	25.0	26.0	24.0	6.3	7.4	13.0
PE ethers	3.9			9.7						
DAG	1.3								1.0	1.3
PC ethers	0.6							1.9		
PG	0.1									0.2
PA	0.1			10.1						3.2
PI	0.1		2.7	10.1	8.9	19.0	1.6	3.9	1.6	3.8
Cer	0.2		0.4					0.3	0.1	0.0
Lipid analysis	MS	MS	MS/GC	TLC	TLC / GLC	TLC / GLC	TLC	MS	MS	MS
EVs preparations	SFM + SUC	SFM + SUC + SG	uFCS + SUC + IG	uFCS + SUC + SG + IC	uFCS + SUC	uFCS + SUC	uFCS + SUC	SUC + IG	SFM + SUC	UF/SEC

* Methods used to isolate EVs preparations: SFM: serum free medium; uFCS: ultracentrifuged fetal calf serum; SUC: sequential centrifugation; SG: sucrose gradient; IG: iodixanol gradient, IC: immunocapture.

Although parental cells were not analyzed, lipidomic data characterization of blood cells was found in the literature[277]. Interestingly, all the lipid species reported in this study are present in our sEVs corroborating the fact that their lipid composition resembles that of the parental cells.

One of the major concerns regarding the purification of EVs is their contamination with other biological vesicles such as lipid droplets or lipoproteins, which cannot be eliminated along the purification steps[273]. CE and TAG are normally found in the core of lipid droplets[267], and cardiolipin in the inner membrane of mitochondria[278]. Therefore, high levels of these lipids in EVs preparations may indicate that lipid droplets, lipoproteins or mitochondria have been co-isolated with sEVs.

Our data shows that the amount of CE and TAG lipids in sEVs isolated with the optimized methodology is negligible which indicates that this new process does not co-isolate lipoproteins and lipid droplets with sEVs.

3.2.2. Proteins

To have further insight about the protein composition of UCB-MNCs-sEVs, LC-MS was performed in three samples that were analyzed as a unique band. 31 proteins were commonly identified between different donor batches (pools of 5 UCB**),** including serum albumin and hemoglobulin subunits in the top 10 list (**Table 3.2).** Ranking the proteins according to the average number of identified peptides with 99% of accuracy, it is possible to observe that top 10 list is mainly composed by blood proteins. Nevertheless, both albumin and annexin A7 are present in the top 100 EV proteins identified in sEVs [279]. Although the majority of top 10 identified protein are present in blood[280] or have red blood cells (RBCs) as their cell of origin[281,282], 9 out the 31 proteins (~29%) were described in sEVs and are at top 100 EV proteins listed on Vesiclepedia [279]. Serum albumin, haptoglobin and hemopexin are mostly described on sEVs derived from plasma or other blood derivatives[283–286] which indicates that these proteins may be contaminants of sEVs preparations rather than specific sEVs markers. In turn, annexins – more specifically in our samples Annexin A4, A5, A7 and A11 - are recognized as classical markers of different EVs subtypes namely sEVs[179]. This group of proteins regulate many aspects of the endocytotic pathway, and is associate with MVBs during their formation following receptor endocytosis, finally localizing into sEVs[287]. Transferrin receptor 1, another of the identified proteins, is a membrane glycoprotein, which can import iron by binding a plasma glycoprotein, transferrin[288]. It can be released in vesicular form during the maturation to erythrocytes[289] and it was through this process that sEVs were firstly described and studied[128]. The presence of this protein in sEVs is mostly reported in samples isolated from RBCs[290–292].

Finally, glyceraldehyde-3-phosphate dehydrogenase (GAPDH) was found in our samples, and it one of the proteins widely found in EVs from different cell sources[179,293–298]. Nevertheless, it is accepted that such protein probably does not qualify as an EV-specific component[139].

If we expand our comparison to all proteins listed on Vesiclepedia and therefore published as founded in EVs preparations, all the identified proteins match with the exception of Immunoglobulin gamma-1 heavy chain.

We have also analyzed parental cell proteome. From the 31 common proteins identified in UCB-MNCs-sEVs, 24 were also detected in cell sample, while the other 7 proteins (desmoglein, sorcin, leucine-rich repeat-containing protein 15, neutrophil defensin 3, desmoplakin, junction plakoglobin and glycogenin-1) were not detected in parental cell analysis. This can be due to the sensitivity of the equipment that varies according to the dynamic molecular range of the proteins, or to the addition of this protein during sEVs isolation/purification method. Most of these proteins are abundant in epithelial cells such as keratinocytes from the skin and can be easily introduced in the system.

All the related sEVs proteins are enriched when compared to the parental cells specifying a particular sorting of those proteins in sEVs **(Figure 3.10)**. Interestingly, hemoglobin protein chains are depleted in UCB-MNCs-sEVs preparation in comparison with parental cells. During SEC, proteins with lower molecular weight are more efficiently separated and they are only recovery in fraction with a higher elution volume[211,299].

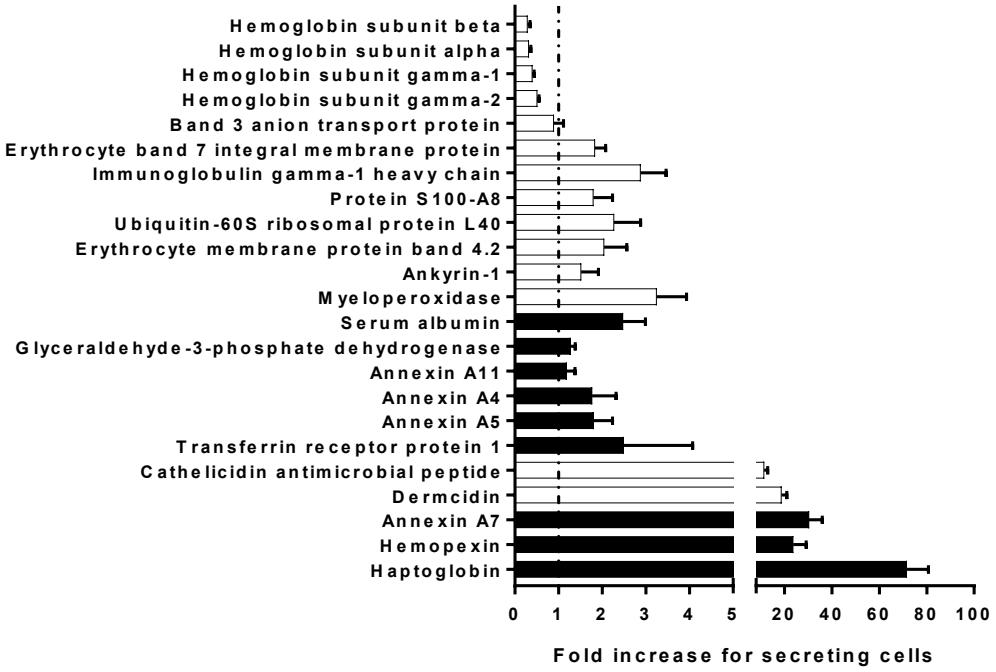

Figure 3.10. Protein enrichment in UCB-MNCs-sEVs samples in comparison to parental cells. 80% of the commonly identified proteins among sEVs and secreting cells samples are enriched in sEVs, indicating possible sorting of these proteins to EVs. Black bars indicate proteins usually described in EVs preparations**.**

Table 3.2. List of 31 identified proteins common to 3 UCB-MNCs-sEVs samples. Liquid chromatography combined with MS was performed and 31 proteins are common to all samples.

Uniprot Accession	Protein Name	Peptides (95%)		
		#1	#2	#3
P02768	Serum albumin	79	32	78
P20073	Annexin A7	26	10	20
P02790	Hemopexin	6	5	10
P02786	Transferrin receptor protein 1	1	1	6
P08758	Annexin A5	3	2	1
P09525	Annexin A4	3	1	1
P50995	Annexin A11	2	1	1
P04406	Glyceraldehyde-3-phosphate dehydrogenase	1	1	1
P00738	Haptoglobin	22	16	26
P02730	Band 3 anion transport protein	47	23	16
P05164	Myeloperoxidase	26	12	29
P69892	Hemoglobin subunit gamma-2	25	14	19
P69891	Hemoglobin subunit gamma-1	23	12	16
P69905	Hemoglobin subunit alpha	17	8	11
P27105	Erythrocyte band 7 integral membrane protein	12	10	7
P46976	Glycogenin-1	9	3	12
P68871	Hemoglobin subunit beta	12	4	8
P16157	Ankyrin-1	10	6	3
P16452	Erythrocyte membrane protein band 4.2	9	7	3
P30626	Sorcin	13	3	3
P59666	Neutrophil defensin 3	7	3	6
P11166	Solute carrier family 2, facilitated glucose transporter member 1	7	4	2
P81605	Dermcidin	4	4	3
P0DOX5	Immunoglobulin gamma-1 heavy chain	3	3	5
Q8TF66	Leucine-rich repeat-containing protein 15	6	3	2
P49913	Cathelicidin antimicrobial peptide	3	3	4
P15924	Desmoplakin	4	2	3
P62987	Ubiquitin-60S ribosomal protein L40	2	2	4
P14923	Junction plakoglobin	4	2	1
Q02413	Desmoglein-1	2	3	1
P05109	Protein S100-A8	3	2	1

Blood is very enriched in soluble proteins and so it was expectable that various blood derived-proteins appeared on UCB-MNCs-sEVs even after the various washing steps that we included in the optimized UF-SEC methodology. Furthermore, relatively few specific vesicle markers were identified, demonstrating how difficult it is to isolate and separate EVs from abundant plasma proteins. Although MS is a very powerful tool and detects a high number of proteins in one single

run, its sensitivity is defined by the dynamic range of the samples and proteins with a low expression may not be detected[300]. Recognizing this limitation, we adopted another MS strategy. Instead of analyzing all the proteins together as a single band, UCB-MNCs-sEVs samples were run in a polyacrylamide gel and four portions were excised and run in separated as described in Materials and Methods section (2.8 - Mass spectrometry). With this strategy, the number of identified peptides increased up to 550 proteins. From the three analyzed UCB-MNCs-sEVs, 300 proteins were common to all samples (approximately 51% of total identifications) which indicates a moderate degree of sample variability, allowing us to define reliable markers for a future quality control of sEVs.

When looking into the subcellular localization of these 300 proteins, we found that 6% are of cytoplasmic origin, 16% nuclear, 36% from the plasma membrane and 37% from the extracellular space **(Figure 3.11A)**; all of them with different functions and belonging to different protein classes **(Figure 3.11B)**. Interestingly, 43% of the identified proteins are enzymes, and among those 52% are proteases, whose role in inflammation resolution is well described. Moreover, proteases, particularly those from neutrophils, including neutrophil elastase, proteinase-3, cathepsin G, and neutrophil serine proteinase-4 display strong antimicrobial functions[301].

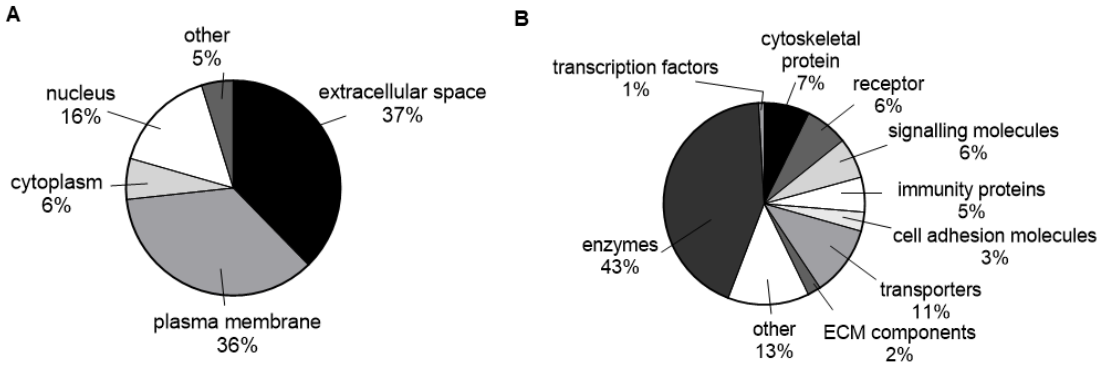

Figure 3.11. Pie chart of (A) localization and (B) molecular function of the identified sEVs proteins by liquid MS.

Vesiclepedia database comprises 11 000 entries related with human proteins reported as identified in EVs preparation by MS. According to this database, 294 out of the 300 proteins identified (98%) were already described in other EVs preparations. However, only 53 proteins of UCB-MNCs-sEVs (~18%) are in the top 100 of the most reported proteins. By segmenting the analysis, several classical markers of sEVs were highlighted. Three different tetraspanins (CD63, CD82 and CD9) were identified. Tetraspanins are specially enriched in the membrane of EVs and they are often used as their biomarkers[176]. Mechanistically, these proteins form clusters and dynamic membrane platforms with other tetraspanins and with different transmembrane and cytosolic proteins, probably acting in the formation of the microdomains that will bud. Moreover, they were also reported as regulators of both the ESCRT-independent endosomal sorting[130] and the intracellular

routing of cargoes, such as integrins[130]. Therefore, these transmembranar proteins are also described as enriched in sEVs[130,139] and we were able to identify seven integrins in our UCB-MNCs-sEVS (integrin alpha-2; integrin alpha-IIb; integrin alpha-4; integrin alpha-M; integrin beta-1; integrin beta-2 and integrin beta-3). Additionally, Rab proteins, that are often anchored on EVs surface and are important on intracellular trafficking routes for EVs were found in our samples. Namely 4 Rab proteins were identified increasing the evidences of an EV-enriched preparation.

At sEVs membrane, cell-type specific proteins are often found depending on the secreting cells[130,139,302]. MNCs comprise lymphocytes and monocytes and therefore it is possible to identify in UCB-MNCs-sEVs in different cell membrane associated molecules present in these cell types. CD14, CD11b, CD36, CD47 and CD97 were cluster differentiation molecules found in SEVS preparations that are particularly enriched in MNCs. Nevertheless, molecules like CD47, linked with both RBCs and platelets[303], and platelet glycoprotein Ib alpha and beta chain, related with platelets[304], are also identified in our samples.

Cytosolic proteins present in EVs with lipid or membrane protein-binding ability such as TSG101, ALIX and flotillin's are also reported in literature to demonstrate the EV nature and the degree of purity of an EV preparation[139]. Accessory proteins from the ESCRT-I/II/III system such as ALIX (PDCD6IP), Flotillins-1 and 2; caveolins; annexins; Heat shock proteins HSC70 (HSPA8), and HSP84 (HSP90AB1) are enriched in EVs[139]. In our MS analysis, Alix, flotillins-1 and 2, eight different annexins (annexin 1,2,3,4,5,6,7 and 11) and heat shock proteins HSC70 and HSP 90 were identified. Interestingly Syntenin-1, that was also identified in our samples, interacts directly with ALIX and supports the intraluminal budding of endosomal membranes, being one of the key pathways regulating sEVs biogenesis[153].

Although we have identified several blood proteins in the top 10 of the identified proteins with this new approach, we were able to reinforce our claim that the new isolation method enriched the EVs preparation with sEVs derived from MNCs. Similarly, to the previous MS analysis, serum albumin, hemopexin and haptoglobin are still the proteins with higher number of identified peptides followed by hemoglobin and RBC-related proteins.

Considering that both albumin and hemoglobin are two proteins with higher number of identified peptides in our samples, we have quantitatively evaluated their presence with specific ELISA kits. The purification with the optimized process still retained a relatively high amount of albumin (1980±1202 ng/mL) and hemoglobin (8.41±3.72 ng/mL) when compared to CD63 and Annexin 2 **(Figure 3.12)** for example. Our UCB-MNC-sEVs samples have an average of 10.61±2.86 pg/mL of CD63 and 1.44±0.233 ng/mL of Annexin 2 **(Figure 3.12 C and D).**

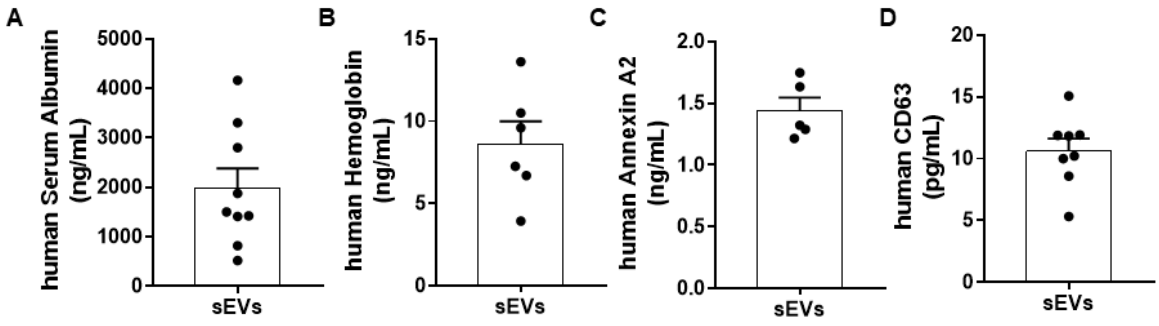

Figure 3.12. Protein quantification of specific and non-specific EVs proteins. At least 5 UCB-MNCs-sEVs samples were used to quantify their content in (A) serum albumin, (B) hemoglobin, (C) Annexin A2 and (D) CD63 by ELISA.

To enrich sEVs protein characterization, surface proteins of UCB-MNCs-sEVs were analyzed by flow cytometry (analysis of beads coated with the sEVs) and by western blot. UCB-MNCs-sEVs purified with the optimized process are positive for classical markers of exosomes such as CD81 (22.22±3.25 %), CD9 (31.8±4.75) and CD63 (62.98±10.41%) **(Figure 3.13)**. The other "non-classical" markers tested on the sEVs were chosen considering their association with the secreting cells. CD45 (hematopoietic cells), CD3 (T lymphocytes), CD19 (B cells) and CD235a (RBCs) were used, however only a residual percentage of the beads (5 to 10%) stained for these markers (data not shown). Interestingly, although highly associated with neutrophils, CD15 was found in 41.81 ± 7.87 % of the analyzed beads **(Figure 3.13A4)**. CD15 has already been detected in EVs being associated with the selective recruitment and compartmentalization during extracellular vesicles biogenesis[305].

The high positiveness of UCB-MNCs-sEVs to CD63 was confirmed by western blot in the three analyzed samples, validating the endosomal origin of these vesicles **(Figure 3.14A)**. Moreover, sEVs samples did not contained calnexin, a 90kDa integral protein of the endoplasmatic reticulum. This protein is recommended by ISEV as a negative control[139] and in fact although its presence was observed in cell lysates and not in UCB-MNCs-sEVs samples **(Figure 3.14B)**.

To complete the protein content study, gene enrichment analysis was performed by using bioinformatic tools such as GO analysis and *Funrich* software. Biological Processes such as 'neutrophil degranulation', 'regulation of leukocyte migration', 'extracellular matrix organization', 'metabolic process' and 'immune system process' were shown to be enriched in the overall proteome **(Table 3.3)**. Moreover, pathways analysis revealed enrichment in the integrin signaling pathways and, in the inflammation, mediated by chemokine and cytokine signaling pathway **(Table 3.3)**. These associated biological processes and pathways mostly related with inflammatory and immune modulation unveiled a potential role of the UCB-MNCs-sEVs in wound healing context as well as in inflammatory skin diseases.

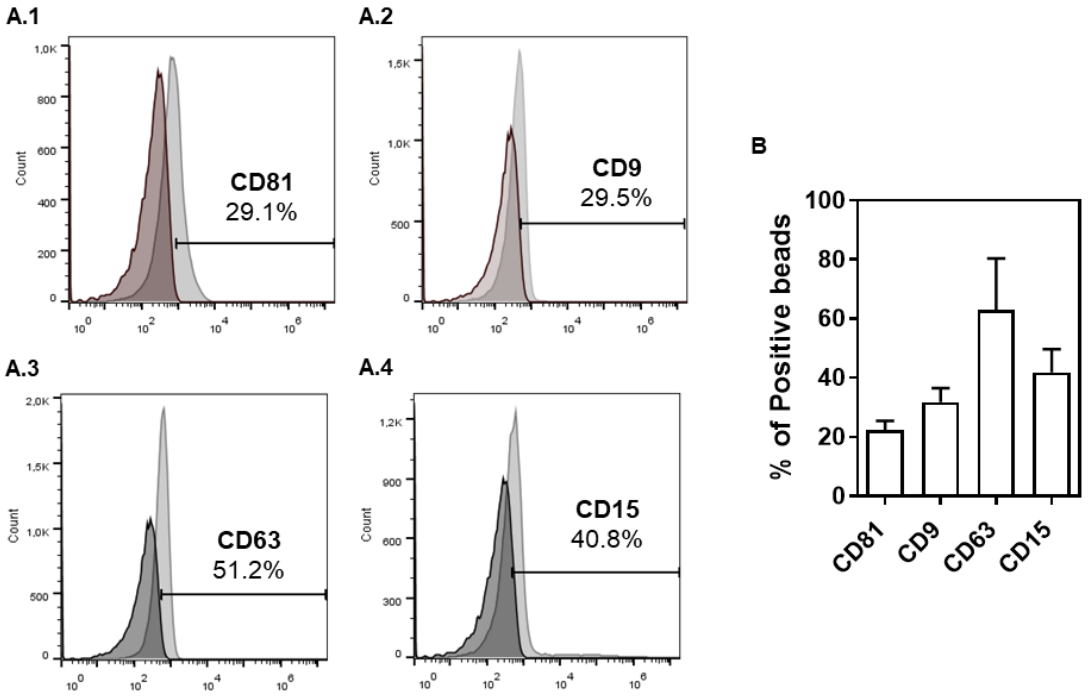

Figure 3.13. Flow cytometry detection of surface molecules in UCB-MNCs-sEVs. UCB-MNCs-sEVs were incubated with aldehyde–sulfate latex beads and stained with monoclonal antibodies or specific isotype-matched control antibodies. Analysis was performed on singlet gate of a forward scatter versus side scatter dot plot. (A) Pallid gray histograms represent sEVs–bead complexes stained with specific monoclonal antibodies; the darker filled histogram represents isotype control antibodies. (B) Graph show the mean percentage of positive beads for each surface molecule evaluated by flow cytometry. (at least n=5)

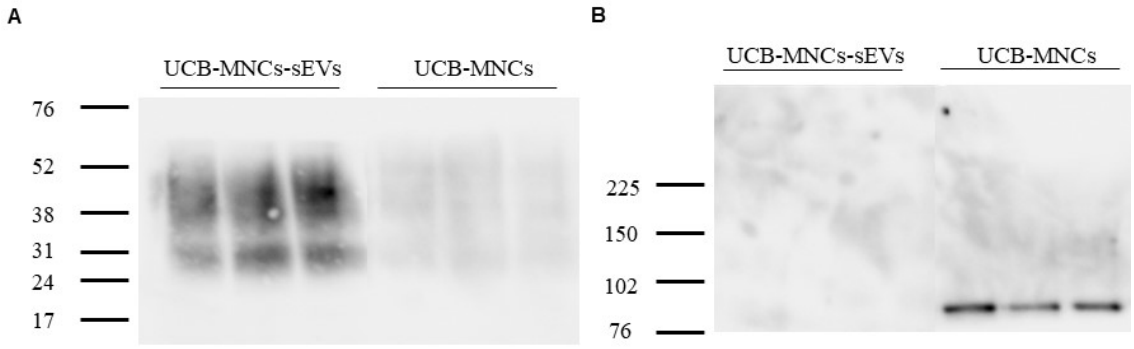

Figure 3.14. Immunoblot protein analysis of UCB-MNCs-sEVs and the parental cells. sEVs and cell lysates were separated on SDS-PAGE and electroblotted onto a nitrocellulose membrane. Samples were incubated with antibodies specific for (A) CD63 and (B) Calnexin.

Table 3.3. Biological processes regulated by the 300 proteins contained in UCB-MNCs-sEVs. Funrich software output with biological process, the correspondent percentage of the total proteins identified which are associated to each biological process and p-value.

Biological process	% proteins	p-value
Neutrophil degranulation	32.43	<0.001
Platelet degranulation	12.5	<0.001
Cell adhesion	9.80	<0.001
Immune response	8.78	<0.001
Cellular protein metabolic process	8.11	<0.001
Regulation of leukocyte migration	7.43	<0.001
Extracellular matrix organization	7.43	<0.001
Inflammatory response	6.76	<0.001
Cytokine-mediated signalling pathways	5.75	0.004
Integrin-mediated signalling pathways	4.72	<0.001
Metabolic process	2.70	0.002
Response to hypoxia	2.71	0.01
Fc-gamma receptor signalling pathway involved in phagocytosis	3.72	<0.001
Fc-epsilon receptor signalling pathway	1.35	0.372
T cell receptor signalling pathway	1.35	0.021

3.2.3. Nucleic acid Content

The genetic cargo of sEVs, namely the small non-coding RNAs, have an important role in their biological function[128]. By the transference of these cargo to recipient cells, SEVS are able to modulate gene expression modifying their cellular phenotype[128,188,306].

UCB-MNCs-sEVs RNA integrity and size distribution was assessed by Bioanalyzer electrophoresis. Globally, sEVs RNA samples are mainly composed by RNA species with sizes lower than 200 nucleotides (nt) (**Figure 3.15A**). The peaks of mRNAs and long RNAs are not well defined as these RNA species are distributed over a greater range of transcript lengths. As expected, rRNAs are present in a residual quantity. In contrast to cellular RNA, in which intact ribosomal RNA dominates the pool of RNA and detection signal, EV samples are mostly devoid of intact large and small ribosomal RNA subunits[190]. Looking specifically to small RNAs (normally defined as RNAs shorter than 200nt), sEVs RNA have a homogenous pattern throughout the nt size, with

around 50% of their content between 20 and 40 nt **(Figure 3.15B)**. This size is compatible with miRNA and tRNAs.

RNA extracted from 10^{10} particles of UCB-MNCs-sEVs have in average 502.2 ± 180.8 pg/µL **(Figure 3.15C)**. This RNA quantification based on a chip system is in general error prone[190] which may justify the high standard error among the 8 analyzed samples. Also, as the detection strategy is based on an RNA non-specific dye, DNA contamination can interfere in measurements.

To discard a possible contamination with gDNA on UCB-MNCs-sEVs samples, an intronic region of CYP1B1 gene was amplified by PCR. This gene encodes for Cytochrome P450 1B1 enzyme which is ubiquitously expressed in all human cells. Interestingly, when we tested side by side the conditioned medium (CM) from where sEVs were isolated (even numbers at **Figure 3.16**) and the final sEVs preparations (odd numbers at **Figure 3.16**), we observed that the UF/SEC method is able to eliminate all gDNA fragments, as evaluated by the presence of one genes' intron. This procedure was tested in 5 different samples and all have a similar result which indicates that UCB-MNCs-sEVs at least do not contain big gDNA fragments (with sizes superior to 649 bp).

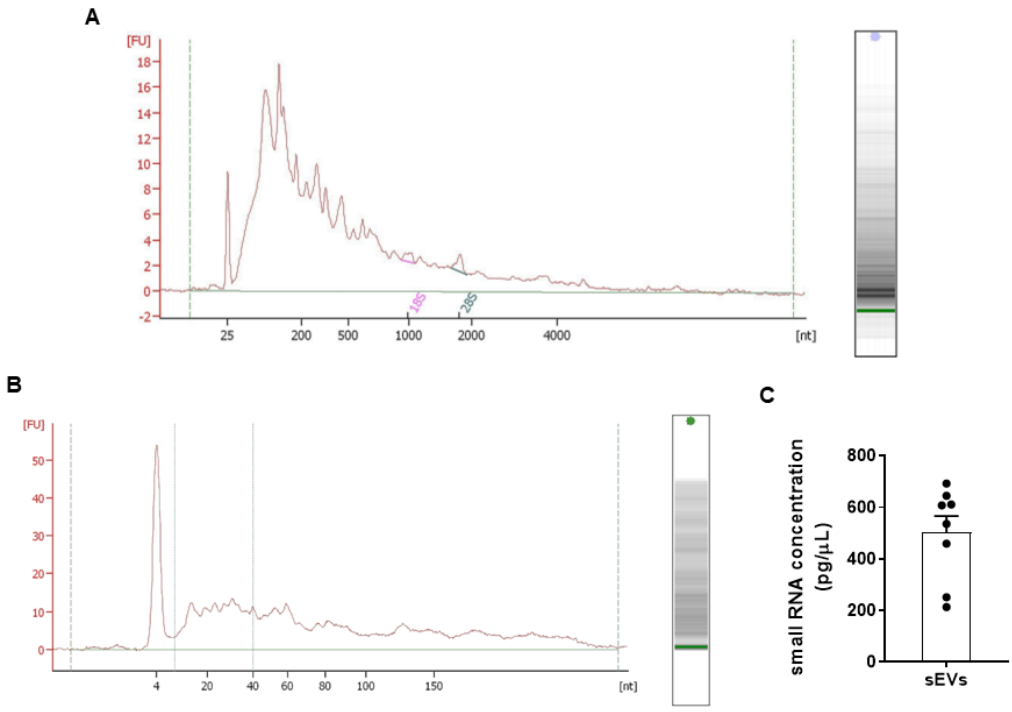

Figure 3.15. UCB-MNCs-sEVs RNA profile. RNA was isolated with a miRNACURY RNA Isolation Kit—Cell and Plant (Exiqon) and analyzed with Bioanalyzer® (Agilent 2100). Bioanalyzer electropherograms for (A) total RNA (25-4000 nt) and (B) small RNA (4-150 nt). (C) Quantification of small RNA concentration obtained by Bioanalyzer small RNA assay. (n= 6)

Figure 3.16. Evaluation of gDNA presence on UCB-MNCs-sEVs samples. Amplification of intronic region of CYP1B1 gene in sEVs (lane: 2,4,6,8 and 10) and its correspondent conditioned medium before UF/SEC methodology (lane 1,3,5,7,9). Positive control was performed with cellular gDNA (37.5ng).

To qualitatively characterize the genetic cargo of the isolated sEVs, next generation sequencing in 6 distinct samples was performed. After RNA alignment to the *RefSeq* human genome GRCh38 (GCF_000001405.26_GRCh38_genomic), more than a half (57.2 ± 6.9 %) were identified as tRNAs. The rest of the reads were identified as miRNAs (26.4 ± 5.4%), rRNA (6.2 ± 0.9%), Y RNA (4.0 ± 0.8%) and other small RNA species (6.1 ± 2.1%) such as snoRNA, snRNA and piwi-interacting (piRNA) **(Figure 3.17A).** Figure **3.17B** shows the distribution of mapped reads for each sample. Although sEVs are derived from different biological donors, the variability among them is minimal, all of them having similar patterns of small RNA distribution. Importantly, UCB-MNCs-sEVs have low abundance of rRNA. Although it is disputable whether or not this RNA species is a contaminant in EVs preparation[190], several evidences pointed out for its enrichment in apoptotic cell–derived materials and also in larger EVs[128].

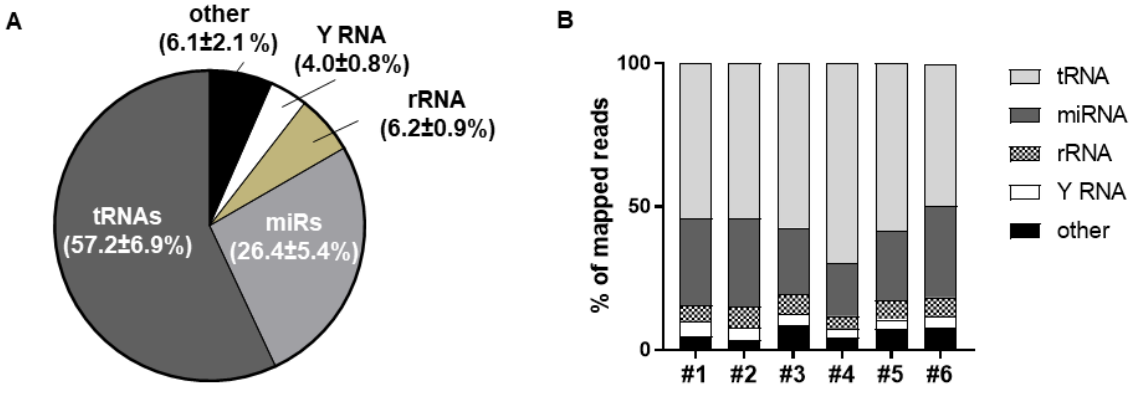

Figure 3.17. Mapping of sequencing reads. Relative composition of diverse RNA classes (A) on average and (B) on each of the 6 analyzed samples. tRNAs are the most frequent small RNA specie identified in UCB-MNCs-sEVs followed by miRNAs. Each of the 6 analyzed samples have similar RNA distribution, showing consistency and low variability among them.

In accordance with literature, tRNA enrichment in sEVs has been described[307–309] namely in EV preparations derived from human stem cells[310–312]. In this analysis, 76 different tRNA species were commonly identified in UCB-MNCs-sEVs; however, none of them was preponderant among others, representing a maximum of 3% each.

Canonically, tRNAs are indispensable components of the protein translation machinery. To execute their role in translation, tRNAs are charged with cognate amino acids through the activity of aminoacyl-tRNA-synthetase[313]. Based on this premise, we checked which aminoacids could be bound to the tRNA species identified in sEVs samples. Interestingly, 30% of tRNAs have anticodon sequences that carry valine while around 24% carries glycine. The impact of UCB-MNCs-sEVs in translation was evaluated by monitorization of incorporation of methionine analogue, HPG, an ubiquous aminoacid that codes for the initiation of the translation process detecting the nascent protein synthesis[314]. A dermal fibroblast cell line was chosen to perform these experiments. After cell seeding, fibroblasts were cultured for 24h to stabilize their cellular function. UCB-MNCS-sEVs were added to treated conditions for 18h as well as saline solution as vehicle control. Then, culture medium was changed for 30m in to a methione-free medium before HPG addition for 4h. In physiological conditions where fibroblasts were incubated in a complete culture medium containing essential and non-essential amino acids, vitamins, organic and inorganic compounds, hormones, growth factors, trace minerals as well as antibiotics and FBS, incubation with UCB-MNCs-sEVs at $1x10^{10}$ part/mL potentiated protein synthesis by 40% **(Figure 3.18B).** As expected, puromycin inhibited protein synthesis. This compound can effectively terminate the mRNA translation elongation and was used as a control. Following a 1h incubation with HPG, newly synthesized proteins were detected both in the cytoplasm and the cell nucleus. Although protein translation occurs mainly at cytoplasm, protein synthesis in the nucleus was long ago described[315]. In the images acquired by confocal microscopy, this phenomenon is perceptible as the modified-aminoacid is clearly visible at the nuclear region. Interestingly, when fibroblasts are challenged in a culture medium without the nutrients present in FBS, the same effect is observed after UCB-MNCs-sEVs administration **(Figure 3.18C)**. UCB-MNCs-sEVs increased the nascent protein synthesis in 30% in this experimental setting. Notably, we did not detect any changes in fibroblasts morphology, nor elevated levels of cell death, indicating no apparent toxicity resulting from HPG incubation or for starvation period tested. Nevertheless, the levels of protein synthesis measured by arbitrary unit of fluorescence were lower in starvation condition when compared with physiological (0.21 ± 0.06 versus 0.33 ± 0.05 a.u.).

These results showed a positive contribution of UCB-MNCs-sEVs to cell protein synthesis. However, as EVs contain lipids, proteins and other nucleic acids in addition to tRNAs, it is yet premature to attribute to these molecules an impact on protein translation. Ways of clarifying tRNAs contribution for this effect could be by silencing tRNAs role – using interfering tRNA halves - or degrading the nucleic acid content in UCB-MNCs-sEVs before applying to the recipient

cells. tRNAs are the major component in our sEVs, and although their selective packaging process into vesicles has been vaguely addressed in the literature, we plan to address their role in depth in the future.

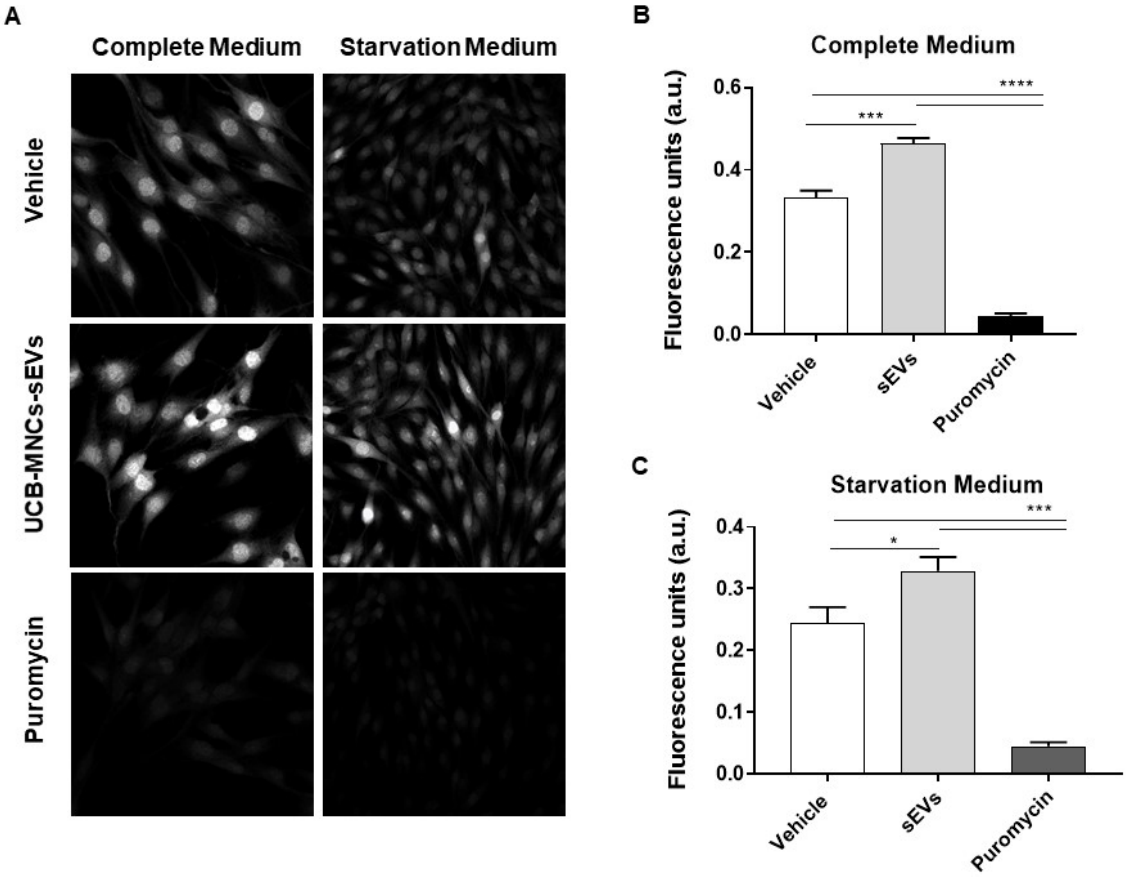

Figure 3.18. UCB-MNCs-sEVs increase protein synthesis capacity of fibroblasts both in physiologic and starvation conditions. HPG is incorporated into newly synthesizing proteins and the inhibition of the protein by puromycin decreases the Click-iT® HPG signal in dermal fibroblast cells. (A) Representative images demonstrating Click-iT® HPG fluorescence (Alexa Fluor® 488) in fibroblasts cells in the presence of either the vehicle or UCB-MNCs-sEVs. Graphs quantify the HPG fluorescent signal in (A) complete medium and (B) starvation medium condition. Quantitative analysis was performed using the Cell Profiler and ImageJ software. p-values were calculated by using one-way ANOVA with Tukey HSD post-hoc. (n=4)

Protein synthesis is a requisite for cell cycle progression. Building on the previous experiment, we decided to correlate protein synthesis levels within each cell cycle phase. Briefly, cell cycle is composed by two major stages, interphase and mitosis. Composing interphase, three distinct steps are segmented: G1, S and G2. In the first phase, cells grow physically larger, copy organelles, and make the molecular building blocks that they will need in later steps. In S phase, the cell synthesizes a complete copy of the DNA in its nucleus. It also duplicates a microtubule-organizing structure called the centrosome. The centrosomes help separate DNA during M phase. Finally, at G2, cells

grow more, make proteins and organelles, and begin to reorganize their contents in preparation for mitosis. During the mitotic phase, each cell separates its DNA into two sets and divide its cytoplasm, forming two new cells. Based on this knowledge, cells were segmented into three groups of cell cycle phase, according to the intensity of its nucleus staining obtained by DAPI. DAPI is a fluorescent stain that binds strongly to adenine–thymine rich regions in DNA. At earlier stages, cells have less DNA content (G0/G1) which is progressively increasing with the development of cell cycle.

In physiological conditions (cells cultured in complete medium with FBS), UCB-MNCs-sEVs have a transversal impact on the increase of translation across all cell cycle phases **(Figure 3.19A)**. However, in starvation conditions, UCB-MNCs-SEVS have a significant higher impact on G0/G1 phase followed by S phase **(Figure 3.19B)**. In these two groups, UCB-MNCs-sEVs significantly boosted protein synthesis, accelerating cell growth and proliferation. In fact, a previous study showed that EVs isolated from UCB-MNCs were able to increase in up 50% skin cell proliferation and migration[253].

Several parameters influence cell translational capacity. For instance, the initiation step remains a key control point of translation. Besides, for the ribosome to elongate at its maximal rate, all its substrates must be present in saturating concentrations which includes the aminoacyl-tRNAs and various elongation factors. Translation elongation rates may be affected by several parameters, including the supply and demand for each tRNA[316]. Accordingly, we hypothesized that UCB-MNCs-sEVs would impact translational rates by increasing tRNA delivery. The differences became attenuated in starvation conditions due to the lack of molecules available at basal levels. In parallel, EVs could carry different transcriptional factors and tRNA-synthetases that would potentiate protein biosynthesis. Of note, in proteomic data of UCB-MNCs-sEVs, two members of aminoacyl-tRNA synthetase were identified (asparagyl-transfer RNA synthetase and lysine-tRNA synthetase). The main function of these proteins is to catalyze the aminoacylation reaction during translation.

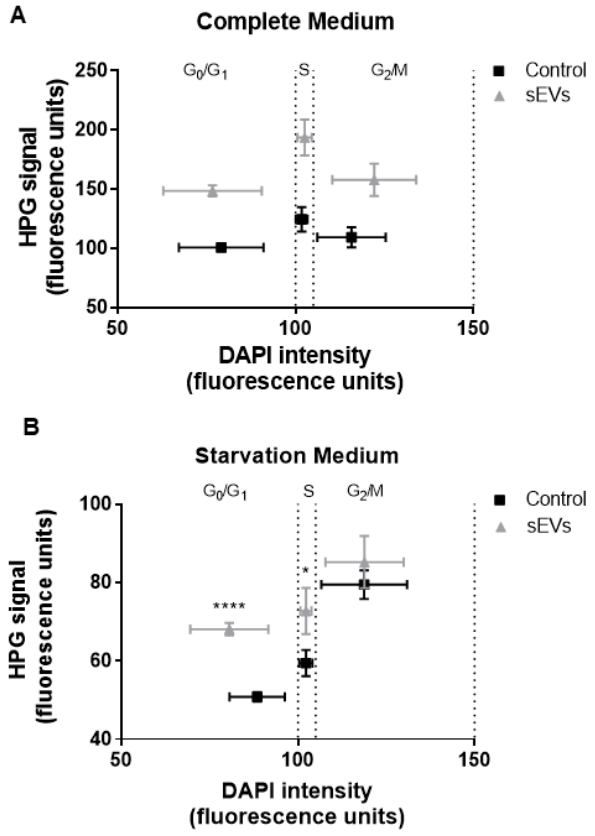

Figure 3.19. Cell cycle analysis in function of protein synthesis cell capacity. UCB-MNCs-sEVs produced a smaller impact on (A) complete medium conditions when compared with (B) fibroblasts cultured in starvation conditions. p-values were calculated by using two-way ANOVA with Tukey HSD post-hoc (n=4).

Using the bioinformatic analysis, we were not able to infer whether the identified tRNAs were full-length or charged with aminoacids. In fact, there is no definitive proof of whether the RNA fragments found in EVs are formed by specific processing steps or are artefacts introduced during EV-isolation procedure[190]. Even though, with the development of high-throughput sequencing technologies, identification of novel non-coding RNAs derived from tRNAs, known as tRNA-derived RNA fragments, has recently gained significant attention. These fragments play important roles in regulating many biological processes, such as gene expression, translation initiation and elongation, stress granule assembly, ribosome biogenesis, intergenerational inheritance, and apoptosis[310,317,318]. Additionally, tRNAs can also function as miRNAs[311,319] and when selective exported into EVs, tRNA fragments were shown to inhibit T cell activation and cytokine production[320].

Therefore, we also conducted a preliminary experiment to evaluate their role on transcription. Again, we created two identical experimental settings to test UCB-MNCs-sEVs. Utilizing an alkyne-modified nucleoside, EU, and click chemistry, newly synthesized RNA was detected. Dermal fibroblasts were treated with the $1x10^{10}$part/mL of UCB-MNCs-sEVs for 18 hours,

followed by a 30 min incubation with EU. Cells were then fixed and permeabilized, and EU incorporated into newly synthesized RNA was detected using the green-fluorescent Alexa Fluor® 488 azide and microscopy. Quantitative analysis was performed using the Cell Profiler and ImageJ software.

In complete medium, a decrease in overall transcription was observed when fibroblasts received UCB-MNCs-sEVs in comparison with the vehicle (88.94±8.31 versus 98.90±6.83) **(Figure 3.20A)**. All eukaryotes have three different RNA polymerases which transcribe different types of genes. RNA polymerase I transcribes ribosomal RNA genes, RNA polymerase II transcribes mRNA, miRNA, snRNA, and snoRNA genes, and RNA polymerase III transcribes tRNA and 5S rRNA genes. Based on signal location, an image analysis routine was created in Cell Profiler (Chapter 2 – 2.18 *In vitro* transcription and translation assays) to distinguish between RNA polymerase I and II. While RNA polymerase II has a disperse and diffuse signal in the nuclei, RNA polymerase I is identified as dark spots where there is no DAPI staining. Moreover, RNA polymerase I requires nucleolin to transcribe. To ensure their distinction, a staining with anti-nucleolin was performed, as described in Chapter 2 – **Figure 2.2..**

By applying image analysis, we were able to segment the transcription signal acquired inside the nuclei. In physiological conditions, the observed decreased in transcription (only 8%) can be explained by a decrease on the activity of RNA polymerase II while RNA polymerase I levels remained constant **(Figure 3.20A.2 and A.3).** In contrast, in starvation conditions, we observed the opposite tendency (increase of 6%) still mediated by RNA polymerase II (**Figure 3.20B**).

At first, based on the experimental conditions, we started to create different hypothesis that would explain the dual role of UCB-MNCs-sEVs on transcription. Nonetheless, the reduced differences among the experimental groups leads us to first implement different assays to confirm they real impact on cell transcription.

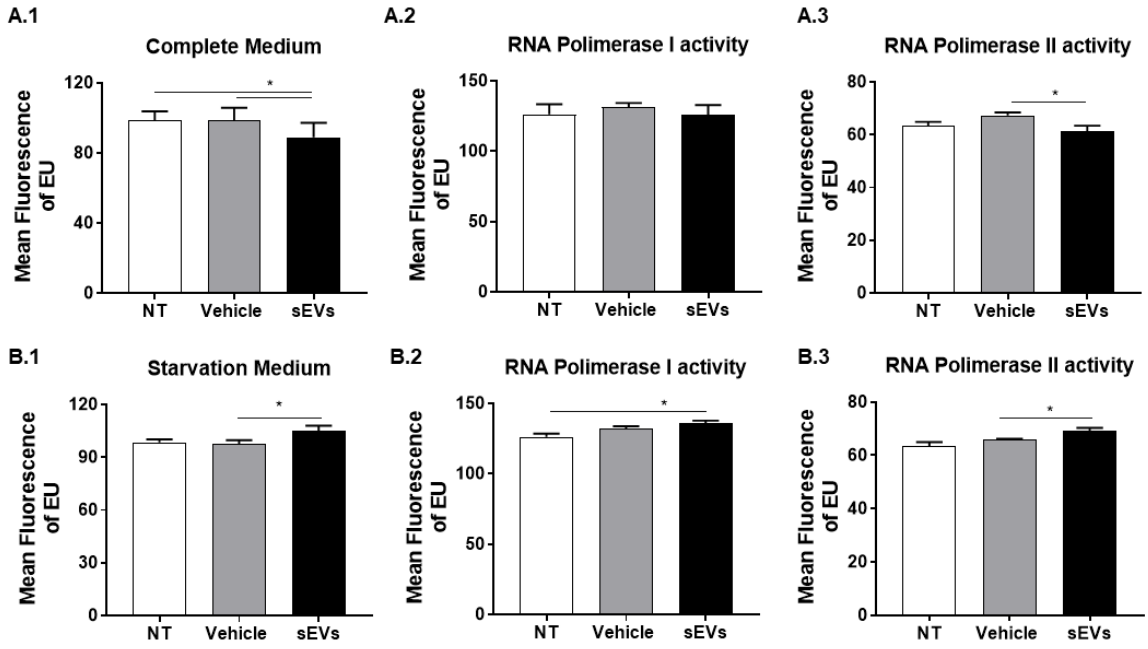

Figure 3.20. Impact of UCB-MNCs-sEVs on cellular transcription. Although significant changes were observed in treated conditions both in (A.1) complete and (B.1) starvation medium, its biological impact remains to be evaluated. Nonetheless, a possible effect is mediated by RNA polymerase II activity. Dermal fibroblasts were treated with the indicated amounts of UCB-MNCs-sEVs for 18 hours, followed by a 1-hour incubation with 5-ethynyl uridine (EU). Cells were then fixed and permeabilized, and EU incorporated into newly synthesized RNA was detected using the green-fluorescent Alexa Fluor® 488 azide. Quantitative analysis was performed using the Cell Profiler and ImageJ software. p-values were calculated by using one-way ANOVA with Tukey HSD post-hoc. (n=9).

In opposition to tRNAs, miRNAs sorting into sEVs is widely described, namely in the context of diagnostic and therapeutic purposes[321]. A total of 175 miRNAs have been identified in the 6 EVs samples studied, and 25% of these (44 miRNAs) are common to 80% of the samples. All the 44 miRNAs listed were previously identified in EVs and have an entry in the vesiclepedia. Interestingly, 6 out 44 miRNAs have the EXOmotifs (GGAG and GGUC) in their sequence. These motifs selectively bind hnRNPA2B1 and hnRNP-Q proteins which has been suggested as a specific mechanism for miRNA sorting into EVs[193,322]. According to sequencing, miRNA-144-3p and miRNA-451a were the most representative sequences in our sEVs, having ten time more reads than the other miRNAs **(Figure 3.21)**. They have been previously identified in EVs from other sources like plasma[323], mesenchymal stem cells[324] and cardiac progenitors cells[325]. Interestingly, miRNA-144/451 compose a miRNA cluster which means they are transcribed from physically adjacent miRNA genes[326]. Moreover the miRNA-144/451 cluster is abundantly expressed in erythrocyte precursors, facilitating their terminal maturation and protecting against oxidant stress[327,328]. The abundance of these miRNAs in sEVs can be justified by a significant amount of RBCs existing in the UCB-MNCs cell mixture after automatic UCB processing. Nevertheless, miRNA-144/451 are

also expressed in non-hematopoietic cells and both members of the cluster (miRNA-144-3p and miRNA-451a) have been respectively proposed to target inflammatory factors including PTGS2/COX2 , TNF-α, IL-1β, IL-6 and YWHAZ[329,330].

Other identified miRNAs in UCB-MNCs-sEVs have also been associated with several important biological functions such as cell proliferation and migration and angiogenesis and inflammation. A pathway analysis was performed in order to generate hypotheses about the relevant biological functions controlled by the miRNA signature. Using KEGG pathway analysis through DIANATOOLS, term like “T cell receptor signaling pathway”, “TGF-beta signaling pathways”, “axon guidance” and “ECM-receptor interaction” were found. However, due to the multiplicity of gene target found, this analysis is strongly biased, leading to the identification of discrepant biological processes.

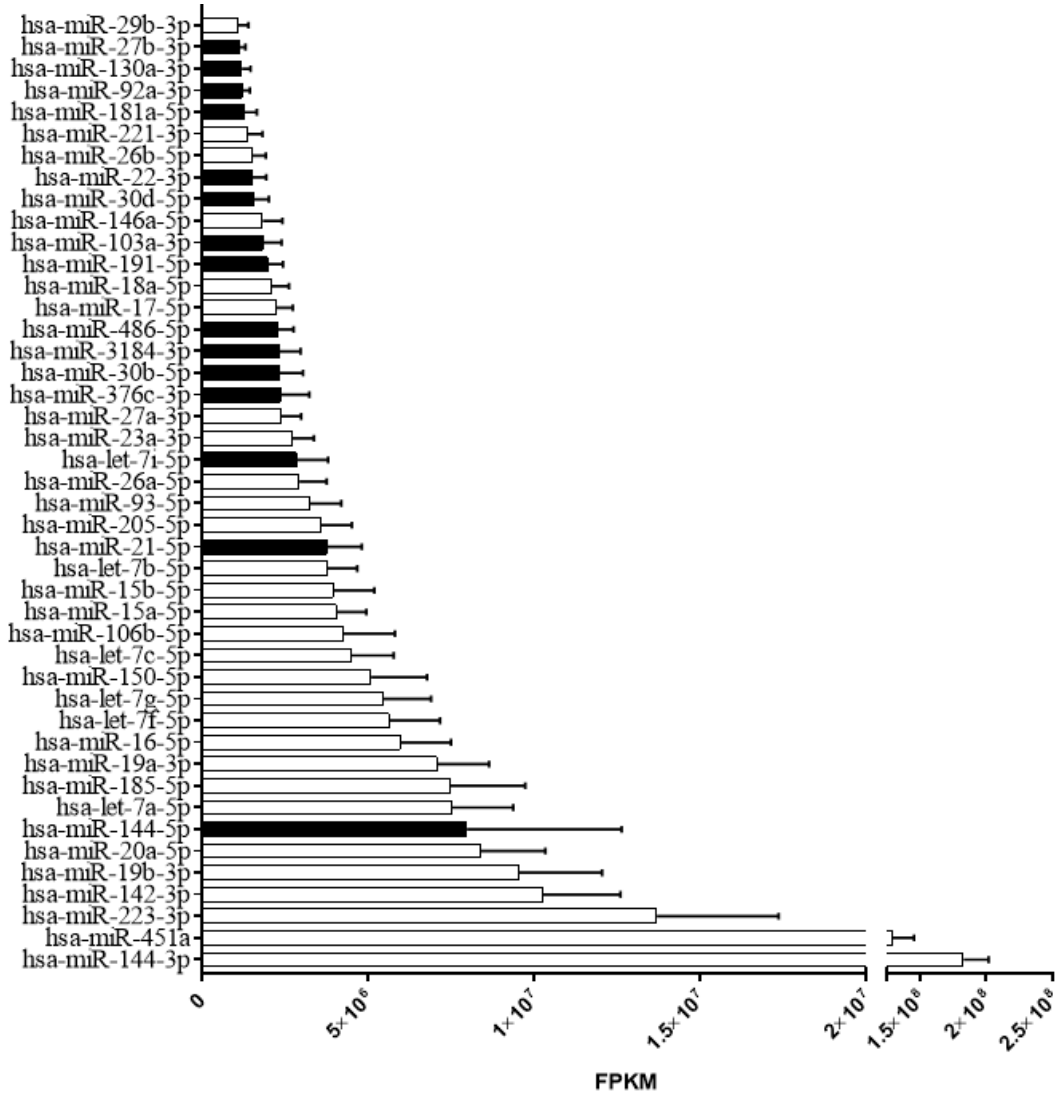

Figure 3.21. UCB-MNCs-sEVs miRNAs with highest number of reads. List of the common miRNAs identified in at least 5 out 6 of the analyzed UCB-MNCs-sEVs samples. The list is organized by isoform-level relative abundance in Fragments Per Kilobase of exon model per Million mapped fragments (FPKM). White bars represent miRNAs sequenced in all samples and black bars the ones that were only detected in 5 out of 6.

As RNA-sequencing is not a quantitative technique, from the top 44 miRNAs identified, we have chosen 6 to quantify by qPCR due to their biological relevance and because they have been previously quantified in the patent owned by Exogenus Therapeutics. We demonstrate that miRNA-150-5p, miRNA-451a, miRNA-223-3p and miRNA-16-5p are the most abundant in UCB-MNCs-sEVs, among the ones analyzed **(Figure 3.22)** Finding a reference gene for normalizing miRNA expressing levels in sEVs is challenging and not consensual in the field[139,190]. Hence, we implemented in our laboratory a standard curve for each miRNA, based on a synthetic analog, to assure the absolute quantification of each molecule instead of relative quantification to a miRNA reference gene **(Figure 3.22A)**. Additionally, to minimize result discrepancy, RNA was always extracted from the same number of particles, as we considered this variable the most reliable one instead of RNA quantification. As expected, the amount of each miRNA is very low, corresponding to approximately 0.2% of the total small RNA **(Figure 3.22B).** Knowing the miRNA concentration and its molar mass, the relation between the number of miRNA copies in each EV was possible to calculate. The miRNAs with the highest concentration have more copies per EV and their lower abundance within each EVs could be a reflex of population heterogenicity **(Figure 3.22C).**

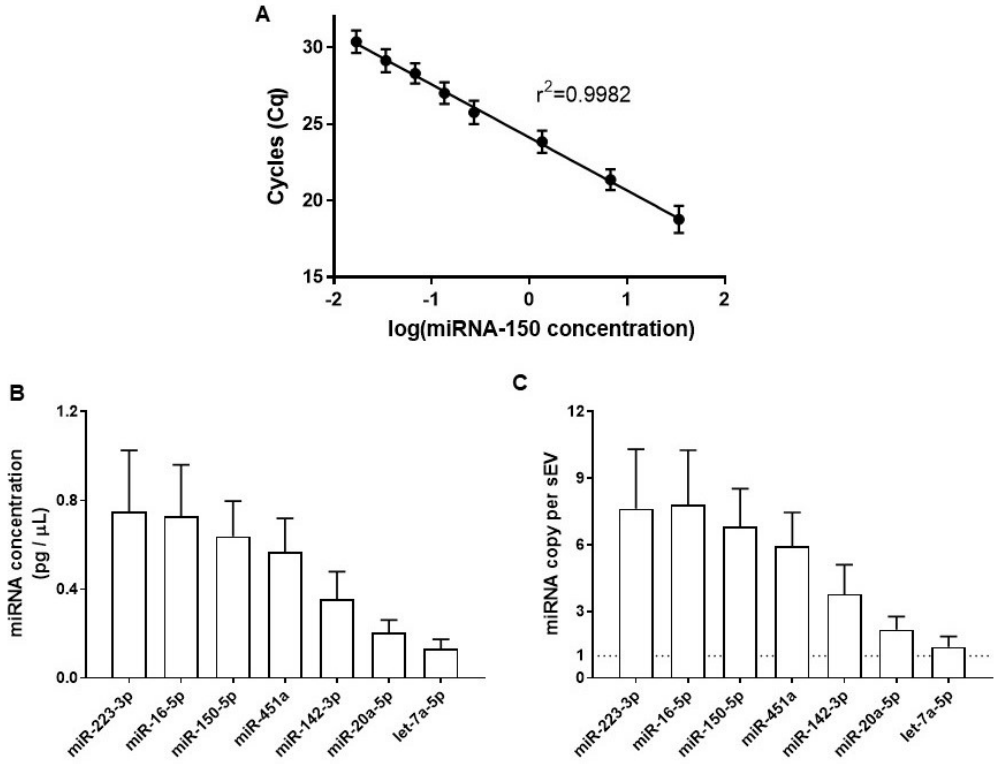

Figure 3.22. Validation and miRNAs quantification on UCB-MNCs-sEVs. UCB-MNCs-sEVs RNA was extracted from $1x10^{10}$ total particles. After cDNA conversion, quantification of several miRNAs was performed by qPCR. Graph (A) shows a representative curve for quantification of miRNA-150 concentration. A range between 0.001 and 16.9 pg/µL was evaluated with optimal fit of linear regression. (B) miRNA concentration in pg/µL. (C) Based on the quantity of each miRNA, the number of copies was calculated and normalized by EV number of each sample. (n=6).

3.3. Validation of the efficacy of UCB-MNCs-sEVs purified by the optimized method for wound healing

Our results show that UCB-MNCs-sEVs obtained by the optimized process maintain biophysical and biochemical characteristics compatible with sEVs. Further, the results demonstrated that sEVs contain several active biomolecules associated with tissue regeneration biological processes. Nonetheless, it was crucial to validate if the therapeutic potential of the optimized sEVs was maintained. It is well now described in the literature that different isolation/purification methods result in different sEVs characteristics at different levels, namely potency[172,331,332].

To confirm the therapeutic potential of UCB-MNCs-sEVs for wound healing, we used a model of type 1 diabetes mice (STZ-induced), with excisional wounds. Each animal was inflicted with two identical wounds in the back, and the sEVs were administrated to both wounds, each wound receiving $2.5x10^7$ sEVs in 10 µl of PBS ($2.5x\ x10^9$ part/mL) twice a day. We aimed to compare the healing kinetics of wounds treated with sEVs produced with the optimized process or with the precedent standard production process. The wound area was daily measured throughout the experimental period.

We compared our standard condition - sEVs purified by UC and derived from MNCs isolated manually - with the optimized condition - sEVs purified by UF/SEC and derived from MNCs isolated automatically. In both experimental groups, we have pooled the sEVs from 10 UCB donors.

In general, the results demonstrate that sEVs obtained with the optimized production process accelerate wound closure in all the animals. The healing kinetics of wounds treated with optimized sEVs is faster than when treated with sEVs obtained with the standard protocol, and the differences between both groups is more prominent in the first 7 days of healing (**Figure 3.23B**). At day 10, all 8 measured wounds treated with UCB-MNCs-sEVs derived from the optimized treatment were significantly smaller than the others that received UCB-MNCs-sEVs purified by standard method ($6.48\pm1.52mm^2$ versus $10.25\pm1.79mm^2$) **(Figure 3.23C**), which corresponds to a significant decrease of 37% of the wound size.

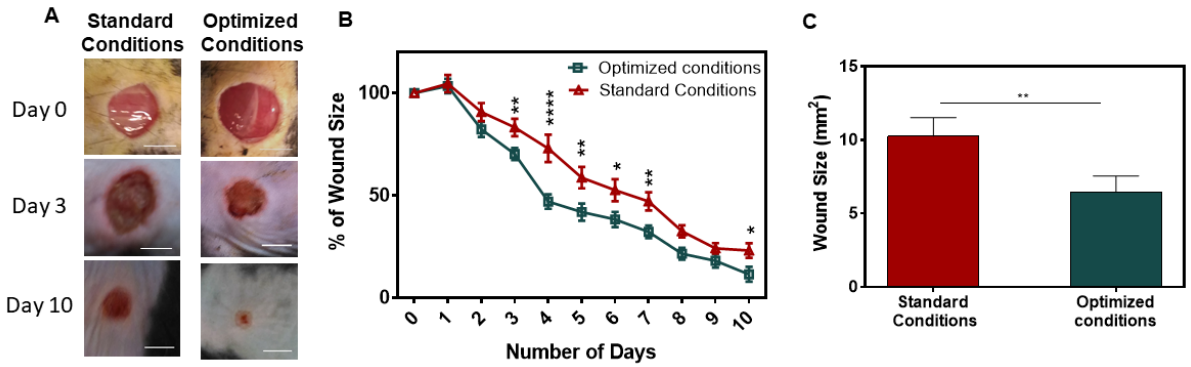

Figure 3.23. UCB-MNCs-sEVs isolated in the optimized conditions exhibit superior pro-healing effect *in vivo*. After having implemented a new production process for UCB-MNCs-sEVs, their efficacy in accelerating wound healing was validated. Full-thickness excisional wounds were performed on the skin of 16 chemically diabetes-induced C57BL/6 mice, which were randomly assigned to each treatment group: standard and optimized process. UCB-MNCs-sEVs treatment was topically applied twice a day in a saline solution. (A) Representative micrographs of wounds of each treatment groups at day 0, 3 and 10. Scale bar: 0.5cm. (B) Arithmetic mean and SEM of the wound size percentage for all the mice, at each time point (every day). (C) Wound size at day 10. p-values were calculated by using unpaired t-test for each day and between sEVs isolation methodologies.

Chapter 4: Inflammatory and immunomodulatory potential of UCB-MNCs-sEVs

UCB cells are one of the most prevalent stem cell sources available. UCB-MNCs which contain high levels of primitive, multipotent stem/progenitor cells have demonstrated their efficacy in preclinical studies via reducing oxidative stress, inflammatory mediators, and fibrogenic markers[333]. Interestingly, UCB-MNCs limited infarct size and improved left ventricular ejection fraction by significantly limiting inflammatory cytokines and inflammatory cells in infarcted myocardium[334]. Various studies on stem cell-derived secreted factors showed that the secreted factor alone without the stem cell itself may cause the same effect on tissue repair in various conditions that involved tissue/organ damage[335,336]. Of note, EVs are one of the main components of secretome.

Although the inflammatory and immunomodulatory potential of UCB-MNCs-EVs remains unexplored, growing evidences support that UCB mesenchymal EVs alleviates inflammation[337] as well as induce immunotolerance[338]. Mechanistically, these EVs are able to affect polarization, maturation, proliferation, and migration of macrophage[236,237]. Besides, a large body of studies have also shown that the immunomodulatory action of MSCs is partially mediated by the suppression of proliferation, differentiation, and activation of T lymphocytes.

Taking this into consideration, in this chapter, the inflammatory and immunomodulatory properties of UCB-MNCs-sEVs were evaluated. For that, regulation of proliferation, maturation and polarization various immune effector cells such as macrophages and T cells were studied.

4.1. In vitro evaluation of UCB-MNCs-sEVs inflammatory impact on macrophages

Monocytes and macrophages possess broad immuno-modulatory, inflammatory, and tissue-repairing capabilities. They actively participate in the development of many inflammatory and autoimmune diseases and are described as one of the major defence against pathogens, inflammatory and autoimmune diseases[339]. In fact, infiltration and exacerbated activation of these cells is generally observed in many autoimmune and inflammatory diseases such as type 1 diabetes, rheumatoid arthritis and others[340].

A number of studies have examined the *in vitro* effects of EVs from different cell sources on macrophage polarization[341,342]. For instance, EVs derived from MSCs have been shown to facilitate M2 polarization by delivering miRNA-21-5p into monocytes[341]. Also, treatment with EVs inhibit M1 markers such as TNF-α and iNOS while enhancing M2 activation[343,344].

Therefore, UCB-MNCs-sEVs biological effect on inflammation was evaluated in an *in vitro* model composed by macrophages differentiated from a monocytic cell line (THP-1) with phorbol 12-myristate-13-acetate (PMA). After differentiation, cells become adherent and the expression of recognized macrophage markers such as CD68 became visible while CD14 is gradually lost[345]. PMA-THP-1 differentiated macrophages are a suitable *in vitro* cell model to study modulation of monocyte and macrophage functions, being well stablished in the literature[346].

Differentiated macrophages were incubated with $1x10^{10}$ part/mL of sEVs and after 24 hours, their phenotype was evaluated by flow cytometry whereas mRNA levels of a panel of inflammatory mediators were evaluated by qPCR. As a positive control, macrophages were incubated with LPS, which induces a strong inflammatory response. LPS stimulates cells through TLR4, causing the release of inflammatory cytokines and upregulation of costimulatory molecules on antigen presenting cells[347].

In response to different stimuli, and as described earlier, macrophages can acquire two different major phenotypes: M1 (pro-inflammatory) and M2 (anti-inflammatory). The classically activated or M1 macrophage phenotype produces inflammatory cytokines such as TNF-α, which trigger acute inflammation, while the alternatively activated M2 phenotype is anti-inflammatory and has been found to play an important role in tissue repair as well as in inflammation resolution[348]. We used CD86 and CD163 staining to distinguish between M1 and M2 phenotype, respectively[62]. We observed a significant decrease in M1 macrophages ($CD14^{-}CD68^{+}CD86^{+}$) when treated with sEVs while the increase in M2 macrophages is less accentuated **(Figure 4.1A and 4.1B, respectively)**. In average, sEVs treatment reduced by 7% the presence of M1 macrophages and increase by 4% M2 macrophages. As a consequence, the ratio of M1/M2 decreased on cells treated with UCB-MNCs-sEVs, reinforcing sEVs potential as an anti-inflammatory product **(Figure 4.1C).**

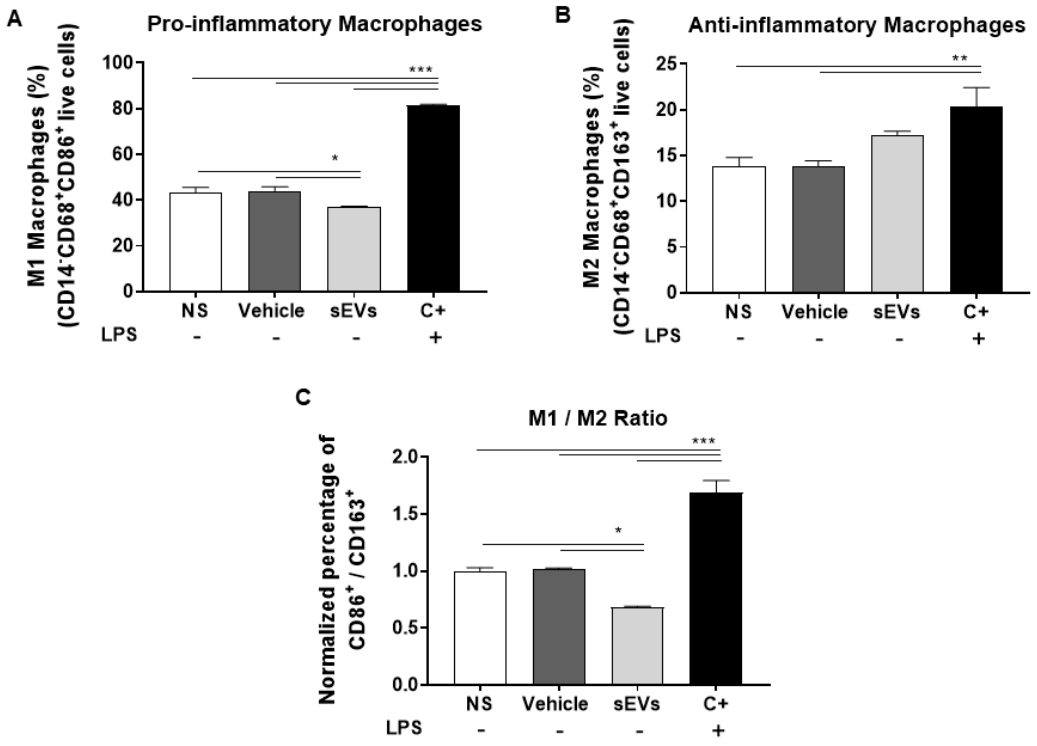

Figure 4.1. Anti-inflammatory effect of UCB-MNCs-sEVs on THP-1 derived macrophages. After differentiation of THP-1 cells into macrophages with PMA (25nM) treatment, macrophages were stimulated with sEVs ($1x10^{10}$ part/mL). LPS (1µg/mL) was used as positive control. 24h after sEVs administration, THP-1 macrophages were analyzed by flow cytometry. (A) M1 macrophages were defined as $CD14^{-}CD68^{+}CD86^{+}$ and M2 macrophages as $CD14^{-}CD68^{+}CD163^{+}$. (C) UCB-MNCs-sEVs treatment decrease M1/M2 ratio. Non-stimulated (NS) represent cells that were not conditioned by any treatment. p-values were calculated by using one-way ANOVA with Tukey HSD post-hoc (n=8).

Besides changes at membrane cell receptors, cells often change their gene expression pattern in response to a stimulus. To confirm that the phenotypic changes were also observed at transcriptional level, mRNA levels of different cytokines were tested. In comparison with the vehicle (saline solution), sEVs decreased the mRNA expression of *IFN-γ*, *IL-1β*, *TNF-α* and *COX-2* (**Figure 4.2)** in macrophages, although the differences were not statistically significant. The major differences are verified in *IFN-γ* and *TNF-α* where the mRNA levels decreased to 50% and 60%, respectively, when compared with the control conditions.

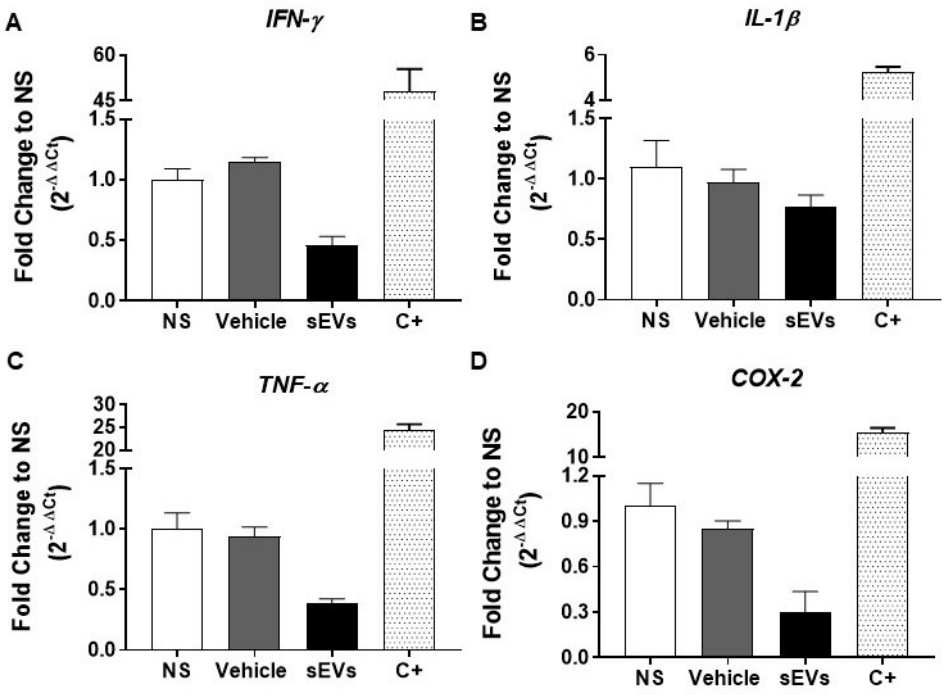

Figure 4.2. UCB-MNCs-sEVs modulate mRNA expression levels of macrophages. The relative expressions of the M1 macrophage phenotype-associated genes were evaluated by qPCR and normalized by *GAPDH*. The expression levels were calculated based on $2^{-\Delta\Delta Ct}$ formula and normalized to non-stimulated (NS) experimental condition. p-values were calculated by using one-way ANOVA with Tukey HSD post-hoc and no significant differences were found (n=8).

We then decided to evaluate if sEVs could counteract the progression to a chronic inflammatory state. For that we used THP-1 derived macrophages stimulated with LPS, and co-incubated with sEVs. Bacterial products such as LPS and cytokines like IFN-γ polarize macrophages to M1 subset. As a result, M1 macrophages induce a strong pro-inflammatory phenotype with the production of cytokines (TNF-α, IL-6, IL-12 and IL-23) and chemokines (CCL-5, CXCL9, CXCL10 and CXCL5), promoting the recruitment of T_H1 and NK cells. In this perspective, M1 macrophages promote T_H1 immune responses, but also contribute to the tissue destruction and tumoricidal activity. Therefore, an over-activation can lead to tissue damage such as occurs in various inflammatory, autoimmune and chronic diseases, including Crohn's disease, rheumatoid arthritis, diabetes, multiple sclerosis and autoimmune hepatitis[340].

UCB-MNCs-sEVs effect was in line with the previous observations. These vesicles were able to shift macrophage phenotype from M1 to M2, has shown in the previous mice model. After UCB-MNCs-sEVs application, M1 macrophage frequency decreased from 81.35 ± 1.52 % to 44.12 ± 5.35% **(Figure 4.3A)** while M2 macrophage increase their presence in the mixture from 17.14 ± 3.22% to 31.68 ± 3.30% **(Figure 4.3B).** sEVs were thus able to decrease M1/M2 ratio at a higher impact than in the previous one (**Figure 4.3C)**.

Concomitantly, mRNA expression of the different proinflammatory cytokine significantly decreased with UCB-MNCs-sEVs treatment (**Figure 4.4)**. This time, we found more pronounced differences with statistically significant differences between the treated groups and the vehicle for the four analyzed genes. As previously, UCB-MNCs-sEVs induce a decrease of approximately 50% in the mRNA expression levels. Although UCB-MNCs-sEVs treatment shutdown the expression of these proinflammatory genes, their administration was not sufficient to resume the levels to a non-inflammatory state. Repeated dose administration in order to evaluate the sustainability of the anti-inflammatory effect leading to total resolution of inflammation.

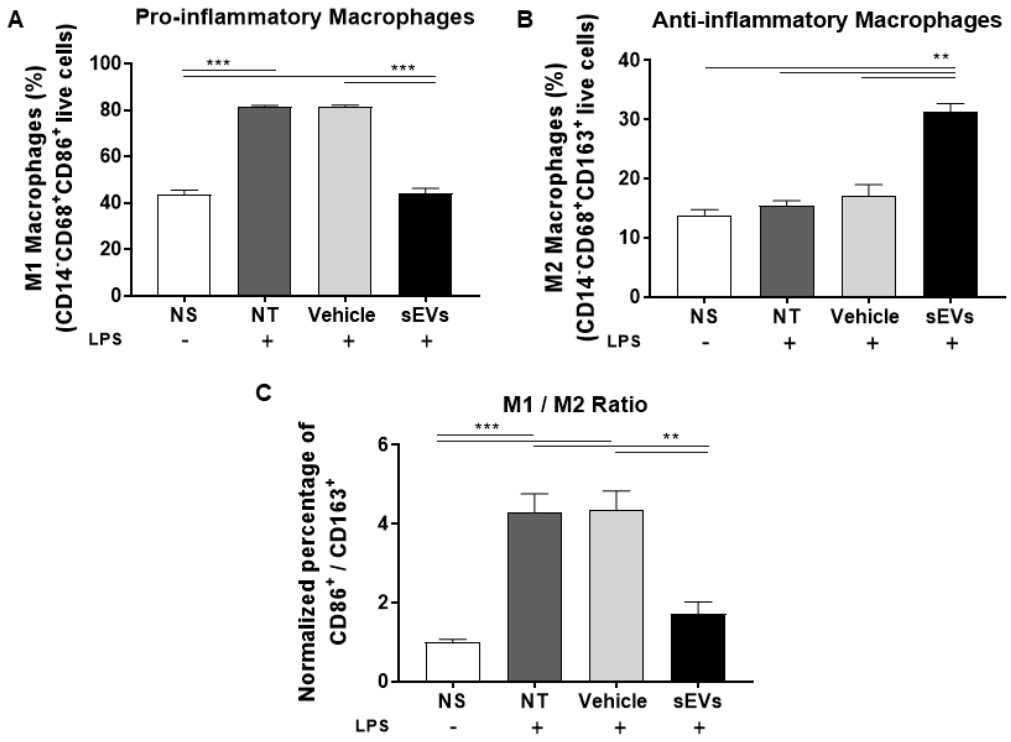

Figure 4.3. UCB-MNCs-sEVs effect on THP-1 derived macrophages are able to counteract a pro-inflammatory stimulus. After differentiation of THP-1 cells into macrophages with PMA (25nM) treatment, THP-1 derived macrophages were stimulated at the same with LPS (1ug/mL) and UCB-MNCs-sEVs ($1x10^{10}$ part/mL). 24h after sEVs administration, THP-1 macrophages cells were used for flow cytometry. (A) M1 macrophages were defined as $CD14^{-}CD68^{+}CD86^{+}$ and M2 macrophages as $CD14^{-}CD68^{+}CD163^{+}$. (C) UCB-MNCs-sEVs treatment was able to decrease M1/M2. Non-stimulated (NS) represent cells that were not conditioned by any treatment. p-values were calculated by using one-way ANOVA with Tukey HSD post-hoc (n=8).

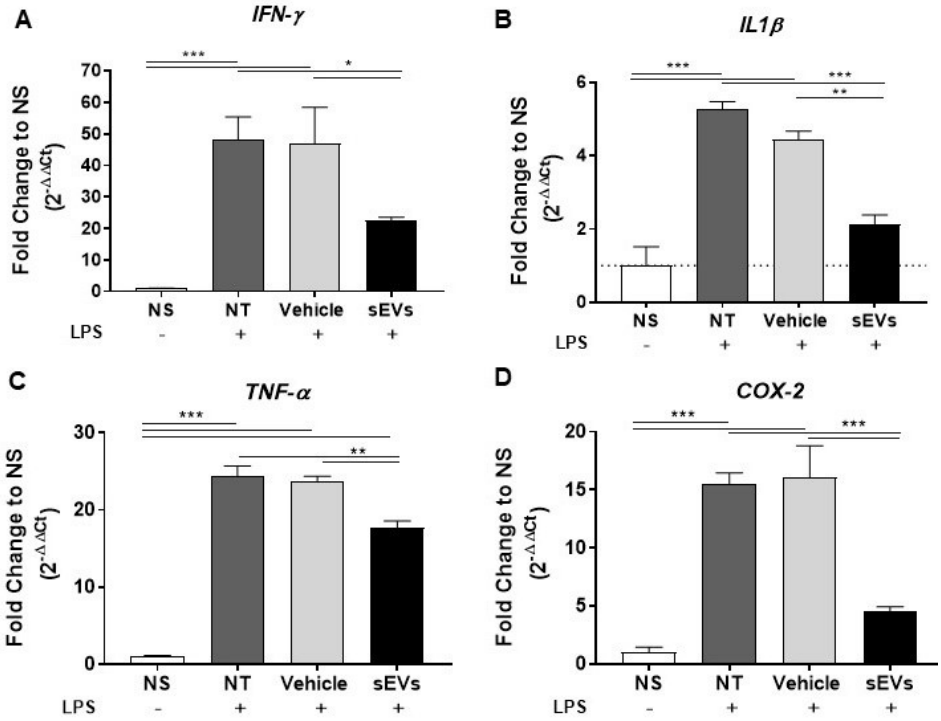

Figure 4.4. UCB-MNCs-sEVs modulate THP-1-derived macrophage gene expression upon a pro-inflammatory stimulus. qPCR analysis different M1 macrophage phenotype-associated genes: (A) *IFN-γ*, (B) *IL1β*, (C) *TNF-α*, (D) *COX-2*. The expression levels were calculated based on $2^{-\Delta\Delta Ct}$ formula and normalized to non-stimulated (NS) experimental condition. Non-treated (NT) corresponds to cells that only received LPS treatment. p-values were calculated by using one-way ANOVA with Tukey HSD post-hoc (n=8).

Additionally, we observed a significant decrease of TNF-α and CCL20 secretion in THP-1 derived macrophages, indicating that the composition of CM become less inflammatory (**Figure 4.5**). As expected, LPS stimulus efficiently elicited a pro-inflammatory response with a significant increase of cytokine production into the CM of THP-1 derived macrophages. The treatment with UCB-MNCs-sEVs reduced the production of these two molecules in 16.53% and 28.41%, respectively. Of note, detection of cytokines was also evaluated in the previous *in vitro* model (without LPS induction), however the secretion levels were too low to be detected.

In summary, these results indicate that UCB-MNCs-sEVs could be involved on macrophage polarization towards an anti-inflammatory phenotype that ultimately may induce resolution of the inflammatory phase. Resolution of inflammation would benefit not only skin inflammatory diseases but also other systemic diseases whose pathogenicity is centered on chronic inflammation.

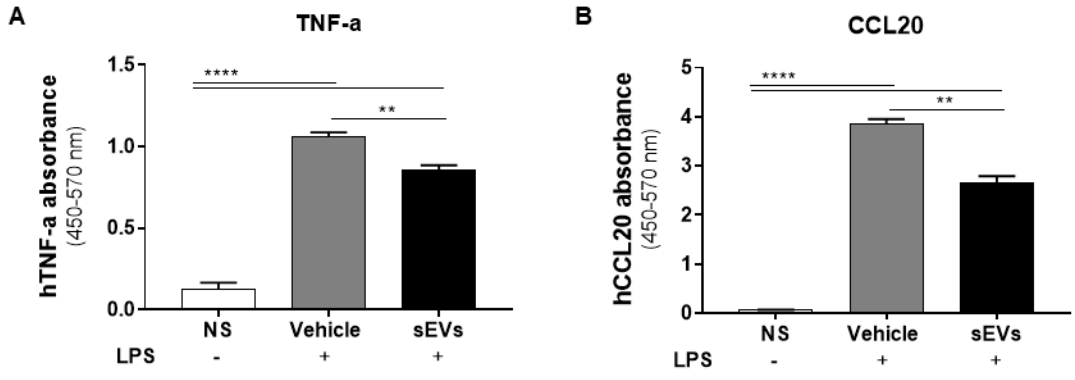

Figure 4.5. Functional effect of UCB-MNCs-sEVs on THP-1-derived macrophages. THP-1-derived macrophages were incubated with vehicle (saline solution) and sEVs for 24 hours with LPS. Cell culture supernatants were collected and the levels of pro-inflammatory molecules, (A) TNF-a and (B) CCL20, were determined by ELISA. p-values were calculated by using one-way ANOVA with Tukey HSD post-hoc (n=8)

4.2. Crosstalk between macrophages and fibroblasts

After skin injury or malfunction or imbalance in the skin, macrophages undergo an adaptive inflammatory response to restore the homeostasis. Macrophages have various functions in the inflammation and proliferation phases of wound healing, including the activation of inflammation, ECM synthesis, and supporting fibroblast proliferation[349]. When macrophages shift their phenotype towards an anti-inflammatory state, they start to secrete factors to promote fibroblast proliferation such as VEGF-α, amphiregulin, TGF-β and IGF-1[350]. Therefore, we hypothesized whether UCB-MNCs-sEVs effect on macrophages would impact not only a phenotypic shift on fibroblasts but also an increased proliferation. Hence, fibroblast proliferation was evaluated after treatment with the CM of THP-1-derived macrophages. In this experiment, dermal fibroblasts cultured in their own culture medium with sEVs or not (vehicle) were included as controls. After two days of treatment, the conditions that were stimulated with sEVs potentiate the same response on fibroblasts **(Figure 4.6A)**. Although not significant different, after six days of treatment, both sEVs and the CM of THP-1 derived macrophages treated with sEVs demonstrated to have an impact in fibroblast proliferation **(Figure 4.6B)**, in accordance with previous results[253]. These results suggest that although UCB-MNCs-sEVs have some direct proliferative effect, when mediated by other cell types, the cell response can be majored. Interestingly, other authors have reported similar evidences where M2 macrophages secrete specific factors to potentiate fibroblast proliferation[96,349]. Interestingly, using gene expression analysis, we observed that fibroblast became "less inflammatory" after two days of treatment as they decrease the expression of *IL-8* and *IL-6* after direct stimulation with sEVs or even less when treated with CM derived from sEVs-treated THP-1 derived-macrophages **(Figure 4.7).**

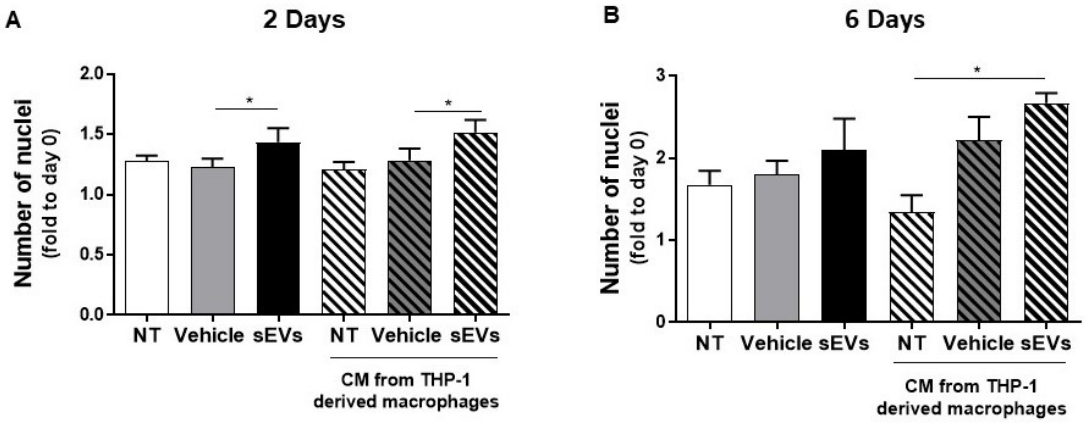

Figure 4.6. Proliferation of dermal fibroblasts is stimulated by CM of sEVs treated THP-1 derived macrophages. At day 0, no differences existed in cell number among the different conditions. The number of nuclei was measured after staining with Hoescht at (A) 48h and (B) 6 days. Statistical analyses were performed by one-way ANOVA with Tukey HSD as a post-hoc test, (n=8)

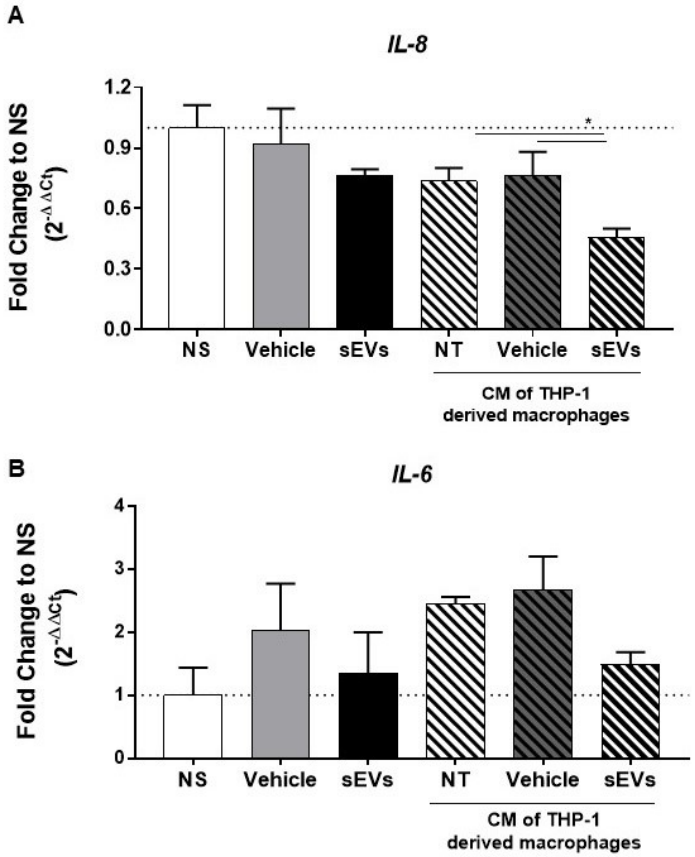

Figure 4.7. UCB-MNCs-sEVs promote a less inflammatory phenotype on dermal fibroblasts at 48h. At the end of experiment, RNA from dermal fibroblasts was extracted and two distinct cytokines were evaluated by qPCR. Levels of (A) *IL-8* and (B) *IL-6* were evaluated and normalized to *GAPDH* expression. The expression levels were calculated based on $2^{-\Delta\Delta Ct}$ formula and normalized to non-stimulated (NS) experimental condition. Non-treated (NT) corresponds to cells that received the CM from non-treated THP-1 differentiated macrophages. Statistical analyses were performed by one-way ANOVA with Tukey HSD as a post-hoc test (n=8).

Concomitantly, at 48h after treatment addition, different growth factors were analyzed. When directly treated with UCB-MNCs-sEVs, fibroblasts increased the production of *PDGF* and *TGF-β* by 10 and 4-fold when compared with non-treated cells **(Figure 4.8C and D).** No significant effect was observed for *bFGF* and *VEGF* **(Figure 4.8A and B).**

Analyzing the mRNA transcripts of fibroblasts treated with CM of THP-1 derived macrophages, the scenario was slightly different. In the non-treated cells (NT), which means fibroblasts treated with CM of macrophages that were not subjected to any substance, the mRNA expression of *bFGF*, *VEGF* and *PDGF* was increased. However, added to this effect, in case of the CM from macrophages treated with, we observe a higher difference in the expression of *bFGF*, *VEGF* and *TGF-β* of 3, 7- and 5-fold, respectively against the vehicle. Except for *PDGF*, the effect on fibroblasts mediated by UCB-MNCs-sEVs-treated macrophages was potentiated when compared with the direct treatment of fibroblasts with UCB-MNCs-sEVs.

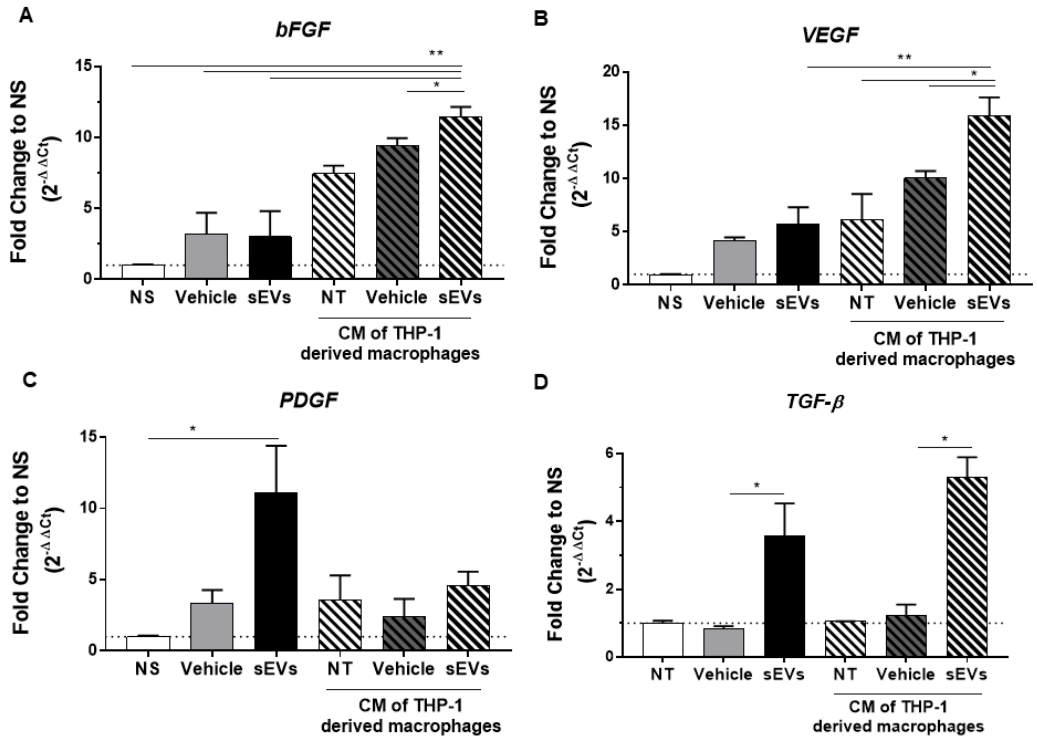

Figure 4.8. Impact of UCB-MNCs-sEVs treatment in growth factors gene expression by dermal fibroblasts at 48h. At the end of experiment, RNA from dermal fibroblasts was extracted and several growth factors were evaluated by qPCR. Levels of (A) bFGF, (B) VEGF, (C) PDGF and (D) TGF-β were evaluated and normalized to GAPDH expression. The expression levels were calculated based on $2^{-\Delta\Delta Ct}$ formula and normalized to non-stimulated (NS) experimental condition. Non-treated (NT) corresponds to cells that received the CM from non-treated THP-1 differentiated macrophages. Statistical analyses were performed by one-way ANOVA with Tukey HSD as a post-hoc test (n=8).

We also evaluated alpha-smooth muscle actin (a-SMA) expression by qPCR, which is an indicator of the status of myofibroblast differentiation. Myofibroblasts exhibit features of smooth muscle cells and play an important role on skin repair by producing extracellular matrix which is needed to restore tissue integrity after injury. As usual, the key for success is the balance and this is also the case for myofibroblasts. Too many myofibroblasts working for too long cause tissue contractures that ultimately obstruct organ function. In turn, insufficient myofibroblast activation and activities, prevent a normal wound healing process[351].

Fibroblasts stimulated with CM of sEVs-treated macrophages showed an upregulation of *α-SMA* compared to fibroblasts stimulated with CM containing the vehicle and the non-treated macrophages, 6 days after treatment **(Figure 4.9B).** The upregulation started 2 days after stimulation and was sustained for 6 days. However, the direct administration of sEVs has the opposite effect, and we believe that this is probably due to a compensatory mechanism to balance myofibroblast differentiation.

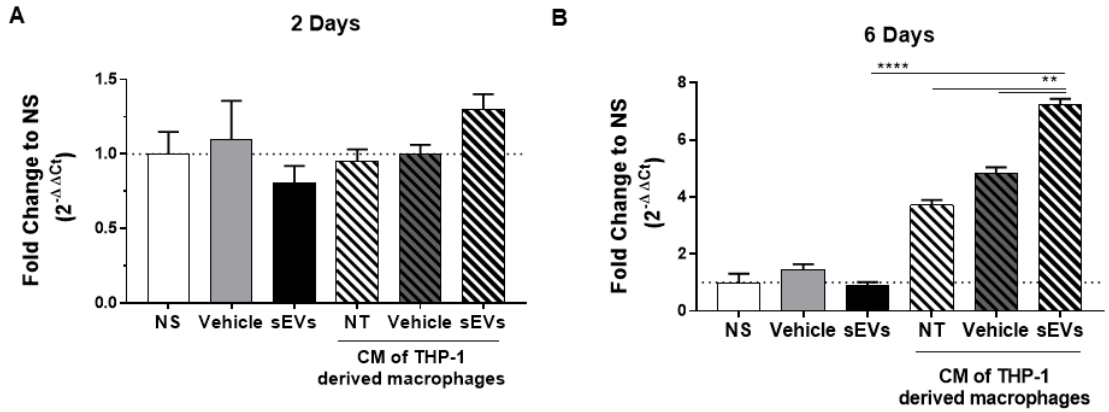

Figure 4.9. CM of UCB-MNCs-sEVs treated THP-1 macrophages increase *α-SMA* expression on dermal fibroblasts. (A) After 48h of incubation, no differences were observed in expression levels of *α-SMA*. (B) However, after 6 days, dermal fibroblasts stimulated with CM of UCB-MNCs-sEVs treated THP-1 macrophages showed an upregulated gene expression when compared with the respective vehicle. Statistical analyses were performed by one-way ANOVA with Tukey HSD as a post-hoc test (n=8)

ECM deposition by fibroblasts is an important process in wound healing and in diverse skin inflammatory disease which have fibrosis as a consequence such as localized scleroderma[88]. Two major collagens produced in these processes are collagen type I (Col1a1) and collagen type III (Col3a1) as well as fibronectin (Fn1). *Col1A1* gene expression in fibroblasts was similarly increased after stimulation with sEVs both directly and when macrophage CM was applied. While no differences were verified 48 hours after UCB-MNCs-sEVs treatment, at 6 days of culture **(Figure 4.10A)**, the *Col1A1* expression was higher in fibroblasts directly treated with UCB-MNCs-sEVs **(Figure 4.10B).** *Col3A1* had a different expression pattern throughout time when treated with UCB-MNCs-sEVs **(Figure 4.10C and D)**. 48 hours after treatment only fibroblasts stimulated with sEVs-treated CM presented a small increase on Col3a1 expression. Compared to vehicle, there is no statistical difference even 6 days after treatment **(Figure 4.10D)**. However, fibroblasts treated directly with sEVs have a more prominent impact in the expression of this gene **(Figure 4.10D).** The expression pattern of fibronectin was also tested. In CM-treated conditions, no differences induced by UCB-MNCs-sEVs were observed. However, UCB-MNCs-sEVs treatment increased in approximately 2-fold face to vehicle, both at 2 and 6 days after treatment, respectively **(Figure 4.11)**.

Activated macrophages produce, in addition to TGF-β, cytokines such as IL-4, IL-10, IL-13, TNF-α, and IL-1β, which have been shown to activate fibroblasts, overproducing proteins of the ECM[88]. Moreover, macrophages also recruit myofibroblasts and exacerbate inflammatory cell infiltration to sites of injury, leading to profound production of a variety of chemokines, cytokines, and growth factors, which lead to and excessive and poorly ordered matrix deposition and fibrosis. Interestingly, our set of results indicate that by inducing a phenotypic shift towards M2 macrophages through UCB-MNCs-sEVs treatment, macrophages paracrine factors would induce not only less inflammatory characteristics on fibroblasts but also a controlled myofibroblast differentiation as well as an equilibrated ECM deposition.

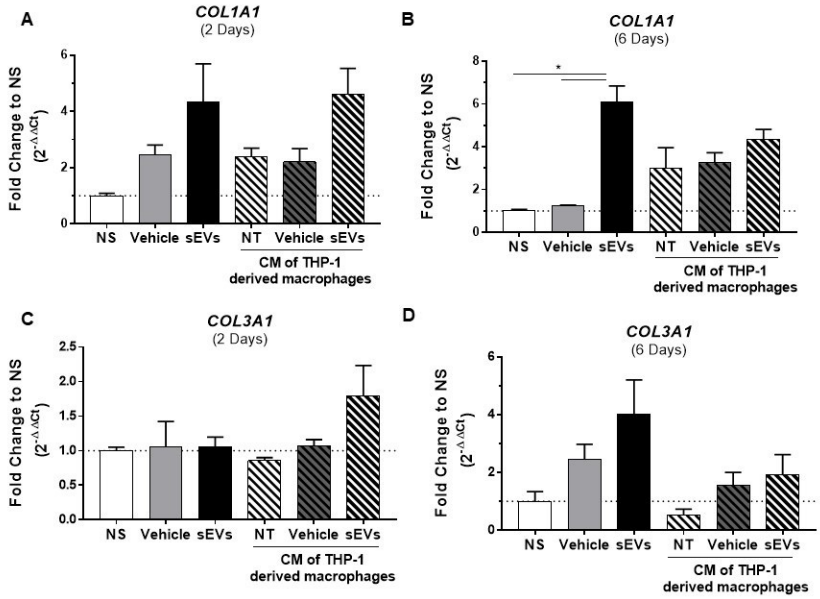

Figure 4.10. Influence of UCB-MNCs-sEVs direct treatment or intermediated by macrophages on collagens gene expression. RNA from dermal fibroblasts was extracted in two different timepoints and ECM-related genes were evaluated by qPCR. (A) Col1a1 gene expression increase in both conditions that received UCB-MNCs-sEVs treatment after 48h while only significative differences were found at day 6 when compared UCB-MNCs-sEVs direct treatment and the respective control (B). No statistical differences were observed on Col3a1 gene expression neither at (C) 48h or (D) 6 days after treatment. Levels of each gene were normalized to GAPDH expression. The expression levels were calculated based on $2^{-\Delta\Delta Ct}$ formula and normalized to non-stimulated (NS) experimental condition. Non-treated (NT) corresponds to cells that received the CM from non-treated THP-1 differentiated macrophages. Statistical analyses were performed by one-way ANOVA with Tukey HSD as a post-hoc test (n=8).

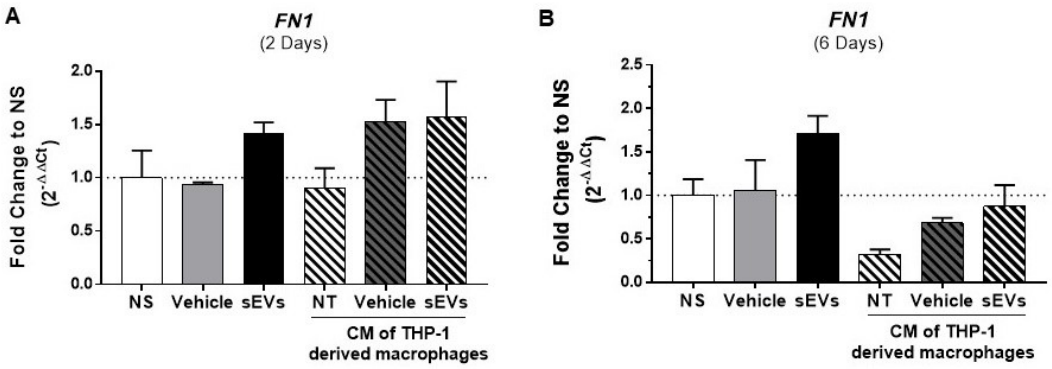

Figure 4.11. Influence of UCB-MNCs-sEVs direct treatment or intermediated by macrophages on *fibronectin* expression. RNA from dermal fibroblasts was extracted in two different timepoints and ECM-related genes were evaluated by qPCR. A tendency to increase Fn1 gene expression is observed in both conditions treated with UCB-MNCs-sEVs both at (A) 48h and (B) 6 days after treatment. Levels of each gene were normalized to *GAPDH* expression. The expression levels were calculated based on $2^{-\Delta\Delta Ct}$ formula and normalized to non-stimulated (NS) experimental condition. Non-treated (NT) corresponds to cells that received the CM from non-treated THP-1 differentiated macrophages. Statistical analyses were performed by one-way ANOVA with Tukey HSD as a post-hoc test. No significant differences were found (n=8).

4.3. *In vitro* evaluation of UCB-MNCs-sEVs immunomodulatory impact on PBMNCs

Immune cell-derived EVs can target many cell types, inducing a wide variety of immune-response effects. These effects range from an immune-promotive response to immunosuppressive effects. Indeed, immunosuppressive effects from EVs may also lead to immune tolerance[352].

Taking this into consideration, our first approach was to infer whether UCB-MNCs-sEVs administration would lead to an activation or deactivation of immune cells. For that, the proliferation ability was determined using carboxyfluorescein succinimidyl ester (CFSE) dilution on PBMNCs. In non-stimulated conditions, no proliferation was observed, indicating that the UCB-MNCs-sEVs by itself did not activate T cells.

Then, we decided to check if UCB-MNCs-sEVs would be able to modulate cell proliferation after a proliferative stimulus. Several forms of T-cell stimulation were tested, including concanavalin A and plate-bound anti-CD3/CD28, yet we decided to work with phytohemagglutinin (PHA) due to its strongest proliferative response. PBMNCs were co-incubated with PHA and either vehicle or UCB-MNCs-sEVs ($1x10^{10}$ part/mL), and no differences in viability were observed between the groups **(Figure 4.12A)**. Non-stimulated PBMNCs were used as negative control (NS), and stimulated PBMNCs without EVs constituted the positive control (NT). As expected, the proliferation rate of non-stimulated cells was very low, and the maximum proliferation rate was reached by stimulated PBMNCs without UCB-MNCs-sEVs. After 6 days of co-incubation with sEVs and PHA, we observed a decrease in overall T lymphocyte population ($CD3^+$ cells) - 58.7 ± 3.8% versus 38.9 ± 6.6% - as well as in $CD4^+$ T lymphocyte subset - 42.9 ± 2.1% versus 28.9 ± 6.5% - and $CD8^+$ T cells - 66.2 ± 4.1% versus 41.54 ± 14.0% **(Figure 4.12B, C and D)**.

Several publications have shown suppressive capacities of sEVs on T cell proliferation, namely MSC-derived EVs[235,319,353]. MSC-derived EVs are immunologically active, and have the potential to attenuate an activated immune system through the induction of anti-inflammatory cytokines and T_{reg}[354]. Additionally, EVs isolated from human adipose MSCs are able to arrest T cell differentiation towards effector and memory cell phenotypes[355]. We acknowledge that within our UCB-MNCs, a small percentage of mesenchymal stem cells exist. Yet, we never quantified their amount. Bieback et al. quantified that the frequency of MSC-like cells ranged from 0 to 2.3 clones per 1 x 10^8 MNCs[356]. Therefore, we cannot discard the hypothesis that EVs secreted by these residual MSCs could be reinforcing UCB-MNCs-sEVs effect.

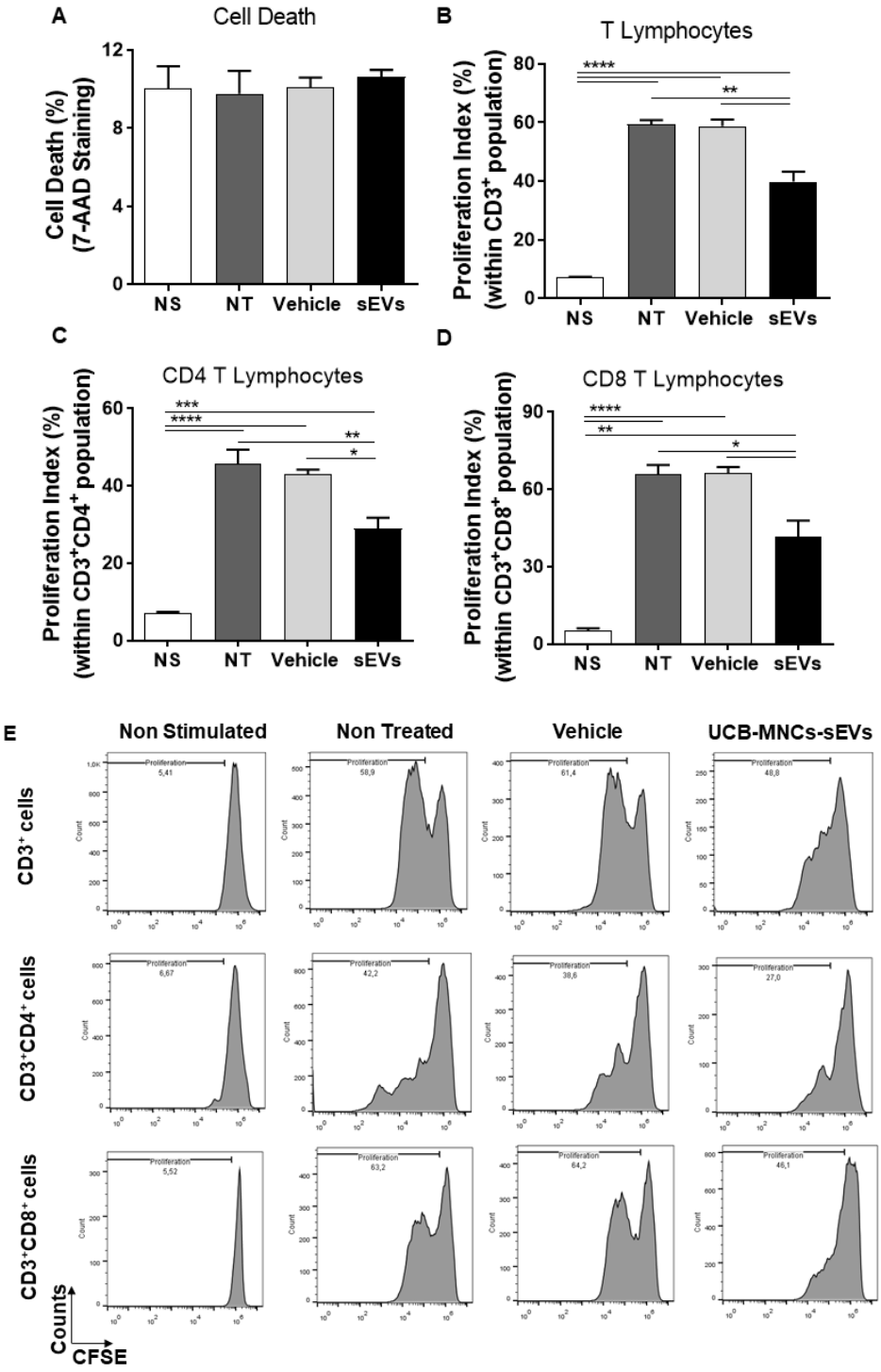

Figure 4.12. UCB-MNCs-sEVs decrease T cell proliferative capacity. PBMNCs were incubated for 6 days with PHA and UCB-MNCs-sEVs or the vehicle. As negative control, PBMNCs were not stimulated with the mitogen (NS) and as positive control, non-treated PBMNCs were used (NT). (A) Cell viability. Internalization of 7-AAD was used to stain death cells. Proliferation index was measured by CFSE intensity of (B) overall T cell proliferation ($CD3^+$ cells); (C) $CD3^+CD4^+$ and (D) $CD3^+CD8^+$ compartment. (E) Representative histograms of cytometric analysis performed on total lymphocyte population ($CD3^+$ cells), $CD3^+CD4^+$ and $CD3^+CD8^+$ T cell subsets. Statistical analyses were performed by one-way ANOVA with Tukey HSD as a post-hoc test (n=6 for UCB-MNCs-sEVs and n=1 for PBMNCs donor).

IFN-γ is a pro-inflammatory cytokine secreted by immune cells under activation[357], an there is a direct correlation between IFN-γ secretion and the level of T cell activation. In order to determine the effect of EVs on the secretory IFN-γ response of T cells, PBMNCs were cultured either in the presence or absence of UCB-MNCs-sEVs for 6 days and intracellular levels of IFN-γ were determined on CD4 and CD8 T cell subsets.

Our results showed that, at day 6, the percentage of intracellular IFN-γ was reduced when PBMNCs were cultured with UCB-MNCs-sEVs, in comparison to positive control, in both T cell subsets. However, this reduction was only statistically significant on gated $CD4^+$ T cells **(Figure 4.13).** In $CD8^+$ T cell subset, although the difference was not significant, we observed a decrease of 3% in IFN-γ expressing cells **(Figure 4.14)**. These results demonstrated that UCB-MNCs-sEVs impaired lymphocytes IFN-γ secretion.

For instance, in psoriatic lesions, Kryczek et al. suggested that one of the main effects of IFN-γ is activating antigen-presenting cells. Particularly, IFN-γ produced by CD4 T cells would program myeloid dendritic cell to produce CCL20, secrete IL-23 thus favoring IL-17 producing cell recruitment and activation. Impairing IFN-γ secretion mainly by $CD4^+$ T cells will suppress T_H17 development, possibly contributing to attenuation of human autoimmune diseases. Notably, while IL-17^+CD4^+ T cells and IL-17 play an active role in inflammation and autoimmune diseases, IL-17^+CD8^+ T cells have not been described as increased in human autoimmune diseases[358].

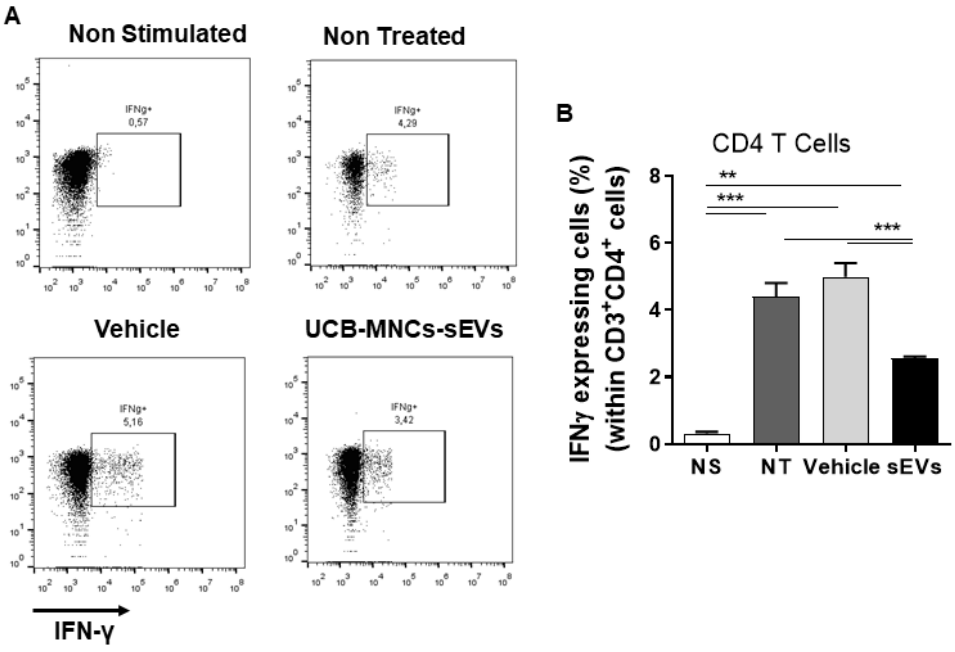

Figure 4.13. UCB-MNCs-sEVs inhibits the IFN-γ production of *in vitro* stimulated CD4+ T cell subset. After activation with αCD3/αCD28, PBMNCs were incubated for 6 days with UCB-MNCs-sEVs ($1x10^{10}$part/mL) or the vehicle. As negative control, PBMNCs were not activated (NS) and as positive control, non-treated PBMNCs were used (NT). (A) Representative dot plots for IFN-γ staining by flow cytometry. (B) Graph indicated the overall percentage of IFN-γ producing cells in each condition within $CD3^+CD4^+$ T cell compartment. p-values were determined using one-way ANOVA with Tukey HSD as post-hoc test. (n=6 for sEVs and n=1 for PBMNCs donor).

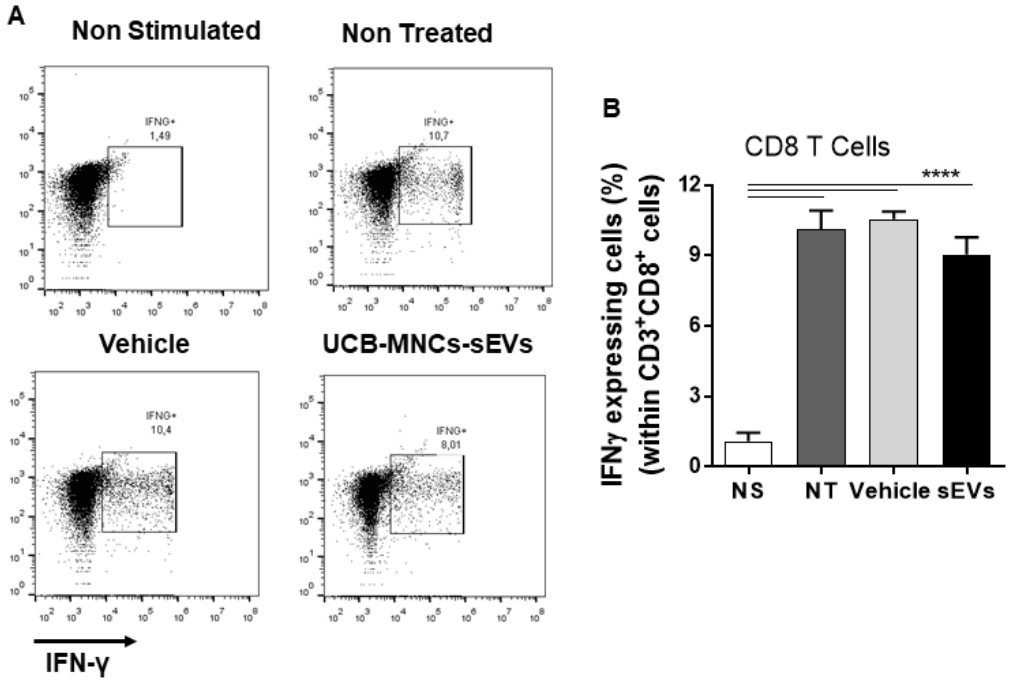

Figure 4.14. sEVs inhibits the IFN-γ production of *in vitro* stimulated CD8$^+$ T cell subset. After activation with αCD3/αCD28, PBMNCs were incubated for 6 days with UCB-MNCs-sEVs ($1x10^{10}$part/mL) or the vehicle. As negative control, PBMNCs were not activated (NS) and as positive control, non-treated PBMNCs were used (NT). (A) Representative dot plots for IFN-γ staining by flow cytometry. (B) Graph indicated the overall percentage of IFN-γ producing cells in each condition within CD3$^+$CD8$^+$ T cell compartment. p-values were determined using one-way ANOVA with Tukey HSD as post-hoc test (n=6 for sEVs and n=1 for PBMNCs donor).

In addition, we wanted to evaluate the UCB-MNCs-sEVs potential on the secretion of cytokines by PBMNCs. Without any stimulus, we were not able to detect the secretion of the analyzed small molecules. However, LPS stimulation highly increased the secretion. This way when stimulated simultaneously with LPS and UCB-MNCs-sEVs, PBMNCs mixture significantly decrease TNF-α secretion **(Figure 4.15A)**. TNF-α is a pro-inflammatory cytokine that is involved in the regulation of immunity and several inflammatory diseases in humans[359,360]. As it plays a critical role in the pathogenesis of autoimmune inflammatory diseases, current biological therapies are designed to block its biological function. Added to UCB-MNCs-sEVs potential of increase T_{reg} in the system, the decrease TNF-α secretion is another indication of the UCB-MNCs-sEVs immunomodulatory effect, which could be explored as a future autoimmune therapy. Additionally, CCL20 secretion was tested **(Figure 4.15B)**. One of the main effects of CCL20 is to promote the recruitment of CCR6$^+$ lymphocytes[361]. CCR6 is expressed by a variety of cells of the innate and/or adaptive immune system, in particular T_H17 cells, which exert multiple functions *via* release of cytokine IL-17A in many chronic inflammatory disorders[361,362]. Again, the decrease of *in vitro* production of this chemokine contributes to the immunomodulatory capacities of UCB-MNCs-sEVs.

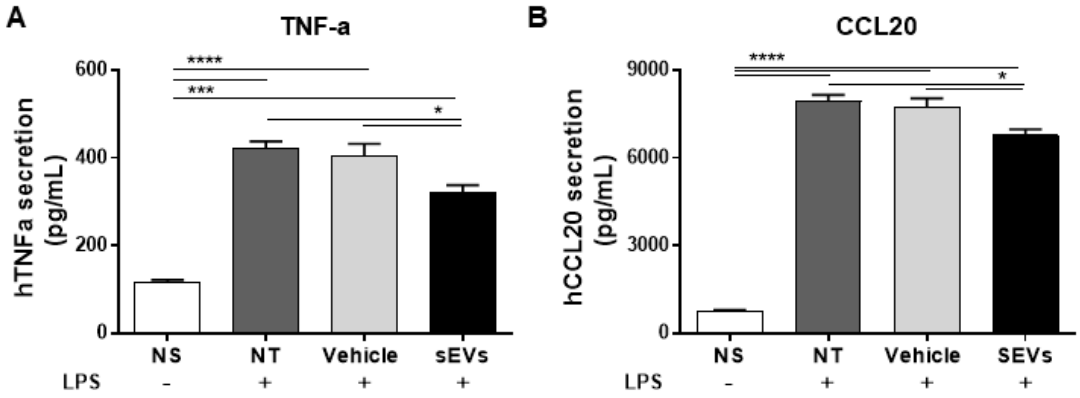

Figure 4.15. UCB-MNCs-sEVs decreases human TNF-a and CCL20 secretion in PBMNCs. PBMNCs were co-incubated with LPS (1µg/mL) and UCB-MNCs-sEVs ($1x10^{10}$ part/mL) for 24h. After this time, the supernatant was collected and analyzed by ELISA. p-values were determined using one-way ANOVA with Tukey HSD as post-hoc test (n=3 for each condition).

Next, the analysis of gene expression levels of master transcription factors was performed after sorting $CD3^+CD4^+$ T cells from PBMNCs mixture. Previously to sorting, PBMNCs were activated and treated for 6 days with UCB-MNCs-sEVs. T cell polarization was evaluated by quantifying the expression of master transcription factors for each helper T cell lineage: *T-BET* for T_H1; *GATA3* for T_H2; *FOXP3* for T_{reg}; and *RORγδ* for T_H17 [363–365] by qPCR.

UCB-MNCs-sEVs do not seem to impact T_H1 and T_H2 T cell subset 6 days after treatment, as observed from the mRNA levels of *T-BET* and *GATA3* **(Figure 4.16A and B)**. Although not significant at 48h for *GATA3* expression, there is a reduction in mRNA expression of the master regulators pointing towards a possible limited T_H1 and T_H2 T cell differentiation face to the control. Interestingly, we observe a significant inhibition of *RORγδ,* which suggest that there is decreased expansion of T_H17 cells upon UCB-MNCs-sEVs treatment **(Figure 4.16C)**. Previous reports showed that approximately 50% of activated T cells expressing this transcription factor produce IL-17A, a key cytokine in the psoriasis and other T_H17 driven-pathophysiology [363].

Moreover, the transcriptional profile indicates a differentiation towards T_{reg} phenotype, with increased expression of *FOXP3* **(Figure 4.16D)**. T_{reg} cells play a pivotal role in the maintenance of peripheral immunological tolerance and control of immune responses toward pathogens and tumors. The identification of *FOXP3* as a specific transcription factor for T_{reg} cells has substantially progressed research on the development, differentiation and suppressive function of T_{reg} cells[366]. Based on these results, we hypothesize that exposing T-lymphocytes to UCB-MNCs-sEVs will increase the population of T_{reg} cells while limiting the T_H17 T-cell subsets.

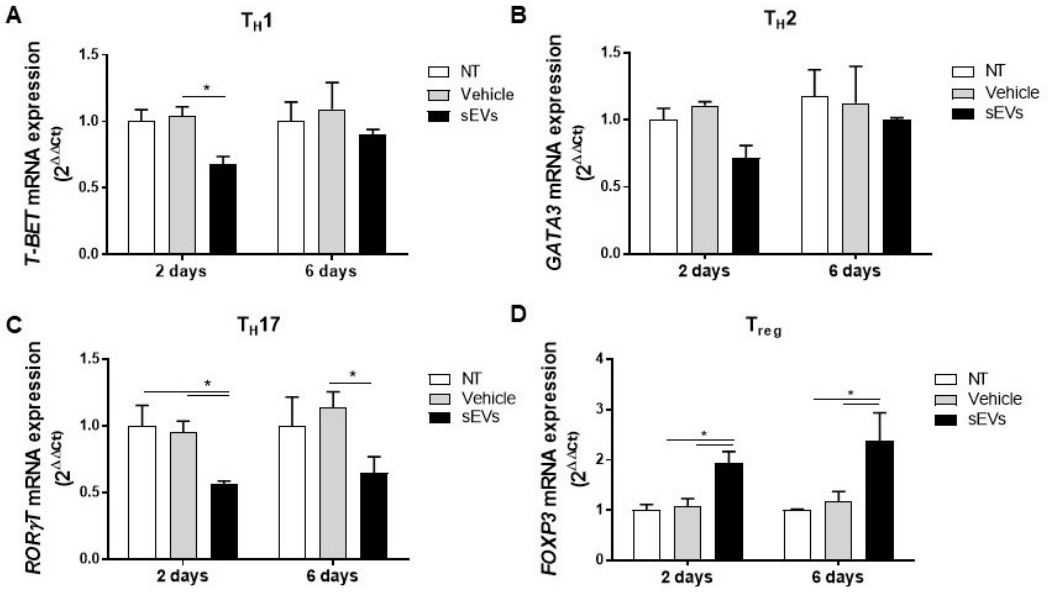

Figure 4.16. UCB-MNCs-sEVs differentially influence master transcriptional T cell factors expression. Activated healthy blood donors PBMNCs were incubated with UCB-MNCs-SEVS ($1x10^{10}$part/mL) or the vehicle (PBS) for 2 and 6 days and the lymphocyte compartment was sorted based on morphological features (FSC and SSC) and $CD3^+CD4^+$ staining. Then, total RNA was extracted, and gene expression analysis was performed using β-actin as reference gene. The normalized expression levels were calculated based on $2^{-\Delta\Delta Ct}$. mRNA expression of (A) T_H1 master transcription factor *T-BET*; (B) T_H2 master transcription factor *GATA3*; (C) T_H17 master transcription factor *RORγδ* and (D) T_{reg} master transcription factor *FOXP3*. p-values were determined using one-way ANOVA with Tukey HSD as post-hoc test (n=6 for UCB-MNCs-sEVs and n=2 for PBMNCs donor).

To confirm these results, we have evaluated the prevalence of T_{reg} (positive for CD25 and FoxP3) within T helper cell subpopulation ($CD4^+$) by flow cytometry. UCB-MNCs-sEVs were able to significantly increase the percentage of T_{reg} in culture (9.68 ±1.89% in treated, against 5.24 ± 2.53% in vehicle) **(Figure 4.17)**. These results indicate that UCB-MNCs-sEVs potentiate the T cell polarization toward T_{reg} cells increasing the immune tolerance and rebalance of Treg/Teff ratio. We believe that the increase on T_{reg} subset is due to a modulation on naïve T cell differentiation rather than promotion of T_{reg} proliferation. After forcing the system with co-stimulation with IL-2 (100 IU/ml) and TGF-β (5ng/mL)[367], UCB-MNCs-sEVs were not able to induce any differences on T_{reg} percentage **(Figure 4.18)**. We hypothesized that if UCB-MNCs-sEVs would induce T_{reg} proliferation, the percentage of this T cell subset would have increased.

Additionally, we aimed to analyzed T_H17 T cell subset upon UCB-MNCs-sEVs stimulation. However, we were not able to confirm the reduction on this T cell subset due to the low prevalence in the PBMNCs mixture (data not shown).

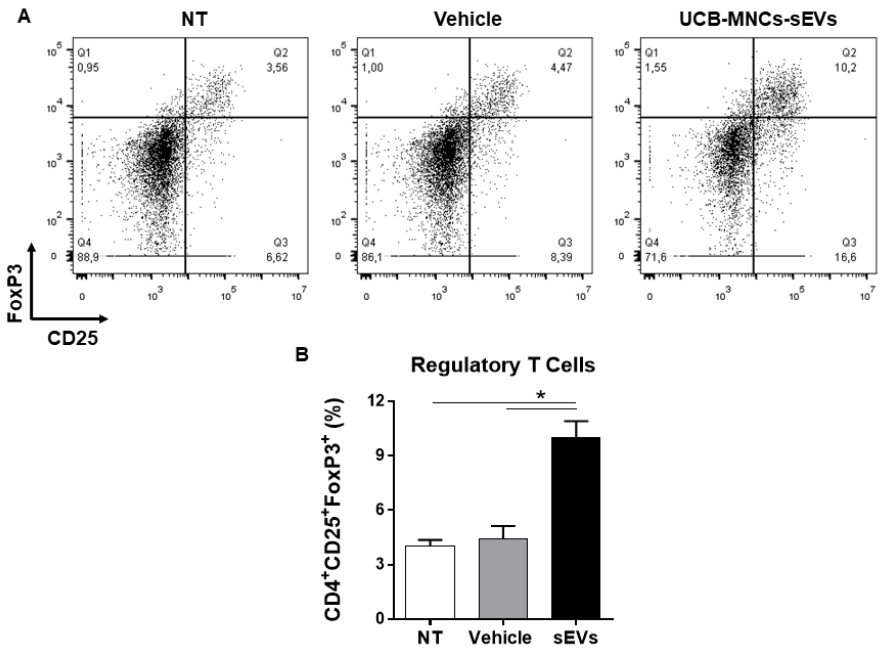

Figure 4.17. UCB-MNCs-sEVs increase regulatory T cells. After activation with αCD3/αCD28, PBMNCs were incubated for 6 days with UCB-MNCs-sEVs ($1x10^{10}$part/mL) or the vehicle. As negative control, PBMNCs were not treated (NT). (A) Representative dot plots for CD25 and FoxP3 staining by flow cytometry. (B) Graph indicated the overall percentage of Regulatory T cells in each condition within CD3 T cell compartment. p-values were determined using one-way ANOVA with Tukey HSD as post-hoc test (n=6 for UCB-MNCs-sEVs and n=2 for PBMNCs).

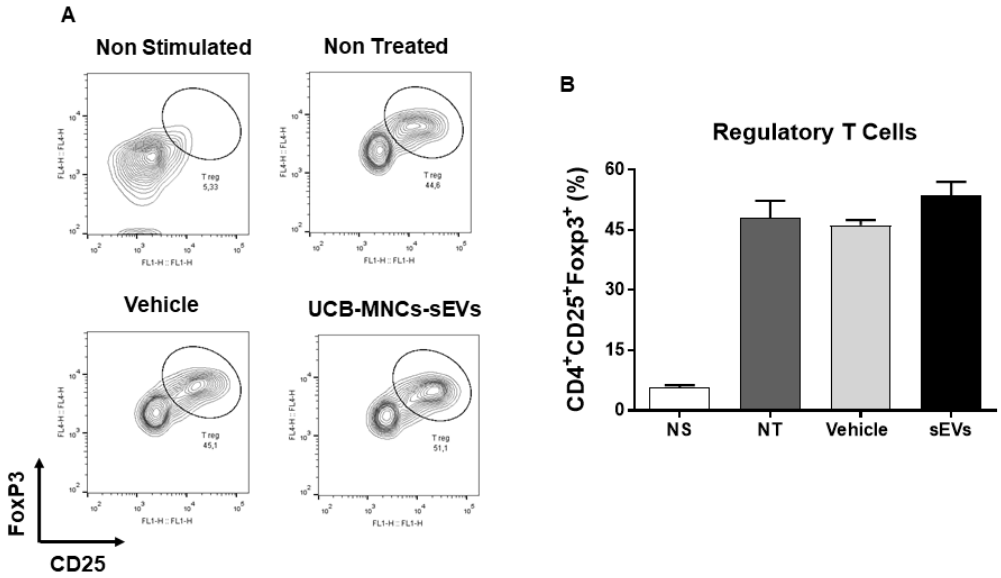

Figure 4.18. After regulatory T cell differentiation, UCB-MNCs-sEVs do not influence cell frequency. After T cell activation with anti-CD3 and anti-CD28, IL-2 and TGF-β was added for 6 days. After that time, the conditioned was renewed and UCB-MNCs-sEVs treatment was added. (A) Representative dot plots for CD25 and FoxP3 staining by flow cytometry. (B) Graph indicated the overall percentage of Regulatory T cells in each condition within CD3 T cell compartment. p-values were determined using one-way ANOVA with Tukey HSD as post-hoc test. No significant differences were found. (n=6 for UCB-MNCs-sEVs and n=1 for PBMNCs).

To reinforce the idea of a rebalance in Treg/Teff ratio and a possible immunotolerant effect derived from UCB-MNCs-sEVs, IL-7 receptor α (CD127) was used as a negative marker of T_{reg} since its expression is inversely correlated with FoxP3 activity and it is reported in the majority of effector and memory T cells[368]. In this experiment, UCB-MNCs-sEVs increase Treg population within $CD4^+$ cells while decreasing the percentage of effector T cells **(Figure 4.19B and C)**. At the end, these differences promote a higher T_{reg}/T_{eff} ratio in PBMNCs mixture **(Figure 4.19D)**. Although increased population of T_{reg} impairs anti-tumor immunity, in an autoimmune disease context, their presence is central to the maintenance of self-tolerance and tissue homeostasis. Moreover, UCB-MNCs-sEVs seem to have an inhibitory effect in cell differentiation toward an effector phenotype. These *in vitro* results agreed with previous data reported for EVs from other sources [221,243,355,369].

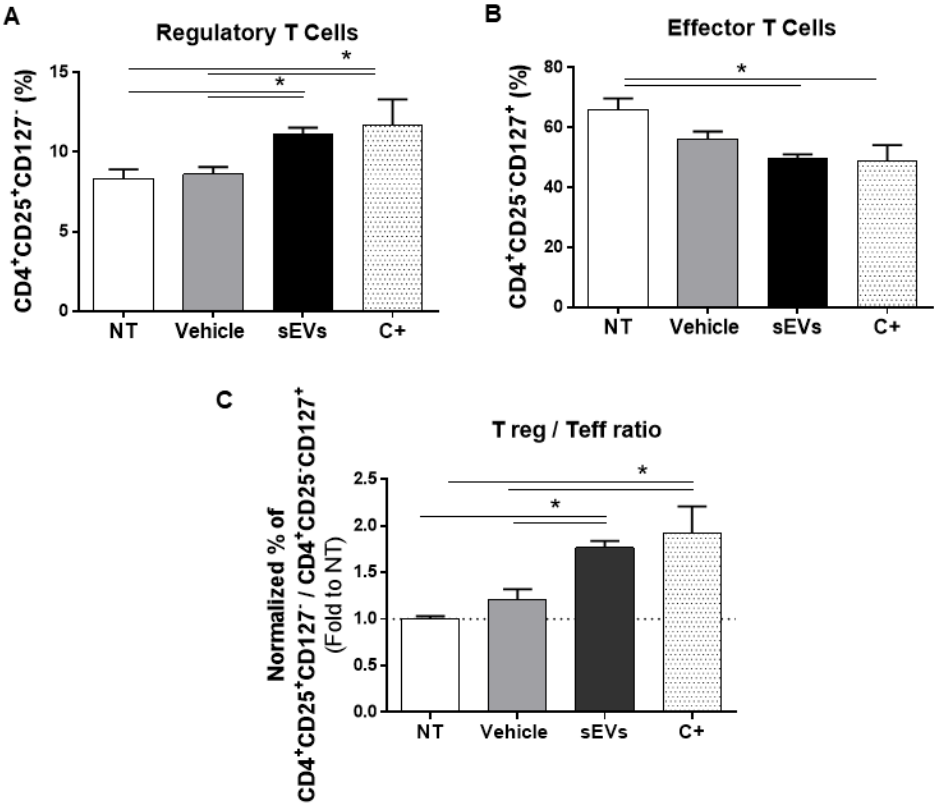

Figure 4.19. UCB-MNCs-sEVs immunomodulatory activity. After activation with anti-CD3 and anti-CD28, healthy blood donors PBMNCs were incubated with SEVS ($1x10^{10}$part/mL) or the vehicle for 6 days. Cells were washed and stained for FACS analysis. For positive control (C+), PBMNCs were additionally stimulated with IL-2 (100 IU/ml) and TGF-β (5ng/mL). A. Percentage of regulatory T cells after 6 days of incubation. Treg were identified as $CD4^+CD25^+CD127^-$; B. Percentage of effector T cells after 6 days of incubation. Teff as $CD4^+CD25^-CD127^+$. C. Ratio Treg/Teff. p-values were determined using one-way ANOVA with Tukey HSD as post-hoc test (n=6 for sEVs and n=1 for PBMNCs donor).

Finally, and because most of the reports test EVs from MSCs, we compared our sEVs derived from UCB-MNCs with EVs purified from UCB-MSCs (MSCs-EVs) and from mononuclear cells extracted from peripheral blood (PBMNCs-EVs).

Similar to the other previous results, UCB-MNCs-sEVs were able to increase T_{reg} percentage while decreasing the percentage of T_{eff} cells **(Figure 4.20)**. Although when compared to Exo-MSCs, based in these two parameters individually, there are no statistical difference. Their ratio (Treg/Teff) is slightly better for the Exo MSCs than for the UCB-MNCs-sEVs. As previously discussed, UCB-MNCs isolated for EVs secretion contain other cells such as RBCs and granulocytes. Although these cells are not the predominant secreting cells, they contribute for sEVs population. Thus, they may hinder MNCs-EVs potential once our normalization values is just particle number. Moreover, EVs isolated from PBMNCs have a smaller impact on T cell subsets when compared with other EVs, despite having some effect on Treg/Teff balance. We believe that these differences can be attributed to the cell source typically used for immune reconstitution in a number of immune deficiencies. Peripheral blood could be considered an attractive alternative tool since the collection of venous blood sample is minimally invasive and an easy procedure that can be performed any time. However, its immunomodulatory potential is smaller when compared with cell sources with a high index of stemness.

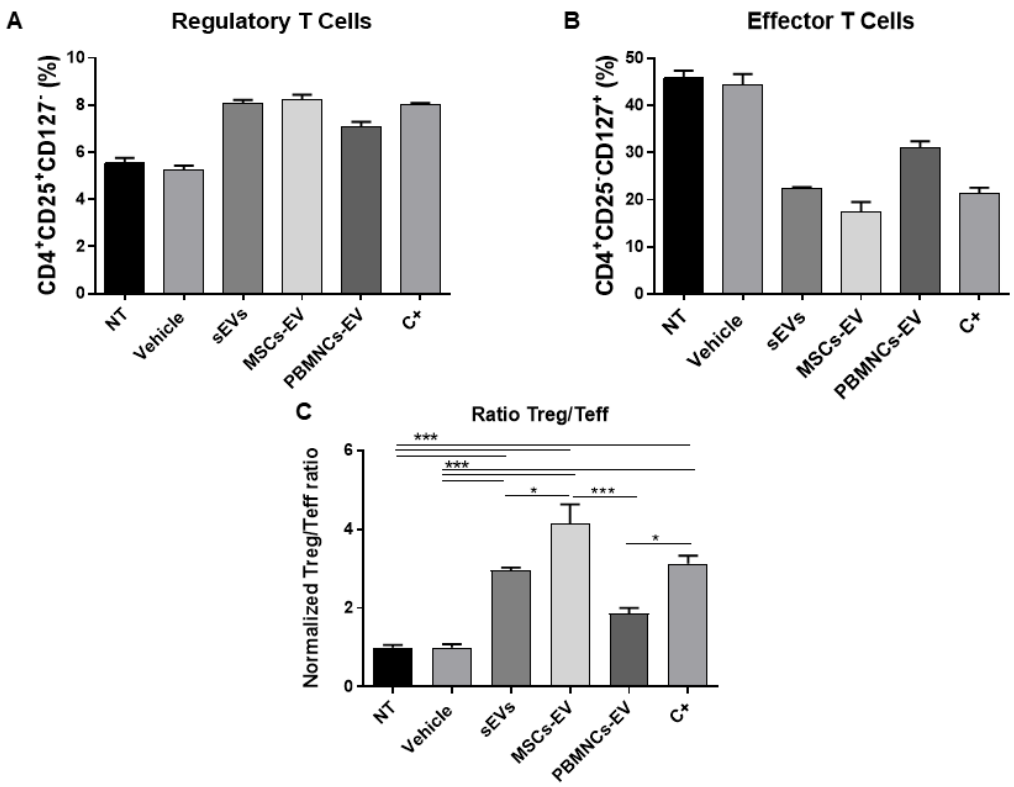

Figure 4.20. Comparison between the immunotolerant effect promoted by UCB-MNCs-sEVs, MSCs-EVs and PBMNCs-EVs. After activation with anti-CD3 and anti-CD28, healthy blood donors PBMNCs were incubated with the same particle concentration ($1x10^{10}$ part/mL) of UCB-MNCs-sEVs, MSCs-EVs and PBMNCs-EVs or the vehicle for 6 days. Cells were washed and stained for FACS analysis. (A) Treg were identified as $CD4^+CD25^+CD127^-$ and (B) Teff as $CD4^+CD25^-CD127^+$. For positive control, PBMNCs were additionally stimulated with IL-2 (100 IU/ml) and TGF-β (5ng/mL). (C) Normalized ratio between regulatory and effector T cells were calculated for each condition. p-values were determined using one-way ANOVA with Tukey HSD as post-hoc test (n=5)

4.4. Gene signature associated to UCB-MNCs-sEVs mode of action in wound healing

During the wound healing process, immune cells reside in the wound site where they regulate inflammation and mediate the tissue repair. The inflammatory response is a crucial component of cutaneous wound healing, as evidenced by severely delayed repair following *in vivo* macrophage ablation[60]. Our team has previously shown that UCB-MNCs-sEVs significantly accelerate healing in different animal models both of acute wounds and delayed healing, such as diabetic animals[253]. The upgrade and upscaling of the manufacturing conditions required that the *in vivo* potency of the UCB-MNCs-sEVs was tested again, in excisional wound healing model of delayed healing (STZ-induced Type 1 Diabetic mice). In this model, the "new" sEVs demonstrated once again their efficacy **(Figure 4.21A)**. Globally, the significant differences are concentrated in the first 6 days of healing, leading to two days of improvement in the total wound healing time, which corresponds

to approximately 13.3%. At day 3, animals treated with UCB-MNCs-sEVs showed a decrease in 20% of wound size and at day 15 almost all treated animals have their wounds closed while in controls animals is still possible to see the injury **(Figure 4.21C and D**).

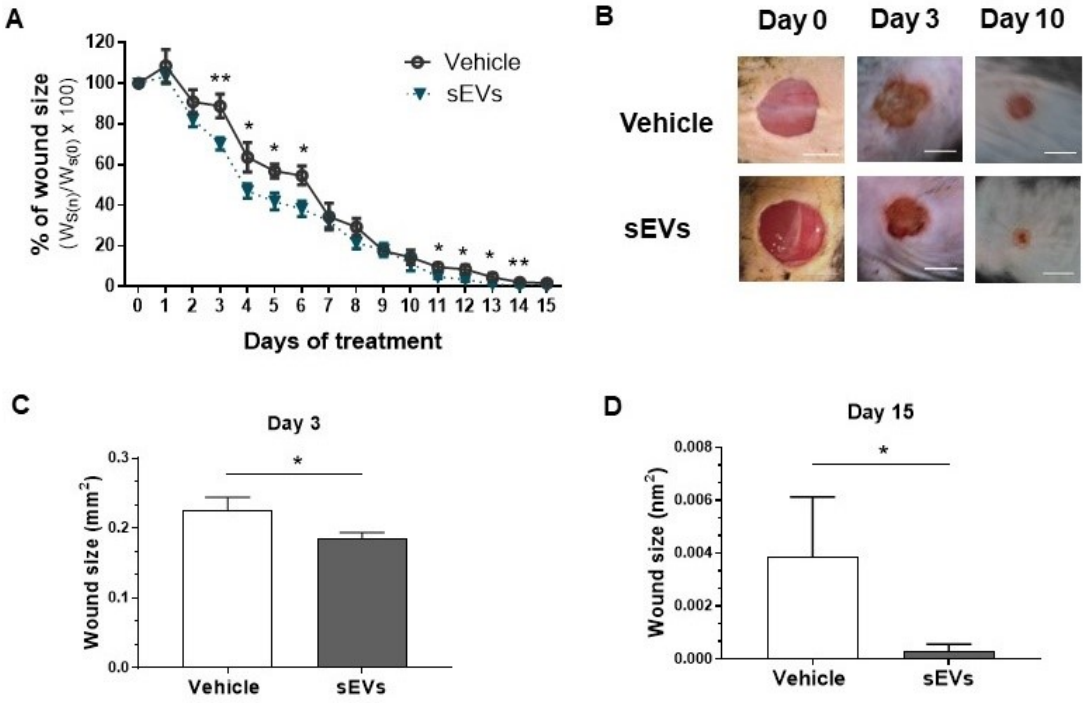

Figure 4.21. UCB-MNCs-sEVs accelerate wound healing in a STZ-induced type 1 diabetic mice. Full-thickness excisional wounds were performed on the skin of 10 chemically induced diabetes C57BL/6 mice, which were randomly assigned to each treatment group: vehicle (PBS) or UCB-MNCs-sEVs. Both treatments were topically applied twice a day. (A) Arithmetic mean and SEM of the wound size percentage for all the mice, at each time point (every day). (B) Representative micrographs of mice wounds at day 0, 3 and 10. Scale bar: 1cm. Wounds size at (C) day 3 and (D) day 10. p-values were calculated by using unpaired t-test (n=10).

STZ-induced type 1 diabetic mice may be not an ideal model to test inflammation because this chemical compound selective destroys pancreatic islet β-cells, resulting in insulin deficiency, hyperglycaemia, polydipsia, and polyuria, all of which mimic human type 1 diabetes mellitus and not inflammatory skin diseases[23]. Nevertheless, we still decided to evaluated mice skin tissues, aiming to characterize and find clues about sEVs mode of action *in vivo* during the inflammatory phase of wound healing. On the other hand, *in vitro* results suggest a strong impact on inflammation and immunomodulation driven by UCB-MNCs-sEVs. In the wound healing process, inflammation is comprehended between day 2 and day 5[70]. Diabetes-associated hyperglycemia induces a significant expansion of the macrophage population in multiple organ tissues namely in the skin. Thus, this increased population triggers a hyperinflammatory reaction and increases proinflammatory cytokines and chemokines, upon an insult[370]. Hence, at day 3, skin biopsies were collected and processed to next generation sequencing analysis. Gene expression analysis allowed

us to globally evaluate 14 269 gene on skin samples of which 19.9% are differentially expressed upon UCB-MNCs-sEVs treatment **(Figure 4.22A)**. Gene enrichment analysis using the *Funrich* software was performed and we observed that the subset of differentially regulated genes for day 3 was enriched in biological processes known to be involved in wound healing, such as cell proliferation, differentiation and adhesion, apoptosis, inflammation and metabolic processes. Interestingly, biological processes such as inflammatory and apoptotic response are more representative on day 3 while cell proliferation and adhesion as well as ECM organization are less prominent as they are mostly related with latter stages of wound healing **(Figure 4.22B)**.

A

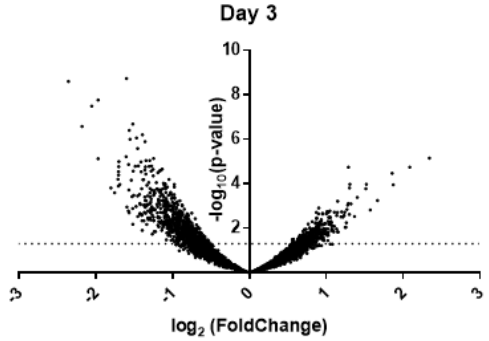

B

Biological Process	# genes	% of total
regulation of transcription	176	13.96
angiogenesis	19	1.51
apoptotic process	104	8.25
cell adhesion	31	2.46
cell differentiation	60	4.76
cell proliferation	87	6.90
ECM organization	3	0.24
immune system process	99	7.85
inflammatory response	95	7.53
ion transport	34	2.70
metabolic process	74	5.87
oxidation-reduction process	94	7.45
translation	45	3.57
Wnt receptor signaling pathway	16	1.27
Total differentially expressed genes	1261	

Figure 4.22. UCB-MNCs-sEVs impact gene expression on mice wounded skin. (A) Volcano plot displaying differential expressed genes between control and UCB-MNCs-sEVs treated skin samples at day 3. The y-axis corresponds to the mean expression value of log 10 (p-value), and the x-axis displays the log2 fold change value. Dash line represents p-value of 0.05, meaning that all the dots above this line have statistical significance. (C) Biological processes/pathways associated to UCB-MNCs-sEVs statistically differential gene expression, as predicted by Funrich software (n=3).

Due to our interest in the inflammatory response, we decided to look closer to the gene subset associated with that phase. Approximately 70% of those were downregulated in UCB-MNCs-sEVs treated animals when compared to the control ones. Among the 65 downregulated genes, 33% of them codified for cytokines, chemokines and interleukins such as *Il-6* (p=0.017), *Il-1β* (p=0.047) and *Cxcl1* (p=0.018). *Cd14* was also found in this list suggesting a decrease on the number of infiltrating macrophages at day 3 (p=0.0091). Notably, GO analysis on these genes showed an association with "negative regulation of T-helper 2 cell differentiation" and "positive regulation of T-helper 1 cell differentiation", suggesting a shutdown on pro-inflammatory mediators while promoting the resolution of inflammation. Interestingly, *Cd163* is among the top up-regulated genes in comparison to the non-treated animals (p=0.0021). This membrane molecule known as

hemoglobin scavenger receptor plays an important role on neutralizing pro-oxidant free heme released during hemolysis in tissue injury and it is also a marker of a "resolving macrophage" phenotype[371]. *Ptgs1* and *Ptgs2*, genes that codified for cyclooxygenase-1 and 2 respectively, are also found as up-regulated genes in treated animals. At first, this result seems contradictory, as prostaglandin production is intimately related with a pro-inflammatory microenvironment. Indeed, prostaglandins have important roles in initiating leukocyte trafficking, stimulating blood flow changes, leading to neutrophil influx to the site of inflammation. However, they also trigger an important switch in neutrophils that later convert proinflammatory prostaglandins into lipoxins, which are anti-inflammatory/pro-resolving mediators, crucial for the transition from inflammation to resolution[372]. In this way, cyclooxygenases have apparently a dual role in the inflammatory process, initially contributing to the onset of inflammation and later helping to resolve the process.

With a strong connection with inflammation, cutaneous immune response is also crucial for healing as reviewed before. Therefore, we also analyzed the immune subset genes differentially expressed upon sEVs treatment (99 genes, 7.85%). The same pattern was observed with 75% of the related genes downregulated. Notably, the gene encoding IL17 receptor α (Il17ra) was found 2.5 times less expressed in treated animals when compared to control (p=6.06E-06).

Complementary, by using Ingenuity Pathway Analysis (Qiagen, Bioinformatics), we were able to predict which upstream regulators may be affected by sEVs at day 3. The software output indicated possible activation or inhibition of different molecule classes that would explain the upregulation or downregulation of the gene used in the input dataset. The software predicted that sEVs treatment downregulated several inflammatory-associated cytokines like IL-1β, IL-6, IFN-γ and TNF-α, indicating a strong anti-inflammatory and immunosuppressive potential at day 3.

The early inflammatory phase of wound repair is characterized by a predominantly granulocytic wave of leukocyte recruitment governed by neutrophil chemoattractants like CXCL1 and CXCL8 and also by monocytes that secrete IL-1, IL-6, TNF-*α*, and MCP-1/CCL2 as prominent chemoattractants[371,373]. As previously identified by RNA-sequencing analysis, we were able to confirm the tendency of decrease in *Il-6*, *Tnf-α* and *Cxcl1* expression by qPCR on UCB-MNCs-sEVs treated animals (**Figure 4.23A, B and C**). No differences were verified on *Il-1β* and *Ccl20* (**Figure 4.23D and E**) and a slight increase was observed for *Il-10* which is an anti-inflammatory cytokine (**Figure 4.23F**). None of these results presented statistical significance maybe due to the low number of samples per group and due to animal associated variability.

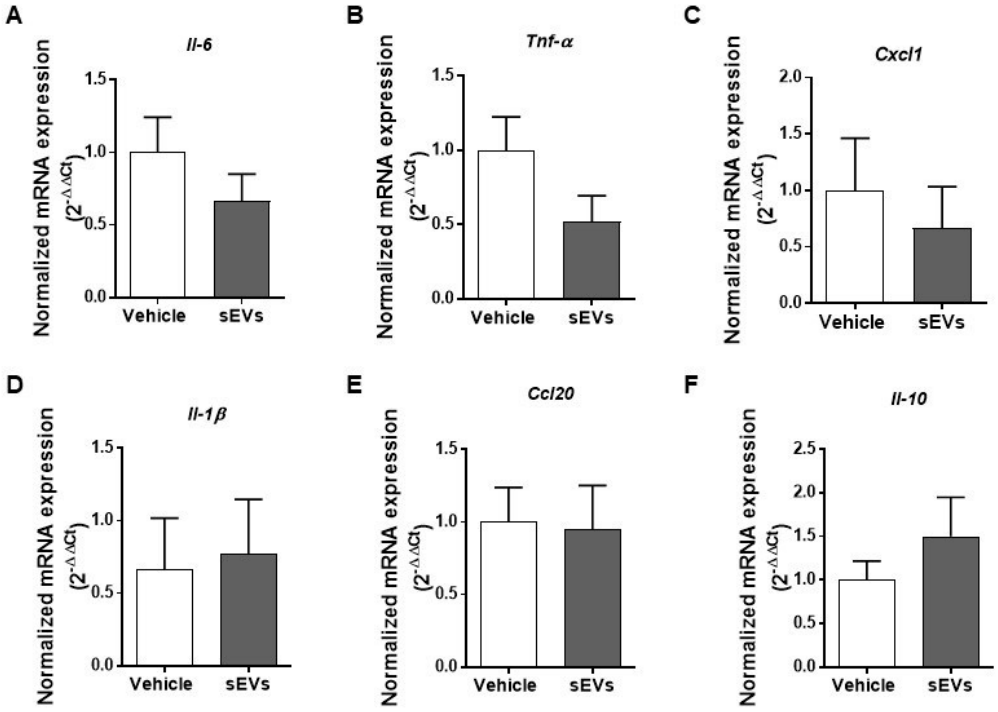

Figure 4.23. Evaluation of UCB-MNCs-sEVs on gene expression of mice wounds at day 3. Fold change of genes associated with inflammatory response by qPCR at day 3: (A) *Il-6*, (B) *Tnf-α*, (C) *Cxcl1*, (D) *Il-1β*, (E) *Ccl20* and (F) *Il-10*. p-values were calculated by using unpaired t-test and no significant differences were found (n=3).

The previous results consolidate a possible UCB-MNCs-sEVs mode of action mediated by macrophages. Therefore, besides validation of *Cd163* expression levels, *Arginase-1* and *iNos* genes were also evaluated. One way of characterizing macrophages into the M1 or M2 population could be by defining their metabolism of one amino acid. The preference of macrophages to metabolize arginine via iNOS to NO or via arginase to ornithine and urea defines them as M1 (NOS) or M2 (arginase)[374].

qPCR results confirmed the RNA-sequencing data, showing an increase on *Cd163* expression levels to almost 4-fold (**Figure 4.24A**). Aligned with this result, *Arginase-1* expression levels were also augmented on sEVs treated skin when compared with control while iNOS expression levels decrease to half (**Figure 4.24B and C)**. These results suggest a modulation of inflammatory macrophage phenotype towards an anti-inflammatory state, indicating that at the same time point (day 3) wounds treated with UCB-MNCs-sEVs are more advanced in wound healing process than the others. Also, we hypothesized that sEVs treatment would help macrophage population to fully switch from a proinflammatory M1 state to an anti-inflammatory M2 program to efficiently promote angiogenesis, connective tissue deposition, and wound repair in the following wound healing phases.

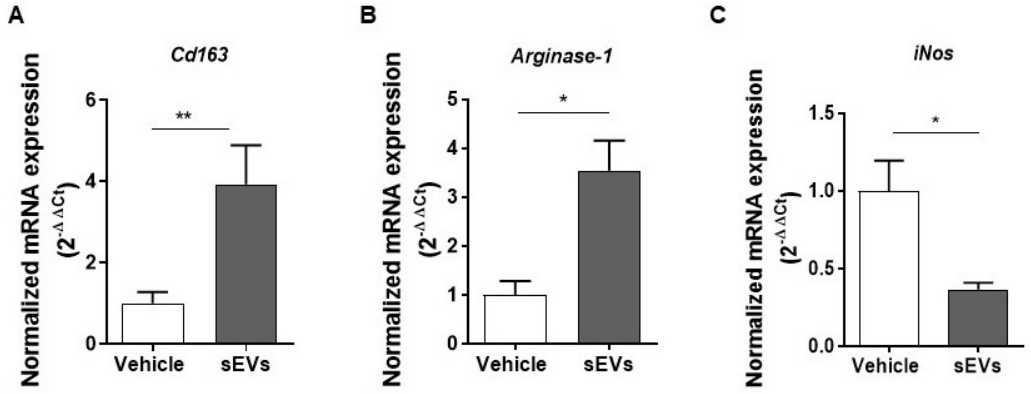

Figure 4.24. UCB-MNCs-sEVs modulate macrophage-associated genes. Fold change of genes associated with macrophages phenotypes: (A) *Cd163*, (B) *Arginase-1* and (C) *iNos*. After RNA was extracted, gene expression was evaluated by qPCR. mRNA expression was normalized for each condition by *GAPDH* and calculated according to $2^{-\Delta\Delta Ct}$. p-values were calculated by using unpaired t-test (n=3).

Additionally, we decided to partially assess the role of the immune system in skin. *In vitro* results have shown that UCB-MNCs-sEVs were able to increase regulatory T cells in PBMNCs mixture as well as decrease T cell activation and cytokine production. Therefore, both *FoxP3* and *Tgf-β* genes were studied in mice skin biopsies. In fact, T_{regs} facilitate cutaneous wound healing[100]. Highly activated Tregs accumulated in skin early after wounding and specific ablation of these cells resulted in delayed wound re-epithelialization and kinetics of wound closure. T_{regs} in wounded skin attenuated IFN-γ production and pro-inflammatory macrophage accumulation[100]. In turn, TGF-β is an important regulator of T cell tolerance, regulating T_{reg} cell homeostasis and modulating Treg cell suppression of T cell proliferation, and T_H1 cell differentiation[375]. Of note, these two genes are upregulated in UCB-MNCs-sEVs treated skins by 2 and 3-fold, respectively (**Figure 4.25**).

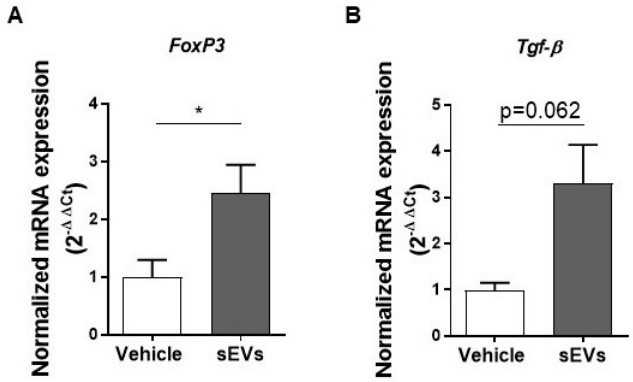

Figure 4.25. UCB-MNCs-sEVs modulate regulatory T cell-associated genes. Fold change of genes associated with immune system namely regulatory T cells: (A) *FoxP3* and (B) *Tgf-β*. After RNA was extracted, gene expression was evaluated by qPCR. mRNA expression was normalized for each condition by *Gapdh* and calculated according to $2^{-\Delta\Delta Ct}$. p-values were calculated by using unpaired t-test (n=3).

Finally, the tissues were also evaluated, at day 15, and despite the lower differences in gene expression among treated and non-treated mice, enrichment in biological process such as ECM production, cell proliferation and angiogenesis were found **(Figure 4.26A)**.

The expression of ECM-related genes was further evaluated in these skin samples and the *Fibronectin* gene was found to be upregulated in treated wounds – 2-fold - **(Figure 4.26B)** while collagen expression was not different in treated and non-treated wounds **(Figure 4.26C and D)**. Interestingly, *Krt10* was also upregulated in treated wounds **(Figure 4.26E)**.

In wound healing, fibronectin plays a critical role in ECM organization and stability. *In vitro* studies revealed that fibronectin is actually required for deposition of collagen I and other structural proteins in the ECM[35]. Probably, our results are indicative of a previous wound healing phase where UCB-MNCs-sEVs treated skin are being prepared for a definitive collagen ECM matrix deposition. Moreover, *in vivo* studies have shown that topical application of fibronectin enhances wound-healing parameters[35]. Nonetheless, as this timepoint correspond to a later wound healing phase of proliferation and remodeling, their analysis is not in the scope of this work and was not included in this PhD thesis.

Overall, these *in vivo* results partially confirmed a mode of action of UCB-MNCs-sEVs mediated by macrophages, modulating at earlier stages inflammation, in a delayed wound healing model.

A

Biological Process	# genes	% of total
regulation of transcription	36	6.33
angiogenesis	17	2.99
apoptotic process	24	4.22
cell adhesion	29	5.10
cell differentiation	23	4.04
cell proliferation	47	8.26
ECM organization	11	1.93
immune system process	13	2.28
inflammatory response	8	1.41
ion transport	6	1.05
metabolic process	5	0.88
oxidation-reduction process	28	4.92
translation	18	3.16
Wnt receptor signaling pathway	14	2.46
Total differentially expressed genes	569	

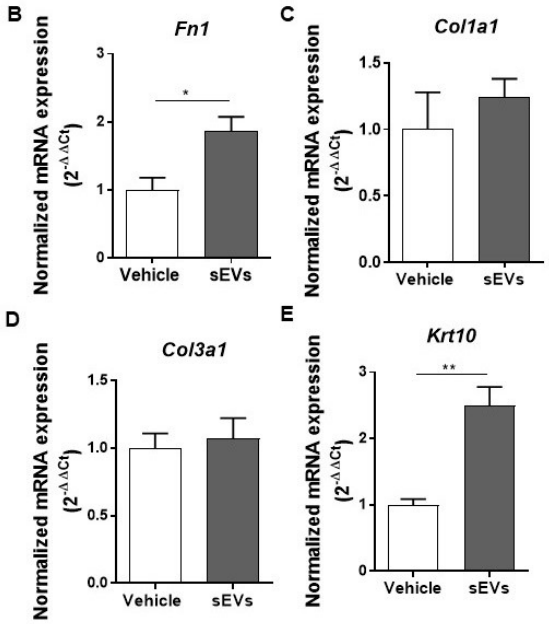

Figure 4.26. UCB-MNCs-sEVs impact on gene expression at day 15 on skin wounds. (A) Biological processes/pathways associated to UCB-MNCs-sEVs statistically differential gene expression; ECM-related genes evaluated by qPCR: (A) FN1, (C) Col1a1, (D) Col3a1 and (E) KRT10. p-values were calculated by using unpaired t-test, only significant differences are indicated (n=3).

Chapter 5: Proof-of-concept UCB-MNCs-sEVs efficacy in Psoriasis

Immune-mediated skin diseases are modulated either by T cells, by the humoral immune system, or by uncontrolled unspecific inflammation. According to the involved T cell subpopulation, T cell–mediated diseases may be further subdivided into T_H1 cell–dominated (e.g., vitiligo), T_H2 cell–dominated (e.g., acute atopic dermatitis), T_H17/T_H22 cell–dominated (e.g., psoriasis), and T_{reg} cell–dominated (e.g., melanoma) responses. The effector mechanisms of the respective T cell subpopulations determine the molecular changes in the local tissue cells, leading to specific microscopic and macroscopic skin alterations[120].

Based on previous results that demonstrated that UCB-MNCs-sEVs have anti-inflammatory and immunosuppressive effects *in vitro*, a pilot study was conducted *in vitro* and *in vivo* in a specific disease model. UCB-MNCs-sEVs modulate macrophage phenotype towards an anti-inflammatory one and soothed the immune system by decreasing T cell proliferation and activation. More specifically, UCB-MNCs-sEVs enhanced the number of T_{reg} increasing immunotolerance and decrease the expression of RORγδ, a master transcriptional factor of T_H17 T cell lineage. Hence, we decided to study the therapeutic potential of UCB-MNCs-sEVs in psoriasis, which is a T_H17-dependent disease.

5.1. *In vitro* experiments

Although some of the most recent treatments are systemically applied, most of the therapeutic approaches for psoriasis remain topical. Currently, human skin equivalents are available, allowing pharmaceutical and cosmetic testing of diverse product formulations. This substitutes are primarily composed of keratinocytes in a three-dimensional arrangement either mimicking or not a pathological condition[376].

Before moving to *in vivo* experiments, a commercial 3D skin model was used ("Psoriasis-like reconstructed human epidermis", Sterlab). This model consists of normal human-derived keratinocytes cultured for 17 days at the air-liquid interface that besides structurally resembling the human epidermis, also exhibit a diseased psoriatic phenotype. Thus, histologically, this 3D model is similar to psoriatic human epidermis and preserves the metabolic activity characteristic of the disease.

This psoriatic human epidermis model was treated for 5 days with a single dose of UCB-MNCs-sEVs twice a day. At the end of experiment, a small piece of the keratinocyte layers was carefully

collected for histological analysis and additional, cells were collected for RNA analysis and supernatant for protein secretion quantification.

At the histological level, no differences were observed **(Figure 5.1)**. In some sections, the inert polycarbonate filter where keratinocytes are cultured is visible. Immediately above, the basal layer composed by oval-shaped cells rich in desmosomes is present **(asterisk, Figure 5.1)** followed by stratum spinosum and granular layers **(black arrows, Figure 5.1)**. Finally, the stratum corneum, the outer layer, is observed and it is composed of dead cells **(cardinal, Figure 5.1)**. Unfortunately, due to scarce raw material, immunohistochemistry was not possible to performed. It would be very interesting to test proliferation markers such as BrdU and overexpressed keratinocyte molecules in human psoriatic lesion like fillagrin or elafin.

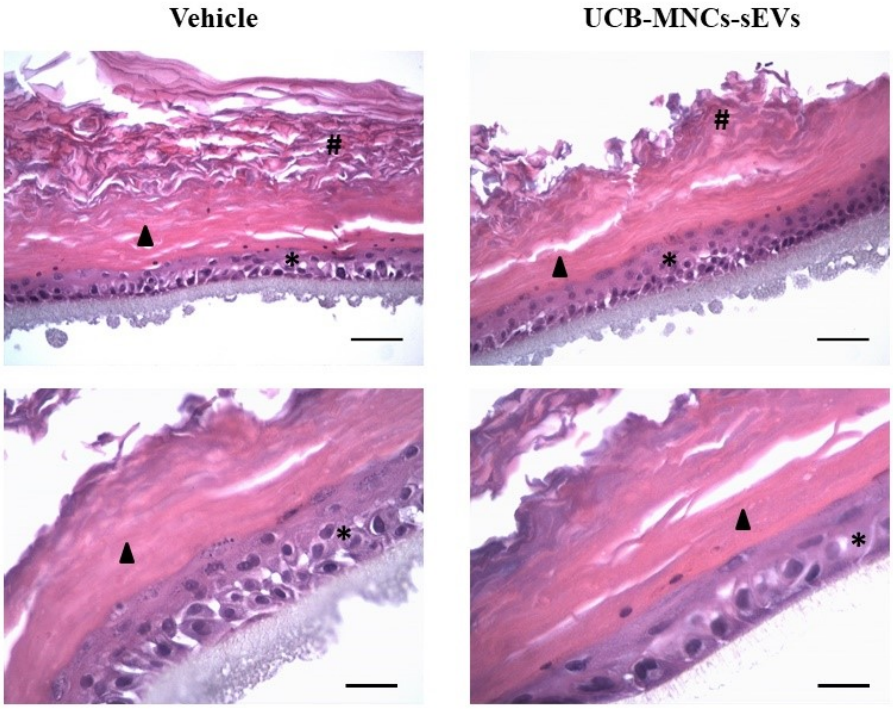

Figure 5.1. Histological cross-section of 3D *in vitro* reconstructed human epidermis. Haematoxylin and eosin staining. Asterisks represent basal layer; black arrows indicate stratum spinosum and granular layer while cardinals point out stratum corneum. Magnification x200 (upper panel) and x400 (bottom panel).

UCB-MNCs-sEVs induced downregulation of the mRNA expression of several cytokines such as *IL-6*, *IL-8*, *TNF-α* and *IFN-γ* **(Figure 5.2)**. Although it was a transversal effect, significant differences were found on *IL-6*, *IL-8* and *CXCL1* ($p<0.05$) decreasing to more than a half the abundance of transcripts found on samples.

Additionally, we have analyzed the expression of antimicrobial peptides (*S100A7* and *DEFB4*) and found consistent downregulation of both **(Figure 5.3A)**. These peptides are largely expressed in

psoriatic epidermis and are responsible for dysregulation of keratinocyte differentiation, a hallmark in psoriasis[377]. Furthermore, these antimicrobial peptides contribute to chemotaxis of neutrophils and T cells[378], exacerbating psoriasis phenotype. Decreasing the expression of these peptides may significantly contribute to ameliorate the psoriatic pathophysiology.

UCB-MNCs-sEVs do not seem to impact the differentiation stage of keratinocytes, as we found no differences in *KRT10* expression **(Figure 5.3B.1)**. Interestingly, *COX-2* expression is downregulated in UCB-MNCs-sEVs treated group, which is expected to contribute to the control of inflammation **(Figure 5.3B.2)**.

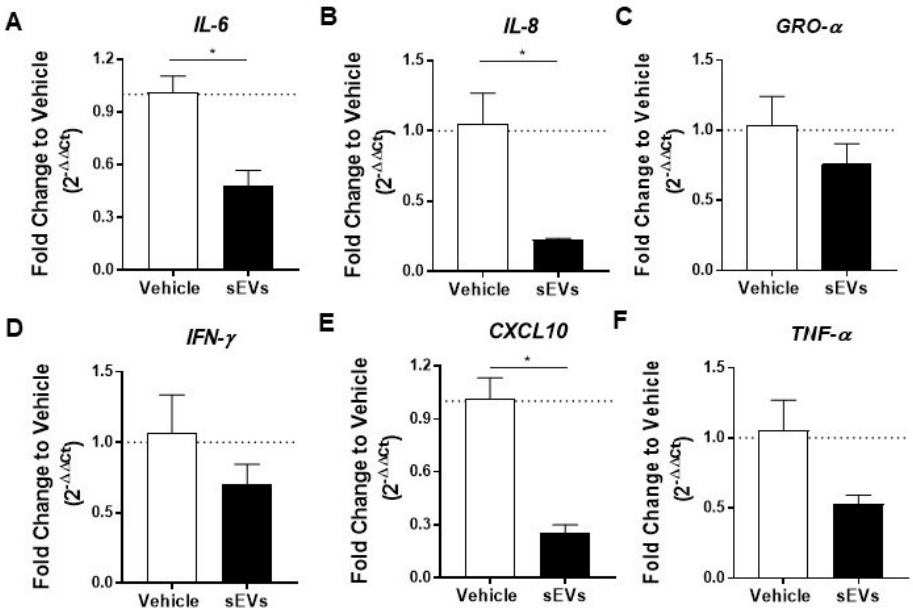

Figure 5.2. UCB-MNCs-sEVs decrease the mRNA gene expression of pro-inflammatory biomolecules on a three dimensional epidermal psoriatic like model. After 5 days of treatment (twice a day with UCB-MNCs-sEVs ($2.5x10^9$part/mL)), RNA was extracted using RNAeasy Mini Kit (Qiagen) according to manufacture recommendations. 500ng of RNA was used for reverse transcription reaction. mRNA expression was normalized by *β-ACTIN* expression gene Gene expression profile of pro-inflammatory mediators: (A) *IL-6*; (B) *IL-8*; (C) *GRO-α*; (D) *IFN-γ*; (E) *CXCL10* and (F) *TNF*-α. p-values were calculated by using unpaired t-test, only significant differences are indicated (n=3 for each condition).

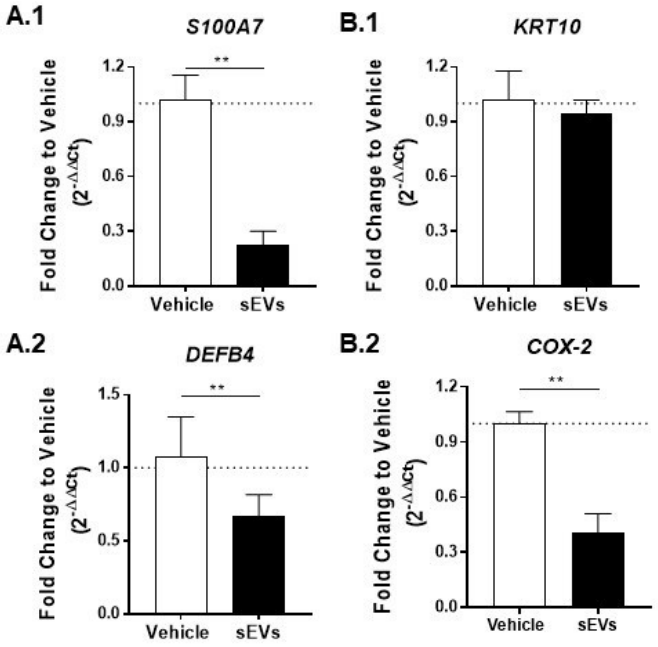

Figure 5.3. UCB-MNCs-sEVs bioactivity on gene expression of different biomolecules in a three dimensional epidermal psoriatic like model. After 5 days of treatment (twice a day with UCB-MNCs-sEVs ($2.5x10^9$part/mL), RNA was extracted using RNAeasy Mini Kit (Qiagen) according to manufacture recommendations. 500ng of RNA was used for reverse transcription reaction. mRNA expression was normalized by *β-ACTIN* expression gene (n=3 for each condition). Gene expression profile of antimicrobial peptides: (A1) *S100A7* and (A2) *DEFB4*. Additionally, (B.1) *KRT10* and (B.2) *COX-2* genes were evaluated. p-values were calculated by using unpaired t-test, only significant differences are indicated (n=3 for each condition).

When analyzing protein secretion we found that UCB-MNCs-sEVs decrease CCL20 and TNF-α **(Figure 5.4A)**, two cytokines involved in psoriasis pathology[379]. UCB-MNCs-sEVs induce a reduction of 40 and 30% on TNF-α and CCL20 secretion, respectively. Moreover, UCB-MNCs-sEVs did not impact IL17A secretion **(Figure 5.4C).**

Similarly to TNF-α, CCL20 is responsible for chemoattracting dendritic and T cells from the blood circulation into inflamed skin tissue. Decreasing these proteins secretion is expected to reduce the local inflammation and hamper immune cell recruitment. Antimicrobial peptides, cytokines, and chemokines such as CCL20 and CXCL1, CXCL3, and CXCL8 are part of the IL-17-induced signature in keratinocytes and play a crucial role in amplifying the immune response in psoriatic plaques[380].

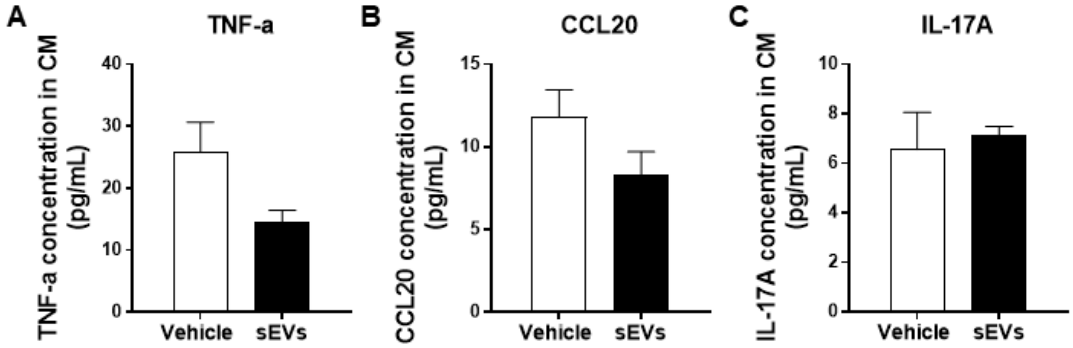

Figure 5.4. Protein secretion in a three-dimensional epidermis-like psoriatic model after UCB-MNCs-sEVs treatment for 5 days. After 5 days of culture, the supernatant was collected and analyzed by ELISA. Protein secretion measured in CM of epidermal psoriatic-like keratinocytes by ELISA: (A) TNF-α, (B) CCL20 and (C) IL17A. p-values were calculated by using unpaired t-test; however, no significant differences were found. (n=3 for each condition).

Overall, these results demonstrated an impact produced by UCB-MNCs-sEVs treatment primarily on keratinocytes with psoriatic characteristics. Nevertheless, as these skin substitutes are derived of only the epidermal layer, constituted by primarily keratinocytes, it limits the result extrapolation for a real use in skin conditions that involve the immune system. The crosstalk between immune cells and keratinocytes and other skin cells is determinant in the pathophysiology of skin inflammatory diseases like psoriasis[82].

5.2. *In vivo* experiment

After the good indicative results obtained *in vitro* but aware of the model limitations, the efficacy of UCB-MNCs-sEVs was tested on a psoriatic *in vivo* model. Although there are few *in vivo* models available, IMQ-induced skin inflammation was chosen as a model that phenotypically resembles psoriasis in mice[43]. IMQ-induced skin inflammation has several advantages compared to other models of psoriasis such as IL23-subcutaneous injected model or genetically modified ones, including rapid and reproducible skin response. While the model does not exactly recapitulate human psoriasis, IMQ treatment of mouse skin can exert specific cytokine expression patterns, histopathological alterations, and cellular infiltrates similar to what is observed in psoriatic patients. IMQ is a ligand for the toll-like receptors TLR7 and TLR8 that exacerbates psoriasis both in the local treated areas as in distant sites. TLR7 and TLR8 are expressed by monocytes, macrophages and DCs that when activated lead to pro-inflammatory cytokines and chemokines production. Application of Aldara, a cream preparation containing 5% IMQ, on hair-free back of mice results in the development of psoriasis-like lesions within 5 days of application and is underpinned by an influx of various cells as well as hyperplasia of the epidermis[41]. The model was induced by topical

application of Aldara, every day. Exogenus Therapeutics' first developed product aimed to be applied topically in a Poloxamer 407 based formulation. This component forms a hydrogel, which allows the emulsion of UCB-MNCs-sEVs in its composition. Poloxamer is generally recognized as a safe excipient widely used in the pharmaceutical industry. It has very low toxicity, weak immunogenic properties, and high stability[381]. From the several attributes of Poloxamer 407, thermoreversibility is emphasized which allows its easy manipulation and consequent successful hydration of the vesicles below 29 ºC and above this temperature it instantaneously jellifies, leading to a slow and controlled release of the vesicles in the site of application. Taking advantage of these characteristics, the efficacy of UCB-MNCs-sEVs was tested topically when incorporated within this hydrogel. Mice were treated during five consecutive days with UCB-MNCs-sEVs. Unfortunately, due a failure in anesthetics equipment, only two mice treated only with gel vehicle survived until day 6. Nevertheless, we proceed with all the analysis with these animals having in mind that due to the low group representativity, statistical analysis is not as robust as we expected. During the course of experiment, mice skin clinical score was monitored. The final value resulted in a sum of three parameters: severity of erythema (redness from 0 to 4), affected area (0-3) and desquamation (scale from 0-2). Clinical signs of psoriasis, such as skin thickening, erythema, and scaling were consistently observed in control animals (IMQ-treated animals) from the third day onwards. Topical application of UCB-MNCs-sEVs or gel only delayed the appearance of psoriatic characteristics and attenuated them over time. Unexpectedly, hydrogel formulation had similar beneficial effects when macroscopic evaluation of clinical score was evaluated **(Figure 5.5B)**. This result may not be representative at day 6 because only 2 animals were evaluated. In the final day of evaluation, treated animals presented significantly less erythema and scales were not observed.

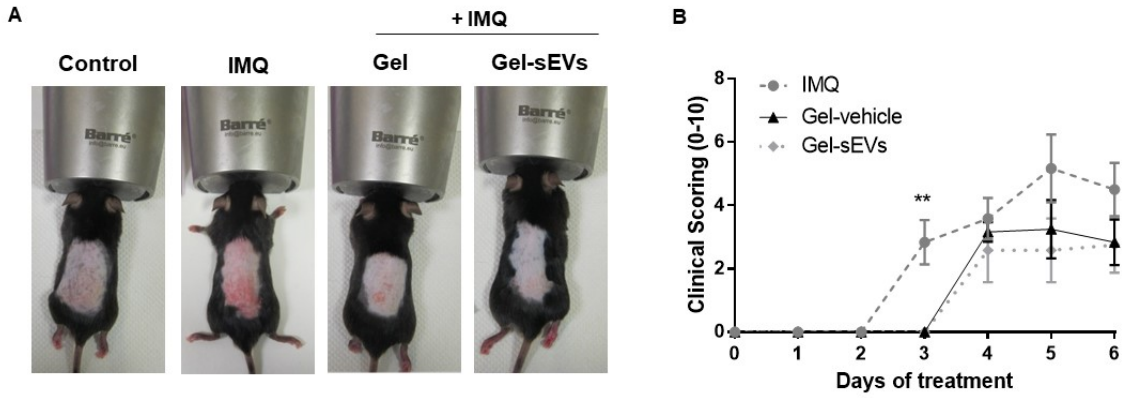

Figure 5.5. Clinical signs of skin inflammation on a psoriatic-like skin inflammation mice model after topical treatment. C57BL/6J mice were used and psoriatic like characteristics were induced by topical application of Aldara, a cream preparation containing 5% IMQ, every day. After one hour of Aldara's applications, UCB-MNCs-sEVs treatment was applied in a topical formulation. (A) Representative photographs of the shaved skin on mice's backs after 6 days of topical treatment. (B) Clinical scoring was performed by ranking severity of erythema (redness from 0 to 4), affected area (0-3) and desquamation (scale from 0-2). p-values were calculated by one-way ANOVA for each time. (n=6 for each group with exception of gel-vehicle: n=2 in the last time point).

Histological skin sections from the back skin of the different experimental groups, with the exception of healthy animals, clearly showed typical alterations present in psoriasis: keratinocytes hyperproliferation, hyperkeratosis, acanthosis, elongation of rete ridges and parakeratosis **(Figure 5.6A)**. Following Aldara treatment the accumulation of neutrophils in the epidermis produced several Munro micro abscesses **(Figure 5.6A, white arrows).** In gel-sEVs treated animals, the number of Munro micro abscesses and epidermal thickness seemed to be apparently less. Also, less rete ridges were observed in this experimental group when compared with gel-vehicle and also with IMQ treatment itself.

Epidermal thickness was measured using hematoxylin and eosin staining. Application of Aldara cream significantly increased the thickness of dorsal skin compared to healthy controls where no product was applied. At day 6, mice in the control and gel group presented a significant difference in epidermal thickness when compared with UCB-MNCs-sEVs treated-animals (69.4 ± 13.8 µm versus 44.2 ± 6.9 µm) **(Figure 5.6B)**. Interestingly, although macroscopically, gel and gel-sEVs groups had similar scores, significant differences were observed microscopically.

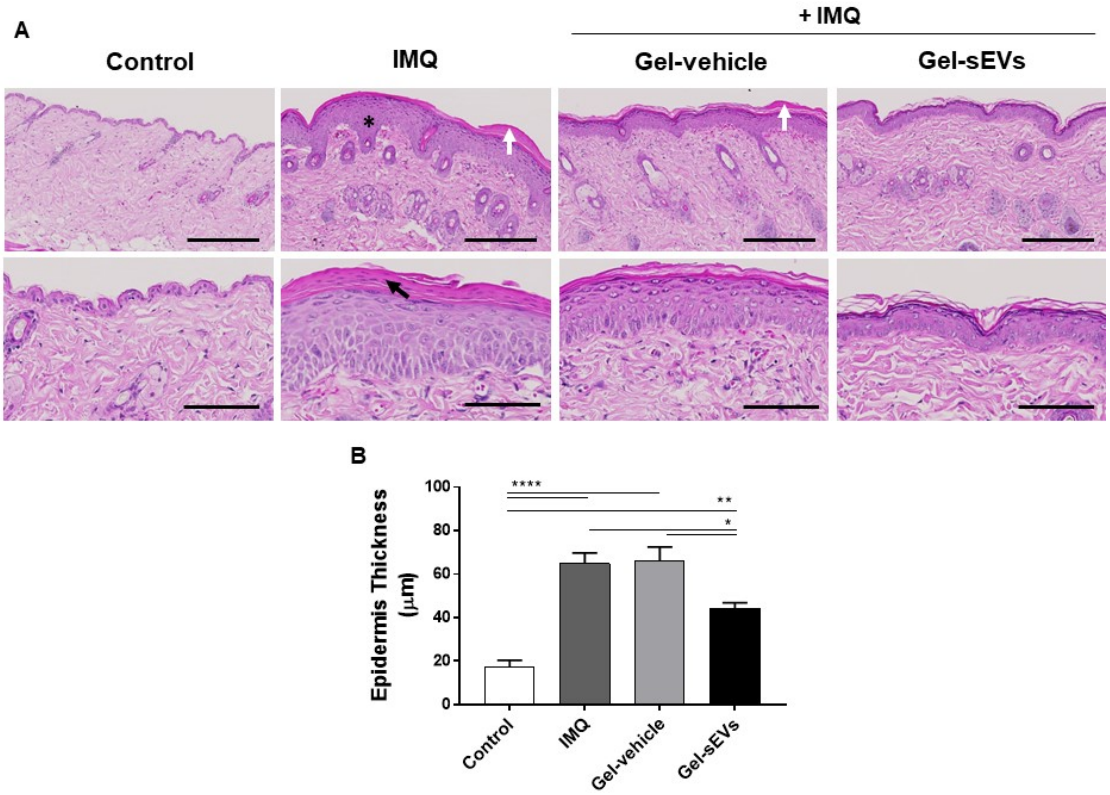

Figure 5.6. UCB-MNCs-sEVs ameliorate histological parameters in a psoriatic-like skin inflammation mice model. (A) Comparison of histological alterations following UCB-MNCs-sEVs topical treatment. Asterisk highlights the increase thickness and elongation of rete ridges provoked by IMQ treatment. Black arrow indicates the nuclei retention of epidermis while white ones point out Munro microabscesses. Upper panel scale bar: 250µm. Bottom panel scale bar: 100 µm. (B) Epidermis thickness was measured in hematoxylin-eosin staining after 6 days of topical treatment in NDP software. p-values were assessed by one-way ANOVA with Tukey HSD for multiple comparisons (n=6 for each condition except Gel-vehicle n=2).

Cellular immunophenotyping analyses by flow cytometry were performed in several mice tissues in the end of the experiment. Skin, blood, LNs and spleen cells were stained with different antibodies to characterize in depth the cellular sub-population that could be affected by sEVs treatment.

The analysis of IMQ-treated skin confirmed infiltration of inflammatory cells, in particular neutrophils, as reported previously[66]. Lin *et al*. reported that mast cells and neutrophils were prominent cells that produced IL-17 in the skin of healthy controls as well as psoriasis patients[382]. Abundant infiltration of $Ly6G^+$cells was observed predominantly in control groups with back to "normal" tendency when treated with the hydrogel formulation **(Figure 5.7A).** Macrophages were also detected on mice skin biopsies and their frequency was not affected by IMQ treatment **(Figure 5.7B)**. Still, we characterized this population of macrophages in two well-defined subsets: classical and nonclassical based on Ly6C expression. Classical macrophages ($CD45^+CD11b^+CD64^+Ly6C^+$) are critical for the initial inflammatory response and can contribute to chronic disease whereas nonclassical macrophages ($CD45^+CD11b_+CD64^+Ly6C^-$) have been widely viewed as anti-inflammatory, as they maintain vascular homeostasis. They are a first line of defense in recognition and clearance of pathogens[383]. Nevertheless, no differences were found within each macrophage subpopulation among the experimental groups **(Figure 5.7C and D).**

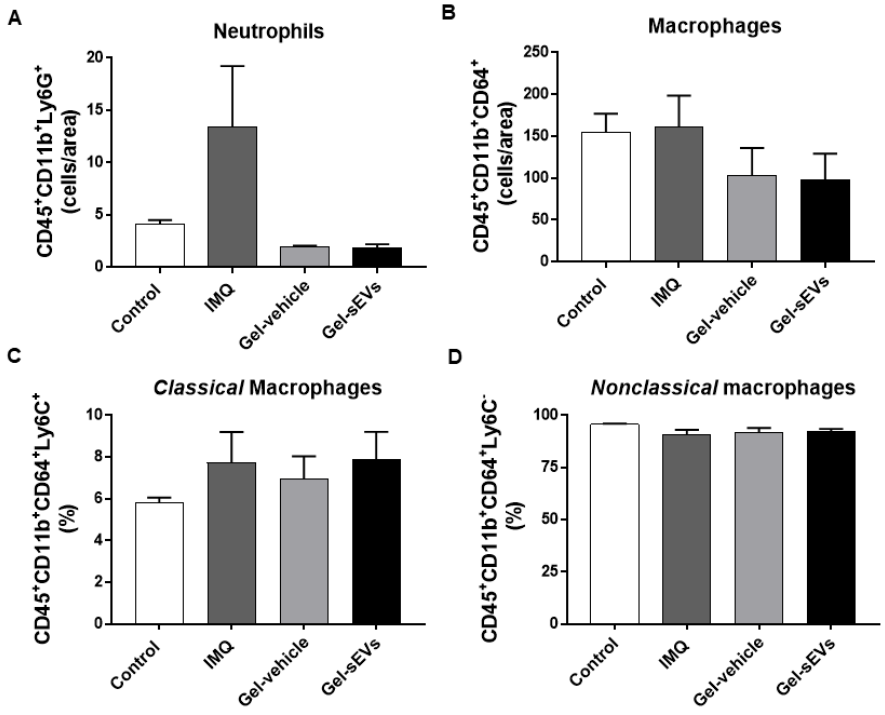

Figure 5.7. Impact of UCB-MNCs-sEVs on infiltration of inflammatory skin cells in skin. Bars indicated quantification of (A) neutrophils ($CD45^+CD11b^+Ly6G^+$) and (B) macrophages ($CD45^+CD11b^+CD64^+$) in skin per area unit harvested from mice. Percentage (%) of (C) classical macrophages ($CD45^+CD11b^+CD64^+Ly6C^+$) and (D) non classical macrophages ($CD45^+CD11b^+CD64^+Ly6C^-$) from live cells are indicated. p-values were assessed by one-way ANOVA with Tukey HSD for multiple comparisons and no differences with statistical meaning were found (n=6 for each condition except Gel-vehicle n=2).

Psoriasis is an autoimmune disease mainly mediated by $CD3^+$ T cells. Flow cytometry results showed that CD3 expression in the skin of IMQ group mice was significantly higher than that of control group **(Figure 5.8A)**. Importantly, a decrease in CD3 expression was observed in mice treated with either gel or gel-sEVs compared to the mice of IMQ group. IMQ treatment elevated the number of CD8 T cells which were significantly decreased by UCB-MNCs-sEVs topical treatment These cells are responsible for IL17 production and so contribute for psoriasis pathogenicity in murine models[45]. UCB-MNCs-sEVs treatment were able to decrease in almost 50% the frequency of CD8 T cells when compared with control animals **(Figure 5.8B)**.

Having in consideration a proposed model by Diani et al. where CD8 T cells may represent the core mechanism of psoriasis pathogenesis, the decreased presence of these cells due to the action of UCB-MNCs-sEVs can have an important role acting on the possible cause of psoriasis and less on the symptom management[380]. These results suggest that UCB-MNCs-sEVs when applied topically hinders $CD3^+$ or $CD8^+$ T cell infiltration in the psoriatic skin.

$CD4^+$ and γδ ($GL3^+$) T cells abundance was similar among experimental groups in skin. We did not observe any quantitative differences in infiltrate composition of γδ T cells nor in their activation state. Interestingly, topical treatment with UCB-MNCs-sEVs was able to significantly increase the number of cells per area of regulatory T cells **(Figure 5.9)**. Of note, Stockenhuber et al. showed that FoxP3 expressing regulatory T cells abolished $CD8^+$ T cell infiltration and excess inflammation through blockage of type I interferon production[384].

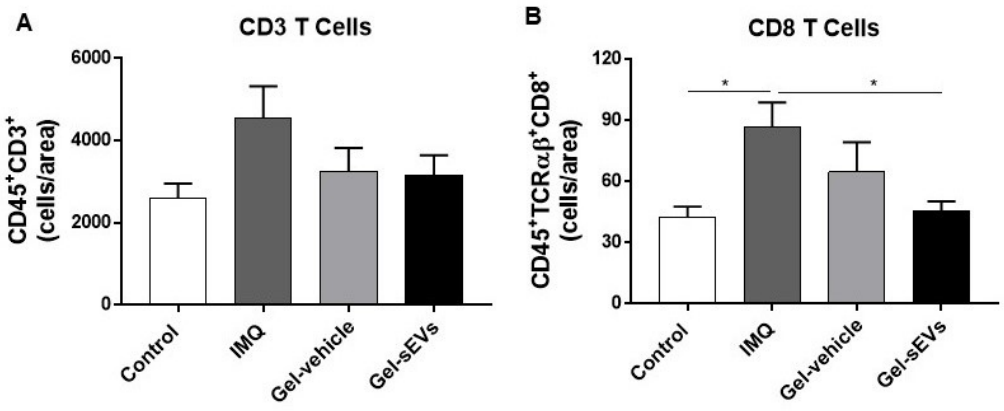

Figure 5.8. Evaluation of infiltrated T cells in IMQ-induced psoriasis like-skin. Bars indicated quantification of (A) CD3 T lymphocytes, (B) CD8 T cells compartment in skin per area unit of skin collected from mice. p-values were assessed by one-way ANOVA with Tukey HSD for multiple comparisons and no differences with statistical meaning were found (n=6 for each condition except Gel-vehicle n=2).

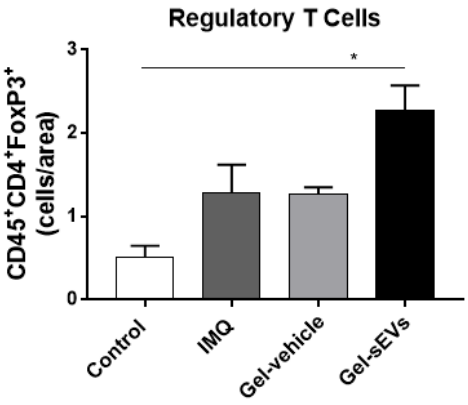

Figure 5.9. UCB-MNCs-sEVs incorporated within the hydrogel promote the infiltration of regulatory T cells on IMQ-induced psoriatic like skin. Bars indicate the number of cells per area unit of collected skin. p-values were assessed by one-way ANOVA with Tukey HSD for multiple comparisons (n=6 for each condition except Gel-vehicle n=2).

We further examined the effects UCB-MNCs-sEVs on mRNA expression of proinflammatory cytokines in the skin of IMQ-induced psoriatic mice using qPCR 6 days after treatment. As shown in Figures 5.10 , the mRNA levels of *Tnf-α*, *Ifn-γ*, *Il-17a*, *Ccl20* and *Cxcl1* in IMQ treated group were significantly higher than those in control group. Application of both gel-vehicle and gel-sEVs significantly reduced the mRNA expressions of these proinflammatory cytokines compared with IMQ-treated mice with the exception of *Ccl20*.

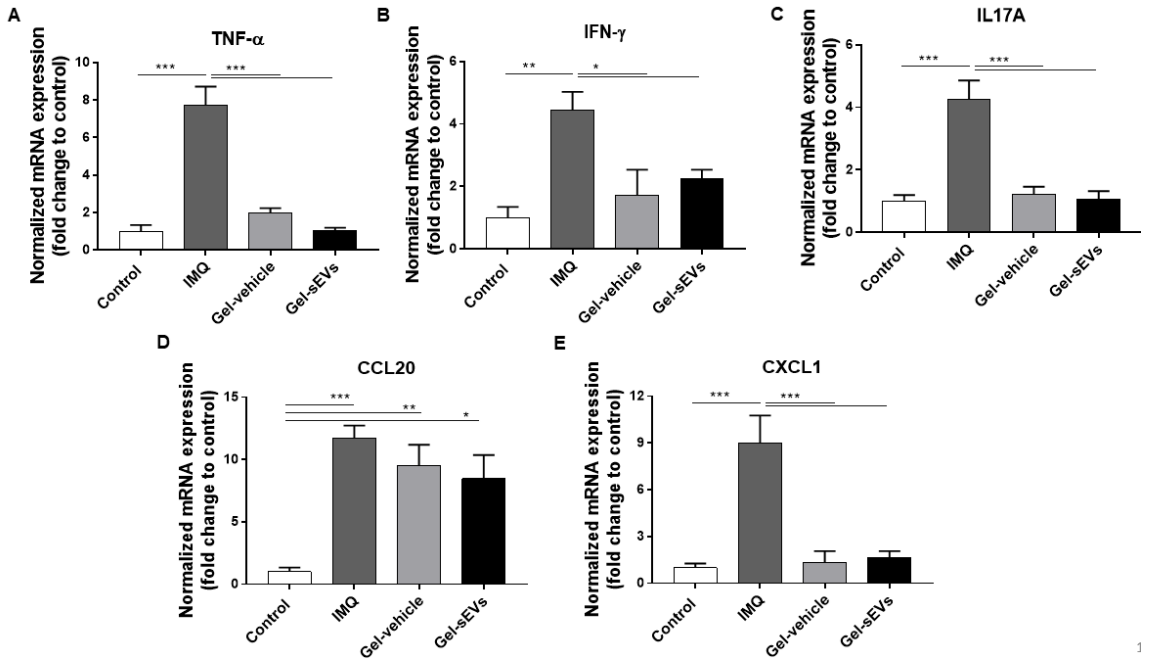

Figure 5.10. UCB-MNCs-sEVs inhibits the mRNA expression of proinflammatory cytokines in psoriatic mouse skin. The mRNA levels of (A) *Tnf-α*, (B) *Ifn-γ*, (C) *Il-17A* (D) *Ccl20* and (E) *Cxcl1* in the skin of IMQ-induced psoriasis-like mice were determined by qPCR analysis 6 days after the treatment without or with UCB-MNCs-sEVs. Values were expressed as fold changes relative to control group that was set as 1.0. Gene expression was normalized to *β-Actin* gene. p-values were assessed by one-way ANOVA with Tukey HSD for multiple comparisons (n=6)

Besides skin, there is now evidence that psoriasis is associated with important systemic manifestations and comorbidities such as cardiovascular disorders, metabolic syndrome, and Crohn's disease. Therefore, the analysis of T cell phenotype in LNs, blood and spleen are important to be evaluated. To determine whether UCB-MNCs-sEVs treatment altered the populations of T cells, the numbers of $CD4^+$, $CD8^+$, and γδ T cells in the spleen, blood and draining LNs, cells harvested from these tissues were assessed on day 6 by flow cytometry.

The numbers of $CD4^+$ and $CD8^+$ T cells in blood did not change during IMQ-induced skin inflammation or when UCB-MNCs-sEVs and hydrogel were applied. Similarly, no differences in γδ T cells number were observed nor in their capacity to produce pro-inflammatory cytokines such as IL17A and IFN-γ, as evaluated by CD27 expression [99].

Both LNs and spleen are lymphoid-type tissues where the immune response is orchestrated, supporting the interaction between peripheral APCs with T cells. In this way, these cell types are expected to migrate into psoriatic lesions while subsequently interacting and thereby generating downstream inflammatory-type responses. Naïve T cells are found primarily within the blood and LNs. When naïve T cells encounter their cognate antigen, they differentiate and gain effector functions including cytotoxicity and cytokine production. During this differentiation process, T cells are imprinted to express tissue specific homing addressins that affect their subsequent migration patterns. Effector T cells are thus programmed during differentiation to migrate to the tissue from which their cognate antigen was originally derived[120].

IMQ trigger a response on CD4 and CD8 T cells in LNs by increasing their number **(Figure 5.11A)**. Both sEVs-gel and gel alone were able to counteract this tendency, decreasing T cell subset population frequency. However, only in CD8 T cell subset the differences between IMQ-treated animals and gel or gel-sEVs were statistically significant **(Figure 5.11A.2)**. Contrarily, in spleen, no significant differences were observed on T cell subpopulations **(Figure 5.11B)**.

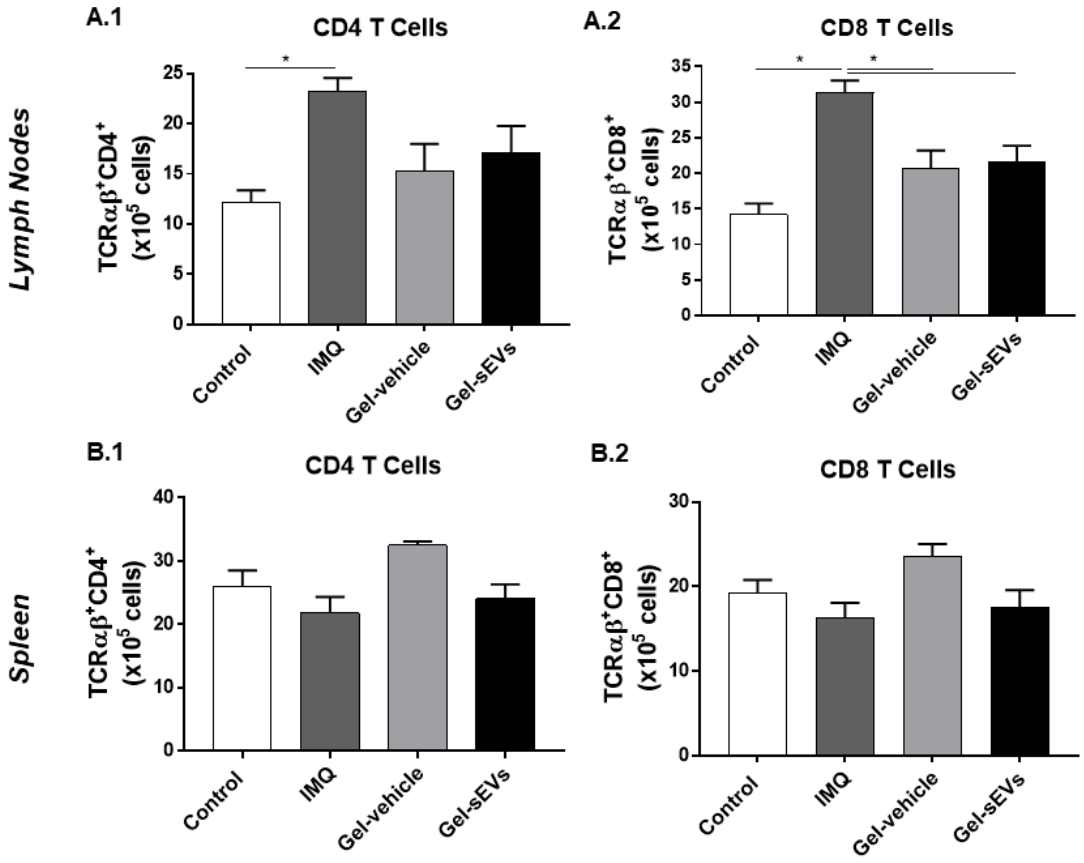

Figure 5.11. T cell frequency on LNs and spleen. Draining LN and spleen cells were isolated from mice 6 days after treatment. The absolute numbers CD4 and CD8 T cells in (A.1 and A.2) LNs and (B.1) and (B.2) spleens of the mice were determined via flow cytometric analysis. p-values were assessed by one-way ANOVA with Tukey HSD for multiple comparisons (n=6 for each condition except Gel-vehicle n=2).

Then, we evaluated whether UCB-MNCs-sEVs topical treatment would suppress effector $CD8^+$ T cells on draining LN and spleen cells isolated from IMQ-induced psoriasis-like mice 6 days after treatment. Flow cytometry analysis revealed that IMQ-treatment significantly increased the percentage of $CD8^+CD44^+CD62L^-$ effector T cells in both LNs and spleens of the mice compared with control group (7.29±1.43 vs. 4.75±0.25 in LNs and 18.55±3.24 vs. 9.29±1.17 in spleens) **(Figure 5.12B and C)**. Both gel and gel-sEVs significantly decreased effector $CD8^+$ T cells percentages in both draining LNs and spleens of psoriasis-like mice. However, as the absolute number only changed in LN, the treatment impact was higher in this lymphoid organ when compared with spleen. These findings suggest that the hydrogel formulation hinders the development of $CD8^+CD44^{high}CD62L^{low}$ effector T cells in psoriatic mice.

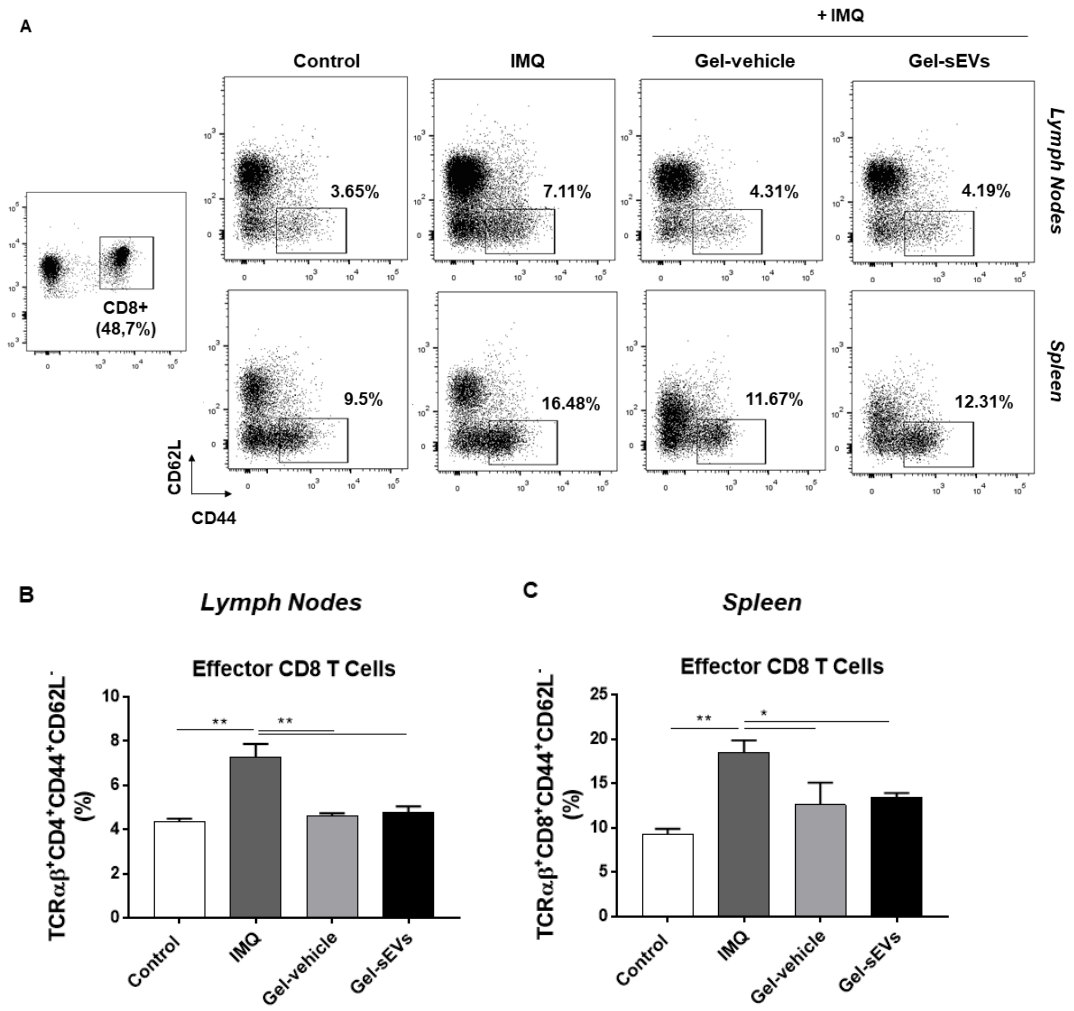

Figure 5.12. Topically treated conditions decrease the frequency of $CD8^+CD44^+CD62L^-$ effector T cells in IMQ-induced psoriasis-like mice. Draining LN and spleen cells were isolated from mice 6 days after treatment. (A) Representative dot plots of effector CD8 T cells in LNs and spleens are shown in the different experimental conditions. The frequencies of $CD8^+CD44^{high}CD62L^{low}$ in (B) LNs and (C) spleens of the mice were determined via flow cytometric analysis. p-values were assessed by one-way ANOVA with Tukey HSD for multiple comparisons (n=6 for each condition except Gel-vehicle n=2).

The effects of topical UCB-MNCs-sEVs treatment on the numbers of $CD4^+FoxP3^+$ Tregs on draining LNs and spleen were also assessed after 6 days of IMQ treatment. T_{reg} numbers in both lymphoid tissues were increased during imiquimod-induced skin inflammation **(Figure 5.13B).** Thus, increased the numbers of T_{reg} did not correlate with the observed, increased disease severity in IMQ-treated mice. This result was observed previously by Sugiyama et al. in skin lesions of psoriasis, they reported that although there is a considerable number of T_{reg}, these cells have decreased suppressive activity[385].

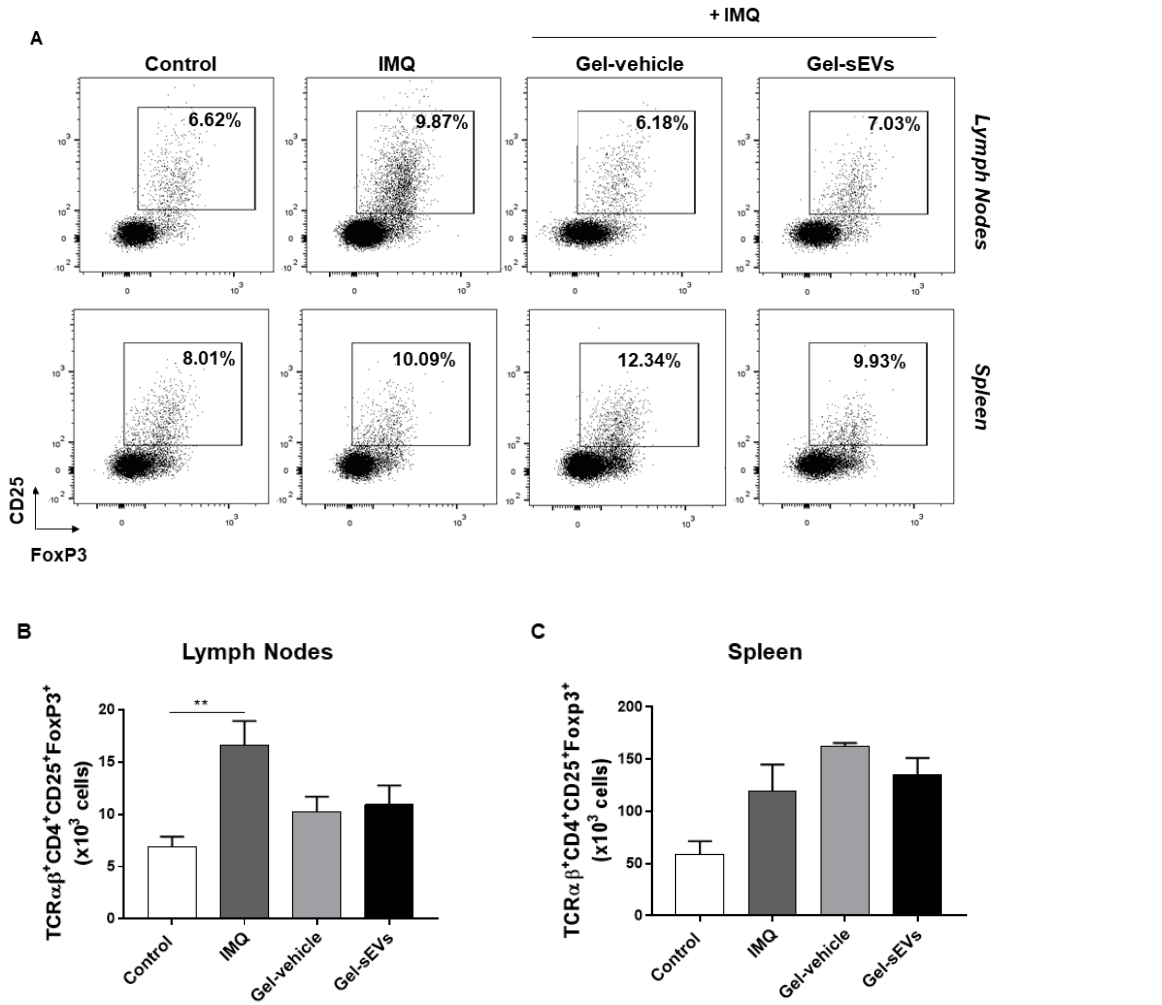

Figure 5.13. Regulatory T cells frequency in LNs and spleen do not correlate with disease severity. Draining LN and spleen cells were isolated from IMQ-induced psoriasis-like mice 7 days after. (A) Representative dot plots of regulatory T cells in lymph nodes and spleens are shown in the different experimental conditions. The absolute numbers of $CD4^{+}Foxp3^{+}$ T_{reg} were measured in (B) lymph nodes and (C) spleens via flow cytometry. p-values were assessed by one-way ANOVA with Tukey HSD for multiple comparisons (n=6 for each condition except Gel-vehicle n=2).

Further, we examined whether topical UCB-MNCs-sEVs treatment would affect cytokine expression during imiquimod-induced skin inflammation by assessing the mRNA expression of several cytokines. Draining LNs were harvested after 6 days of imiquimod treatment, and the expression of *Tnf-α*, *Ifn-γ*, *Il-22* and *Il-17a* was quantified by qPCR. Relative mRNA expression of *Il-17a* was not altered by IMQ treatment (**Figure 5.14A**). However, IMQ treatment was able to significantly increase the other cytokine transcripts when compared to control. Both Gel-vehicle and Gel-sEVs groups impact the abundance of cytokine transcripts, promoting their significant downregulation **(Figure 5.14B to D)**. Furthermore, *Rorγδ* and *FoxP3* expression was also evaluated. In accordance with what we have observed in cell phenotyping, both treatment groups seemed to impact on the frequency of IL17A producing cells which is regulated by *Rorγδ.* In this way, *Rorγδ* transcripts were less prevalent in these conditions **(Figure 5.14E).** Additionally, *FoxP3*

expression, the master transcription factor associated with T_{reg}, have a contrary pattern to what we expected. IMQ increased significantly *FoxP3* transcripts while treatment group oppose this tendency **(Figure 5.14F).** Nevertheless, these results are in accordance with the previous cell evaluation **(Figure 5.13B).**

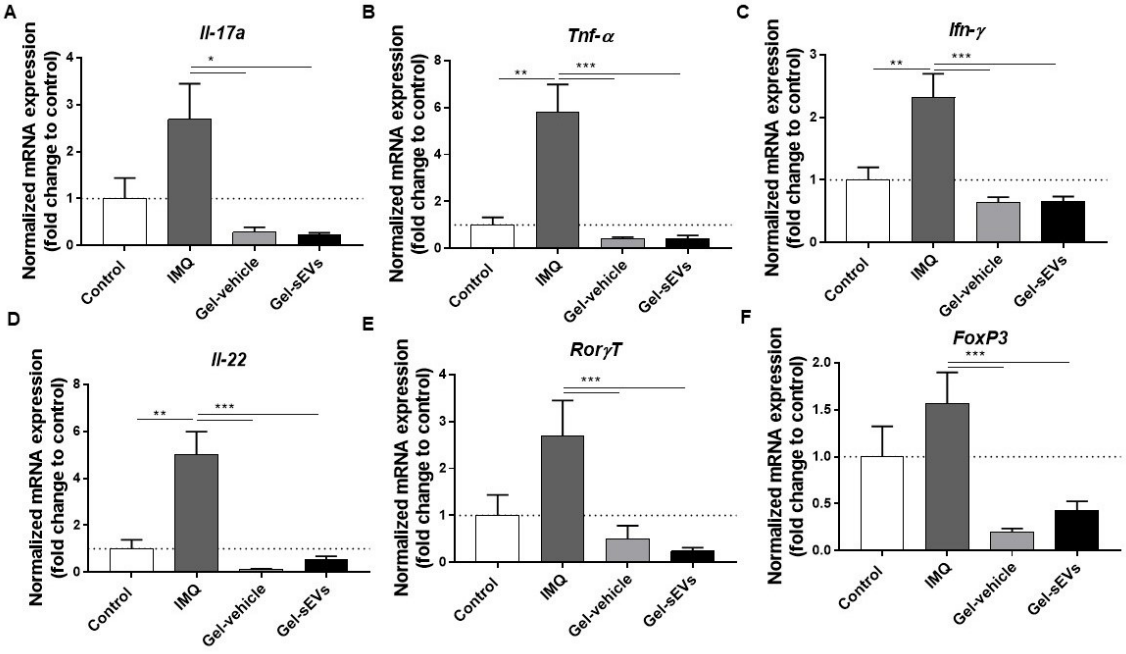

Figure 5.14. mRNA expression analysis in LNs. Mice skin-draining lymph nodes were taken on day 6 of treatment, cells were dissociated, and their RNA was extracted. Analysis of mRNA transcripts of pro-inflammatory mediators: (A) *Il-17a*, (B) *Tnf-α*, (C) *Ifn-γ* and (D) *Il-22*. (E) T_H17 (*Rorγδ*) and (F) T_{reg} (*FoxP3*) transcriptional factor were also evaluated. p-values were assessed by one-way ANOVA with Tukey HSD for multiple comparisons. (n=6 for each condition).

Based on the above presented results, we questioned whether UCB-MNCs-sEVs potency may have been partially hindered by hydrogel formulation or the formulation itself had interfered with IMQ action, blocking the development of psoriatic features. Moreover, our results in PBMNCs suggested a systemic immunomodulation rather than local. Therefore, we decided to repeat the experiment using a different route of administration. Notably, the route of administration can affect whether EVs will induce an activating or inhibitory immune response due to their biodistribution pattern[386]. For instance, administration into the footpad resulted in EVs localization into LNs[387]; intranasal administration delivered EVs to the brain[388], across the blood brain barrier, opening exciting opportunities on the exploitation of EVs as drug delivery system to the brain; periocular injection of EVs reached the neurosensory retina[386]. In the new experimental settings, UCB-MNCs-sEVs were injected intravenously in mice tail vein every day ($5x10^9$ part total corresponding to 5 µg of total protein).

As expected, the control mice without IMQ did not show any sign of skin inflammation. The symptoms of psoriasis-like lesions, including skin erythema, scaling, and thickening, started to appear three days after the beginning of IMQ application in both IMQ and sEVs-treated group. IV UCB-MNCs-sEVs treatment exacerbated erythema, scaling and thickening, and overall skin lesion being markedly different at day 4 and 6 **(Figure 5.15B).** Taken together, our data suggest that intravenously UCB-MNCs-sEVs intensified skin lesions of IMQ-induced psoriatic mice.

Psoriatic lesions are mainly characterized by hyperkeratosis and epidermal hyperplasia. Based on HE staining, IMQ group mice exhibited significant epidermal hyperplasia, acanthosis, and hyperkeratosis in the epidermis 6 days after the experiment starting day **(Figure 5.15C).** The clinical score showed that the intravenous injection of UCB-MNCs-sEVs did not alleviated any histological parameter, having no impact on epidermal thickness **(Figure 5.15D).**

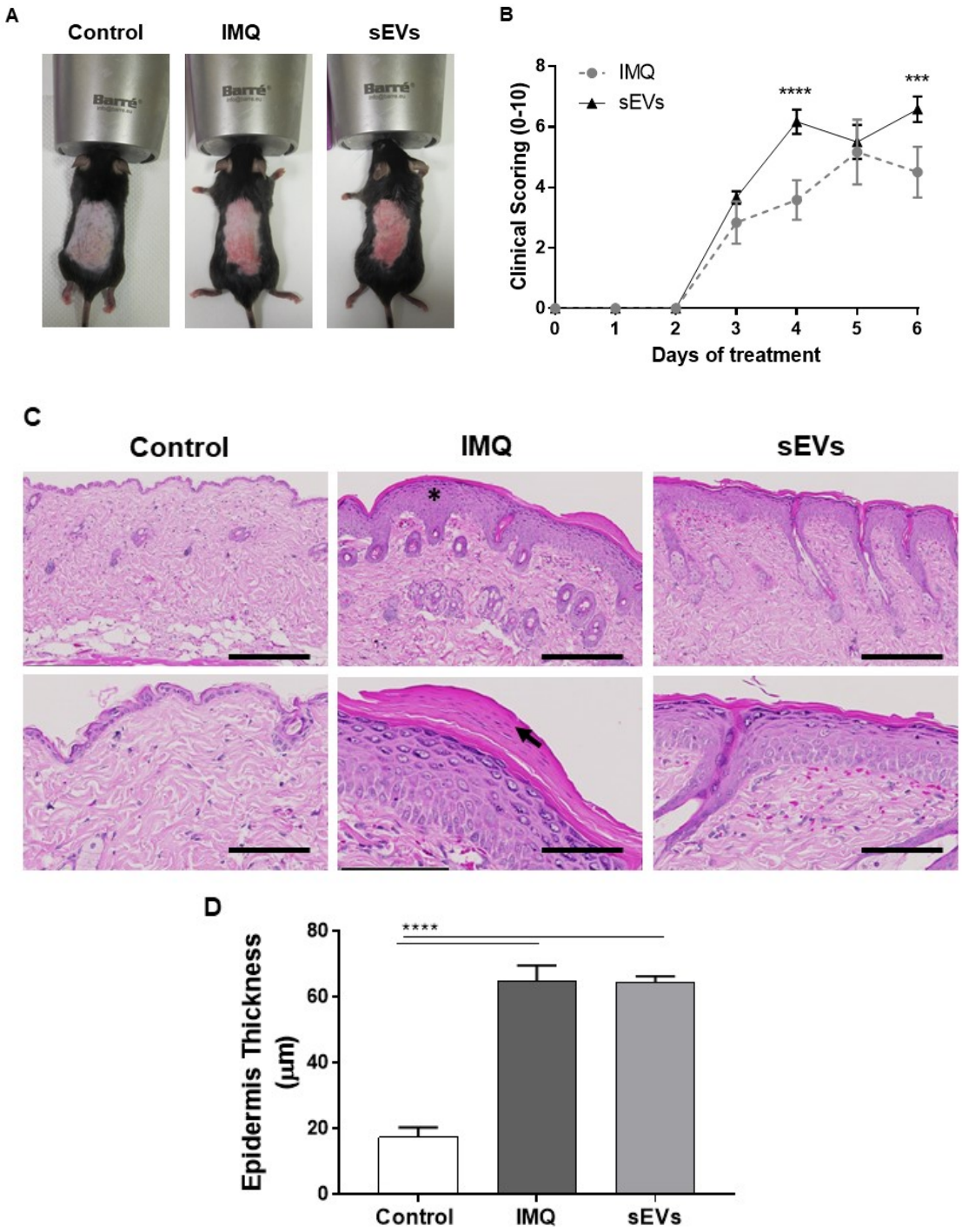

Figure 5.15. IV injection of UCB-MNCs-sEVs did not alleviated skin lesions on IMQ-induced skin inflammation mice model. (A) The representatives of photos of dorsal skin in IMQ-induced psoriasis-like mice 6 days after IMQ-treatment without or with UCB-MNCs-sEVs. (B) Clinical scores of the skin lesion in IMQ-induced psoriasis-like mice throughout the experiment. (C) Comparison of histological alterations following UCB-MNCs-sEVs topical treatment. Asterisk highlights the increase thickness and elongation of rete ridges provoked by IMQ treatment. Black arrow indicates the nuclei retention of epidermis. Upper panel scale bar: 250µm. Bottom panel scale bar: 100 µm. (D) Epidermis thickness was measured in hematoxylin-eosin staining after 6 days of topical treatment. p-values were assessed by one-way ANOVA with Tukey HSD for multiple comparisons (n=6 mice per group).

Although the results were not promising for the systemic use of UCB-MNCs-sEVs as a therapeutic tool for psoriasis, we decided to analyze the samples, in attempt to evaluate whether it could be a dosage limitation or an active stimulation of the immune system due to human/mice incompatibility. Hence, skin innate immune cells were analyzed by flow cytometry. The abundance of neutrophils and macrophages was similar in both sEVs treated and non-treated animals. However, IMQ, as expected, elevated the infiltration of these cell type. Curiously, the frequency of classical macrophages was significantly higher (23.76 ± 8.52 versus 10.56 ±7.01) on UCB-MNCs-sEVs treated animals **(Figure 5.16C)**, unveiling a possible specific mechanism of activation of macrophages.

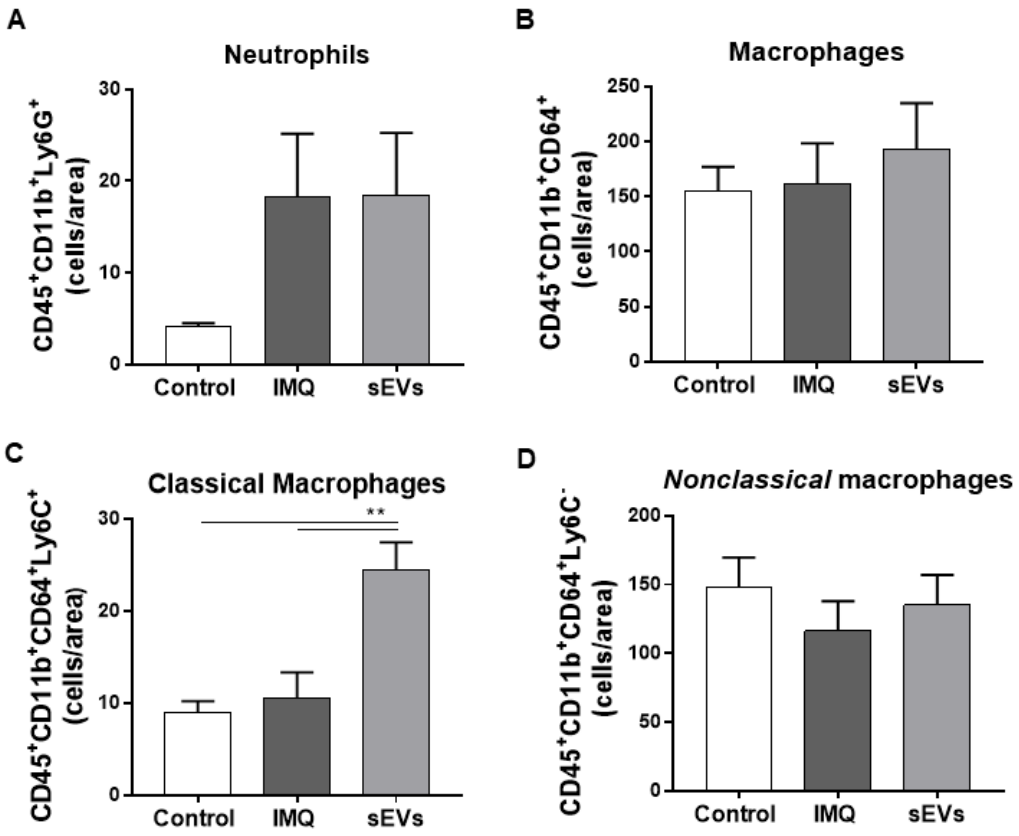

Figure 5.16. Impact of intravenous UCB-MNCs-sEVs on skin infiltrating inflammatory cells. Bars indicate quantification of (A) neutrophils ($CD45^+CD11b^+Ly6G^+$) and (B) macrophages ($CD45^+CD11b^+CD64^+$) in skin per area unit harvested from mice. Percentage (%) of (C) classical macrophages ($CD45^+CD11b^+CD64^+Ly6C^+$) and (D) non classical macrophages ($CD45^+CD11b^+CD64^+Ly6C^-$) from live cells are indicated. p-values were assessed by one-way ANOVA with Tukey HSD for multiple comparisons (n=6 mice per group).

On infiltrating skin T cells, no differences were found in any specific subset**.** Nevertheless, although not statistically significant, there is a tendency of decrease on IL17A producing cells within CD4 compartment **(Figure 5.17).** In absolute number, UCB-MNCs-sEVs reduced from 6 to 4 cells per unit area.

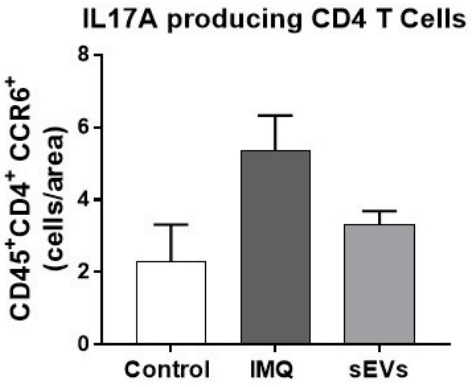

Figure 5.17. Evaluation of CCR6 expressing cells within skin CD4 compartment upon UCB-MNCs-sEVs intravenous treatment. Upon collection of dorsal mice skin, cells were extracted and prepared to flow cytometry analysis. Graph shows the absolute number of cells per area of IL17A producing cells ($CCR6^+$). p-values were assessed by one-way ANOVA with Tukey HSD for multiple comparisons and no differences with statistical meaning were found (n=6 mice per group).

Due to the route of administration, we questioned whether the effect was first concentrated in the lymphoid organs instead of skin. Thus, cells harvested from lymph nodes and spleen were analyzed by flow cytometry.

In LNs, the total amount of CD4 T cells did not vary with UCB-MNCs-sEVs injection, although in comparison with the control, IMQ treatment elevated the number of these cells. Within this compartment, effector CD4 T cells percentage was also maintained. Nevertheless, UCB-MNCs-sEVs treatment decreased the number of IL17A secreting cells and regulatory T cells **(Figure 5.18C and D)**. This decrease towards control levels could indicate a delayed but positive response of UCB-MNCs-sEVs in the treatment of psoriasis. After activation in LNs, CD4 T cells home to skin where they can play a role of restraining inflammation. Therefore, less cells secreting pathogenic molecules will limit for instance IL-17 mediated responses, attenuating important clinical manifestation of the disease.

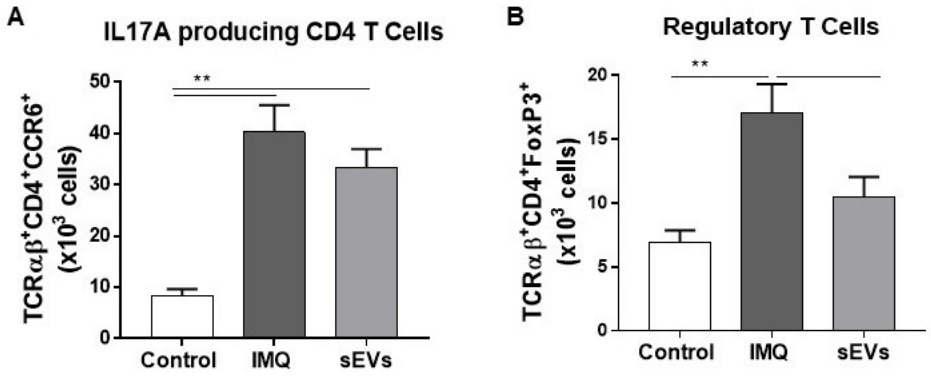

Figure 5.18. CD4 T cell distribution within lymph nodes of IMQ-induced psoriatic-like mice. Mice skin-draining lymph nodes were taken on day 6 of treatment and dissociated for flow cytometry analysis. A small impact of UCB-MNCs-sEVs was observed in (B) IL17A producing CD4 T cells while a statistically significant decrease was induced by UCB-MNCs-sEVs intravenous treatment on (B) regulatory T cells. p-values were assessed by one-way ANOVA with Tukey HSD for multiple comparisons (n=6 mice per group).

Besides CD4 T cells, CD8 T cells and γδ T cells represent other important players on inhibiting effector arms of an autoimmune reaction. When analyzing these two T cell compartments, no differences were found in CD8 T cells nor in the percentage of effector cells in this population. Moreover, while the same number of γδ T cells was observed in both conditions treated with IMQ (**Figure 5.19A)**, UCB-MNCs-sEVs significantly decreased the number of activations in this subset **(Figure 5.19B).**

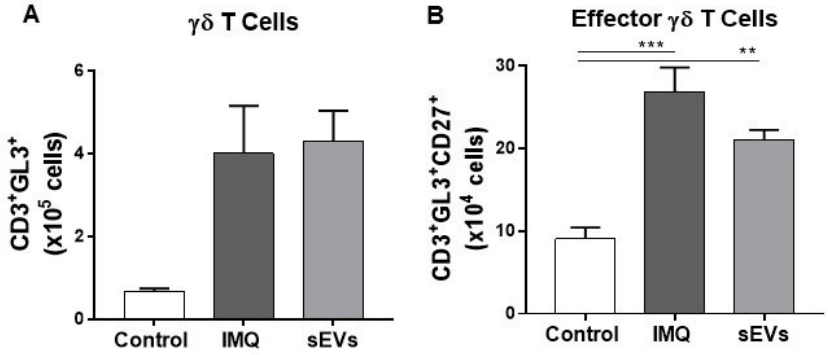

Figure 5.19. γδ T cell distribution within lymph nodes of IMQ-induced psoriatic-like mice. Mice skin draining LNs were taken on day 6 of treatment and dissociated for flow cytometry analysis. No differences induced by UCB-MNCs-sEVs were found in absolute number of (A) γδ T cells. A small impact of UCB-MNCs-sEVs was observed in (B) activated γδ T cells. p-values were assessed by one-way ANOVA with Tukey HSD for multiple comparisons (n=6 mice per group).

At the mRNA level, the impact of UCB-MNCs-sEVs was more visible. UCB-MNCs-sEVs treated animals have less abundance of transcripts of different pro-inflammatory cytokines namely *Il-22*, *Ifn-γ*, *Tnf-α* and *Il-17a* **(Figure 5.20A to D).** Allied to this downregulation, *Rorγδ* (T_H17 master transcription factor) expression was also affected by UCB-MNCs-sEVs treatment, and expression levels tend to be more similar to healthy controls than IMQ (**Figure 5.20E**). No differences were observed in *FoxP3* **(Figure 5.20F)**.

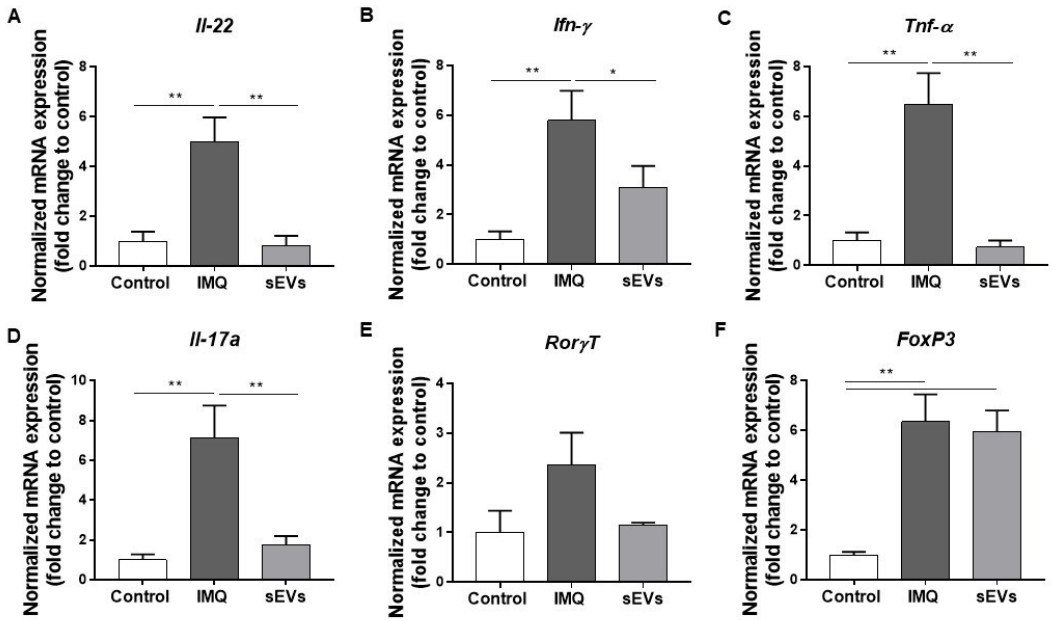

Figure 5.20. mRNA expression analysis in lymph nodes upon UCB-MNCs-sEVs intravenous injection. Mice skin-draining LNs were taken on day 6 of treatment, cells were dissociated, and their RNA was extracted. Analysis of mRNA transcripts of pro-inflammatory mediators: (A) *Il-17a*, (B) *Tnf-α*, (C) *Ifn-γ* and (D) *Il-22*. (E) T_H17 (*Rorγδ*) and (F) T_{reg} (*FoxP3*) transcriptional factor were also evaluated. p-values were assessed by one-way ANOVA with Tukey HSD for multiple comparisons (n=6 mice per group).

To validate the secretion of these molecules, cells extracted from draining LNs were cultured *in vitro* with IL-23 and IL-1β. After 48hours, the production of IL-22, IL-17A, IFN-γ and IL-10 was evaluated both in CD4 and γδ T cells compartments.

Imiquimod treatment enhanced the frequencies of IFN-γ, IL-17A, IL-22 and IL-10-producing $CD4^+$ and γδ T cells under the stimulated cell-inducing conditions **(Figure 5.21 and Figure 5.22).** The frequencies of IFN-γ and IL-22-producing $CD4^+$ T cells were significantly decreased in UCB-MNCs-sEVs treated animals when compared with IMQ **(Figure 5.21B and C)**. However, IL-17A-producing $CD4^+$ T cells frequency remained stable in both IMQ treated animals, higher than healthy controls **(Figure 5.21D)**. Interestingly, IL-10 producing CD4 T cells number increased upon UCB-MNCs-sEVs intravenous treatment **(Figure 5.21E)**.

Similar pattern was found inside γδ T cells. Intravenous treatment with UCB-MNCs-sEVs significantly decrease the frequency of IFN-γ and IL-22 producing cells with increase the number of IL-10 producing cells.

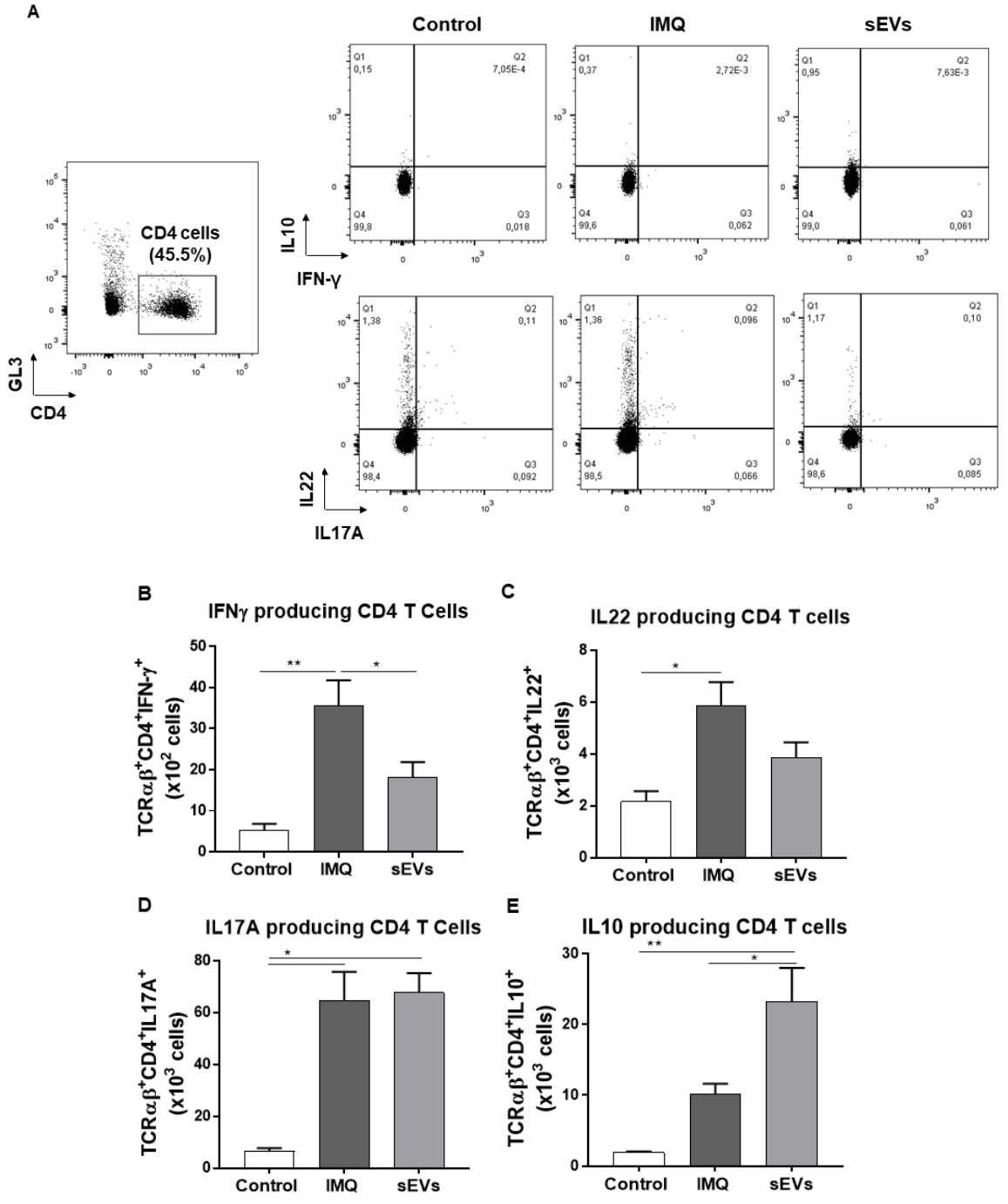

Figure 5.21. Intravenous UCB-MNCs-sEVs injection modulates cytokine production on *in vitro* stimulated CD4 lymph node T cells. LNs cell suspensions of IMQ-treated mice and control were stimulated *in vitro* with IL-23 and IL-1β for 48h. Flow cytometry analysis of stimulated lymph nodes cells was performed. (A) Representative dot plots of cytokine production within each condition. Bars indicated the absolute number of (B) IFN-γ, (C) IL-22, (D) IL-17A and (E) IL-10 cell secretion on CD4 T cell compartment. p-values were assessed by one-way ANOVA with Tukey HSD for multiple comparisons (n=6 mice per group).

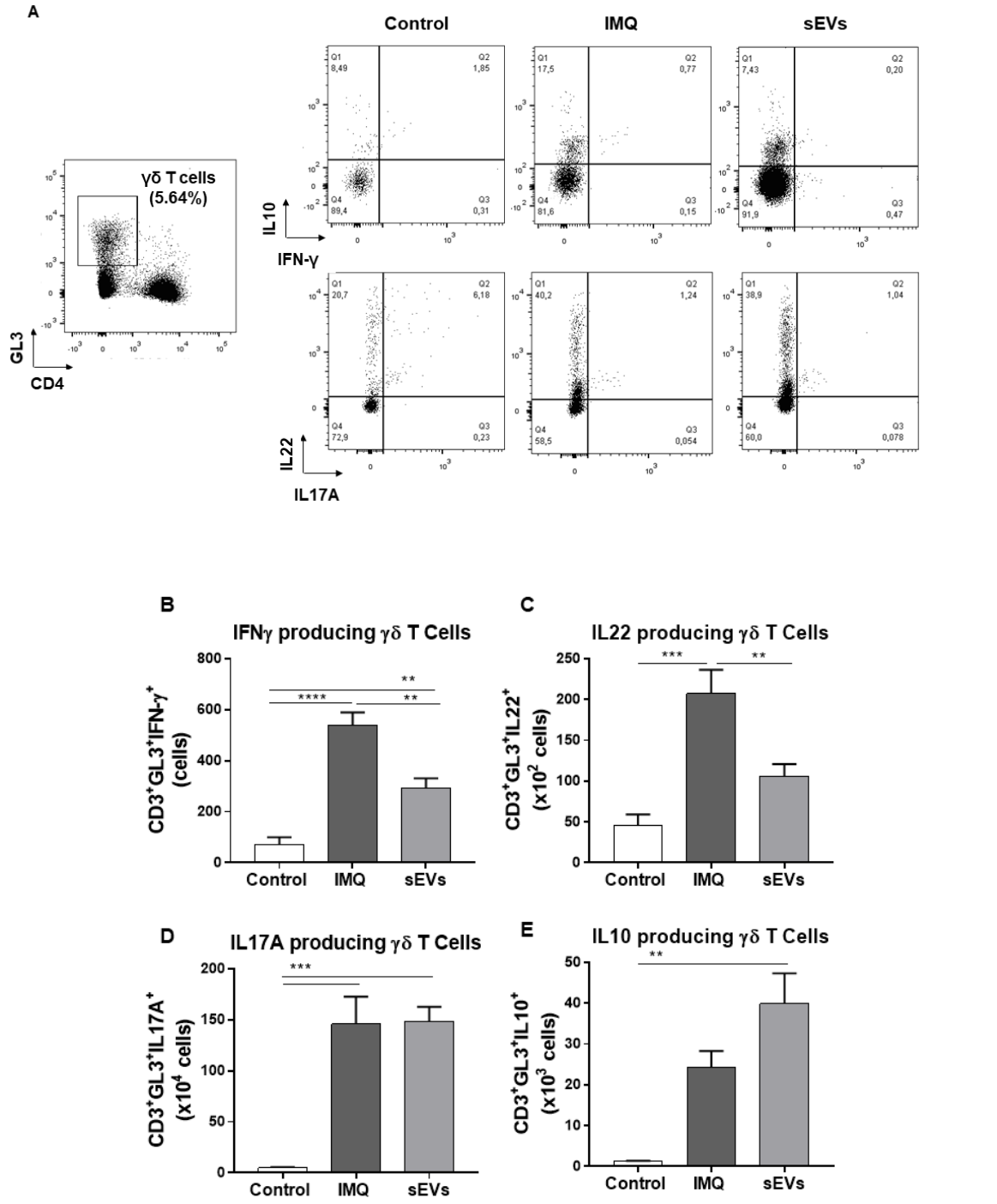

Figure 5.22. Intravenous UCB-MNCs-sEVs injection modulates cytokine production on *in vitro* stimulated γδ lymph node T cells. LN cell suspensions of IMQ-treated mice and control were stimulated *in vitro* with IL-23 and IL-1β for 48h. Flow cytometry analysis of stimulated lymph nodes cells was performed. (A) Representative dot plots of cytokine production within each condition. Bars indicated the absolute number of (B) IFN-γ, (C) IL-22, (D) IL-17A and (E) IL-10 cell secretion on γδ T cell compartment. p-values were assessed by one-way ANOVA with Tukey HSD for multiple comparisons (n=6 mice per group).

T cells were also analyzed in spleen cells. Although in αβ lymphocytes no alteration in cell frequency nor in the percentage of effector cells was found, within CD4 T cell compartment changes in some specific T cell subset occurred**.** Interestingly, less IL17A-producer and regulatory T cells were generated within spleens of UCB-MNCs-sEVs treated mice when compared with IMQ **(Figure 5.23**). The decrease in the frequency could indicate that in a longer time period UCB-MNCs-sEVs could have benefit from the treatment.

γδ T cell subset did not suffer any alteration in terms of frequency in the intravenously UCB-MNCs-sEVs treated mice, however the representativity of IFN-γ producing cells significantly decrease **(Figure 5.24).**

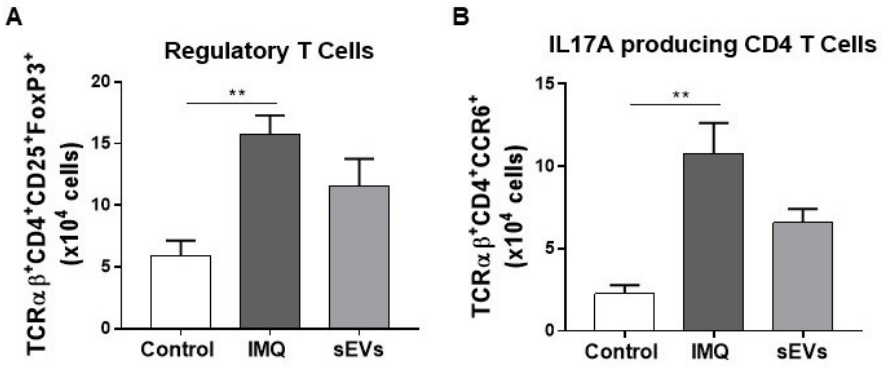

Figure 5.23. CD4 T cell distribution within spleen cells of IMQ-induced psoriatic-like mice. Mice spleens were collected on day 6 of treatment and dissociated for flow cytometry analysis. No differences induced by UCB-MNCs-sEVs was found in absolute number of (A) overall CD4 T cells neither (B) in the percentage of effector CD4 T cells. A small impact of UCB-MNCs-sEVs was observed in both (C) IL17A producing CD4 T cells and on (D) regulatory T cells. p-values were assessed by one-way ANOVA with Tukey HSD for multiple comparisons (n=6 mice per group)

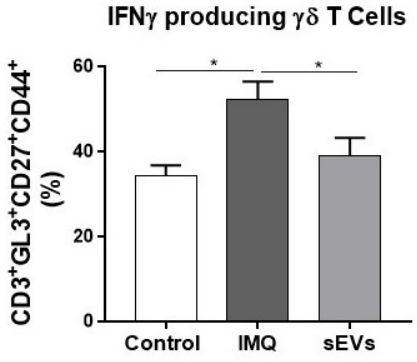

Figure 5.24. CD8 and γδ T cell distribution within spleen cells of IMQ-induced psoriatic-like mice. Mice spleens were collected on day 6 of treatment and dissociated for flow cytometry analysis. No differences induced by UCB-MNCs-sEVs was found in absolute number of (A) overall CD8 T cells neither (B) effector CD8 T cells nor in (C) γδ T cells. Within γδ T cells, no impact was observed on (D) IL17A producing γδ T cells while a statistically significant reduction was visible on (E) IFN-γ producing γδ T cells. p-values were assessed by one-way ANOVA with Tukey HSD for multiple comparisons (n=6 mice per group).

Upon naïve T cells differentiation and polarization in lymphoid organs, effector T cells migrate through the bloodstream and are distributed to all parts of the skin. Therefore, complementary, blood cells were analyzed by flow cytometry. At 6 days of daily treatment, within the bloodstream, only altered levels of IL-17A and IFN-γ producing γδ T cells were observed **(Figure 5.25B and C).** αβ lymphocytes were not affected by UCB-MNCs-sEVs treatment. Nevertheless, together with some results highlighted before, the decrease of homing of IL-17A and IFN-γ producing cells could alleviate psoriasis pathophysiology.

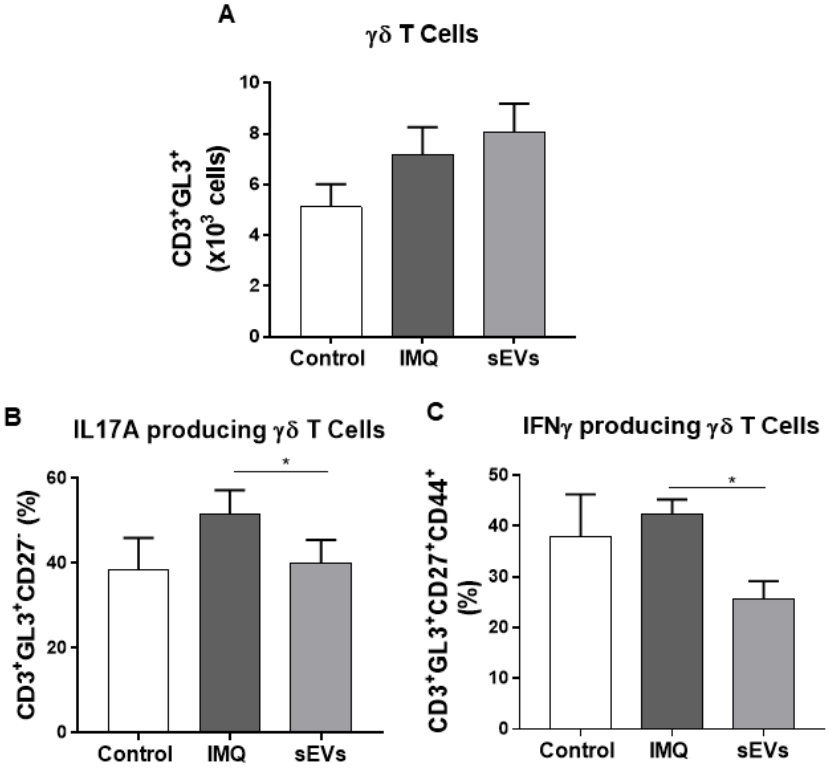

Figure 5.25. Blood γδ T cell distribution after UCB-MNCs-sEVs intravenous injection. Distribution of γδ T lymphocyte populations in peripheral blood were analyzed by flow cytometry. (A) Bars indicate the absolute number of γδ T cells among PBMNCs harvested from blood. Within this T population, percentage distribution of (B) IL-17A and (C) IFN-γ producing cells was calculated. p-values were assessed by one-way ANOVA with Tukey HSD for multiple comparisons (n=6 mice per group).

In summary, these results suggest important effects of UCB-MNCs-sEVs in psoriatic features. In the one hand, although we had technical limitations related to the hydrogel application (which may have partially impaired IMQ effect), the results indicate that topical application ameliorates psoriatic skin characteristics, decreasing epidermis thickness. Furthermore, a decrease in CD8 T cells and increase in Treg would promote an immunotolerant microenvironment, improving disease severity. On the other hand, systemic administration mainly acts in T cells of lymphoid tissues like LNs and spleen. The phenotype modulation of those cells, decreasing effector and pro-inflammatory cells and modulating mRNA expression, would posteriorly ameliorate disease symptoms once these cells migrate to skin.

It is important to stress that this was the first *in vivo* proof-of-concept study for evaluating the use of this biological product in psoriasis and therefore we consider that the experimental conditions should be optimized in the future and the results shall be confirmed before considering application in humans.

Chapter 6: Discussion

The skin is the largest multifunctional organ in the body and provides a barrier between the body interior and the environment to protect against assault by foreign organisms or toxic substances. Dysfunction of the skin can lead to a range of diseases whose patients not only face a decreased quality of life, but also are often uncomfortable about the appearance of their skin, which can cause an immense psychological burden. Although increasing evidences have shown that EVs are involved in the pathogenesis of skin diseases, their therapeutic potential for chronic inflammatory skin diseases is only starting to be explored.

EVs are nano-sized membrane-bound vesicles constantly released by almost all cell types with the ability to travel between cells and deliver numerous biomolecules, such as miRNAs and proteins, that make them an appealing cell-free therapy option to treat multiple diseases. MSCs and MNCs obtained from the UCB are among the most promising and versatile tools for regenerative medicine and immunotherapy, constituting a rich source of EVs[311,389,390]. Indeed, isolated from these types of cells, EVs have been demonstrated to successfully replace cell-based therapies[391]. Moreover, UCB is considered as a medical waste, its collection is noninvasive, and its access has not been encumbered with ethical problems. Therefore, it consists in a highly promising cell source to sustain the development of new therapies. UCB mononuclear fraction, the one used for transplants, is composed by different cell populations with several potential roles namely immunomodulatory. Although in comparison with peripheral blood, UCB contains less T lymphocytes, they are phenotypically and functionally immature, potentiating allogeneic transplantation. Even though UCB-derived T_{reg} present a higher expansion capacity, they have the same potent suppressor cell phenotype and function as adult T_{reg}[392,393]. Given the potent anti-inflammatory activity of T_{reg}, it has been suggested that these cells exert a significant role promoting immunotolerance through IL-10 secretion[366]. Nevertheless, the anti-inflammatory and immunomodulatory potential of EVs derived from UCB-MNCs remains unexplored in comparison with the existing literature about MSCs-EVs. Hence, in this work, the molecular mechanisms of the UCB-MNCs-sEVs immunomodulatory effect were assessed, envisioning the development of a new therapy for skin lesions.

The progress of EV isolation techniques has improved the efficiency of exosome isolation, however, difficulties in upscaling are real. Therefore, before starting testing UCB-MNCs-EVs mode of action, an optimized process for future clinically compatible GMP-compliant production of an EV-based therapy was developed. The UCB-MNCs-sEVs were purified from UCB-MNCs conditioned media by a process that combines centrifugation (clearance), followed by microfiltration (clarification) and ultrafiltration (UF) for the concentration of the vesicles, and size exclusion chromatography (SEC) as a final purification step. With this optimized method, we

generate a population of vesicles highly enriched in sizes smaller than 200nm (~80%) and 20% of microvesicles (200-400nm), which is the most frequent population associated to other sEVs isolation methods[394]. Furthermore, a final higher yield in particle recovery was achieved in comparison to when standard methods were applied.

Interestingly, detection of CD63 by immunolabeling and flow cytometry was possible with the new processing method, validating their use as purification method for vesicles with endosomal origin such as exosomes. Additionally, other evidences substantiate the enrichment of the final product in sEVs rather than microvesicles. In comparison with larger vesicles, sEVs/exosomes contain proteins with GTPase activity involved in transportation and fusion (Annexin, Rab proteins), heat shock proteins (Hsp 60, Hsp70, Hsp90), and proteins co-responsible for the vesicle biogenesis (Alix, TSG101) that were detected by mass spectrometry analysis in UCB-MNCs-sEVs. sEVs also express tetraspanins (CD63, CD81, CD9) required for the fusion between EVs and recipient cells. These surface markers were also detected among different UCB-MNCs-sEVs. Besides, the analysis of the lipid composition of UCB-MNCs-sEVs showed that phosphatidylcholines, phosphatidylserines and sphingomyelin are the three major phospholipid constituents, which is in line with the results observed in sEVs obtained from other cell sources[275]. These results reinforced the evidences found in the literature that sEVs have a higher membrane rigidity than microvesicles and apoptotic bodies[395]. Regarding the small RNA content, UCB-MNCs-sEVs contain the expected RNA species for sEVs, being enriched in tRNAs. The dominance of tRNAs in exosomes is consistent with their function and abundance in the cellular cytoplasm. Of note, *Baglio et al*. had already described an enrichment in this RNA class in EVs from MSCs[311]. The UCB-MNCs-sEVs boost of protein synthesis in target cells may be due to their enrichment in this small RNA specie. Although the sorting of tRNAs into vesicles has been scarcely addressed in the literature, the presence and function of miRNAs in sEVs has been frequently described. Interestingly, EXOmotifs, short sequence motifs over-represented in miRNAs, were also found among the detected miRNA species in UCB-MNCs-sEVs, indicating a possible specific sorting mechanism into sEVs.

Overall and based on the adequate UCB-MNCs-sEVs characteristics, we conclude that the developed methodology is more suitable for future clinical applications rather than differential centrifugations. Besides its alignment with the technological demands regarding of standardization, upscaling, and yield, this method allows a recovery of a very pure fraction of sEVs with a superior efficacy on accelerating wound healing.

Regarding UCB-MNCs-sEVs action on inflammatory phase of wound healing, it was shown that they are able to influence macrophage phenotype and gene expression state, promoting M2-like polarization both *in vitro* and *in vivo*. Interestingly, *in vitro*, this effect was superior in a pro-inflammatory environment. While synthetic molecules are developed to act on a specific target

potentiating direct inhibition of for example inflammatory effector cells, EVs have a differential inflammatory effect due to their nature perhaps based in environmental cues.

The action of UCB-MNCs-EVs was not only concentrated on mRNA modulation of different inflammatory modulators but also protein secretion. The UCB-MNCs-EVs changed macrophage phenotype and modulate gene expression promoting a decrease production of TNF-α and CCL20 by macrophages. This data corroborates with previously published literature on the effects of EVs from different sources on macrophage polarization[239,396–398].

EVs seem to play a crucial role in inflammation processes thanks to their ability to carry inflammatory modulators, such as miRNA and proteins, which can act at distant and close-range tissues. In fact, biochemical composition of UCB-MNCs-sEVs suggests a possible effect in inflammatory response. Among the confirmed miRNAs carried by UCB-MNCs-sEVs, miRNA-223 represents a novel regulator of macrophage polarization. This miRNA is responsible for suppressing classic pro-inflammatory pathways and enhancing the alternative anti-inflammatory responses[239,399]. In turn, enforced expression of miRNA-142-3p in human monocytes leads to a significant reduction in the production of several proinflammatory cytokines and chemokines, such as IL6[400,401]. A single miRNA can exert therapeutic efficacy on multiple targets. Therefore, these correlations raise important questions about the specific contents of EVs to determine whether UCB-MNCs-sEVs effect is based on a plethora of molecules or there is one that has a key potential. Of note, this comment is valid for either miRNAs but also for other RNA species as well as growth factors, proteins, and lipids enclosed in UCB-MNCs-sEVs. Some of the identified proteins constitute also important clues for promoting macrophage polarization. The complex between hemoglobin and haptoglobin, two of the proteins with higher peptides reads in mass spectrometry of UCB-MNCs-sEVs, when engulfed by macrophages leads to the production of the anti-inflammatory agents, IL-10 and heme oxygenase[371,402,403]. Identically, although lipids are mainly recognized as key players in cells membrane and signaling, they also regulate immunity. A recent study suggested that choline and PC supplementation may have anti-inflammatory implications[404]. The authors showed that by inhibiting choline uptake for a period of 48 h followed by a 6h stimulation with LPS, the secretion of inflammatory cytokines, such as TNFα and IL-6, was higher, whereas IL-10 secretion was lower.

Previous studies have shown that paracrine factors of M1/M2 polarized macrophages influence the phenotypical state of dermal fibroblasts[96,405]. To promote wound healing, transition from inflammatory to proliferative phase is crucial[70]. Therefore, we investigated the influence of secreted factors (conditioned medium) of UCB-MNCs-sEVs treated macrophages on dermal fibroblasts.

Beforehand, we have characterized that UCB-MNCs-sEVs induced a macrophage shift from M1 to M2 macrophages promoting a less inflammatory environment. In accordance with previous reported results, secreted factors of macrophages influence fibroblasts phenotype and fibroblast proliferation[96]. In wound repair, M2 macrophages are responsible for reversing the inflammatory

response, thereby initiating the healing process. Interestingly, in this study we show that UCB-MNCs-sEVs are able to act not only directly on fibroblasts but also through macrophage action. In fact, the cross action among environmental clues seemed to potentiate the anti-inflammatory phenotype in fibroblasts as well as fibroblast proliferation. A significant increase was seen in the expression of α-SMA, indicating a possible differentiation into the myofibroblast phenotype. Nevertheless, this result should be confirmed in the future with the evaluation of other parameters like surface markers and quantification of ECM production.

Controlling inflammation involves a tight regulation from the immune system. Although inflammatory cells like macrophages are the first line of response, immune cells such as T lymphocytes are crucial to moderate the intensity of such response. M1 or M2 dominant macrophages direct T lymphocytes to produce T_H1 or T_H2 responses, respectively, to further amplify M1 or M2 type responses in positive feed-back loops. Thus, modulating not only macrophage phenotype but also derivatives of T_H1 such as IL-2, IFN-γ and T_H2 such as IL-10, IL-4 will also down regulate M1 and M2 activity, respectively[349]. The balance of macrophages and T lymphocytes derivatives dominate the balance of cellular and humoral immunity, which is severely altered in skin inflammatory diseases.

In order to address the possible modulation of adaptative immunity by UCB-MNCs-sEVs, PBMNCs from healthy donors were used to access cell proliferation, cytokine secretion and gene expression. Our results showed a suppressive activity of UCB-MNCs-sEVs on T cell proliferation after induction by a mitogen in PBMNCs culture. The effect was extended to CD4 and CD8 subsets. EV-mediated effects on T cell proliferation are controversially discussed in the literature with diminished[243,406,407] or unaffected[408,409] T cell proliferation for EVs from different cell sources such as glioma stem cells or MSCs from bone marrow or umbilical cord. This might reflect the heterogeneity within study design, such as different EV isolation methods or differences in the conducted immunomodulation assays. Additionally, we observed that the profile of released cytokines was altered in PBMNCs cultures treated UCB-MNCs-sEVs, displaying reduced pro-inflammatory cytokine levels (IFN-γ, TNF-α, CCL20).

The ability of UCB-MNCs-EVs to enhance the proportion of regulatory T cells is supported by the present data, showing that besides increasing frequency of $CD25^+FoxP3^+$ expressing cells, they also promote significant upregulation of FoxP3 at the mRNA level. Overall, we suggest that UCB-MNCs-sEVs enhance the differentiation of naïve T cells into immunosuppressive T_{reg} cells rather than promoting their proliferation. Tolerance can be driven both locally in the skin and systemically. Under certain circumstances in which the balance between tolerance and immune response has been lost, such as in autoimmunity or allergy, it is essential to have available therapeutic options that boost tolerogenic pathways and control the aberrant immunogenicity.

MSCs are one of the most prominent cell sources responding to the need of promoting immunotolerance. Therefore, a direct comparison with EVs from umbilical cord MSCs and

PBMNCs was performed. UCB-MNCs-sEVs potential to increase T_{reg}/T_{eff} ratio was higher than the observed sEVs derived from adult PBMNCs, but slightly lower than the one observed for MSCs-EVs. This was the only comparative study performed by us and should be complemented with others experiments, to evaluate if UCB-MNCs-sEVs have a differentiated mechanism of action, depending on the experimental settings, and can be useful for different therapeutic indications. Further studies are needed to determine the involvement of particular molecules, like microRNAs, in the mode of action.

In vitro results observed for UCB-MNCs-sEVs were partially confirmed *in vivo* during the wound healing phases. Besides demonstrating *de novo* the efficacy of UCB-MNCs-sEVs in accelerating wound healing, we were able to partially validate their predominant effect on the inflammatory phase. At day 3, gene expression analysis showed a suppression of immune and inflammatory pathways, demonstrating the capacity of UCB-MNCs-sEVs to promote the resolution of this phase earlier than the control. In fact, gene expression confirmed by qPCR, concluded that skin macrophages were expressing less pro-inflammatory genes and mediators in contrast with the expression of markers related with an anti-inflammatory state like A*rginase-1* and *Cd163*. Accordingly, it was shown, *in vivo,* that the application of UCB-MNCs-sEVs also increased the expression of *FoxP3* and Tgf-β genes in treated-skin, suggesting a more prominent presence of regulatory T cells in these animals. Interestingly, we observed in the mass spectrometry analysis of UCB-MNCs-sEVs that galectin-1 and several proteins from the annexin family were present. They are known to be modulators of immune responses by binding of galectin-1 to CD69 and mimicking a signal cascade which promotes regulatory T cell development[410]cd. Furthermore, increasing FoxP3 expressing cells in skin during wound healing promote a faster wound closure[100]. The acceleration of wound closure was also observed the in remodelling phase, where a faster resolution of inflammation also accelerates the process of RCM deposition and remodeling.

Based on the discovered immunomodulatory UCB-MNCs-sEVs effects in our study, a potential clinical application could be feasible namely for skin inflammatory diseases. Modulation of adverse immune processes could be dampened via the observed shift of macrophages cells into a pro-regenerative and anti-inflammatory phenotype and the enhanced induction of regulatory T cells. Therefore, we decided to continue the study on a psoriatic disease model. Firstly, a three-dimensional psoriatic *in vitro* model was used. Although it was only constituted by keratinocytes in various stages of differentiation, UCB-MNCs-sEVs administration induced a reduction on mRNA abundance of strong inflammatory cytokines, including *IFN-γ*, *TNF-α, IL-1β and IL-6*[411]. Elevated levels of IFN-γ have been considered a pathogenic mechanism of different skin inflammatory diseases such as systemic lupus erythematosus and pemphigus. Moreover, in pemphigus, the production by keratinocytes of TNF-α, CXCL8 and IL-6 act through the extracellular signal-regulated kinase 1/2 and signal transducer and activator of transcription 3

signaling pathways, exacerbating disease symptoms [412]. With these observations, UCB-MNCs-sEVs application could be envisaged for other therapeutic uses within the universe of skin lesions. Overexpression of IL-17 induces epithelial cells to release CXCL8 and CXCL1, potent neutrophil chemoattractant, granulocyte colony-stimulating factor, a survival factor for neutrophils, CCL20 and antimicrobial peptides such as b-defensin-4, mucins (MUC5AC and MUC5B), and S100 proteins (S100A7, S100A8, and S100A9). Concomitantly, *in vitro*, UCB-MNCs-sEVs were able to modulate the expression of these genes as well as to decrease TNF-α and CCL20 secretion, reinforcing their potential in the pathophysiology of IL-17 driven skin diseases.

In line with these results, we moved forward for a *in vivo* proof-of-concept study in a model of psoriasis disease. Skin application of IMQ, a TLR7/8 ligand, in mice, initiates inflammation through the IL-23/IL-17 axis with characteristics of human psoriasis. IMQ also induced systemic inflammation with increased spleen weight and increased inflammatory cells in skin and in ski-draining lymph nodes[43].

The topical application of UCB-MNCs-sEVs was done with hydrogel formulation where vesicles were emulsified. This mode of application decreased the epidermis thickness and increased the number of Tregs on the skin compared to untreated animals. Despite the apparent good performance of the developed formulation, it was not possible to distinguish between UCB-MNCs-sEVs activity and the respective control consisting of the gel vehicle. We believe that the hydrogel formulation may have blocked IMQ action, although 1 hour has been left between the application of these compounds. Therefore, we decided to perform systemic administration of the biological compound for 6 consecutive days. Intravenous injection of UCB-MNCs-sEVs did not relieved psoriatic-like symptoms in skin, in fact it seems that they had been intensified, while no influence in the skin histological analysis was noticed. In accordance with the exacerbated clinical signs, flow cytometry analysis of skin inflammatory cells revealed a high number of inflammatory macrophages on UCB-MNCs-sEVs treated mice.

T cell recirculation from the skin to lymphoid organs play a role both in the amplification of the cutaneous manifestations and in the development of comorbidities associated with psoriasis. In the early stages of a primary immune response, proliferating T cells are also released from the skin draining lymph nodes and give rise to new populations of effector T cells that migrate to skin or take up residence in the gut, lungs and other peripheral tissues[78]. As UCB-MNCs-sEVs were not applied topically but instead intravenously, we investigated a possible effect on these tissues. After tail vein injection, UCB-MNCs-sEVs enter the bloodstream interacting with blood cells being then redistributed in the body before being eliminated. Interestingly, UCB-MNCs-sEVs modulate systemic inflammation in this mice model as there are cellular alterations in lymph nodes and spleen. In skin-draining lymph nodes, UCB-MNCs-sEVs decreased the frequency of IL17A-producing CD4 T cells, effector γδ T cells and regulatory T cells. While in UCB-MNCs-sEVs treated spleen, this effect was not so pronounced, similar decrease in those cellular populations

were verified. Additionally, alteration of gene expression profile in both lymph nodes and spleen of UCB-MNCs-sEVs treated mice was observed. Overall, cytokines such as IL-17A, IL-22, IFN-γ and TNF-α were downregulated. These changes were further validated after *in vitro* cell stimulation with IL-1β and IL-23 of lymph nodes cells. While no differences were found on IL-17A producing cells (both within CD4 and γδ T cells), a significant reduction was observed in IFN-γ producing cells and IL-22. In mice, IL-22 release is preferentially associated with T_H17 differentiation which are centrally involved in psoriasis. In general, impaired signaling of IL-17 and IL-22 promotes a disturbed wound healing, while over-activation of the cascade results in inflammatory processes with tissue remodeling as observed in rheumatoid arthritis or psoriasis. Hence, a possible mechanism of action of UCB-MNCs-sEVs through modulation of IL-22 secretion can be hypothesized both for wound healing and skin inflammatory diseases.

Moreover, IL-10 is thought to play a protective role in the development of psoriasis[413]. It is secreted by multiple cell types (T cells, B cells, monocytes, macrophages, mast cells, and eosinophils) and can suppress T_H1 and polarization and inhibit macrophage antigen presentation and proinflammatory cytokine production. In psoriasis patients, plasma IL-10 levels are significantly decreased when compared with healthy individuals and, are negatively correlated with the severity of skin lesions[414]. Consistently, the systemic application of human recombinant IL-10 (rIL-10) reduces the severity of skin lesions in psoriasis patients. However, a larger, randomized, double-blind, placebo-controlled study demonstrated that systemic human rIL-10 administration resulted in a temporary improvement[415]. As the serum half-life of rIL-10 is only 2.6 h in humans[416], it is the likely cause of the disappointing results of rIL-10 treatment for psoriasis.

The pilot study described herein suggests a role for UCB-MNCs-sEVs in immune modulation in a psoriasis *in vivo* model, offering a future biologic cell-free therapy for this disease. Nonetheless, studies are needed to confirm their potential therapeutic effect at longer time points, higher dosages or using different administration routes. Footpad injection could be an interesting next step as with this route UCB-MNCs-sEVs will be delivery to lymph nodes in a direct and reliable way.

Importantly, although UCB-MNCs-sEVs efficacy have been tested on a psoriatic model, relevant findings were unveiling, hypothesizing their potential application in other skin inflammatory diseases. For instance, the literature consensus suggests that the multitude of effects of IL-10 contribute to the pathogenesis of different skin disorders. In certain circumstances IL-10 could represent novel therapeutic approach to treating cutaneous diseases. Similarly, modulation of IL-17/IL-22 axis in conjugation with increment of immunotolerance appears to be the future for the development of skin inflammatory diseases.

6.1. Future work

Biochemical composition of UCB-MNCs-sEVs was also characterized to support possible clues about mechanism of action through the identification of specific biomolecules. In fact, their composition suggests various effects in inflammatory and immune response when lipids, proteins and RNA are analyzed in detail. Although at functional level, some of these effects were tested, mechanistically, further investigation is needed. Now that the most promising processes influenced by UCB-MNCs-sEVs on immunomodulation were identified, identification of the most probable molecules responsible for that on the biochemical composition would be very valuable. To achieve that for the different types of biomolecules (lipids, proteins or RNA) their concentration should be quantified in UCB-MNCs-sEVs and their direct impact of manipulating its concentration in the outcome of each specific process (eg, anti-inflammatory effect, impact on T cell proliferation, or influence in frequency of T_{reg}) should be evaluated. Similar *in vitro* assays from those used in chapter 4 can be used or even improved ones such as using cells obtained from patients or cell lines stimulated *in vitro* with clues that closely resemble specific disease pathologies. These results will validate which molecules present in UCB-MNCs-sEVs can govern its mode of action, potentiating the development of an improved version of UCB-MNCs-sEVs and to acknowledge their positioning in the market.

After the generation of this knowledge, generating EVs with higher therapeutic potential would be the next aim to reach. To optimize UCB-MNCs-sEVs therapeutic potential, two different strategies should be equated: (i) cell manipulation or pre-conditioning to indirectly enrich EVs with the selected biomolecules and (ii) direct functionalization/loading of specific molecules into EVs[417]. Cell manipulation can be achieved by tailoring the cell stimuli[417]. Electric stimulation, hypoxia or chemical addition (i.e. LPS) to cell culture are some of the variables that can be altered, and can potentiate EVs contents and functions[235,418,419]. In addition, genetic modification of the secreting cells can also be attempted, to force the expression of a given specific biomolecule of interest. On the other hand, directly enrichment of EVs content can be performed. Similarly to the majority of drug loading EVs studies, direct transfection with the molecule of interest can be used using for instance electroporation[420,421]. Finally, *in vivo* validation of the therapeutic effect of an optimized version of UCB-MNCs-sEVs should be tested in appropriated models according to the improved potential.

Depending on the chosen disease model, and after validation of the most relevant UCB-MNCs-sEVs mechanism for that, route of administration and consequently an appropriate formulation should be designed.

Chapter 7: Conclusion

The results from this thesis demonstrate that a newly developed methodology for UCB-MNCs-sEVs purification, based on UF and SEC, is more suitable for future clinical applications than differential centrifugation. It results in sEVs with higher purity and with higher yield. Besides the technical questions regarding standardization, upscaling, and yield, this method allows for the recovery of a very pure fraction of sEVs as observed from the protein and lipid content and, more importantly, with a superior efficacy for accelerating wound healing. UCB-MNCs-sEVs boost cellular translation and proteins synthesis in both physiological and starvation condition whereas only a slight modulation of transcription was observed in starvation conditions.

Furthermore, we have successfully demonstrated that UCB-MNCs-sEVs have an anti-inflammatory and immunomodulatory potential. Overall, our data demonstrate that UCB-MNCs-sEVs (1) promote a shift on macrophage phenotype towards an anti-inflammatory state, (2) suppress PBMNCs cell proliferation, reducing their activation and pro-inflammatory cytokines secretion, and enhance induction of T_{reg} phenotype *in vitro*.

In a psoriatic-like *in vitro* system, UCB-MNCs-sEVs modulate not only the gene expression but also cytokines secretion. On the other hand, i*n vivo*, although we may have faced significant technical limitations related to the topical application of UCB-MNCs-sEVs emulsified in a hydrogel, the results indicate they promote decrease of epidermis thickness, skin infiltrating neutrophils as well as downregulation of proinflammatory cytokine expression at mRNA level. Importantly, topical application of UCB-MNCs-sEVs increased the number of T_{regs} on the skin. However, in the other parameters analyzed, emulsified UCB-MNCs-sEVs did not show any incremental action when compared with the formulation itself in a psoriatic-like mice model, suggesting that the application of the hydrogel (with or without vesicles) may have interfered with the induction of psoriatic features by IMQ. Interestingly, when UCB-MNCs-sEVs were given intravenously, immunomodulatory effects on LNs and spleens cells were observed. It is noteworthy the decreased of pro-inflammatory cytokines such as IL-22 and IL-17A and the number of effector cells in both tissues. In addition, *in vitro* stimulated LNs and spleen cells treated with these vesicles decreased IFN-γ secretion and increased IL-10 expression. Although UCB-MNCs-sEVs had no impact on psoriatic clinical signs, the results show a systemic effect in controlling inflammation, but further studies are needed to consolidate these potential beneficial effects.

By studying in detail the immunomodulatory and anti-inflammatory properties of sEVs, derived from the UCB-MNCs and stimulated with hypoxia, this information adds a new avenue to EVs field. In this way, UCB-MNCs-sEVs emerge as a valid option for controlling immune-derived

diseases, namely those with cutaneous manifestations. Besides, the multifactorial effect on different experimental settings support a competitive advantage over products available in the market, which typically stimulate only one target/pathway/function. As EVs are loaded differentially and combinatorial with multiple types of proteins together with coding and regulatory nucleic acids, the responses they induce may be more complex and longer lasting compared to those elicited by individual biomolecules. Nevertheless, further investigation about the molecular mechanism involved, and their potential for the treatment of skin diseases should be considered.

Chapter 8: References

1. Lim, H. W. *et al.* The burden of skin disease in the United States. *J. Am. Acad. Dermatol.* **76**, 958-972.e2 (2017).
2. Hay, R. J. *et al.* The Global Burden of Skin Disease in 2010: An Analysis of the Prevalence and Impact of Skin Conditions. *J. Invest. Dermatol.* **134**, 1527–1534 (2014).
3. Karimkhani, C. *et al.* Global Skin Disease Morbidity and Mortality: An Update From the Global Burden of Disease Study 2013. *JAMA dermatology* **153**, 406–412 (2017).
4. Seth, D., Cheldize, K., Brown, D. & Freeman, E. F. Global Burden of Skin Disease: Inequities and Innovations. *Curr. Dermatol. Rep.* **6**, 204–210 (2017).
5. Elishmereni, M. & Levi-Schaffer, F. Skin Disorders of Inflammation and Immune Suppression in Young and Elder: A Special Role for Mast Cells. in *Skin Aging Handbook* (ed. Dyan, N.) 105–128 (William Andrew Publishing, 2009). doi:10.1016/B978-0-8155-1584-5.50010-7
6. Leong, S. P. L. *et al.* Progression of cutaneous melanoma: implications for treatment. *Clin. Exp. Metastasis* **29**, 775–796 (2012).
7. Maxson, T. & Mitchell, D. A. Targeted treatment for bacterial infections: prospects for pathogen-specific antibiotics coupled with rapid diagnostics. *Tetrahedron* **72**, 3609–3624 (2016).
8. Naran, K., Nundalall, T., Chetty, S. & Barth, S. Principles of Immunotherapy: Implications for Treatment Strategies in Cancer and Infectious Diseases. *Front. Microbiol.* **9**, (2018).
9. Branco, A. C. C. C., Yoshikawa, F. S. Y., Pietrobon, A. J. & Sato, M. N. Role of Histamine in Modulating the Immune Response and Inflammation. *Mediators Inflamm.* **2018**, (2018).
10. Gooderham, M. J., Papp, K. A. & Lynde, C. W. Shifting the focus - the primary role of IL-23 in psoriasis and other inflammatory disorders. *J. Eur. Acad. Dermatology Venereol.* **32**, 1111–1119 (2018).
11. Shankaran, V., Brooks, M. & Mostow, E. Advanced therapies for chronic wounds: NPWT, engineered skin, growth factors, extracellular matrices. *Dermatol. Ther.* **26**, 215–221 (2013).
12. Patel, S., Srivastava, S., Singh, M. R. & Singh, D. Mechanistic insight into diabetic wounds: Pathogenesis, molecular targets and treatment strategies to pace wound healing. *Biomedicine and Pharmacotherapy* **112**, (2019).
13. Soleymani-Goloujeh, M., Saberi, S. & Shekari, F. Extracellular Vesicles in Regenerative Medicine, a Brief Review. *Rev. Artic. | Mod Med Lab J* **2**, 6–14 (2018).
14. Hodgkinson, C. P., Bareja, A., Gomez, J. A. & Dzau, V. J. Emerging Concepts in Paracrine Mechanisms in Regenerative Cardiovascular Medicine and Biology. *Circ. Res.* **118**, 95–107 (2016).
15. Murphy, D. E. *et al.* Extracellular vesicle-based therapeutics: natural versus engineered targeting and trafficking. *Exp. Mol. Med.* **51**, 32 (2019).
16. McBride, J. D., Rodriguez-Menocal, L. & Badiavas, E. V. Extracellular Vesicles as Biomarkers and Therapeutics in Dermatology: A Focus on Exosomes. *J. Invest. Dermatol.* **137**, 1622–1629 (2017).
17. Choi, E. W. *et al.* Exosomes from human adipose-derived stem cells promote proliferation and migration of skin fibroblasts. *Exp. Dermatol.* **27**,
18. Kim, Y.-L. Y.-J. *et al.* Exosomes derived from human umbilical cord blood mesenchymal stem cells stimulates rejuvenation of human skin. *Biochem. Biophys. Res. Commun.* **493**, 1102–1108 (2017).
19. Cicero, A. Lo *et al.* Exosomes released by keratinocytes modulate melanocyte pigmentation. *Nat. Commun.* **6**, 7506 (2015).
20. El-Tookhy, O. S., Shamaa, A. A., Shehab, G. G., Abdallah, A. N. & Azzam, O. M. Histological evaluation of experimentally induced critical size defect skin wounds using exosomal solution of mesenchymal stem cells derived microvesicles. *Int. J. Stem Cells* **10**,

1–10 (2017).
21. Wang, L. *et al.* Exosomes secreted by human adipose mesenchymal stem cells promote scarless cutaneous repair by regulating extracellular matrix remodelling. *Sci. Rep.* **7**, (2017).
22. Zhao, B. *et al.* Exosomes derived from human amniotic epithelial cells accelerate wound healing and inhibit scar formation. *J. Mol. Histol.* **48**, 121–132 (2017).
23. Albanna, M. Z., Holmes IV, J. H., Allen-Hoffmann, B. L. & Rooney, P. J. *Skin Tissue Engineering and Regenerative Medicine*. *Skin Tissue Engineering and Regenerative Medicine* (2016). doi:10.1016/B978-0-12-801654-1.00013-9
24. Matejuk, A. Skin Immunity. *Arch. Immunol. Ther. Exp. (Warsz).* **66**, 45–54 (2018).
25. Yousef, H., Alhajj, M. & Sharma, S. *Anatomy, Skin (Integument), Epidermis*. *StatPearls* (StatPearls Publishing, 2019).
26. Rognoni, E. & Watt, F. M. Skin Cell Heterogeneity in Development, Wound Healing, and Cancer. *Trends Cell Biol.* **28**, 709–722 (2018).
27. Nguyen, A. V. & Soulika, A. M. The Dynamics of the Skin's Immune System. *Int. J. Mol. Sci.* **20**, 1811 (2019).
28. Woodley, D. T. Distinct Fibroblasts in the Papillary and Reticular Dermis: Implications for Wound Healing. *Dermatol. Clin.* **35**, 95–100 (2017).
29. Kular, J. K., Basu, S. & Sharma, R. I. The extracellular matrix: Structure, composition, age-related differences, tools for analysis and applications for tissue engineering. *J. Tissue Eng.* **5**, 204173141455711 (2014).
30. Kusindarta, D. L. & Wihadmadyatami, H. The Role of Extracellular Matrix in Tissue Regeneration. in *Tissue Regeneration* (InTech, 2018). doi:10.5772/intechopen.75728
31. Cichorek, M., Wachulska, M., Stasiewicz, A. & Tymińska, A. Skin melanocytes: biology and development. *Adv. Dermatology Allergol.* **1**, 30–41 (2013).
32. Jaitley, S. & Saraswathi, T. Pathophysiology of Langerhans cells. *J. Oral Maxillofac. Pathol.* **16**, 239–44 (2012).
33. Shetty, S. & Gokul, S. Keratinization and its disorders. *Oman Med. J.* **27**, 348–357 (2012).
34. Richmond, J. M. & Harris, J. E. Immunology and skin in health and disease. *Cold Spring Harb. Perspect. Med.* **4**, a015339 (2014).
35. Tracy, L. E., Minasian, R. a. & Caterson, E. J. Extracellular Matrix and Dermal Fibroblast Function in the Healing Wound. *Adv. wound care* **5**, 119–136 (2016).
36. Gomes, C. O. Implementation of biomolecular methods to explore the mode of action of Exo-Wound in vitro. (Aveiro University, 2018).
37. Rittié, L. Cellular mechanisms of skin repair in humans and other mammals. *J. Cell Commun. Signal.* **10**, 103–120 (2016).
38. Di Meglio, P., Perera, G. K. & Nestle, F. O. The multitasking organ: recent insights into skin immune function. *Immunity* **35**, 857–69 (2011).
39. Wong, V. W., Sorkin, M., Glotzbach, J. P., Longaker, M. T. & Gurtner, G. C. Surgical Approaches to Create Murine Models of Human Wound Healing. *J. Biomed. Biotechnol.* **2011**, 1–8 (2011).
40. Debeer, S. *et al.* Comparative histology and immunohistochemistry of porcine versus human skin. *Eur. J. Dermatology* **23**, 456–466 (2013).
41. Ueyama, A. *et al.* Mechanism of pathogenesis of imiquimod-induced skin inflammation in the mouse: A role for interferon-alpha in dendritic cell activation by imiquimod. *J. Dermatol.* **4**, 135–143 (2014).
42. Yang, B. *et al.* IL-27 Facilitates Skin Wound Healing through Induction of Epidermal Proliferation and Host Defense. *J. Invest. Dermatol.* **137**, 1166–1175 (2017).
43. van der Fits, L. *et al.* Imiquimod-Induced Psoriasis-Like Skin Inflammation in Mice Is Mediated via the IL-23/IL-17 Axis. *J. Immunol.* **182**, 5836–5845 (2009).
44. Pasparakis, M., Haase, I. & Nestle, F. O. Mechanisms regulating skin immunity and inflammation. *Nat. Rev. Immunol.* **14**, 289–301 (2014).
45. Cruz, M. S., Diamond, A., Russell, A. & Jameson, J. M. Human αβ and γδ T Cells in Skin Immunity and Disease. *Front. Immunol.* **9**, 1304 (2018).
46. Clark, R. & Kupper, T. Old meets new: The interaction between innate and adaptive immunity. *J. Invest. Dermatol.* **125**, 629–637 (2005).

47. Hirano, T. *et al.* The Fab fragment of anti-IgE Cε2 domain prevents allergic reactions through interacting with IgE-FcεRIα complex on rat mast cells. *Sci. Rep.* **8**, 14237 (2018).
48. Hellman, L. T., Akula, S., Thorpe, M. & Fu, Z. Tracing the Origins of IgE, Mast Cells, and Allergies by Studies of Wild Animals. *Front. Immunol.* **8**, 1749 (2017).
49. Moon, T. C. *et al.* Advances in mast cell biology: new understanding of heterogeneity and function. *Mucosal Immunol.* **3**, (2009).
50. Tsai, M., Grimbaldeston, M. & Galli, S. J. Mast Cells and Immunoregulation/Immunomodulation. in *Advances in experimental medicine and biology* **716**, 186–211 (2011).
51. Wang, Z. *et al.* Skin microbiome promotes mast cell maturation by triggering stem cell factor production in keratinocytes. *J. Allergy Clin. Immunol.* **139**, 1205-1216.e6 (2017).
52. Tordesillas, L. *et al.* PDL2+ CD11b+ dermal dendritic cells capture topical antigen through hair follicles to prime LAP+ Tregs. *Nat. Commun.* **9**, 5238 (2018).
53. Kashem, S. W., Haniffa, M. & Kaplan, D. H. Antigen-Presenting Cells in the Skin. *Annu. Rev. Immunol.* **35**, 469–499 (2017).
54. Nestle, F. O. *et al.* Plasmacytoid predendritic cells initiate psoriasis through interferon-α production. *J. Exp. Med.* **202**, 135–143 (2005).
55. Ah Kioon, M. D. *et al.* Plasmacytoid dendritic cells promote systemic sclerosis with a key role for TLR8. *Sci. Transl. Med.* **10**, eaam8458 (2018).
56. Clayton, K., Vallejo, A. F., Davies, J., Sirvent, S. & Polak, M. E. Langerhans Cells—Programmed by the Epidermis. *Front. Immunol.* **8**, 1676 (2017).
57. Takagi, H. *et al.* Plasmacytoid Dendritic Cells Are Crucial for the Initiation of Inflammation and T Cell Immunity In Vivo. *Immunity* **35**, 958–971 (2011).
58. Mann, E. R. *et al.* Review: Skin and the Immune System. *J. Clin. Exp. Dermatology Res.* **S3**, (2012).
59. Manuscript, A. Inflammation and wound healing : The role of the macrophage. *Expert Rev Mol Med* **16**, 19–25 (2013).
60. Mirza, R., DiPietro, L. A. & Koh, T. J. Selective and specific macrophage ablation is detrimental to wound healing in mice. *Am. J. Pathol.* **175**, 2454–62 (2009).
61. Yanez, D. A., Lacher, R. K., Vidyarthi, A. & Colegio, O. R. The role of macrophages in skin homeostasis. *Pflugers Arch.* **469**, 455–463 (2017).
62. Martinez, F. O. & Gordon, S. The M1 and M2 paradigm of macrophage activation: time for reassessment. *F1000Prime Rep.* **6**, 13 (2014).
63. Italiani, P. & Boraschi, D. From monocytes to M1/M2 macrophages: Phenotypical vs. functional differentiation. *Front. Immunol.* **5**, 1–22 (2014).
64. Nahrendorf, M. & Swirski, F. K. Abandoning M1/M2 for a Network Model of Macrophage Function. *Circ. Res.* **119**, 414–7 (2016).
65. Mills, C. D. Anatomy of a discovery: m1 and m2 macrophages. *Front. Immunol.* **6**, 212 (2015).
66. Wang, Y. *et al.* Monocytes/Macrophages play a pathogenic role in IL-23 mediated psoriasis-like skin inflammation. *Sci. Rep.* **9**, 5310 (2019).
67. Zhao, R., Liang, H., Clarke, E., Jackson, C. & Xue, M. Inflammation in Chronic Wounds. 1–14 (2016). doi:10.3390/ijms17122085
68. Schebesch, C. *et al.* Alternatively activated macrophages actively inhibit proliferation of peripheral blood lymphocytes and CD4+ T cells in vitro. *Immunology* **92**, 478–86 (1997).
69. Kotwal, G. J. & Chien, S. Macrophage Differentiation in Normal and Accelerated Wound Healing. *Results Probl. Cell Differ.* **62**, 353–364 (2017).
70. Landén, N. X., Li, D. & Ståhle, M. Transition from inflammation to proliferation: a critical step during wound healing. *Cell. Mol. Life Sci.* **73**, 3861–3885 (2016).
71. Eming, S., Krieg, T. & Davidson, J. M. Inflammation in wound repair: Molecular and cellular mechanisms. *J. Invest. Dermatol.* **127**, 514–525 (2007).
72. Cañedo-Dorantes, L. & Cañedo-Ayala, M. Skin Acute Wound Healing: A Comprehensive Review. *Int. J. Inflam.* **2019**, 1–15 (2019).
73. Larouche, J., Sheoran, S., Maruyama, K. & Martino, M. M. Immune Regulation of Skin Wound Healing: Mechanisms and Novel Therapeutic Targets. *Adv. wound care* **7**, 209–231

(2018).
74. Mantovani, A., Cassatella, M. A., Costantini, C. & Jaillon, S. Neutrophils in the activation and regulation of innate and adaptive immunity. *Nat. Rev. Immunol.* **11**, 519–531 (2011).
75. Clark, R. A. *et al.* The vast majority of CLA+ T cells are resident in normal skin. *J. Immunol.* **176**, 4431–9 (2006).
76. Suwanpradid, J., Holcomb, Z. E. & MacLeod, A. S. Emerging Skin T-Cell Functions in Response to Environmental Insults. *J. Invest. Dermatol.* **137**, 288–294 (2017).
77. Mueller, S. N. & Mackay, L. K. Tissue-resident memory T cells: local specialists in immune defence. *Nat. Rev. Immunol.* **16**, 79–89 (2016).
78. Clark, R. A. Skin-resident T cells: the ups and downs of on site immunity. *J. Invest. Dermatol.* **130**, 362–70 (2010).
79. Ali, N. & Rosenblum, M. D. Regulatory T cells in skin. *Immunology* **152**, 372–381 (2017).
80. Cai, Y. *et al.* Pivotal role of dermal IL-17-producing γδ T cells in skin inflammation. *Immunity* **35**, 596–610 (2011).
81. Egbuniwe, I. U., Karagiannis, S. N., Nestle, F. O. & Lacy, K. E. Revisiting the role of B cells in skin immune surveillance. *Trends Immunol.* **36**, 102–111 (2015).
82. Klicznik, M. M., Szenes-Nagy, A. B., Campbell, D. J. & Gratz, I. K. Taking the lead – how keratinocytes orchestrate skin T cell immunity. *Immunol. Lett.* **200**, 43–51 (2018).
83. Wollenberg, A., Räwer, H.-C. & Schauber, J. Innate Immunity in Atopic Dermatitis. *Clin. Rev. Allergy Immunol.* **41**, 272–281 (2011).
84. de Jongh, G. J. *et al.* High Expression Levels of Keratinocyte Antimicrobial Proteins in Psoriasis Compared with Atopic Dermatitis. *J. Invest. Dermatol.* **125**, 1163–1173 (2005).
85. Pivarcsi, A., Kemény, L. & Dobozy, A. Innate Immune Functions of the Keratinocytes. *Acta Microbiol. Immunol. Hung.* **51**, 303–310 (2004).
86. Bautista-Hernández, L. A., Gómez-Olivares, J. L., Buentello-Volante, B. & Bautista-de Lucio, V. M. Fibroblasts: The Unknown Sentinels Eliciting Immune Responses Against Microorganisms. *Eur. J. Microbiol. Immunol. (Bp).* **7**, 151–157 (2017).
87. Yao, C. *et al.* Toll-like receptor family members in skin fibroblasts are functional and have a higher expression compared to skin keratinocytes. *Int. J. Mol. Med.* **35**, 1443–1450 (2015).
88. Van Linthout, S., Miteva, K. & Tschope, C. Crosstalk between fibroblasts and inflammatory cells. *Cardiovasc. Res.* **102**, 258–269 (2014).
89. Tsepkolenko, A. *et al.* The regenerative potential of skin and the immune system. *Clin. Cosmet. Investig. Dermatol.* **12**, 519–532 (2019).
90. Xiao, T. S. Innate immunity and inflammation. *Cell. Mol. Immunol.* **14**, 1 (2017).
91. Chen, L. *et al.* Inflammatory responses and inflammation-associated diseases in organs. *Oncotarget* **9**, 7204–7218 (2018).
92. MacLeod, A. S. & Mansbridge, J. N. The Innate Immune System in Acute and Chronic Wounds. *Adv. wound care* **5**, 65–78 (2016).
93. Dasu, M. R. & Isseroff, R. R. Toll-like receptors in wound healing: location, accessibility, and timing. *J. Invest. Dermatol.* **132**, 1955–8 (2012).
94. Greenlee-Wacker, M. C. Clearance of apoptotic neutrophils and resolution of inflammation. *Immunol. Rev.* **273**, 357–70 (2016).
95. McCormick, T. S., Stevens, S. R. & Kang, K. Macrophages and cutaneous inflammation. *Nat. Biotechnol.* **18**, 25–26 (2000).
96. Ploeger, D. T. *et al.* Cell plasticity in wound healing: paracrine factors of M1/ M2 polarized macrophages influence the phenotypical state of dermal fibroblasts. *Cell Commun. Signal.* **11**, 29 (2013).
97. Novak, M. L. & Koh, T. J. Phenotypic transitions of macrophages orchestrate tissue repair. *Am. J. Pathol.* **183**, 1352–1363 (2013).
98. Atri, C., Guerfali, F. Z. & Laouini, D. Role of Human Macrophage Polarization in Inflammation during Infectious Diseases. *Int. J. Mol. Sci.* **19**, (2018).
99. Tan, S.-Y., Tay, S. S., Sumaria, N., Roediger, B. & Weninger, W. Gamma-Delta T Cells in the Skin. in *Clinical and Basic Immunodermatology* 51–66 (Springer International Publishing, 2017). doi:10.1007/978-3-319-29785-9_4
100. Nosbaum, A. *et al.* Cutting Edge: Regulatory T Cells Facilitate Cutaneous Wound Healing.

J. Immunol. **196**, 2010–4 (2016).
101. Haertel, E., Joshi, N., Hiebert, P., Kopf, M. & Werner, S. Regulatory T cells are required for normal and activin-promoted wound repair in mice. *Eur. J. Immunol.* **48**, 1001–1013 (2018).
102. Schneider, D. F. *et al.* A novel role for NKT cells in cutaneous wound repair. *J. Surg. Res.* **168**, 325–33.e1 (2011).
103. Brubaker, A. L., Schneider, D. F. & Kovacs, E. J. Neutrophils and natural killer T cells as negative regulators of wound healing. *Expert Rev. Dermatol.* **6**, 5–8 (2011).
104. Dainichi, T., Hanakawa, S. & Kabashima, K. Classification of inflammatory skin diseases: a proposal based on the disorders of the three-layered defense systems, barrier, innate immunity and acquired immunity. *J. Dermatol. Sci.* **76**, 81–9 (2014).
105. Qu, X., Tang, Y. & Hua, S. Immunological Approaches Towards Cancer and Inflammation: A Cross Talk. *Front. Immunol.* **9**, 563 (2018).
106. Hanses, F., Park, S., Rich, J. & Lee, J. C. Reduced neutrophil apoptosis in diabetic mice during staphylococcal infection leads to prolonged Tnfα production and reduced neutrophil clearance. *PLoS One* **6**, e23633 (2011).
107. Wynn, T. A. & Barron, L. Macrophages: master regulators of inflammation and fibrosis. *Semin. Liver Dis.* **30**, 245–57 (2010).
108. Krzyszczyk, P., Schloss, R., Palmer, A. & Berthiaume, F. The Role of Macrophages in Acute and Chronic Wound Healing and Interventions to Promote Pro-wound Healing Phenotypes. *Front. Physiol.* **9**, 419 (2018).
109. Sindrilaru, A. *et al.* An unrestrained proinflammatory M1 macrophage population induced by iron impairs wound healing in humans and mice. *J. Clin. Invest.* **121**, 985–97 (2011).
110. Rosenblum, M. D., Remedios, K. A. & Abbas, A. K. Mechanisms of human autoimmunity. *J. Clin. Invest.* **125**, 2228–33 (2015).
111. Ye, C., Brand, D. & Zheng, S. G. Targeting IL-2: an unexpected effect in treating immunological diseases. *Signal Transduct. Target. Ther.* **3**, 2 (2018).
112. Whangbo, J. S. *et al.* Functional analysis of clinical response to low-dose IL-2 in patients with refractory chronic graft-versus-host disease. *Blood Adv.* **3**, 984–994 (2019).
113. Marín Morales, J. M. *et al.* Automated Clinical Grade Expansion of Regulatory T Cells in a Fully Closed System. *Front. Immunol.* **10**, 38 (2019).
114. Yanaba, K. *et al.* Regulatory B cells suppress imiquimod-induced, psoriasis-like skin inflammation. *J. Leukoc. Biol.* **94**, 563–73 (2013).
115. Rendon, A. & Schäkel, K. Psoriasis pathogenesis and treatment. *International Journal of Molecular Sciences* **20**, (2019).
116. De, R. & Mignogna, C. The histopathology of psoriasis. *Reumatismo* **59**, 46–48 (2007).
117. Roberson, E. D. O. & Bowcock, A. M. Psoriasis genetics: Breaking the barrier. *Trends in Genetics* **26**, 415–423 (2010).
118. Albanesi, C. & Pastore, S. Pathobiology of chronic inflammatory skin diseases: interplay between keratinocytes and immune cells as a target for anti-inflammatory drugs. *Curr. Drug Metab.* **11**, 210–27 (2010).
119. Benhadou, F., Mintoff, Di. & Del Marmol, V. Psoriasis: Keratinocytes or Immune Cells - Which Is the Trigger? *Dermatology* **235**, 91–100 (2019).
120. Sabat, R., Wolk, K., Loyal, L., Döcke, W. D. & Ghoreschi, K. T cell pathology in skin inflammation. *Seminars in Immunopathology* **41**, 359–377 (2019).
121. Casciano, F., Pigatto, P. D., Secchiero, P., Gambari, R. & Reali, E. T cell hierarchy in the pathogenesis of psoriasis and associated cardiovascular comorbidities. *Frontiers in Immunology* **9**, (2018).
122. Claudia, C. D. *et al.* Small molecules under development for psoriasis: on the road to the individualized therapies. *Archives of Dermatological Research* 1–17 (2020). doi:10.1007/s00403-020-02056-3
123. McKay, C., Kondratuk, K. E., Miller, J. P., Stumpf, B. & Boh, E. Biologic therapy in psoriasis: Navigating the options. *Cutis* **102**, 13–17 (2018).
124. Gunter, N. V., Yap, B. J. M., Chua, C. L. L. & Yap, W. H. Combining Understanding of Immunological Mechanisms and Genetic Variants Toward Development of Personalized

Medicine for Psoriasis Patients. *Front. Genet.* **10**, 395 (2019).
125. Calzada, D., Baos, S., Cremades-Jimeno, L. & Cárdaba, B. Immunological Mechanisms in Allergic Diseases and Allergen Tolerance: The Role of Treg Cells. *J. Immunol. Res.* **2018**, 1–10 (2018).
126. Nauta, A. J., Engels, F., Knippels, L. M., Garssen, J. & Redegeld, F. A. Mechanisms of allergy and asthma. *Eur. J. Pharmacol.* **585**, 354–360 (2008).
127. Raposo, G. & Stoorvogel, W. Extracellular vesicles: exosomes, microvesicles, and friends. *J. Cell Biol.* **200**, 373–83 (2013).
128. Colombo, M., Raposo, G. & Théry, C. Biogenesis, Secretion, and Intercellular Interactions of Exosomes and Other Extracellular Vesicles. *Annu. Rev. Cell Dev. Biol* **30**, 255–89 (2014).
129. Gould, S. J. & Raposo, G. As we wait: coping with an imperfect nomenclature for extracellular vesicles. *J. Extracell. vesicles* **2**, (2013).
130. van Niel, G., D'Angelo, G. & Raposo, G. Shedding light on the cell biology of extracellular vesicles. *Nat. Rev. Mol. Cell Biol.* **19**, 213–228 (2018).
131. Pan, B. T. & Johnstone, R. M. Fate of the transferrin receptor during maturation of sheep reticulocytes in vitro: Selective externalization of the receptor. *Cell* **33**, 967–978 (1983).
132. Raposo, G. *et al.* B lymphocytes secrete antigen-presenting vesicles. *J. Exp. Med.* **183**, 1161–72 (1996).
133. Zitvogel, L. *et al.* Eradication of established murine tumors using a novel cell-free vaccine: dendritic cell derived exosomes. *Nat. Med.* **4**, 594–600 (1998).
134. Pitt, J. M., Kroemer, G. & Zitvogel, L. Extracellular vesicles : masters of intercellular communication and potential clinical interventions. *J. Clin. Invest.* **126**, 1139–1143 (2016).
135. Gurunathan, S., Kang, M.-H., Jeyaraj, M., Qasim, M. & Kim, J.-H. Review of the Isolation, Characterization, Biological Function, and Multifarious Therapeutic Approaches of Exosomes. *Cells* **8**, (2019).
136. Riazifar, M., Pone, E. J., Lötvall, J. & Zhao, W. Stem Cell Extracellular Vesicles: Extended Messages of Regeneration. *Annu. Rev. Pharmacol. Toxicol.* **57**, 125–154 (2017).
137. Wolf, P. The Nature and Significance of Platelet Products in Human Plasma. *Br. J. Haematol.* **13**, 269–288 (1967).
138. Minciacchi, V. R., Freeman, M. R. & Di Vizio, D. Extracellular Vesicles in Cancer: Exosomes, Microvesicles and the Emerging Role of Large Oncosomes. *Semin. Cell Dev. Biol.* **40**, 41–51 (2015).
139. Théry, C. *et al.* Minimal information for studies of extracellular vesicles 2018 (MISEV2018): a position statement of the International Society for Extracellular Vesicles and update of the MISEV2014 guidelines. *J. Extracell. Vesicles* **7**, 1535750 (2018).
140. Stoorvogel, W., Strous, G. J., Geuze, H. J., Oorschot, V. & Schwartz, A. L. Late endosomes derive from early endosomes by maturation. *Cell* **65**, 417–27 (1991).
141. Hessvik, N. P. & Llorente, A. Current knowledge on exosome biogenesis and release. *Cell. Mol. Life Sci.* **75**, 193–208 (2018).
142. Möbius, W. *et al.* Immunoelectron Microscopic Localization of Cholesterol Using Biotinylated and Non-cytolytic Perfringolysin O. *J. Histochem. Cytochem.* **50**, 43–55 (2002).
143. Christ, L., Raiborg, C., Wenzel, E. M., Campsteijn, C. & Stenmark, H. Cellular Functions and Molecular Mechanisms of the ESCRT Membrane-Scission Machinery. *Trends Biochem. Sci.* **42**, 42–56 (2017).
144. Stuffers, S., Sem Wegner, C., Stenmark, H. & Brech, A. Multivesicular Endosome Biogenesis in the Absence of ESCRTs. *Traffic* **10**, 925–937 (2009).
145. Trajkovic, K. *et al.* Ceramide Triggers Budding of Exosome Vesicles into Multivesicular Endosomes. *Science (80-.).* **319**, 1244–1247 (2008).
146. Kajimoto, T., Okada, T., Miya, S., Zhang, L. & Nakamura, S. Ongoing activation of sphingosine 1-phosphate receptors mediates maturation of exosomal multivesicular endosomes. *Nat. Commun.* **4**, 2712 (2013).
147. Theos, A. C. *et al.* A Lumenal Domain-Dependent Pathway for Sorting to Intralumenal Vesicles of Multivesicular Endosomes Involved in Organelle Morphogenesis. *Dev. Cell* **10**, 343–354 (2006).

148. van Niel, G. *et al.* The Tetraspanin CD63 Regulates ESCRT-Independent and -Dependent Endosomal Sorting during Melanogenesis. *Dev. Cell* **21**, 708–721 (2011).
149. Hurwitz, S. N. *et al.* CD63 Regulates Epstein-Barr Virus LMP1 Exosomal Packaging, Enhancement of Vesicle Production, and Noncanonical NF-κB Signaling. *J. Virol.* **91**, (2017).
150. Gauthier, S. A. *et al.* Enhanced exosome secretion in Down syndrome brain - a protective mechanism to alleviate neuronal endosomal abnormalities. *Acta Neuropathol. Commun.* **5**, 65 (2017).
151. Hurwitz, S. N. *et al.* Nanoparticle analysis sheds budding insights into genetic drivers of extracellular vesicle biogenesis. *J. Extracell. vesicles* **5**, 31295 (2016).
152. Ostrowski, M. *et al.* Rab27a and Rab27b control different steps of the exosome secretion pathway. *Nat. Cell Biol.* **12**, 19–30 (2010).
153. Baietti, M. F. *et al.* Syndecan–syntenin–ALIX regulates the biogenesis of exosomes. *Nat. Cell Biol.* **14**, 677–685 (2012).
154. Pfeffer, S. R. Unsolved Mysteries in Membrane Traffic. *Annu. Rev. Biochem.* **76**, 629–645 (2007).
155. Jadli, A. S., Ballasy, N., Edalat, P. & Patel, V. B. Inside(sight) of tiny communicator: exosome biogenesis, secretion, and uptake. *Molecular and Cellular Biochemistry* **467**, 77–94 (2020).
156. del Conde, I., Shrimpton, C. N., Thiagarajan, P. & López, J. A. Tissue-factor-bearing microvesicles arise from lipid rafts and fuse with activated platelets to initiate coagulation. *Blood* **106**, 1604–1611 (2005).
157. Piccin, A., Murphy, W. G. & Smith, O. P. Circulating microparticles: pathophysiology and clinical implications. *Blood Rev.* **21**, 157–171 (2007).
158. Beer, K. B. & Wehman, A. M. Mechanisms and functions of extracellular vesicle release in vivo-What we can learn from flies and worms. *Cell Adh. Migr.* **11**, 135–150 (2017).
159. Skotland, T., Sandvig, K. & Llorente, A. Lipids in exosomes: Current knowledge and the way forward. *Prog. Lipid Res.* **66**, 30–41 (2017).
160. Llorente, A. *et al.* Molecular lipidomics of exosomes released by PC-3 prostate cancer cells. *Biochim. Biophys. Acta - Mol. Cell Biol. Lipids* **1831**, 1302–1309 (2013).
161. Brouwers, J. F. *et al.* Distinct lipid compositions of two types of human prostasomes. *Proteomics* **13**, 1660–1666 (2013).
162. Record, M., Silvente-Poirot, S., Poirot, M. & Wakelam, M. J. O. Extracellular vesicles: lipids as key components of their biogenesis and functions. *J. Lipid Res.* **59**, 1316–1324 (2018).
163. Podbielska, M. *et al.* Cytokine-induced release of ceramide-enriched exosomes as a mediator of cell death signaling in an oligodendroglioma cell line. *J. Lipid Res.* **57**, 2028–2039 (2016).
164. Kakazu, E., Mauer, A. S., Yin, M. & Malhi, H. Hepatocytes release ceramide-enriched pro-inflammatory extracellular vesicles in an IRE1α-dependent manner. *J. Lipid Res.* **57**, 233–45 (2016).
165. Esser, J. *et al.* Exosomes from human macrophages and dendritic cells contain enzymes for leukotriene biosynthesis and promote granulocyte migration. *J. Allergy Clin. Immunol.* **126**, 1032-1040.e4 (2010).
166. Lukic, A. *et al.* Pulmonary epithelial cancer cells and their exosomes metabolize myeloid cell-derived leukotriene C4 to leukotriene D4. *J. Lipid Res.* **57**, 1659–69 (2016).
167. Hough, K. P. *et al.* Unique Lipid Signatures of Extracellular Vesicles from the Airways of Asthmatics. *Sci. Rep.* **8**, 10340 (2018).
168. Sharma, S. *et al.* Targeting myeloid-derived suppressor cells augments antitumor activity against lung cancer. *ImmunoTargets Ther.* **2012**, 7 (2012).
169. Subra, C. *et al.* Exosomes account for vesicle-mediated transcellular transport of activatable phospholipases and prostaglandins. *J. Lipid Res.* **51**, 2105–2120 (2010).
170. Putz, U. *et al.* The Tumor Suppressor PTEN Is Exported in Exosomes and Has Phosphatase Activity in Recipient Cells. *Sci. Signal.* **5**, ra70–ra70 (2012).
171. Mathivanan, S., Ji, H. & Simpson, R. J. Exosomes: Extracellular organelles important in

intercellular communication. *J. Proteomics* **73**, 1907–1920 (2010).
172. Doyle, L. M. & Wang, M. Z. Overview of Extracellular Vesicles, Their Origin, Composition, Purpose, and Methods for Exosome Isolation and Analysis. *Cells* **8**, 727 (2019).
173. Escola, J.-M. M. *et al.* Selective enrichment of tetraspan proteins on the internal vesicles of multivesicular endosomes and on exosomes secreted by human B-lymphocytes. *J. Biol. Chem.* **273**, 20121–20127 (1998).
174. Witwer, K. W. *et al.* Standardization of sample collection, isolation and analysis methods in extracellular vesicle research. *J. Extracell. vesicles* **2**, (2013).
175. Sinha, A., Ignatchenko, V., Ignatchenko, A., Mejia-Guerrero, S. & Kislinger, T. In-depth proteomic analyses of ovarian cancer cell line exosomes reveals differential enrichment of functional categories compared to the NCI 60 proteome. *Biochem. Biophys. Res. Commun.* **445**, 694–701 (2014).
176. Andreu, Z. & Yáñez-Mó, M. Tetraspanins in Extracellular Vesicle Formation and Function. *Front. Immunol.* **5**, (2014).
177. Tauro, B. J. *et al.* Two distinct populations of exosomes are released from LIM1863 colon carcinoma cell-derived organoids. *Mol. Cell. Proteomics* **12**, 587–98 (2013).
178. Crescitelli, R. *et al.* Distinct RNA profiles in subpopulations of extracellular vesicles: apoptotic bodies, microvesicles and exosomes. *J. Extracell. vesicles* **2**, (2013).
179. Kowal, J. *et al.* Proteomic comparison defines novel markers to characterize heterogeneous populations of extracellular vesicle subtypes. *Proc. Natl. Acad. Sci. U. S. A.* **113**, E968-77 (2016).
180. Lo Cicero, A., Stahl, P. D. & Raposo, G. Extracellular vesicles shuffling intercellular messages: for good or for bad. *Curr. Opin. Cell Biol.* **35**, 69–77 (2015).
181. Blanc, L. & Vidal, M. New insights into the function of Rab GTPases in the context of exosomal secretion. *Small GTPases* **9**, 95–106 (2018).
182. Stenmark, H. Rab GTPases as coordinators of vesicle traffic. *Nat. Rev. Mol. Cell Biol.* **10**, 513–525 (2009).
183. Pathan, M. *et al.* Vesiclepedia 2019: a compendium of RNA, proteins, lipids and metabolites in extracellular vesicles. *Nucleic Acids Res.* **47**, D516–D519 (2019).
184. Chalmin, F. *et al.* Membrane-associated Hsp72 from tumor-derived exosomes mediates STAT3-dependent immunosuppressive function of mouse and human myeloid-derived suppressor cells. *J. Clin. Invest.* **120**, 457–71 (2010).
185. Sheng, H. *et al.* Insulinoma-released exosomes or microparticles are immunostimulatory and can activate autoreactive T cells spontaneously developed in nonobese diabetic mice. *J. Immunol.* **187**, 1591–600 (2011).
186. Zhao, H. *et al.* Exosomes From Adipose-Derived Stem Cells Attenuate Adipose Inflammation and Obesity Through Polarizing M2 Macrophages and Beiging in White Adipose Tissue. *Diabetes* **67**, 235–247 (2018).
187. Barros, F. M., Carneiro, F., Machado, J. C. & Melo, S. A. Exosomes and Immune Response in Cancer: Friends or Foes? *Front. Immunol.* **9**, (2018).
188. Valadi, H. *et al.* Exosome-mediated transfer of mRNAs and microRNAs is a novel mechanism of genetic exchange between cells. *Nat. Cell Biol.* **9**, 654–659 (2007).
189. Wahlgren, J. *et al.* Plasma exosomes can deliver exogenous short interfering RNA to monocytes and lymphocytes. *Nucleic Acids Res.* **40**, e130–e130 (2012).
190. Mateescu, B. *et al.* Obstacles and opportunities in the functional analysis of extracellular vesicle RNA – an ISEV position paper. *J. Extracell. Vesicles* **6**, 1286095 (2017).
191. Turchinovich, A., Drapkina, O. & Tonevitsky, A. Transcriptome of Extracellular Vesicles: State-of-the-Art. *Front. Immunol.* **10**, 202 (2019).
192. Nolte-'t Hoen, E. N. M. *et al.* Deep sequencing of RNA from immune cell-derived vesicles uncovers the selective incorporation of small non-coding RNA biotypes with potential regulatory functions. *Nucleic Acids Res.* **40**, 9272–9285 (2012).
193. Villarroya-Beltri, C. *et al.* Sumoylated hnRNPA2B1 controls the sorting of miRNAs into exosomes through binding to specific motifs. *Nat. Commun.* **4**, 2980 (2013).
194. Mukherjee, K. *et al.* Reversible HuR-micro RNA binding controls extracellular export of

miR-122 and augments stress response. *EMBO Rep.* **17**, 1184–1203 (2016).
195. Temoche-Diaz, M. M. *et al.* Distinct mechanisms of microRNA sorting into cancer cell-derived extracellular vesicle subtypes. *Elife* **8**, (2019).
196. Kahlert, C. *et al.* Identification of double-stranded genomic DNA spanning all chromosomes with mutated KRAS and p53 DNA in the serum exosomes of patients with pancreatic cancer. *J. Biol. Chem.* **289**, 3869–75 (2014).
197. Thakur, B. K. *et al.* Double-stranded DNA in exosomes: a novel biomarker in cancer detection. *Cell Res.* **24**, 766–9 (2014).
198. Lázaro-Ibáñez, E. *et al.* Different gDNA content in the subpopulations of prostate cancer extracellular vesicles: Apoptotic bodies, microvesicles, and exosomes. *Prostate* **74**, 1379–1390 (2014).
199. García-Romero, N. *et al.* DNA sequences within glioma-derived extracellular vesicles can cross the intact blood-brain barrier and be detected in peripheral blood of patients. *Oncotarget* **8**, 1416–1428 (2017).
200. Németh, A. *et al.* Antibiotic-induced release of small extracellular vesicles (exosomes) with surface-associated DNA. *Sci. Rep.* **7**, 8202 (2017).
201. Guescini, M., Genedani, S., Stocchi, V. & Agnati, L. F. Astrocytes and Glioblastoma cells release exosomes carrying mtDNA. *J. Neural Transm.* **117**, 1–4 (2010).
202. Sansone, P. *et al.* Packaging and transfer of mitochondrial DNA via exosomes regulate escape from dormancy in hormonal therapy-resistant breast cancer. *Proc. Natl. Acad. Sci.* **114**, E9066–E9075 (2017).
203. Jabalee, J., Towle, R. & Garnis, C. The Role of Extracellular Vesicles in Cancer: Cargo, Function, and Therapeutic Implications. *Cells* **7**, 93 (2018).
204. Momen-Heravi, F., Getting, S. J. & Moschos, S. A. Extracellular vesicles and their nucleic acids for biomarker discovery. *Pharmacol. Ther.* **192**, 170–187 (2018).
205. Dai, Y. D. & Dias, P. Exosomes or Microvesicles, a Secreted Subcellular Organelle Contributing to Inflammation and Diabetes. *Diabetes* **67**, 2154–2156 (2018).
206. Zheng, G. *et al.* Mesenchymal stromal cell-derived extracellular vesicles: regenerative and immunomodulatory effects and potential applications in sepsis. *Cell Tissue Res.* **374**, 1–15 (2018).
207. Galieva, L. R., James, V., Mukhamedshina, Y. O. & Rizvanov, A. A. Therapeutic Potential of Extracellular Vesicles for the Treatment of Nerve Disorders. *Front. Neurosci.* **13**, 163 (2019).
208. Dai, G. H. *et al.* MicroRNA-223-3p inhibits the angiogenesis of ischemic cardiac microvascular endothelial cells via affecting RPS6KB1/hif-1a signal pathway. *PLoS One* **9**, 1–14 (2014).
209. Li, P., Kaslan, M., Lee, S. H., Yao, J. & Gao, Z. Progress in Exosome Isolation Techniques. *Theranostics* **7**, (2017).
210. Théry, C., Amigorena, S., Raposo, G. & Clayton, A. Isolation and Characterization of Exosomes from Cell Culture Supernatants and Biological Fluids. *Curr. Protoc. Cell Biol.* **30**, 3.22.1-3.22.29 (2006).
211. Lane, R. E., Korbie, D., Trau, M. & Hill, M. M. Optimizing Size Exclusion Chromatography for Extracellular Vesicle Enrichment and Proteomic Analysis from Clinically Relevant Samples. *Proteomics* **19**, 1800156 (2019).
212. Monguió-Tortajada, M., Gálvez-Montón, C., Bayes-Genis, A., Roura, S. & Borràs, F. E. Extracellular vesicle isolation methods: rising impact of size-exclusion chromatography. *Cell. Mol. Life Sci.* **76**, 2369–2382 (2019).
213. Zeringer, E., Barta, T., Li, M. & Vlassov, A. V. Strategies for Isolation of Exosomes. *Cold Spring Harb. Protoc.* **2015**, 319–323 (2015).
214. Zarovni, N. *et al.* Integrated isolation and quantitative analysis of exosome shuttled proteins and nucleic acids using immunocapture approaches. *Methods* **87**, 46–58 (2015).
215. Conde-Vancells, J. *et al.* Characterization and comprehensive proteome profiling of exosomes secreted by hepatocytes. *J. Proteome Res.* **7**, 5157–66 (2008).
216. Hartjes, T., Mytnyk, S., Jenster, G., van Steijn, V. & van Royen, M. Extracellular Vesicle Quantification and Characterization: Common Methods and Emerging Approaches.

Bioengineering **6**, 7 (2019).
217. Bæk, R. & Jørgensen, M. M. Multiplexed phenotyping of small extracellular vesicles using protein microarray (EV array). in *Methods in Molecular Biology* **1545**, 117–127 (2017).
218. Eldh, M., Lötvall, J., Malmhäll, C. & Ekström, K. Importance of RNA isolation methods for analysis of exosomal RNA: Evaluation of different methods. *Mol. Immunol.* **50**, 278–286 (2012).
219. Théry, C. *et al.* Indirect activation of naïve CD4+ T cells by dendritic cell–derived exosomes. *Nat. Immunol.* **3**, 1156–1162 (2002).
220. Segura, E., Amigorena, S. & Théry, C. Mature dendritic cells secrete exosomes with strong ability to induce antigen-specific effector immune responses. *Blood Cells, Mol. Dis.* **35**, 89–93 (2005).
221. Robbins, P. D. & Morelli, A. E. Regulation of immune responses by extracellular vesicles. *Nat. Rev. Immunol.* **14**, 195–208 (2014).
222. Campana, S., De Pasquale, C., Carrega, P., Ferlazzo, G. & Bonaccorsi, I. Cross-dressing: an alternative mechanism for antigen presentation. *Immunol. Lett.* **168**, 349–354 (2015).
223. Altevogt, P., Bretz, N. P., Ridinger, J., Utikal, J. & Umansky, V. Novel insights into exosome-induced, tumor-associated inflammation and immunomodulation. *Semin. Cancer Biol.* **28**, 51–57 (2014).
224. Schorey, J. S. & Harding, C. V. Extracellular vesicles and infectious diseases : new complexity to an old story. **126**, 1181–1189 (2016).
225. Carrasco, E., Soto-Heredero, G. & Mittelbrunn, M. The Role of Extracellular Vesicles in Cutaneous Remodeling and Hair Follicle Dynamics. *Int. J. Mol. Sci.* **20**, (2019).
226. Kotzerke, K. *et al.* Immunostimulatory activity of murine keratinocyte-derived exosomes. *Exp. Dermatol.* **22**, 650–655 (2013).
227. Medina, A. & Ghahary, A. Transdifferentiated circulating monocytes release exosomes containing 14-3-3 proteins with matrix metalloproteinase-1 stimulating effect for dermal fibroblasts. *Wound Repair Regen.* **18**, 245–253 (2010).
228. Basu, J. & Ludlow, J. W. Exosomes for repair, regeneration and rejuvenation. *Expert Opin. Biol. Ther.* **16**, 489–506 (2016).
229. Ha, D., Yang, N. & Nadithe, V. Exosomes as therapeutic drug carriers and delivery vehicles across biological membranes : current perspectives and future challenges. *Acta Pharm. Sin. B* **6**, 287–296 (2016).
230. Yamashita, T., Takahashi, Y. & Takakura, Y. Possibility of exosome-based therapeutics and challenges in production of exosomes eligible for therapeutic application. *Biological and Pharmaceutical Bulletin* **41**, 835–842 (2018).
231. Koniusz, S. *et al.* Extracellular Vesicles in Physiology, Pathology, and Therapy of the Immune and Central Nervous System, with Focus on Extracellular Vesicles Derived from Mesenchymal Stem Cells as Therapeutic Tools. *Front. Cell. Neurosci.* **10**, 109 (2016).
232. Bobrie, A., Colombo, M., Raposo, G. & Théry, C. Exosome Secretion: Molecular Mechanisms and Roles in Immune Responses. *Traffic* **12**, 1659–1668 (2011).
233. Beer, L. *et al.* Analysis of the secretome of apoptotic peripheral blood mononuclear cells: Impact of released proteins and exosomes for tissue regeneration. *Sci. Rep.* **5**, 1–18 (2015).
234. Wilgus, T. A., Roy, S. & McDaniel, J. C. Neutrophils and Wound Repair: Positive Actions and Negative Reactions. *Adv. Wound Care* **2**, 379–388 (2013).
235. Ti, D. *et al.* LPS-preconditioned mesenchymal stromal cells modify macrophage polarization for resolution of chronic inflammation via exosome-shuttled let-7b. *J. Transl. Med.* **13**, 308 (2015).
236. Song, J. Y. *et al.* Umbilical cord-derived mesenchymal stem cell extracts reduce colitis in mice by re-polarizing intestinal macrophages. *Sci. Rep.* **7**, (2017).
237. Spinosa, M. *et al.* Human mesenchymal stromal cell-derived extracellular vesicles attenuate aortic aneurysm formation and macrophage activation via microRNA-147. *FASEB J.* **32**, fj201701138RR (2018).
238. Li, X. *et al.* Exosome Derived From Human Umbilical Cord Mesenchymal Stem Cell Mediates MiR-181c Attenuating Burn-induced Excessive Inflammation. *EBioMedicine* **8**, 72–82 (2016).

239. He, X. *et al.* MSC-Derived Exosome Promotes M2 Polarization and Enhances Cutaneous Wound Healing. *Stem Cells Int.* **2019**, 1–16 (2019).
240. Kou, X. *et al.* The Fas/Fap-1/Cav-1 complex regulates IL-1RA secretion in mesenchymal stem cells to accelerate wound healing. *Sci. Transl. Med.* **10**, eaai8524 (2018).
241. Budoni, M. *et al.* The Immunosuppressive Effect of Mesenchymal Stromal Cells on B Lymphocytes is Mediated by Membrane Vesicles. *Cell Transplant.* **22**, 369–379 (2013).
242. Mokarizadeh, A. *et al.* Microvesicles derived from mesenchymal stem cells: Potent organelles for induction of tolerogenic signaling. *Immunol. Lett.* **147**, 47–54 (2012).
243. Muraca, M. *et al.* Immunoregulatory Effects of Mesenchymal Stem Cell-Derived Extracellular Vesicles on T Lymphocytes. *Cell Transplant.* **24**, 2615–2627 (2015).
244. Kordelas, L. *et al.* MSC-derived exosomes: a novel tool to treat therapy-refractory graft-versus-host disease. *Leukemia* **28**, 970–973 (2014).
245. Peche, H., Heslan, M., Usal, C., Amigorena, S. & Cuturi, M. C. Presentation of donor major histocompatibility complex antigens by bone marrow dendritic cell-derived exosomes modulates allograft rejection1. *Transplantation* **76**, 1503–1510 (2003).
246. Kim, S.-H. *et al.* Exosomes Derived from IL-10-Treated Dendritic Cells Can Suppress Inflammation and Collagen-Induced Arthritis. *J. Immunol.* **174**, 6440–6448 (2005).
247. Yang, X., Meng, S., Jiang, H., Chen, T. & Wu, W. Exosomes derived from interleukin-10-treated dendritic cells can inhibit trinitrobenzene sulfonic acid-induced rat colitis. *Scand. J. Gastroenterol.* **45**, 1168–1177 (2010).
248. Miksa, M. *et al.* Dendritic cell-derived exosomes containing milk fat globule epidermal growth factor-factor VIII attenuate proinflammatory responses in sepsis. *Shock* **25**, 586–593 (2006).
249. Miksa, M. *et al.* Immature dendritic cell-derived exosomes rescue septic animals via milk fat globule epidermal growth factor-factor VIII. *J. Immunol.* **183**, 5983–90 (2009).
250. Hedlund, M. *et al.* Human Placenta Expresses and Secretes NKG2D Ligands via Exosomes that Down-Modulate the Cognate Receptor Expression: Evidence for Immunosuppressive Function. *J. Immunol.* **183**, 340–351 (2009).
251. Azari, O., Babaei, H. & Derakhshanfar, A. Effects of transplanted mesenchymal stem cells isolated from Wharton's jelly of caprine umbilical cord on cutaneous wound healing ; histopathological evaluation. *Vet. Res. Community* **35**, 211–222 (2011).
252. Luo, G., Cheng, W., He, W. & Wang, X. Promotion of cutaneous wound healing by local application of mesenchymal stem cells derived from human umbilical cord blood. *Wound Pract. Res.* **18**, 506–513 (2010).
253. Henriques-Antunes, H. *et al.* The Kinetics of Small Extracellular Vesicle Delivery Impacts Skin Tissue Regeneration. *ACS Nano* **13**, 8694–8707 (2019).
254. Wang, L. *et al.* Extracellular Vesicles Released from Human Umbilical Cord-Derived Mesenchymal Stromal Cells Prevent Life-Threatening Acute Graft-Versus-Host Disease in a Mouse Model of Allogeneic Hematopoietic Stem Cell Transplantation. *Stem Cells Dev.* **25**, 1874–1883 (2016).
255. Nassar, W. *et al.* Umbilical cord mesenchymal stem cells derived extracellular vesicles can safely ameliorate the progression of chronic kidney diseases. *Biomater. Res.* **20**, (2016).
256. Lai, P., Weng, J., Guo, L., Chen, X. & Du, X. Novel insights into MSC-EVs therapy for immune diseases. *Biomark. Res.* **7**, (2019).
257. AXP automatic UCB processing. (2019). Available at: http://cescatherapeutics.com/blood-marrow-processing/axp-autoxpress/). (Accessed: 15th May 2020)
258. Sigma Aldrich. Phospholipid Assay Kit. Available at: https://www.sigmaaldrich.com/catalog/product/sigma/mak122?lang=pt&region=PT. (Accessed: 15th May 2020)
259. Cheng, L. & Hill, A. F. Small RNA library construction for exosomal RNA from biological samples for the ion torrent PGM™ and ion S5™ system. in *Methods in Molecular Biology* **1545**, 71–90 (2017).
260. Nordin, J. Z. *et al.* Ultrafiltration with size-exclusion liquid chromatography for high yield isolation of extracellular vesicles preserving intact biophysical and functional properties. *Nanomedicine Nanotechnology, Biol. Med.* **11**, 879–883 (2015).

261. Szatanek, R. *et al.* The Methods of Choice for Extracellular Vesicles (EVs) Characterization. *Int. J. Mol. Sci.* **18**, (2017).
262. Kornek, M. *et al.* extracellular vesicle Heterogeneity: Subpopulations, isolation Techniques, and Diverse Functions in Cancer Progression. **9**, 1 (2018).
263. Kreimer, S. *et al.* Mass-Spectrometry-Based Molecular Characterization of Extracellular Vesicles: Lipidomics and Proteomics. *J. Proteome Res.* **14**, 2367–2384 (2014).
264. de Gassart, A., Geminard, C., Fevrier, B., Raposo, G. & Vidal, M. Lipid raft-associated protein sorting in exosomes. *Blood* **102**, 4336–44 (2003).
265. Brzozowski, J. S. *et al.* Lipidomic profiling of extracellular vesicles derived from prostate and prostate cancer cell lines. *Lipids Health Dis.* **17**, 211 (2018).
266. Sampaio, J. L. *et al.* Membrane lipidome of an epithelial cell line. *Proc. Natl. Acad. Sci.* **108**, 1903–1907 (2011).
267. van Meer, G., Voelker, D. R. & Feigenson, G. W. Membrane lipids: where they are and how they behave. *Nat. Rev. Mol. Cell Biol.* **9**, 112–124 (2008).
268. Chapuy-Regaud, S. *et al.* Characterization of the lipid envelope of exosome encapsulated HEV particles protected from the immune response. *Biochimie* **141**, 70–79 (2017).
269. Wubbolts, R. *et al.* Proteomic and biochemical analyses of human B cell-derived exosomes. Potential implications for their function and multivesicular body formation. *J. Biol. Chem.* **278**, 10963–72 (2003).
270. Laulagnier, K. *et al.* Mast cell- and dendritic cell-derived exosomes display a specific lipid composition and an unusual membrane organization. *Biochem. J.* **380**, 161–71 (2004).
271. Vidal, M., Sainte-Marie, J., Philippot, J. R. & Bienvenue, A. Asymmetric distribution of phospholipids in the membrane of vesicles released during in vitro maturation of guinea pig reticulocytes: Evidence precluding a role for ?aminophospholipid translocase? *J. Cell. Physiol.* **140**, 455–462 (1989).
272. Durcin, M. *et al.* Characterisation of adipocyte-derived extracellular vesicle subtypes identifies distinct protein and lipid signatures for large and small extracellular vesicles. *J. Extracell. vesicles* **6**, 1305677 (2017).
273. Skotland, T., Hessvik, N. P., Sandvig, K. & Llorente, A. Exosomal lipid composition and the role of ether lipids and phosphoinositides in exosome biology. *J. Lipid Res.* **60**, 9–18 (2019).
274. Correia, B. S. B., Susana Torrinhas, R., Yutaka Ohashi, W. & Tasic, L. Analytical Tools for Lipid Assessment in Biological Assays. in *Advances in Lipid Metabolism* (ed. Baez, R. V.) (IntechOpen, 2018). doi:10.5772/intechopen.81523
275. Yang, K. & Han, X. Lipidomics: Techniques, Applications, and Outcomes Related to Biomedical Sciences. *Trends Biochem. Sci.* **41**, 954–969 (2016).
276. Haraszti, R. A. *et al.* Serum Deprivation of Mesenchymal Stem Cells Improves Exosome Activity and Alters Lipid and Protein Composition. *iScience* **16**, 230–241 (2019).
277. Rübsaamen, K. Lipidomic analysis of circulating human blood cells. (2010).
278. Horvath, S. E. & Daum, G. Lipids of mitochondria. *Prog. Lipid Res.* **52**, 590–614 (2013).
279. Vesiclepedia - A community compendium for extracellular vesicles. Available at: http://microvesicles.org/index.html. (Accessed: 15th September 2019)
280. Schaller, J. *Human blood plasma proteins : structure and function*. (John Wiley & Sons, 2008).
281. Bryk, A. H. & Wiśniewski, J. R. W. Quantitative Analysis of Human Red Blood Cell Proteome. *ACS Nano* **16**, 2752–2761 (2017).
282. Kakhniashvili, D. G., Bulla, L. A. & Goodman, S. R. The human erythrocyte proteome: analysis by ion trap mass spectrometry. *Mol. Cell. Proteomics* **3**, 501–9 (2004).
283. Gómez-Molina, C. *et al.* Small Extracellular Vesicles in Rat Serum Contain Astrocyte-Derived Protein Biomarkers of Repetitive Stress. *Int. J. Neuropsychopharmacol.* **22**, 232–246 (2019).
284. Kittivorapart, J. *et al.* Quantitative proteomics of plasma vesicles identify novel biomarkers for hemoglobin E/β-thalassemic patients. *Blood Adv.* **2**, 95–104 (2018).
285. Prieto, D. *et al.* S100-A9 protein in exosomes from chronic lymphocytic leukemia cells promotes NF-κB activity during disease progression. *Blood* **130**, 777–788 (2017).

286. Vallabhajosyula, P. *et al.* Tissue-specific exosome biomarkers for noninvasively monitoring immunologic rejection of transplanted tissue. *J. Clin. Invest.* **127**, 1375–1391 (2017).
287. Monastyrskaya, K. Functional Association between Regulatory RNAs and the Annexins. *Int. J. Mol. Sci.* **19**, (2018).
288. Shen, Y. *et al.* Transferrin receptor 1 in cancer: a new sight for cancer therapy. *Am. J. Cancer Res.* **8**, 916–931 (2018).
289. Pasricha, S.-R. S. *et al. Diagnosis and management of iron deficiency anaemia: a clinical update*. *The Medical Journal of Australia* **193**, (2010).
290. Díaz-Varela, M. *et al.* Proteomics study of human cord blood reticulocyte-derived exosomes. *Sci. Rep.* **8**, 14046 (2018).
291. Carayon, K. *et al.* Proteolipidic composition of exosomes changes during reticulocyte maturation. *J. Biol. Chem.* **286**, 34426–39 (2011).
292. Géminard, C., Nault, F., Johnstone, R. M. & Vidal, M. Characteristics of the interaction between Hsc70 and the transferrin receptor in exosomes released during reticulocyte maturation. *J. Biol. Chem.* **276**, 9910–6 (2001).
293. Rong, Y. *et al.* Neural stem cell-derived small extracellular vesicles attenuate apoptosis and neuroinflammation after traumatic spinal cord injury by activating autophagy. *Cell Death Dis.* **10**, 340 (2019).
294. Choi, D. *et al.* The Impact of Oncogenic EGFRvIII on the Proteome of Extracellular Vesicles Released from Glioblastoma Cells. *Mol. Cell. Proteomics* **17**, 1948–1964 (2018).
295. Kishore, A. *et al.* Expression analysis of extracellular microRNA in bronchoalveolar lavage fluid from patients with pulmonary sarcoidosis. *Respirology* **23**, 1166–1172 (2018).
296. Pavlyukov, M. S. *et al.* Apoptotic Cell-Derived Extracellular Vesicles Promote Malignancy of Glioblastoma Via Intercellular Transfer of Splicing Factors. *Cancer Cell* **34**, 119-135.e10 (2018).
297. Oeyen, E. *et al.* Ultrafiltration and size exclusion chromatography combined with asymmetrical-flow field-flow fractionation for the isolation and characterisation of extracellular vesicles from urine. *J. Extracell. Vesicles* **7**, 1490143 (2018).
298. Bruschi, M. *et al.* Metabolic Signature of Microvesicles from Umbilical Cord Mesenchymal Stem Cells of Preterm and Term Infants. *Proteomics - Clin. Appl.* **12**, 1700082 (2018).
299. Hong, P., Koza, S. & Bouvier, E. S. P. A review size-exclusion chromatography for the analysis of proteins biopharmaceuticals and their aggregates. *J. Liq. Chromatogr. Relat. Technol.* **35**, 2923–2950 (2012).
300. Olver, C. & Vidal, M. Proteomic analysis of secreted exosomes. *Subcell. Biochem.* **43**, 99–131 (2007).
301. Deraison, C., Bonnart, C. & Vergnolle, N. Proteases. in *Inflammation - From Molecular and Cellular Mechanisms to the Clinic* (eds. Cavaillon, J. -M. & Singer, M.) 727–766 (2017). doi:10.1002/9783527692156.ch28
302. Théry, C., Zitvogel, L. & Amigorena, S. Exosomes: composition, biogenesis and function. *Nat. Rev. Immunol.* **2**, 569–579 (2002).
303. Velliquette, R. W. *et al.* Monoclonal anti-CD47 interference in red cell and platelet testing. *Transfusion* **59**, 730–737 (2019).
304. Lopez, J. A. *et al.* The α and β chains of human platelet glycoprotein Ib are both transmembrane proteins containing a leucine-rich amino acid sequence. *Proc. Natl. Acad. Sci. U. S. A.* **85**, 2135–2139 (1988).
305. Belov, L. *et al.* Extensive surface protein profiles of extracellular vesicles from cancer cells may provide diagnostic signatures from blood samples. *J. Extracell. vesicles* **5**, 25355 (2016).
306. Qiu, G. *et al.* Mesenchymal stem cell-derived extracellular vesicles affect disease outcomes via transfer of microRNAs. *Stem Cell Res. Ther.* **9**, 320 (2018).
307. Sork, H. *et al.* Heterogeneity and interplay of the extracellular vesicle small RNA transcriptome and proteome. *Sci. Rep.* **8**, 10813 (2018).
308. Bellingham, S. A., Coleman, B. M. & Hill, A. F. Small RNA deep sequencing reveals a distinct miRNA signature released in exosomes from prion-infected neuronal cells. *Nucleic Acids Res.* **40**, 10937–49 (2012).

309. Lässer, C. *et al.* Two distinct extracellular RNA signatures released by a single cell type identified by microarray and next-generation sequencing. *RNA Biol.* **14**, 58–72 (2017).
310. Kaur, S. *et al.* Small non-coding RNA landscape of extracellular vesicles from human stem cells. *Sci. Rep.* **8**, 15503 (2018).
311. Baglio, S. R. *et al.* Human bone marrow- and adipose-mesenchymal stem cells secrete exosomes enriched in distinctive miRNA and tRNA species. *Stem Cell Res. Ther.* **6**, 127 (2015).
312. Wei, Z. *et al.* Coding and noncoding landscape of extracellular RNA released by human glioma stem cells. *Nat. Commun.* **8**, 1145 (2017).
313. Oberbauer, V. & Schaefer, M. R. tRNA-Derived Small RNAs: Biogenesis, Modification, Function and Potential Impact on Human Disease Development. *Genes (Basel).* **9**, (2018).
314. Click-IT™ L-Homopropargylglycine (HPG). Available at: https://www.thermofisher.com/order/catalog/product/C10186?SID=srch-srp-C10186. (Accessed: 9th September 2019)
315. Reid, D. W. & Nicchitta, C. V. The enduring enigma of nuclear translation. *J. Cell Biol.* **197**, 7–9 (2012).
316. Polymenis, M. & Aramayo, R. *Translate to divide: control of the cell cycle by protein synthesis*. *Microbial Cell* **2**, 94–104 (2015).
317. Anderson, P. & Ivanov, P. tRNA fragments in human health and disease. *FEBS Lett.* **588**, 4297–304 (2014).
318. Li, S., Xu, Z. & Sheng, J. tRNA-Derived Small RNA: A Novel Regulatory Small Non-Coding RNA. *Genes (Basel).* **9**, 246 (2018).
319. Phinney, D. G. & Pittenger, M. F. Concise Review: MSC-Derived Exosomes for Cell-Free Therapy. *Stem Cells* **35**, 851–858 (2017).
320. Chiou, N.-T., Kageyama, R., Mark, K. & Correspondence, A. Selective Export into Extracellular Vesicles and Function of tRNA Fragments during T Cell Activation. *Cell Rep.* **25**, 3356–3370 (2018).
321. Zhang, J. *et al.* Exosome and exosomal microRNA: trafficking, sorting, and function. *Genomics. Proteomics Bioinformatics* **13**, 17–24 (2015).
322. Bhome, R. *et al.* Exosomal microRNAs (exomiRs): Small molecules with a big role in cancer. *Cancer Lett.* **420**, 228–235 (2018).
323. Cheng, L., Sharples, R. A., Scicluna, B. J. & Hill, A. F. Exosomes provide a protective and enriched source of miRNA for biomarker profiling compared to intracellular and cell-free blood. *J. Extracell. Vesicles* **3**, 23743 (2014).
324. Liang, Y. *et al.* Exosomal microRNA-144 from bone marrow-derived mesenchymal stem cells inhibits the progression of non-small cell lung cancer by targeting CCNE1 and CCNE2. *Stem Cell Res. Ther.* **11**, 87 (2020).
325. Chen, L. *et al.* Cardiac progenitor-derived exosomes protect ischemic myocardium from acute ischemia/reperfusion injury. *Biochem. Biophys. Res. Commun.* **431**, 566–571 (2013).
326. Lai, X. & Vera, J. MicroRNA Clusters. in *Encyclopedia of Systems Biology* (eds. W., D., O., W., KH., C. & H., Y.) 1310–1314 (Springer New York, 2013). doi:10.1007/978-1-4419-9863-7_1121
327. Xu, P. *et al.* Regulation of gene expression by miR-144/451 during mouse erythropoiesis. *Blood* **133**, 2518–2528 (2019).
328. Kohrs, N. *et al.* MiR144/451 Expression Is Repressed by RUNX1 During Megakaryopoiesis and Disturbed by RUNX1/ETO. *PLOS Genet.* **12**, e1005946 (2016).
329. Nothnick, W. B., Swan, K., Flyckt, R., Falcone, T. & Graham, A. Human endometriotic lesion expression of the miR-144-3p/miR-451a cluster, its correlation with markers of cell survival and origin of lesion content. *Sci. Rep.* **9**, 8823 (2019).
330. Wang, T., Wu, F. & Yu, D. miR-144/451 in hematopoiesis and beyond. *ExRNA* **1**, 16 (2019).
331. Freitas, D. *et al.* Different isolation approaches lead to diverse glycosylated extracellular vesicle populations. *J. Extracell. vesicles* **8**, 1621131 (2019).
332. Patel, G. K. *et al.* Comparative analysis of exosome isolation methods using culture supernatant for optimum yield, purity and downstream applications. *Sci. Rep.* **9**, 5335 (2019).

333. Elmahdy, N. A., Sokar, S. S., Salem, M. L., Sarhan, N. I. & Abou-Elela, S. H. Anti-fibrotic potential of human umbilical cord mononuclear cells and mouse bone marrow cells in CCl4-induced liver fibrosis in mice. *Biomed. Pharmacother.* **89**, 1378–1386 (2017).
334. Henning, R. J. *et al.* Human cord blood mononuclear cells decrease cytokines and inflammatory cells in acute myocardial infarction. *Stem Cells Dev.* **17**, 1207–19 (2008).
335. Pawitan, J. A. Prospect of Stem Cell Conditioned Medium in Regenerative Medicine. *Biomed Res. Int.* **2014**, (2014).
336. Kim, J., Lee, J. H., Yeo, S. M., Chung, H. M. & Chae, J. Il. Stem cell recruitment factors secreted from cord blood-derived stem cells that are not secreted from mature endothelial cells enhance wound healing. *Vitr. Cell. Dev. Biol. - Anim.* **50**, 146–154 (2014).
337. Ding, M. *et al.* Exosomes Isolated From Human Umbilical Cord Mesenchymal Stem Cells Alleviate Neuroinflammation and Reduce Amyloid-Beta Deposition by Modulating Microglial Activation in Alzheimer's Disease. *Neurochem. Res.* **43**, 2165–2177 (2018).
338. Ma, Z. J. *et al.* Immunosuppressive Effect of Exosomes from Mesenchymal Stromal Cells in Defined Medium on Experimental Colitis. *Int. J. stem cells* **12**, 440–448 (2019).
339. Ma, W.-T., Gao, F., Gu, K. & Chen, D.-K. The Role of Monocytes and Macrophages in Autoimmune Diseases: A Comprehensive Review. *Front. Immunol.* **10**, 1140 (2019).
340. Navegantes, K. C. *et al.* Immune modulation of some autoimmune diseases: the critical role of macrophages and neutrophils in the innate and adaptive immunity. *J. Transl. Med.* **15**, (2017).
341. Ren, W. *et al.* Extracellular vesicles secreted by hypoxia pre-challenged mesenchymal stem cells promote non-small cell lung cancer cell growth and mobility as well as macrophage M2 polarization via miR-21-5p delivery. *J. Exp. Clin. Cancer Res.* **38**, (2019).
342. Lo Sicco, C. *et al.* Mesenchymal Stem Cell-Derived Extracellular Vesicles as Mediators of Anti-Inflammatory Effects: Endorsement of Macrophage Polarization. *Stem Cells Transl. Med.* **6**, 1018–1028 (2017).
343. Abumaree, M. H. *et al.* Human Placental Mesenchymal Stem Cells (pMSCs) Play a Role as Immune Suppressive Cells by Shifting Macrophage Differentiation from Inflammatory M1 to Anti-inflammatory M2 Macrophages. *Stem Cell Rev. Reports* **9**, 620–641 (2013).
344. Vasandan, A. B. *et al.* Human Mesenchymal stem cells program macrophage plasticity by altering their metabolic status via a PGE 2 -dependent mechanism. *Sci. Rep.* **6**, (2016).
345. Maeß, M. B., Sendelbach, S. & Lorkowski, S. Selection of reliable reference genes during THP-1 monocyte differentiation into macrophages. *BMC Mol. Biol.* **11**, 90 (2010).
346. Chanput, W., Mes, J. J. & Wichers, H. J. THP-1 cell line: An in vitro cell model for immune modulation approach. *International Immunopharmacology* **23**, 37–45 (2014).
347. McAleer, J. P. & Vella, A. T. Understanding how lipopolysaccharide impacts CD4 T-cell immunity. *Critical Reviews in Immunology* **28**, 281–299 (2008).
348. Adamson, S. & Leitinger, N. Phenotypic modulation of macrophages in response to plaque lipids. *Curr. Opin. Lipidol.* **22**, 335–342 (2011).
349. Delavary, B. M., van der Veer, W. M., van Egmond, M., Niessen, F. B. & Beelen, R. H. J. Macrophages in skin injury and repair. *Immunobiology* **216**, 753–762 (2011).
350. Mescher, A. L. Macrophages and fibroblasts during inflammation and tissue repair in models of organ regeneration. *Regeneration* **4**, 39–53 (2017).
351. Hinz, B. The role of myofibroblasts in wound healing. *Curr. Res. Transl. Med.* **64**, 171–177 (2016).
352. Wen, C. *et al.* Biological roles and potential applications of immune cell-derived extracellular vesicles. *J. Extracell. vesicles* **6**, 1400370 (2017).
353. Arutyunyan, I., Elchaninov, A., Makarov, A. & Fatkhudinov, T. Umbilical Cord as Prospective Source for Mesenchymal Stem Cell-Based Therapy. *Stem Cells Int.* **2016**, (2016).
354. Zhang, B. *et al.* Mesenchymal Stem Cells Secrete Immunologically Active Exosomes. *Stem Cells Dev.* **23**, 1233–1244 (2014).
355. Blazquez, R. *et al.* Immunomodulatory Potential of Human Adipose Mesenchymal Stem Cells Derived Exosomes on in vitro Stimulated T Cells. *Front. Immunol.* **5**, 556 (2014).
356. Bieback, K. Critical Parameters for the Isolation of Mesenchymal Stem Cells from

Umbilical Cord Blood. *Stem Cells* **22**, 625–634 (2004).
357. Siegel, J. P. Effects of interferon-γ on the activation of human T lymphocytes. *Cell. Immunol.* **111**, 461–472 (1988).
358. Kryczek, I. *et al.* Induction of IL-17+ T cell trafficking and development by IFN-gamma: mechanism and pathological relevance in psoriasis. *J. Immunol.* **181**, 4733–41 (2008).
359. Li, P., Zheng, Y. & Chen, X. Drugs for Autoimmune Inflammatory Diseases: From Small Molecule Compounds to Anti-TNF Biologics. *Front. Pharmacol.* **8**, 460 (2017).
360. Kassiotis, G. & Kollias, G. TNF and receptors in organ-specific autoimmune disease: multi-layered functioning mirrored in animal models. *J. Clin. Invest.* **107**, 1507–8 (2001).
361. Hirota, K. *et al.* Preferential recruitment of CCR6-expressing Th17 cells to inflamed joints via CCL20 in rheumatoid arthritis and its animal model. *J. Exp. Med.* **204**, 2803–12 (2007).
362. Li, Q., Laumonnier, Y., Syrovets, T. & Simmet, T. Recruitment of CCR6-expressing Th17 cells by CCL20 secreted from plasmin-stimulated macrophages. *Acta Biochim. Biophys. Sin. (Shanghai).* **45**, 593–600 (2013).
363. Zhu, J., Yamane, H. & Paul, W. E. Differentiation of effector CD4 T cell populations (*). *Annu. Rev. Immunol.* **28**, 445–89 (2010).
364. Fang, D. & Zhu, J. Dynamic balance between master transcription factors determines the fates and functions of CD4 T cell and innate lymphoid cell subsets. *J. Exp. Med.* **214**, 1861–1876 (2017).
365. Shih, H.-Y. *et al.* Transcriptional and epigenetic networks of helper T and innate lymphoid cells. *Immunol. Rev.* **261**, 23–49 (2014).
366. Li, Z., Li, D., Tsun, A. & Li, B. FOXP3+ regulatory T cells and their functional regulation. *Cell. Mol. Immunol.* **12**, 558–65 (2015).
367. Schmidt, A., Eriksson, M., Shang, M.-M., Weyd, H. & Tegnér, J. Comparative Analysis of Protocols to Induce Human CD4+Foxp3+ Regulatory T Cells by Combinations of IL-2, TGF-beta, Retinoic Acid, Rapamycin and Butyrate. *PLoS One* **11**, e0148474 (2016).
368. Liu, W. *et al.* CD127 expression inversely correlates with FoxP3 and suppressive function of human CD4+ T reg cells. *J. Exp. Med.* **203**, 1701–11 (2006).
369. Veerman, R. E., Güçlüler Akpinar, G., Eldh, M. & Gabrielsson, S. Immune Cell-Derived Extracellular Vesicles – Functions and Therapeutic Applications. *Trends Mol. Med.* **25**, 382–394 (2019).
370. Niu, S. *et al.* Broad Infiltration of Macrophages Leads to a Proinflammatory State in Streptozotocin-Induced Hyperglycemic Mice. *J. Immunol.* **197**, 3293–3301 (2016).
371. Evans, B. J., Haskard, D. O., Sempowksi, G. & Landis, R. C. Evolution of the Macrophage CD163 Phenotype and Cytokine Profiles in a Human Model of Resolving Inflammation. *Int. J. Inflam.* **2013**, 780502 (2013).
372. Sugimoto, M. A., Sousa, L. P., Pinho, V., Perretti, M. & Teixeira, M. M. Resolution of inflammation: What controls its onset? *Frontiers in Immunology* **7**, (2016).
373. Engelhardt, E. *et al.* Chemokines IL-8, GROalpha, MCP-1, IP-10, and Mig are sequentially and differentially expressed during phase-specific infiltration of leukocyte subsets in human wound healing. *Am. J. Pathol.* **153**, 1849–60 (1998).
374. Rath, M., Müller, I., Kropf, P., Closs, E. I. & Munder, M. Metabolism via arginase or nitric oxide synthase: Two competing arginine pathways in macrophages. *Frontiers in Immunology* **5**, (2014).
375. Konkel, J. E. *et al.* Transforming Growth Factor-β Signaling in Regulatory T Cells Controls T Helper-17 Cells and Tissue-Specific Immune Responses. *Immunity* **46**, 660–674 (2017).
376. Teimouri, A., Yeung, P. & Agu, R. 2D vs. 3D Cell Culture Models for In Vitro Topical (Dermatological) Medication Testing. in *Cell Culture* (IntechOpen, 2019). doi:10.5772/intechopen.79868
377. Martinsson, H., Yhr, M. & Enerback, C. Expression patterns of S100A7 (psoriasin) and S100A9 (calgranulin-B) in keratinocyte differentiation. *Exp. Dermatol.* **14**, 161–168 (2005).
378. Jinquan, T. *et al.* Psoriasin: a novel chemotactic protein. *J. Invest. Dermatol.* **107**, 5–10 (1996).
379. Baliwag, J., Barnes, D. H. & Johnston, A. Cytokines in psoriasis. *Cytokine* **73**, 342–350 (2015).

380. Diani, M., Altomare, G. & Reali, E. T Helper Cell Subsets in Clinical Manifestations of Psoriasis. *J. Immunol. Res.* **2016**, 7692024 (2016).
381. Giuliano, E., Paolino, D., Fresta, M. & Cosco, D. Drug-Loaded Biocompatible Nanocarriers Embedded in Poloxamer 407 Hydrogels as Therapeutic Formulations. *Medicines* **6**, 7 (2018).
382. Lin, A. M. *et al.* Mast cells and neutrophils release IL-17 through extracellular trap formation in psoriasis. *J. Immunol.* **187**, 490–500 (2011).
383. Narasimhan, P. B., Marcovecchio, P., Hamers, A. A. J. & Hedrick, C. C. Nonclassical Monocytes in Health and Disease. *Annu. Rev. Immunol.* **37**, 439–456 (2019).
384. Stockenhuber, K. *et al.* Foxp3+ T reg cells control psoriasiform inflammation by restraining an IFN-I–driven CD8+ T cell response. *J. Exp. Med.* **215**, 1987–1998 (2018).
385. Sugiyama, H. *et al.* Dysfunctional blood and target tissue CD4+CD25high regulatory T cells in psoriasis: mechanism underlying unrestrained pathogenic effector T cell proliferation. *J. Immunol.* **174**, 164–73 (2005).
386. Di Rocco, G., Baldari, S. & Toietta, G. Towards Therapeutic Delivery of Extracellular Vesicles: Strategies for In Vivo Tracking and Biodistribution Analysis. *Stem Cells International* **2016**, (2016).
387. Hu, L., Wickline, S. A. & Hood, J. L. Magnetic resonance imaging of melanoma exosomes in lymph nodes. *Magn. Reson. Med.* **74**, 266–271 (2015).
388. Alvarez-Erviti, L. *et al.* Delivery of siRNA to the mouse brain by systemic injection of targeted exosomes. *Nat. Biotechnol.* **29**, 341–345 (2011).
389. Damien, P. & Allan, D. S. Regenerative Therapy and Immune Modulation Using Umbilical Cord Blood-Derived Cells. *Biology of Blood and Marrow Transplantation* **21**, 1545–1554 (2015).
390. Rizk, M., Aziz, J., Shorr, R. & Allan, D. S. Cell-Based Therapy Using Umbilical Cord Blood for Novel Indications in Regenerative Therapy and Immune Modulation: An Updated Systematic Scoping Review of the Literature. *Biology of Blood and Marrow Transplantation* **23**, 1607–1613 (2017).
391. Willis, G. R., Kourembanas, S. & Mitsialis, S. A. Toward Exosome-Based Therapeutics: Isolation, Heterogeneity, and Fit-for-Purpose Potency. *Front. Cardiovasc. Med.* **4**, 1–13 (2017).
392. Torelli, G. F. *et al.* Functional analysis and gene expression profile of umbilical cord blood regulatory T cells. *Ann. Hematol.* **91**, 155–161 (2012).
393. Godfrey, W. R. *et al.* Cord blood CD4+CD25+-derived T regulatory cell lines express FoxP3 protein and manifest potent suppressor function. *Blood* **105**, 750–758 (2005).
394. Lobb, R. J. *et al.* Optimized exosome isolation protocol for cell culture supernatant and human plasma. *J. Extracell. Vesicles* **4**, (2015).
395. Osteikoetxea, X. *et al.* Improved Characterization of EV Preparations Based on Protein to Lipid Ratio and Lipid Properties. *PLoS One* **10**, e0121184 (2015).
396. Singla, D. K., Johnson, T. A. & Tavakoli Dargani, Z. Exosome Treatment Enhances Anti-Inflammatory M2 Macrophages and Reduces Inflammation-Induced Pyroptosis in Doxorubicin-Induced Cardiomyopathy. *Cells* **8**, 1224 (2019).
397. Deng, S. *et al.* Exosomes from adipose-derived mesenchymal stem cells ameliorate cardiac damage after myocardial infarction by activating S1P/SK1/S1PR1 signaling and promoting macrophage M2 polarization. *Int. J. Biochem. Cell Biol.* **114**, (2019).
398. Bardi, G. T., Smith, M. A. & Hood, J. L. Melanoma exosomes promote mixed M1 and M2 macrophage polarization. *Cytokine* **105**, 63–72 (2018).
399. Ying, W. *et al.* MicroRNA-223 is a crucial mediator of PPAR??-regulated alternative macrophage activation. *J. Clin. Invest.* **125**, 4149–4159 (2015).
400. Wang, Y. *et al.* Elevated expression of miR-142-3p is related to the pro-inflammatory function of monocyte-derived dendritic cells in SLE. *Arthritis Res. Ther.* **18**, 263 (2016).
401. Sun, Y. *et al.* PU.1-Dependent Transcriptional Regulation of miR-142 Contributes to Its Hematopoietic Cell-Specific Expression and Modulation of IL6. *J. Immunol.* **190**, 4005-4013; (2013).
402. Schaer, C. A., Schoedon, G., Imhof, A., Kurrer, M. O. & Schaer, D. J. Constitutive

endocytosis of CD163 mediates hemoglobin-heme uptake and determines the noninflammatory and protective transcriptional response of macrophages to hemoglobin. *Circ. Res.* **99**, 943–950 (2006).
403. Crayne, C. B., Albeituni, S., Nichols, K. E. & Cron, R. Q. The immunology of macrophage activation syndrome. *Frontiers in Immunology* **10**, (2019).
404. Snider, S. A. *et al.* Choline transport links macrophage phospholipid metabolism and inflammation. *J. Biol. Chem.* **293**, 11600–11611 (2018).
405. Zhu, Z., Ding, J., Ma, Z., Iwashina, T. & Tredget, E. E. Alternatively activated macrophages derived from THP-1 cells promote the fibrogenic activities of human dermal fibroblasts. *Wound Repair Regen.* **25**, 377–388 (2017).
406. Domenis, R. *et al.* Systemic T cells immunosuppression of glioma stem cell-derived exosomes is mediated by monocytic myeloid-derived suppressor cells. *PLoS One* **12**, (2017).
407. Pachler, K. *et al.* An in vitro potency assay for monitoring the immunomodulatory potential of stromal cell-derived extracellular vesicles. *Int. J. Mol. Sci.* **18**, (2017).
408. Di Trapani, M. *et al.* Differential and transferable modulatory effects of mesenchymal stromal cell-derived extracellular vesicles on T, B and NK cell functions. *Sci. Rep.* **6**, (2016).
409. Chen, W. *et al.* Immunomodulatory effects of mesenchymal stromal cells-derived exosome. *Immunol. Res.* **64**, 831–840 (2016).
410. Cibrián, D. & Sánchez-Madrid, F. CD69: from activation marker to metabolic gatekeeper. *European Journal of Immunology* **47**, 946–953 (2017).
411. Lee, J. Y., Park, J. K., Lee, E. Y., Lee, E. B. & Song, Y. W. Circulating exosomes from patients with systemic lupus erythematosus induce an proinflammatory immune response. *Arthritis Res. Ther.* **18**, (2016).
412. Fang, H. *et al.* Proinflammatory role of blister fluid-derived exosomes in bullous pemphigoid. *J. Pathol.* **245**, 114–125 (2018).
413. Weiss, E. *et al.* The role of interleukin 10 in the pathogenesis and potential treatment of skin diseases. *Journal of the American Academy of Dermatology* **50**, 657–675 (2004).
414. Owczarczyk-Saczonek, A., Czerwińska, J., Orylska, M. & Placek, W. Evaluation of selected mechanisms of immune tolerance in psoriasis. *Postep. Dermatologii i Alergol.* **36**, 315–324 (2019).
415. Kimball, A. B. *et al.* Clinical and immunologic assessment of patients with psoriasis in a randomized, double-blind, placebo-controlled trial using recombinant human interleukin 10. *Arch. Dermatol.* **138**, 1341–1346 (2002).
416. Van Deventer, S. J. H., Elson, C. O. & Fedorak, R. N. Multiple doses of intravenous interleukin 10 in steroid-refractory Crohn's disease. *Gastroenterology* **113**, 383–389 (1997).
417. Armstrong, J. P. K., Holme, M. N. & Stevens, M. M. Re-Engineering Extracellular Vesicles as Smart Nanoscale Therapeutics. *ACS Nano* **11**, 69–83 (2017).
418. Fakoya, A. O. J. New Delivery Systems of Stem Cells for Vascular Regeneration in Ischemia. *Front. Cardiovasc. Med.* **4**, 1–20 (2017).
419. Feng, Y., Huang, W., Wani, M., Yu, X. & Ashraf, M. Ischemic preconditioning potentiates the protective effect of stem cells through secretion of exosomes by targeting Mecp2 via miR-22. *PLoS One* **9**, 1–8 (2014).
420. Gilligan, K. E. Engineering Exosomes for Cancer Therapy. *Int. J. Mol. Sci.* **18**, 1122 (2017).
421. Luan, X. *et al.* Engineering exosomes as refined biological nanoplatforms for drug delivery. *Acta Pharmacol. Sin.* **38**, 754–763 (2017).